Thèse

Présentée et soutenue publiquement pour l'obtention du titre de

DOCTEUR DE L'UNIVERSITÉ DE LORRAINE
ET DE L'UNIVERSITE CADI AYYAD-MAROC

Mentions : GÉNIE DES PROCÉDÉS ET DES PRODUITS ET DES MOLÉCULES (SIMPPE)
ET
CHIMIE ET GENIE DE L'ENVIRONNEMENT (CED)

par

Amina LISSANEDDINE

Formulation d'adsorbant à base de matériaux naturels et leurs combinaisons aux procédés électrochimiques pour traiter des effluents industriels

le 15 décembre 2021

Membres du jury :

Rapporteurs :	**Ali ASSABBANE**	Professeur, Faculté des Sciences, Agadir, Maroc (Président du jury)
	Pierre-Louis TABERNA	Directeur de recherche, CNRS - Université de Toulouse 3, France
Examinateurs :	**Marc CRETIN**	Professeur, Université de Montpellier, France
	Rachid MAMOUNI	Professeur, Université Ibn Zohr, Agadir, Maroc.
Directrices de thèse :	**Marie-Noëlle PONS**	Directrice de recherche, CNRS - Université de Lorraine, France
	Laila MANDI	Professeure, Faculté des Sciences Semlalia, Université Cadi Ayyad, Marrakech, Maroc
Co-directeurs de thèse :	**Emmanuel MOUSSET**	Chargé de recherche, CNRS - Université de Lorraine, France
	Faissal AZIZ	Professeur, Faculté polydisciplinaire de Safi, Université Cadi Ayyad, Maroc
Invité :	**Mohammadine EL HADDAD**	Professeur, Faculté polydisciplinaire de Safi, Université Cadi Ayyad, Maroc

LABORATOIRE RÉACTIONS ET GÉNIE DES PROCÉDÉS
1, rue Grandville – BP 20451
54001 Nancy Cedex, France

B. P 511, Av. Abdelkrim Elkhattabi
40000 Marrakech, Maroc

To my dear parents Abderrahman and Malika

No dedication can express my great love, my esteem, my deep gratitude, my intimate attachment and my deep affection. I cannot and will not be able to thank you for all that you do for me, and all that you do until now.

May God protect you.

To my dear husband Soufian

All my love, thank you for supporting and encouraging me to finish this work and for being there when I needed advice.

To my dear brothers, my sister-in-law and my niece Soufiya

For their patience and comfort in moments of doubt and discouragement. They have advised me, supported me and put up with me throughout these years.

To my dearest friends Fadwa, Sana, Ahlam and Chaima

You are the only ones who can understand me, advise me and support me in a complicity that is ours, thank you for the moral support during all these long years.

To all those who have helped me from near or far in the realization of this work.

Scientific Publications

Publications:

- **Lissaneddine, A.,** Mandi, L., Achaby, M. El, Mousset, E., Eldon, R., Ouazzani, N., Pons, M.-N., Aziz, F. (2021). Performance and dynamic modeling of a continuously operated pomace olive packed bed for olive mill wastewater treatment and phenol recovery. Chemosphere, 130797.https://doi.org/10.1016/j.chemosphere.2021.130797.
- **Lissaneddine, A.,** Pons, M.-N., Aziz, F., Ouazzani, N., Mandi, L., Mousset, E. (2021). A critical review on the electrosorption of organic compounds in aqueous effluent – Influencing factors and engineering considerations, Environmental Research, 112128. https://doi.org/10.1016/j.envres.2021.112128.
- **Lissaneddine, A.,** Pons, M.-N., Aziz, F., Ouazzani, N., Mandi, L., Mousset, E. (2022). Electrosorption of phenolic compounds from olive mill wastewater: Mass transport consideration under a transient regime through an alginate-activated carbon fixed-bed electrode, Journal of Hazardous Materials, 128480. https://doi.org/10.1016/j.jhazmat.2022.128480.

Communications:

- Lissaneddine, A., Aziz, F., Pons, M.-N., Ouazzani, N., Mandi, L., Mousset, E. Key criteria for selective electrosorption of phenolic compounds on a novel biosourced material for olive mill wastewater treatment, 72nd Annual Meeting of the International Society of Electrochemistry held in Jeju Island, South Korea (online), August 29- September 3,2021. (Oral presentation)

- Lissaneddine, A., Aziz, F., Pons, M.-N., Ouazzani, N., Mandi, L., Mousset, E. Electrosorption using new biosourced porous electrode material for phenolic compounds removal and valorization – electrochemical engineering aspects, 12th European symposium on electrochemical engineering, Leeuwarden, The Netherlands (online), June 14-17, 2021. (Oral presentation)

- Lissaneddine, A., Aziz, F., El Achaby, M., Ouazzani, N., Mandi, L. Adsorption of chromium from highly concentrated tannery wastewater with novel porous composite beads: Central composite design optimization study, Water Resources in the Mediterranean Basin (WATMED9), Marrakech, Morocco, May 26-28, 2021. (Oral presentation)

- Lissaneddine, A., Aziz, F., Ouazzani, N., Mandi, L., Mousset, E., Pons, M.-N. Formulation of adsorbents based on natural materials and their combinations with electrochemical processes to treat industrial effluents, Seminar of SIMPEE doctoral school, Nancy, France, March 12, 2019. (Poster)

- Lissaneddine, A., Aziz, F., Pons, M.-N., Ouazzani, N., Mousset, E., Mandi, L. Formulation of adsorbent based on natural materials and their combinations to the electrochemical process for treating industrial effluents, CNEREE PhD Students Day, Faculty of Sciences and Techniques of Marrakech, Marrakech, Morocco, July 11, 2019. (Poster)

- Lissaneddine, A., Aziz, F., El Achaby, M., Ouazzani, N., Mandi, L. Removal of chromium (Cr(VI)) of tannery effluent by adsorption using beads based on natural materials, Africa sustainable solid waste management workshop, Marrakech, Morocco, November 7-9, 2018. (Poster)

- Lissaneddine, A., Aziz, F., El Achaby, M., Ouazzani, N., Mandi, L. Formulation of adsorbents based on natural materials for the removal of heavy metals from industrial effluents, CNEREE PhD Students Day, Faculty of Sciences and Techniques of Marrakech, Morocco, June 27, 2018. (Poster)

- Lissaneddine, A., Aziz, F., El Achaby, M., Ouazzani, N., Mandi, L. Bioadsorbents for tannery water treatment, CNEREE Open House, Marrakech, Morocco, June 5-7, 2018. (Poster)

- Lissaneddine, A., Aziz, F., El Achaby, M., Ouazzani, N., Mandi, L. Valorization of cultural heritage in Africa: Ecological development of tanneries, 23rd edition of the scientific and cultural week of the student, Faculty of Sciences Semlalia of Marrakech, Morocco, April 17-22, 2018. (Poster)

Patent:

Mandi Laila; Ouazzani Naaila; **Lissaneddine Amina**; Aziz Faissal (2020)."Procédé à flux continu à base des bioadsorbants pour traiter les effluents industriels" MA 44429 A1, B01D 15/00; B01J 20/04; C02F 1/288; C02F 1/28; B01J 20/043; B01J 20/24.

Acknowledgments

This work would not have been possible without the contribution of several people. I want to express my deepest gratitude by thanking all those who helped me to complete this work.

This PhD was completed as a co-shared thesis (Cotutelle) between the Faculty of Sciences Semlalia, Cadi Ayyad University, Marrakech, Morocco and Lorraine University, Nancy, France, under the Partenariat Hubert Curien (PHC) Toubkal/19/84 project (Campus France: 41525VG). For that reason, I would like to express my gratitude towards the CED Cadi Ayyad and the ED SIMPEE for facilitating the paperwork and allowing me to join this program, thus allowing me to benefit from this amazing collaboration.

My sincere thanks to my thesis directors. It has been my good fortune to do my thesis under the supervision of Pr. Laila MANDI (Cadi Ayyad University, Morocco) and Dr. Marie-Noëlle PONS (Lorraine University, France) who have supervised this work with great interest and optimism. Through their professional qualities, they have transmitted to me valuable knowledge in the field as well as scientific rigor that will be very useful in my professional future. Their rigor, patience and great efficiency make them irreplaceable supervisors. I am grateful for all the guidance and sustainably assistance.

I am profoundly grateful to my co-supervisors Pr. Faissal AZIZ (Cadi Ayyad University, Morocco) and Dr. Emmanual MOUSSET (Lorraine University, France). I want to thank them for believing in me, providing me with the right advice and giving me the necessary pep talks whenever I started doubting myself. Without their assistance and dedicated involvement in every step throughout the process, this thesis would have never been accomplished. I want to thank you very much for your support and understanding over these past years. I am deeply thankful to both of them for all their support, guidance and time.

I want to thank Pr. Naaila OUAZZANI, director of the Water, Biodiversity and Climate Change Laboratory (FSSM). I am deeply grateful for her support, advice and time.

It is important for me also to mention all the National Center for Studies and Research on Water and Energy staff that helped me get prepared with the thesis world by showing me the ropes, mainly Dr. HEJJAJ Abdessamad. The deepest appreciations are also

due to all the Water, Biodiversity and Climate change Laboratory members in Cadi Ayyad Univesity, mainly Aafaf KRIMECH, Khadija ZIDAN, Taoufiq ELHAKIM ELMANSOUR, and Imane HAYDARI as well as LRGP members of Lorraine University; Bastien JALLY and Nicolas MAURICE. I cannot forget Mohd Faidzul Hakim Mohd ADNAN for his invaluable help on many occasions.

I want to show my appreciation to all the members of my thesis committee Mr. Ali ASSABBANE, Mr. Pierre-Louis TABERNA, Mr. Mohammadine EL HADDAD, Mr. Marc CRETIN and Mr. Rachid MAMOUNI. I thank them for taking their valuable time to revise my manuscript carefully.

I warmly thank my dear parents, my dear husband Soufian, my wonderful brothers (Mohammed, Abdelilah, Zakaria and Abderazaq) and as well as my adorable sister-in-law Fatima Zahra, my princess Soufiya and my cousin Fatima for their encouragement and their unconditional support throughout these last years. May they find here the expression of my high consideration.

Last but not least, I would like to address massive thanks to my dearest friends Fadwa, Sana, Ahlam and Chaima for always being there as wonderful friends and supporting me in their way.

Abstract

Olive mill technology generates a considerable amount of solid (olive pomace) and liquid (olive mill wastewater) by-products during olives milling season, usually between November and March. These wastes represent a great challenge for olive oil producers since they must find technical, environmental and economical solutions to manage these by-products. The main objective of this thesis was to explore and propose a complete cycle of olive mill wastes treatment. This is in the framework of a zero liquid and waste discharge approach and promotes the circular economy concept. Two sorbents based on olive pomace chemical activation, i.e., powdered activated carbon within composite alginate beads and granular activated carbon (GAC), were successfully synthetized. Both materials had a structure and a porous morphology that revealed their feasibilities as potential and low-cost bio-sorbents. They were employed in either adsorption or electrosorption for phenolic compounds (PCs) recovery from olive mill wastewater (OMWW). The adsorption of PCs fitted second-order kinetics (R^2 = 0.997) and Langmuir isotherms (R^2 = 0.995). The thermodynamic parameters for the PCs adsorption onto the bio-adsorbent suggested a spontaneous nature of adsorption, an endothermic reaction and a modification of bio-adsorbent surface during the adsorption process. Thomas model was better at predicting PCs column adsorption (R^2 =0.97). Finally, the investigation of bio-adsorbent regeneration showed that the recovery of phenols from OMWW could be carried out with ethanol (43% of PCs recovered) or hydrochloric acid (90% of PCs recovered). The results of electrochemical characterization of the two bio-adsorbent electrodes showed that the high electroactive surface area, the high value of exchange current intensity (I_0) and the low value of charge transfer resistance (R_{CT}) could be promising properties for electrosorption studies. Electrosorption improved the adsorption capacity of the composite beads from 123 to 170 mg g^{-1} and the removal rate of PCs from 66 to 74% for GAC. Furthermore, the electrosorption of organic compounds was shown for the first time with real wastewater. New models were developed to better understand and predict PCs electrosorption kinetics, including transient mass transport. The remaining organic compounds in OMWW were then eliminated (91% of chemical oxygen demand (COD) removed) by advanced electro-oxidation treatment, while the bio-adsorbent was regenerated (34.5% of PCs recovered) by an electrochemical method.

Keywords: Adsorption; Biosourced materials; Electrosorption; Phenolic compounds; Powder or granular activated carbon; Regeneration.

Résumé

Les procédés d'extraction d'huile d'olive génèrent d'énormes quantités de déchets solides (grignons d'olive) et liquides (margines) pendant la saison de l'extraction de l'huile d'olives, généralement entre novembre et mars. Ces déchets représentent un grand défi pour les producteurs d'huile d'olive car ils doivent trouver des solutions techniques, environnementales et économiques pour gérer ces sous-produits. L'objectif principal de cette thèse était d'explorer et de proposer un cycle complet de traitement des déchets de l'extraction de l'huile d'olives. Cette démarche s'inscrit dans le cadre d'une approche zéro rejet liquide et déchets et promeut le concept d'économie circulaire. Deux adsorbants basés sur l'activation chimique des grignons d'olive, c'est-à-dire du charbon actif en poudre incorporé au sein de billes d'alginate composite et du charbon actif en grains (CAG), ont été synthétisés avec succès. Les deux matériaux avaient une structure et une morphologie poreuse et ont révélé leur applicabilité en tant que bio-adsorbants potentiels et peu coûteux. Ils ont été utilisés en adsorption ou électrosorption pour la récupération des composés phénoliques (CPs) des margines. L'adsorption des CPs correspond à la cinétique de second ordre (R^2 = 0.997) et aux isothermes de Langmuir (R^2 = 0.995). Les paramètres thermodynamiques pour l'adsorption des CPs sur le bio-adsorbant suggèrent une nature spontanée de l'adsorption et une modification de la surface du bio-adsorbant pendant le processus d'adsorption. Le modèle de Thomas a mieux prédit l'adsorption sur colonne de CPs (R^2 =0.97). Enfin, l'étude de la régénération du bio-adsorbant a montré que la récupération des phénols à partir des margines peut être effectuée avec de l'éthanol (43% des CPs récupérés) ou de l'acide chlorhydrique (90% des CPs récupérés). Les résultats de la caractérisation électrochimique des deux électrodes de bio-adsorbant ont montré que la surface électro-active élevée, la valeur élevée de l'intensité du courant d'échange (I_0) et la faible valeur de la résistance de transfert de charge (R_{CT}) pourraient être des propriétés prometteuses pour les études d'électrosorption. L'électrosorption a amélioré la capacité d'adsorption des billes composites de 123 à 170 mg g^{-1} et le taux d'élimination des CPs de 66 à 74% pour le CAG. De plus, l'électrosorption de composés organiques a été démontrée pour la première fois avec des eaux usées réelles. De nouveaux modèles ont été développés pour mieux comprendre et prédire la cinétique d'électrosorption des CPs, y compris le transport de masse transitoire. Les composés organiques restants dans les margines ont ensuite été éliminés (91% de la demande chimique en oxygène (DCO) éliminée) par un

traitement d'électro-oxydation avancé, tandis que le bio-adsorbant a été régénéré (34,5% des CPs récupérés) par une méthode électrochimique.

Mots clés : Adsorption ; Charbon actif en poudre ou en grains ; Composés phénoliques ; Electrosorption ; Matériaux biosourcés ; Régénération.

Résumé des travaux de thèse : Formulation d'adsorbants à base de matériaux naturels et leurs combinaisons aux procédés électrochimiques pour traiter des effluents industriels

Introduction

La présence de polluants dans l'eau est devenue une préoccupation environnementale majeure depuis la dernière décennie. Les rejets industriels couvrent un large spectre de polluants de natures différentes : matières organiques (hydrocarbures, composés phénoliques, pesticides...) et minérales (métaux lourds, radioéléments, fluorures, ...) à divers degrés de toxicité (Selvaraj et al., 2018). Parmi ces industries, on trouve les usines de production d'huile d'olive qui revêtent une grande importance économique dans les pays méditerranéens puisqu'elles représentent 98% de la production mondiale (Bampalioutas et al., 2019). Les procédés d'extraction d'huile d'olive génèrent d'énormes quantités de déchets solides (grignons d'olive) et liquides (margines) dans de courts intervalles de temps (Annab et al., 2019). Les margines représentent ainsi une source de pollution importante par l'acidification du milieu, la destruction de la microflore bactérienne du sol, la pollution des oueds, des retenues d'eau et des nappes souterraines ainsi que par les atteintes portées à la vie aquatique (Achak, 2016). Les composés phénoliques sont les principaux contributeurs de la pollution organique des margines ; il s'agit principalement du tyrosol, de l'hydroxytyrosol, de l'acide p-hydroxyphénylacétique, de l'acide vanillique, de l'acide gallique, de l'acide p-coumarique et de l'acide caféique (Bressan et al., 2004). En outre, ces composés phénoliques présentent de fortes propriétés antioxydantes, anti-inflammatoires et antimicrobiennes, et plusieurs effets positifs sur la santé ont été attribués à la consommation d'aliments riches en polyphénols (Annab et al., 2019), d'où l'intérêt de récupérer les composés phénoliques présents dans les margines.

Les procédés physico-chimiques et biologiques traditionnels employés pour le traitement des margines ont souvent une efficacité limitée. Par conséquent, d'autres méthodes de traitement sont nécessaires pour fournir une solution satisfaisante pour la récupération de ces composés (Kilic et al., 2019). Les procédés d'adsorption ont démontré une certaine efficacité pour une large gamme de polluants à l'échelle du laboratoire et réelle. Dans une volonté d'amélioration de l'efficacité de cette technologie, des matériaux poreux conducteurs

ont été polarisés par l'application de faibles intensités, selon le procédé dénommé électrosorption. Cette technologie s'est révélée être une alternative prometteuse aux techniques traditionnelles. Elle permet d'améliorer la séparation sélective des polluants organiques, tout en intensifiant les phénomènes de transport et donc d'augmenter les cinétiques d'électrosorption (Bayram et al., 2018 ; Nainamalai et al., 2018).

Dans ce contexte, l'objectif principal de cette thèse est de proposer une approche intégrée qui consiste en la formulation d'adsorbants à base de matériaux naturels et leurs combinaisons aux procédés électrochimiques pour traiter des effluents industriels.

Les déchets de grignons d'olive générés pendant le processus de production d'huile d'olive sont réutilisés comme bio-adsorbant dans l'adsorption ou l'électrosorption pour la récupération des composés phénoliques à partir des margines. Les composés organiques restants dans les margines sont ensuite éliminés par un traitement d'électro-oxydation avancée, tandis que l'adsorbant est régénéré par une méthode chimique ou électrochimique. Une approche systématique a été adoptée en augmentant le degré de complexité de l'effluent jusqu'à la réalisation d'études avec de véritables eaux usées d'usine de production d'huile d'olive. L'accent est mis sur l'amélioration de la connaissance des mécanismes d'adsorption et d'électrosorption de l'élimination des composés phénoliques dans des matrices aqueuses complexes, à travers la proposition de nouveaux modèles comparés à des données expérimentales cohérentes. Une attention particulière a été accordée à l'influence du transport de matière et des propriétés physico-chimiques des composés phénoliques sur l'efficacité d'adsorption et d'électrosorption. Ces considérations ont été prises en compte dans les modèles pour une meilleure prédiction de l'évolution du système en fonction du temps.

Ce travail de recherche a été réalisé dans le cadre d'une convention de cotutelle entre l'Université Cadi Ayyad et l'Université de Lorraine, dans le cadre du Partenariat Hubert Curien (PHC) Toubkal/19/84 (Campus France : 41525VG). La formulation des adsorbants ainsi que les tests d'adsorption et de désorption ont été réalisés au Maroc (Centre National d'Etudes et de Recherches sur l'Eau et l'Energie (CNEREE) et Laboratoire Eau, Biodiversité et Changements Climatiques, Faculté des Sciences Semlalia). La conception de l'électrode tridimensionnelle ainsi que les expériences d'électrosorption, d'électrodésorption et d'électro-oxydation ont été réalisées en France (Laboratoire Réactions et Génie des Procédés (LRGP)).

La structure de la thèse est illustrée en Figure R1, et le contenu de chaque partie est résumé ci-après.

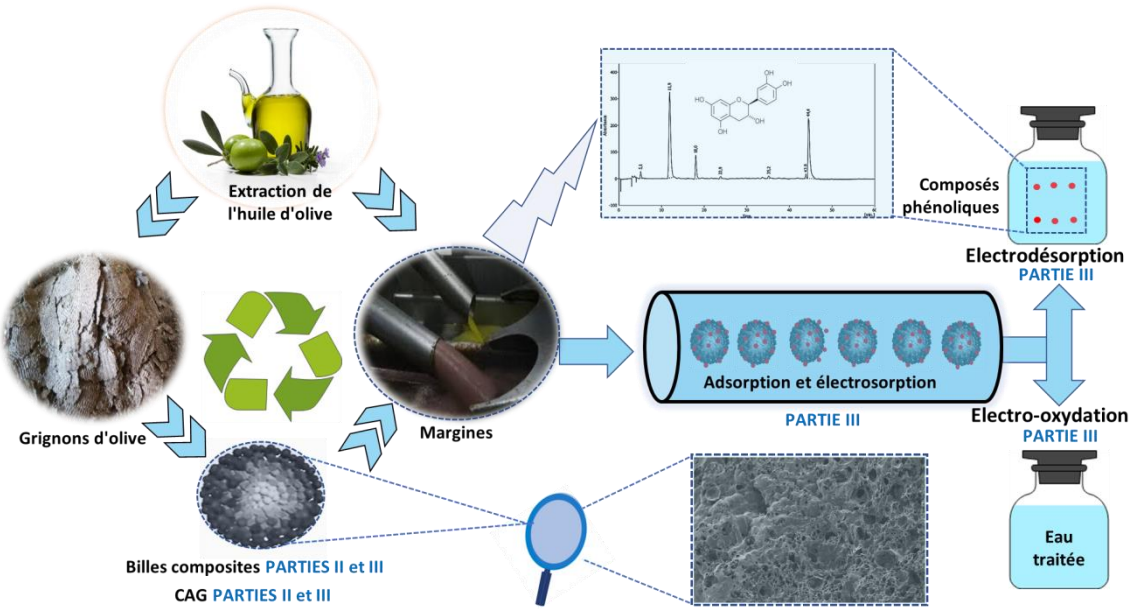

Fig. R1. Approche intégrée innovante de la thèse.

Les différents axes développés dans ce travail ont porté premièrement sur une étude bibliographique mettant l'accent sur l'adsorption et l'électrosorption. Cette partie commence par exposer le contexte et le principe des technologies d'adsorption et d'électrosorption. L'influence des paramètres, tels que les matériaux d'électrode, la densité de courant, la physico-chimie des électrolytes et la conception du réacteur, est ensuite abordée. Ensuite, l'identification des principaux facteurs d'influence combinée à la modélisation de l'électrosorption a permis de définir les stratégies de conception pour la mise en œuvre d'électrodes poreuses. Enfin, des orientations sont présentées, afin d'apporter de nouvelles opportunités pour l'optimisation et le développement futur de ces technologies, y compris dans le cadre de cette thèse.

La deuxième partie de la thèse est focalisée sur la présentation de l'approche expérimentale, en commençant par l'origine des margines étudiées et les différentes techniques physico-chimiques appliquées pour les caractériser. Ensuite, la préparation des adsorbants et électrodes poreuses à base de grignons d'olive a été décrite ainsi que les

méthodes pour déterminer leurs propriétés physico-chimiques. Enfin, un aperçu sur les protocoles expérimentaux d'adsorption et d'électrosorption des composés phénoliques a été donné avec les différentes techniques d'analyse utilisées.

La troisième et dernière partie de ce travail rassemble les résultats et discussions de cette étude. Cette partie est constituée de deux chapitres :

Le premier chapitre détaille l'étude d'adsorption et d'électrosorption des composés phénoliques sur des billes composites. Le grignon d'olive est d'abord transformé en un charbon actif hautement poreux puis en billes composites à base du charbon actif en poudre qui ont ensuite été utilisées pour le traitement des margines par adsorption. La cinétique, le mécanisme et les caractéristiques de l'adsorption des composés phénoliques ont été étudiés. Les expériences ont été réalisées dans différentes conditions expérimentales (temps, concentration, pH, température) afin de déterminer le comportement de l'adsorbant dans des réacteurs à lit fixe et à lit agité. La récupération des composés phénoliques et la réutilisation des billes composites ont été réalisées dans des réacteurs à lit fixe. Ensuite, l'électrosorption des composés phénoliques avec les billes composites en tant qu'électrode a été étudiée. De nouveaux modèles théoriques sont proposés pour prédire l'évolution de l'électrosorption des composés organiques dans des effluents simulés et réels en tenant compte du transport de matière et de la différence des constantes de dissociation acide (pKa) des composés phénoliques.

Le deuxième chapitre développe l'adsorption et l'électrosorption des composés phénoliques sur le charbon actif en grain (CAG). Pour l'adsorption, plusieurs paramètres ont été explorés tels que la cinétique d'équilibre, l'effet du pH et celui de la concentration initiale sur l'adsorption. Les effets de la profondeur du lit et du débit sur l'élimination des composés phénoliques ont également été étudiés. Ensuite une étude sur l'électrosorption des composés phénoliques sur CAG a été réalisée. La régénération électrochimique des électrodes de CAG et la dégradation électrochimique des margines ont également été étudiées.

1- Synthèse bibliographique

1.1- Adsorption

Les approches vertes sont devenues primordiales pour résoudre les enjeux actuels liés à l'eau, dans le but de satisfaire pleinement les trois piliers du développement durable, à savoir les garanties environnementales et sociales ainsi que la prospérité économique. Parmi ces procédés, l'adsorption est une des techniques la plus utilisée pour séparer les polluants organiques des eaux usées (Chkirida et al., 2021). L'adsorption est un processus efficace qui a été largement exploité dans l'élimination d'ions organiques dans les solutions aqueuses. L'adsorbant le plus généralement utilisé est le charbon actif. Bien qu'il soit efficace dans l'élimination des ions organiques à partir des eaux usées, il est coûteux (Pollard et al., 1992) et nécessite un agent chélateur pour améliorer ses performances, ce qui augmente le coût du traitement (Oliveira et al., 2005). Ceci a donc encouragé des travaux de recherche orientés vers des procédés de traitement faisant appel à des matériaux naturels moins coûteux et largement disponibles (Bailey et al., 1999 ; Fiset et al., 2000). Divers matériaux bio-sourcés ont été proposés tels que les zéolithes naturelles, les cendres volcaniques, les argiles (Paradas et al., 1993 ; Aziz et al., 2016), la peau de banane, la paille de blé, la sciure de bois (Jauad et al., 2016 ; Achak et al., 2016). En effet la performance et l'efficacité de la technique d'adsorption dépend d'une façon prépondérante de la nature du support utilisé comme adsorbant, son coût, son abondance, sa facilité de régénération, etc. Les principaux adsorbants employés dans les applications industrielles sont les charbons actifs, les argiles (terres décolorantes), les zéolithes, les gels de silice et les alumines activées (Sun & Meunier, 2007). Divers matériaux bio-sourcés et granulaires ont été employés pour les technologies d'adsorption.

Il existe plusieurs façons de mettre en œuvre l'adsorption en laboratoire, la manière la plus couramment utilisée étant la technique en mode batch. C'est une méthode statique qui consiste à mettre en contact un volume fixe de solution à épurer avec une masse d'adsorbant donnée, dans des conditions préalablement établies. Aussi efficace soit-elle en terme de capacité d'adsorption, il reste un problème lié à la récupération de ces adsorbants. Pour surmonter ce problème, une autre méthode largement utilisée en milieu industriel du fait des volumes d'eau à traiter, est la méthode dynamique en colonne ouverte qui utilise l'adsorbant

sous forme d'un lit filtrant. La solution à traiter est percolée à travers le matériau adsorbant (McKay, 1996 ; Franca & Oliveira, 2010). Par rapport à l'adsorption discontinue, l'adsorption sur colonne est plus pratique dans les applications industrielles en raison de sa simplicité, c'est-à-dire qu'elle ne nécessite aucun procédé supplémentaire, tel que la filtration ou la centrifugation (Zhang et al., 2002). Les expériences en mode continu dans une colonne aident à intensifier le processus d'adsorption à des fins pratiques. En procédé continu, le temps de contact entre l'adsorbant et l'adsorbat est presque instantané par rapport au mode discontinu où le temps de contact est relativement prolongé. Un dispositif en fonctionnement continu permet d'éliminer les polluants d'un volume considérable d'eaux usées, contrairement au procédé discontinu, tout en exploitant au maximum la capacité d'adsorption, ce qui est l'une des principales exigences des applications industrielles (Gupta & Sankararamakrishnan, 2010 ; Chatterjee & Schiewer, 2014). Le grand défi de telles utilisations des adsorbants pulvérulents dans le traitement des eaux en flux continu (colonne) est que les particules ont très facilement tendance à s'agglomérer et former des amas qui conduisent au colmatage du système dans un laps de temps très court et à des pertes de charges très significatives. Pour surmonter ce problème les chercheurs ont recours à l'encapsulation des adsorbants sous forme de bille, à l'aide de polymères comme liant (Aziz et al., 2019).

L'encapsulation est un procédé économique pour immobiliser un matériau dans une matrice d'hydrogel, tout en conservant ses propriétés d'adsorption. Ces billes gélifiées de taille uniforme offrent des avantages liés non seulement à la teneur élevée en composants actifs, mais aussi à leur facilité d'utilisation en réacteur (Xu et al., 2021). Les matériaux encapsulés peuvent être, après usage et saturation, récupérés par une simple séparation dans le cas de réacteur batch ou régénérés in situ s'ils sont mis en œuvre sous la forme de filtres dans un réacteur ouvert. L'alginate agit comme un milieu d'encapsulation pour aider à la préparation d'adsorbants faciles à séparer et à recycler. De nombreux chercheurs utilisent des billes avec des revêtements d'alginate sur plusieurs types de matériaux adsorbants ou les fonctionnalisent pour être plus efficaces. Des tests avec les billes composites ont été réalisés pour l'élimination de polluants organiques dans les eaux usées. L'adsorption dans les billes composites s'est produite en deux étapes : (i) l'adsorption par film, suivie par (ii) la diffusion intra-particulaire, comme le décrit le modèle de diffusion intra-particulaire. La capacité d'adsorption élevée, la capacité de régénération ainsi que la méthode de préparation simple font des billes composites un adsorbant prometteur pour l'élimination sélective des polluants

organiques dans les applications de traitement des eaux usées (Khan et al., 2021 ; Xu et al., 2021 ; Chkirida et al., 2021 ; Girijan et al., 2021).

Actuellement, le CAG est utilisé comme adsorbant en raison de sa grande surface et de sa grande affinité pour l'élimination des polluants organiques dans les eaux usées. Le modèle cinétique d'adsorption des polluants organiques dans le CAG est un modèle de pseudo-second ordre et de diffusion intraparticulaire, c'est-à-dire que l'adsorption est principalement contrôlée par la chimisorption et la diffusion (Islam et al., 2018 ; Díaz-Blancas et al., 2018 ; Eeshwarasinghe et al., 2019 ; Cai et al., 2020). Le modèle d'isotherme d'adsorption des polluants organiques dans le CAG suit celui de Langmuir (Islam et al., 2018 ; Cai et al., 2020). L'utilisation de billes composites et de CAG a montré un énorme potentiel dans les applications de remédiation environnementale en raison de leurs caractéristiques uniques (forme granulaire, morphologie poreuse et surface spécifique élevée) et de leur grande affinité d'adsorption vis-à-vis de divers polluants organiques (Islam et al., 2018 ; Díaz-Blancas et al., 2018 ; Jamil et al., 2019 ; Piai et al., 2019 ; Barhoumi et al., 2019 ; Eeshwarasinghe et al., 2019 ; Golovko et al., 2020 ; Cai et al., 2020).

Ainsi, bien qu'un nombre important d'articles de recherche aient été publiés sur l'adsorption des composés organiques sur des billes composites ou du CAG, il existe encore de nombreuses lacunes qui nécessitent une plus grande attention. Les faits suivants ont été pris en compte dans le cadre de cette thèse et peuvent également constituer des pistes pour des recherches futures :

● La recherche sur la sélectivité de l'adsorption et de la désorption est très importante et doit être étendue, en particulier pour les composés organiques à grande valeur ajoutée (par exemple les composés phénoliques).

● Peu de travaux sont réalisés sur l'utilisation de matériaux de recyclage comme adsorbants pour éliminer les composés organiques. Cela peut constituer un potentiel pour de futures recherches.

● Des matériaux plus efficaces, réutilisables et respectueux de l'environnement devraient être développés. Leur efficacité devrait être démontrée plus souvent avec des effluents réels.

● La possibilité de combiner la technologie d'adsorption basée sur le CAG ou les billes avec d'autres technologies de séparation potentiellement plus sélective, comme l'électrosorption, pourrait également être explorée.

● La plupart des articles ont porté sur l'adsorption de composés organiques en mode batch et continu à l'échelle laboratoire. Seuls quelques chercheurs ont traité le sujet à une échelle pilote voire industrielle.

1.2- Electrosorption

Au-delà des techniques d'adsorption seule, le couplage entre l'adsorption et l'électrochimie, dénommée électrosorption, suscite un regain d'intérêt ces dernières années, bien qu'il s'agisse d'un procédé ancien datant de la fin du 19ème siècle. Cela s'explique par ses propriétés et avantages uniques par rapport aux autres technologies de séparation. Le développement concomitant de nouveaux matériaux d'électrodes poreux a également permis son nouvel essor. L'électrosorption offre l'avantage de séparer les polluants des eaux usées avec la possibilité d'adsorber et de désorber sélectivement les composés ciblés. Une revue complète et critique sur l'électrosorption a été publiée dans le journal *Environmental Research* (Elsevier) au cours de cette thèse. Une attention particulière a été accordée à l'électrosorption des composés organiques, contrairement aux revues existantes sur la déionisation capacitive qui se concentrent uniquement sur les sels inorganiques. Le contexte et le principe de l'électrosorption sont d'abord présentés. L'influence des principaux paramètres (par exemple, les matériaux d'électrode, le potentiel d'électrode, la physico-chimie des solutions électrolytiques, le type de composés, l'effet de co-sorption, la conception du réacteur, etc.) est ensuite détaillée. Les aspects de modélisation et d'ingénierie sont discutés par la suite. Enfin, les principaux résultats et les perspectives d'avenir concernant les études de récupération de composés à forte valeur ajoutée ainsi que la combinaison entre les procédés d'électro-sorption/désorption et de dégradation sont exposés. L'analyse bibliographique met particulièrement en évidence le fait que les matériaux à base de carbone ont été principalement utilisés (85% des études) comme électrode poreuse dans l'électrosorption des substances organiques, alors que les études existantes manquent en termes de tests de stabilité et de durabilité des électrodes en conditions réelles. Ces électrodes ont été mises en œuvre dans des réacteurs à lit fixe la plupart du temps (43% des études) en raison de l'amélioration

du transport de matière. De plus, le potentiel d'électrode est un critère majeur : il doit être appliqué dans le domaine non faradique sinon des réactions indésirables peuvent facilement se produire, notamment la corrosion du carbone à partir de 0,21 V/électrode standard à hydrogène ou encore l'oxydation/réduction de l'eau. En outre, il n'existe pas d'études réalisées avec des effluents réels et sans ajout d'électrolyte support, ce qui est crucial pour tester l'efficacité réelle du procédé sans rajouter de pollution. Le développement de modèles prédictifs associés sera nécessaire en considérant l'effet de matrice ainsi que les phénomènes de transport et les caractéristiques physico-chimiques des composés organiques ciblés. Ces perspectives font en partie l'objet de cette thèse.

2- Méthodologie

2.1- Échantillonnage et caractérisation des margines

Les margines ont été collectées dans des huileries moderne et traditionnelle situées dans la région de Marrakech au Maroc pendant la saison d'extraction de l'huile d'olive de décembre à mars, durant les campagnes successives de 2019/2020 et 2020/2021. Les échantillons collectés ont été soumis à différentes analyses physico-chimiques. Le pH, la température, la teneur en solide dissous, la salinité et la conductivité électrique ont été mesurés par une sonde Hanna HI 9829 (Kallang Road, Singapour). La demande chimique en oxygène (DCO), les matières en suspension et les matières volatiles en suspension, l'ammonium, le phosphore total et les orthophosphates ont été analysés selon les normes AFNOR. Les composés phénoliques ont été dosés par la méthode Folin-Ciocalteu (Singleton & Rossi, 1965) en utilisant l'acide caféique comme standard.

2.2- Préparation des billes composites

Les grignons d'olive ont été séchés à 105°C pendant une nuit, puis broyés pour avoir des granulats pas trop fins. Le processus d'activation a été réalisé en utilisant l'activation chimique. Dix grammes de précurseur (grignons d'olive) ont été physiquement mélangés avec de l'hydroxyde de sodium 5 M (pureté 98 - 100,5%, Sigma-Aldrich) à un rapport pondéral (activateur/précurseur) (1 : 1), sous agitation pendant une heure. Le mélange ainsi obtenu a été lavé à plusieurs reprises avec de l'eau ultrapure jusqu'à pH neutre. La température de carbonisation a été stabilisée à 700°C pendant 30 min.

Le procédé de préparation des billes composites d'alginate de sodium/charbon actif a consisté à suivre les étapes successives suivantes (Figure R2) :

a) réaliser un mélange primaire d'hydrogel de l'alginate de sodium (BioChemica) (1%),
b) ajouter un mélange primaire de poudre de charbon actif (1%),
c) agiter le mélange pendant 24 h,
d) verser le mélange secondaire, goutte à goutte, dans une solution de fer(III) à 20 g L^{-1} (Iron (III) chloridehexahydrate, 99%, ACROS Organics),
e) réaliser la réticulation des billes.

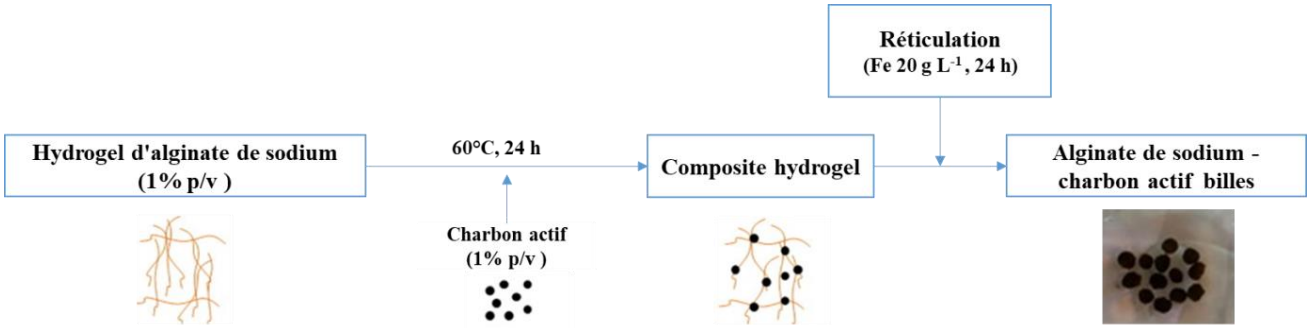

Fig. R2. Représentation schématique de la préparation des billes composites.

2.3- Préparation du charbon actif en grain

Le processus d'activation des granulats de grignons d'olive a été effectué en utilisant une méthode d'imprégnation. Dix grammes de précurseur (granulats du grignon d'olive) ont été mélangés avec de l'hydroxyde de sodium 5 M (pureté 98 - 100,5%, Sigma-Aldrich) à un rapport massique (activateur/précurseur) (1 : 1, 2 : 1, 3 : 1, 5 : 1), sous agitation pendant une heure. Après carbonisation, le CAG obtenu a été lavé plusieurs fois avec de l'eau ultra pure afin de neutraliser le pH.

2.4- Caractérisation des billes composites et du CAG

La spectroscopie infrarouge à transformée de Fourier (FTIR) a été utilisée pour évaluer les groupes fonctionnels sur la surface du charbon actif, des billes et du CAG. Les spectres FTIR ont été obtenus sur un spectromètre FT-IR ALPHA (ALPHA-P, Allemagne) dans la gamme de nombres d'onde comprise entre 400 et 4000 cm^{-1}. Chaque spectrogramme était composé d'une moyenne de 60 balayages.

L'examen morphologique des billes composites et de CAG a été réalisé à l'aide de mesures par microscopie électronique à balayage (MEB) de type TESCAN™ VEGA3 (Fuveau, France), en combinaison avec un système de détection dispersif en énergie (EDS) (TEAM™ EDS). L'EDS a permis d'analyser les éléments et leur distribution à l'échelle microscopique à la surface des billes et du CAG. La méthode de Brunauer, Emmett et Teller (BET) par adsorption d'azote à -196°C (via un système d'analyse de surface Micromeritics ASAP 2020) a été utilisée pour calculer la surface spécifique (S_{BET}) et le volume total (V_T) des billes et du CAG préalablement dégazés.

Les propriétés électrochimiques de l'électrode constituée de billes composites ou bien de CAG ont été évaluées à l'aide d'un potentiostat (AMETEK, Massy, France) dans un système à trois électrodes. Les billes composites ou bien le CAG ont été utilisés comme électrode de travail, une tige de graphite (Final Advanced Material, Didenheim, France) ou bien un fil de platine (Ögussa, Vienne, Autriche) comme contre-électrode et une électrode de référence de type Ag/AgCl. La surface électroactive du matériau poreux a été déterminée par voltampérométrie cyclique (CV) avec -0,2 à 0,8 V comme plage de tension et 0,01 V s^{-1} comme vitesse de balayage, suivie de l'utilisation de l'équation de Randles-Sevcik pour déterminer la surface à partir du pic d'intensité du courant (Mousset et al., 2016a). Les droites de Tafel ont été obtenues à partir de la voltampérométrie à balayage linéaire (LSV) avec une plage de tension variant de -2 à 2 V et une vitesse de balayage de 0,01 V s^{-1}. Elles ont été utilisées pour calculer l'intensité de courant d'échange (I_0) de l'électrode poreuse (Mousset et al., 2016b ; Fang et al., 2017 ; Adnan et al., 2021b). Des mesures de spectroscopie d'impédance électrochimique (EIS) utilisant la gamme de fréquences de 50 000 à 0,1 Hz avec une amplitude de 10 mV ont été réalisées pour caractériser l'interface électrode de travail/électrolyte en utilisant la méthode du circuit électrique équivalent (EEC) (Mousset et al., 2016a). Les données EIS ont été ajustées à l'aide du logiciel d'analyse de données ZSimpWin (AMETEK, Massy, France).

2.5- Adsorption

2.5.1- Billes composites

Les capacités d'adsorption du charbon actif préparé à base de grignons ont été étudiées en mode batch (réacteur fermé parfaitement agité) et en colonne (réacteur fermé

recirculé à flux ascendant). Lors des essais sur batch, les échantillons ont été agités pendant 4 h à la température ambiante (20°C) et avec une vitesse d'agitation de 200 tr min^{-1}. Les expériences en système continu ont été réalisées dans une colonne de 4 cm de diamètre intérieur et de 30 cm de hauteur. Les billes à base de charbon actif (140 g) ont été introduites dans la colonne. L'effluent a été introduit en flux ascendant à l'aide d'une pompe péristaltique, en appliquant un débit constant de 25 mL min^{-1}. Les échantillons de la solution d'effluent ont été recueillis à des intervalles de temps définis (1 h) et analysés par la méthode colorimétrique de Folin–Ciocalteu (Singleton et Rossi, 1965) en utilisant l'acide caféique comme standard.

2.5.2- Charbon actif en grain

Des expériences en batch ont été réalisées en ajoutant 5 g de CAG à 5 mL d'échantillon de margines, pendant un temps optimisé dans des tubes sous agitation continue dans un mélangeur rotatif (KS 3000 i control, Allemagne) tournant à 200 tr min^{-1}. Les études d'isothermes ont été réalisées sur le CAG préparé avec des margines de différentes concentrations (20, 50, 100, 250, 1000, 2000, 3000, 4000 et 5000 mg L^{-1}) pendant 24 h et à pH 4, ce qui correspondait à celui de l'effluent réel. Dans un sous-ensemble d'expériences, le pH de la solution des margines a été ajusté de 2 à 6 en utilisant du HCl ou du NaOH à 1 M. Des tests de contrôle ont été effectués dans les mêmes conditions mais en absence de CAG. Toutes les expériences ont été réalisées à température ambiante (entre 20°C et 25°C) et ont été effectuées en double.

Une colonne de 1 cm de diamètre et de hauteur variant entre 10, 15 et 20 cm a été remplie de CAG dont la masse variait entre 3 et 6 g. Les margines ont été introduites en flux ascendant en utilisant une pompe péristaltique (Antlia - 3C Dutscher, France) et en appliquant un débit constant de 0,5, 0,8 ou 1,5 mL min^{-1}. Les margines ont été collectées à la sortie de la colonne à intervalles réguliers et la concentration des composés phénoliques a été mesurée. Toutes les expériences ont été réalisées en double.

2.6- Electrosorption

2.6.1- Billes composites

La performance de l'électrosorption avec l'électrode de travail composée de billes composites a été testée sur un réacteur à colonne à lit fixe (diamètre intérieur de 2,6 cm et hauteur de 15 cm) en utilisant une tige de graphite (210 mm de longueur et 12 mm de diamètre) comme collecteur de courant pour connecter en mode monopolaire les billes de composites (35 g) avec le potentiostat. La contre-électrode était constituée d'une tige de graphite (100 mm de longueur et 8 mm de diamètre) et a servi en tant qu'anode. Dans toutes les expériences, 100 mL d'effluent ont été introduits en flux ascendant à l'aide d'une pompe péristaltique (Fisher Scientific, Illkirch-Graffenstaden, France) à un débit constant de 10 mL min^{-1}. Le potentiel de la cathode a été varié de -0,8 à -1,3 V/(Ag/AgCl) et une expérience a été réalisée en tant que contrôle en l'absence de courant électrique.

2.6.2- Charbon actif en grain

L'électrosorption avec le CAG a été réalisée avec une colonne à lit fixe, suivant un montage similaire à celui employé avec les billes d'alginate. 10 g de CAG ont été introduits dans la colonne avec une tige de graphite (210 mm de longueur et 12 mm de diamètre) comme collecteur de courant entre le générateur de courant et le CAG poreux, en considérant un mode de connexion monopolaire. La contre-électrode était une tige de platine (80 mm de longueur et 1 mm de diamètre). L'intensité du courant appliqué a été variée de 1 à 150 mA. Dans toutes les expériences, 100 mL d'effluent ont été introduits en flux ascendant à l'aide d'une pompe péristaltique à un débit constant de 10 mL min^{-1}. A la sortie de la colonne, l'effluent a été échantillonné à intervalles de temps réguliers, et la concentration en composés phénoliques a été mesurée.

3- Résultats et discussions

3.1- Billes composites

3.1.1- Performance et modélisation dynamique du lit fixe de grignons d'olives fonctionnant en continu pour le traitement des margines et la récupération du phénol.

Les résultats des caractéristiques physico-chimiques des margines étudiées ont montré que les composés phénoliques sont fortement présents dans les margines (4 et 10 g L^{-1} pour l'huilerie moderne et huilerie traditionnelle, respectivement). Une concentration élevée en matière organique a été notée, avec une valeur de DCO très élevée (110 g-O_2 L^{-1} pour l'huilerie traditionnelle). Elles avaient un pH acide de l'ordre de 4 : cette faible valeur rend le traitement biologique des margines brutes très difficile. La concentration en matières sèches totales était relativement élevée, soit 128,5 g L^{-1}. La conductivité électrique enregistrée dans cette étude était de l'ordre de 24 mS cm^{-1}, ce qui constitue un avantage pour conduire une électrolyse.

De nouvelles billes composites à base de grignons d'olive et d'hydrogel d'alginate ont été formulées avec succès pour l'élimination des composés phénoliques des margines. La structure et la morphologie poreuse des billes ont été confirmées par FTIR, MEB et EDS, ce qui a révélé la faisabilité des billes d'alginate en tant que biosorbants potentiels et peu coûteux. L'adsorption des composés phénoliques par les billes correspond à la cinétique de second ordre et à l'isotherme de Langmuir. Les résultats indiquent que l'adsorption des composés phénoliques sur les billes dépend fortement du pH et de la solubilité des phénols. L'analyse thermodynamique indique que l'adsorption des composés phénoliques est spontanée. Les modèles de Thomas et de Yoon-Nelson ont été choisis pour ajuster les données expérimentales. Le modèle de Thomas modifié a été le meilleur pour prédire l'adsorption des composés phénoliques en colonne (Figure R3). Enfin, l'étude de la régénération des billes a montré que la récupération des phénols à partir des margines pouvait être effectuée avec de l'éthanol.

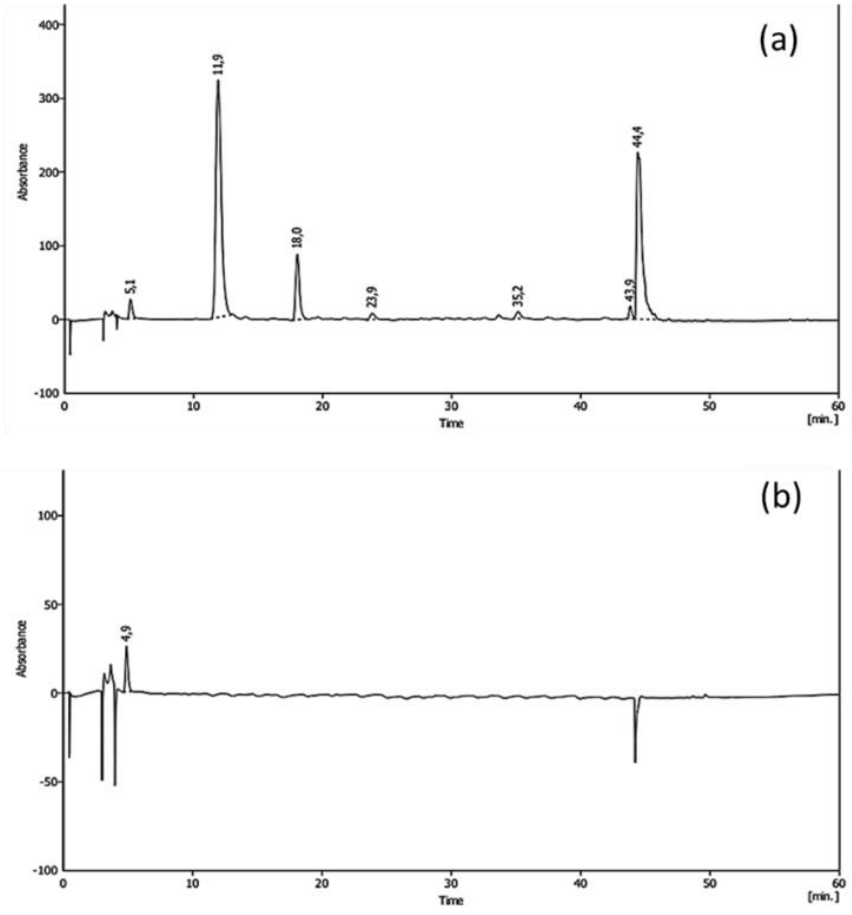

Fig. R3. Chromatogrammes (HPLC) des margines avant (a) et après (b) traitement.

3.1.2- Electrosorption des composés phénoliques des margines : considération du transport de matière en régime transitoire à travers une électrode à lit fixe en charbon actif-alginate.

Cette étude a permis de proposer une nouvelle approche pour éliminer les composés phénoliques des eaux usées simulées et réelles en mettant en œuvre l'électrosorption avec des billes en tant qu'électrode poreuse. Les impacts des paramètres clés (agent de réticulation (fer et calcium), teneur en charbon actif en poudre et potentiel de la cathode) sur l'efficacité de l'élimination des composés phénoliques ont été explorés. Les principaux résultats obtenus sont résumés ci-après (Figure R4). La conductivité plus élevée obtenue avec le fer comme agent de réticulation a conduit à une efficacité d'électrosorption légèrement supérieure par rapport à la présence de calcium. La teneur en charbon actif dans les billes a eu un impact sur le transfert de matière et les coefficients de diffusion ainsi que sur la résistance ohmique interne. Une quantité optimale de charbon actif a été déterminée (1% p/v), car une concentration trop

élevée induisait une agglomération des particules. Un potentiel cathodique de -1,1 V/(Ag/AgCl) a été trouvé optimal en considérant à la fois la capacité d'électrosorption et les besoins énergétiques. Une tension trop élevée a conduit à des réactions faradiques qui entravaient le mécanisme d'électrosorption. De plus, l'efficacité de l'électrosorption était plus élevée avec les eaux usées réelles qu'avec les effluents simulés. Cela peut être dû à la présence de nombreux composés organiques qui ont des pKa différents. De nouveaux modèles discrets ont été proposés pour comprendre et prédire l'efficacité d'électrosorption. La cinétique est principalement limitée par la diffusion en régime transitoire dans l'effluent synthétique, tandis que l'électromigration des composés phénoliques ioniques a également eu un impact sur l'électrosorption avec les eaux usées réelles. Les résultats obtenus, le modèle de circuit électrique équivalent ainsi que les modèles cinétiques ont permis de confirmer que l'électrosorption se produisait principalement à l'intérieur des billes et non à l'interface électrode/électrolyte, contrairement à ce qui est souvent supposé.

La bonne efficacité de l'électrosorption obtenue pour l'élimination des composés phénoliques des margines est prometteuse pour leur récupération en vue d'une valorisation ultérieure. Une autre possibilité serait de combiner l'électrosorption pour la récupération des composés phénoliques avec un procédé de dégradation pour l'élimination des composés indésirables, ce qui a fait l'objet de recherche d’une partie de la thèse.

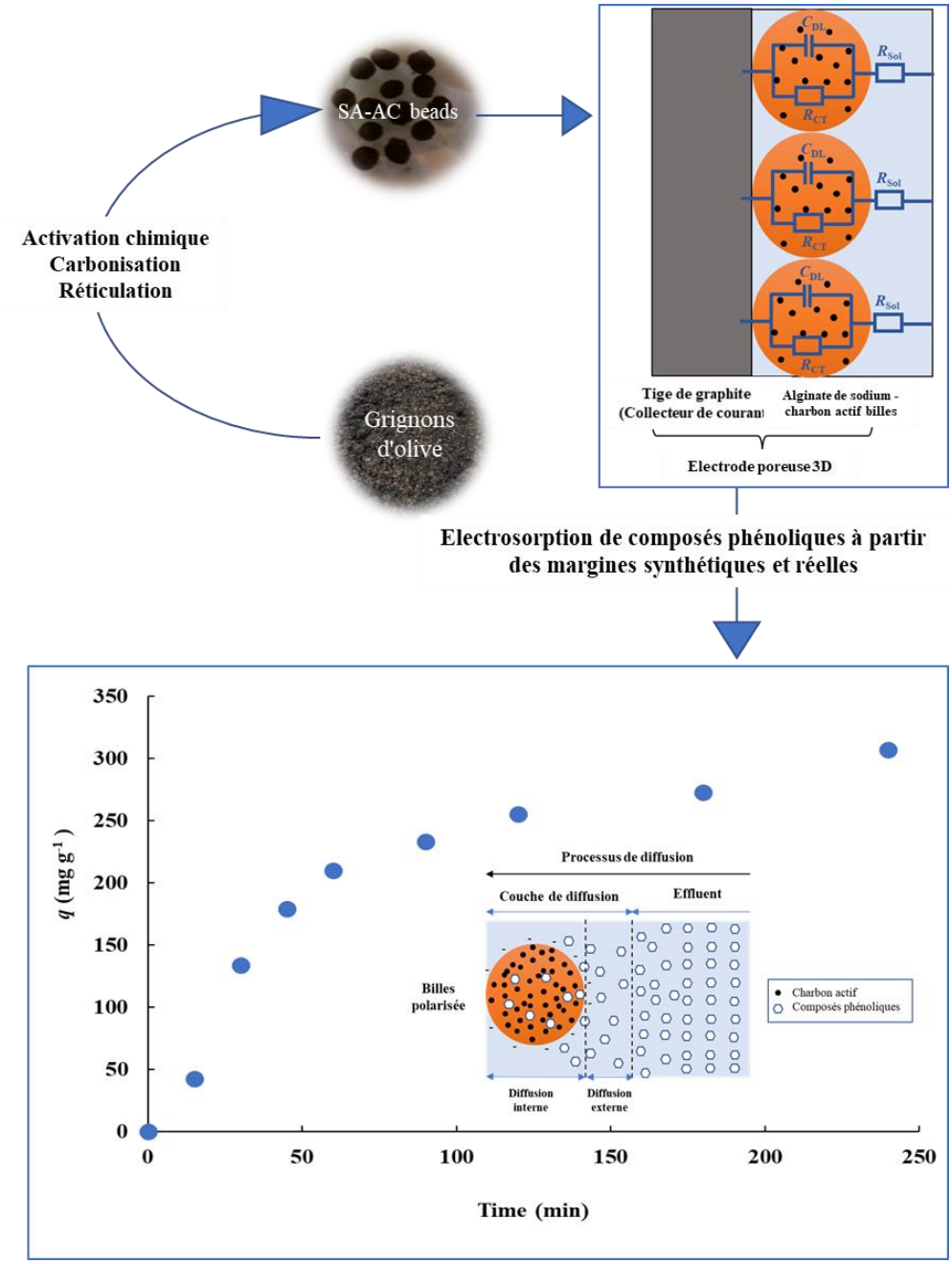

Fig. R4. Représentation schématique des résultats de l'électrosorption des composés phénoliques avec des billes en tant qu'électrode poreuse.

3.2- Charbon actif en grain

3.2.1- Charbon actif en grain à base de grignons d'olive pour le traitement des margines et la récupération des composés phénoliques

Dans le cadre de nos recherches, une tentative a été faite pour optimiser les paramètres du procédé qui conduisent à un CAG ayant de bonnes caractéristiques. Les

résultats de préparation du CAG avec différents rapports massiques d'activateur/précurseur (1 : 1, 2 : 1, 3 : 1, 5 : 1) ont montré qu'après trois répétitions le rapport massique de 3 : 1 était le meilleur. Le volume des pores du CAG augmentait en continu avec le taux d'imprégnation. Par conséquent, la structure de micropores ainsi que l'élargissement des micropores aux mésopores augmentaient également (Sudaryanto et al., 2006). De plus, l'adsorption des composés phénoliques (petites tailles : diamètre moléculaire moyen = 0,557 nm) était favorisée sur des charbons actifs microporeux. Par conséquent, nous avons utilisé par la suite ce rapport massique (3 : 1) pour la production du CAG.

Les caractéristiques du CAG, nécessaires pour une bonne adsorption, ont été confirmées par des études de FTIR, MEB, EDS et BET. La capacité d'adsorption monocouche de Langmuir des composés phénoliques sur le CAG était de 1666 mg g^{-1}. Les données expérimentales cinétiques s'adaptaient très bien au modèle cinétique de pseudo second ordre. Les paramètres thermodynamiques pour l'adsorption des composés phénoliques sur le CAG ont montré que la valeur négative d'enthalpie libre (ΔG) confirmait la faisabilité du processus et la nature spontanée de l'adsorption. Les valeurs d'enthalpie (ΔH) et d'entropie (ΔS) de l'adsorption des composés phénoliques sur le CAG suggérent une modification de la surface du CAG pendant le processus d'adsorption. L'étude en condition dynamique a permis de mettre en évidence que le temps de percée diminuait avec le débit lors de l'élimination des composés phénoliques, mais augmentait avec la hauteur du lit. La capacité d'adsorption des composés phénoliques dépendait donc de la hauteur du lit et du débit. La modélisation de l'adsorption en colonne a montré que les modèles de Thomas et de Yoon-Nelson s'adaptaient bien aux données expérimentales. Par conséquent, le CAG, avec ses divers avantages (faible coût et haute efficacité dans cette application), pourrait être utilisé comme un adsorbant prometteur pour une séparation et récupération efficace des composés phénoliques des margines.

3.2.2- Electrosorption avec l'électrode de charbon actif en grain bio-sourcé pour la récupération des composés phénoliques et combinaison avec l'électro-oxydation pour le traitement des margines

La performance de l'électrosorption basée sur l'électrode en CAG a été étudiée pour les composés phénoliques provenant des margines. Les résultats de la caractérisation électrochimique de l'électrode en CAG ont montré une surface électro-active élevée (7.8×10^3

cm^2), une valeur élevée de I_0 (5.5×10^{-3} A), et une faible valeur de R_{CT} (4 Ω) comparées à la littérature. Ainsi les propriétés de l'électrode en CAG promettaient une grande efficacité d'électrosorption. L'étude de l'électrosorption qui a suivi en présence de composés phénoliques a été réalisée à différentes intensités de courant pour les margines artificielles (1 à 200 mA) et pour les margines réelles (1 à 100 mA). L'intensité de courant la plus appropriée était de 1 mA (potentiel de cathode : 0,26 V/(Ag/AgCl)) pour l'effluent artificiel et de 10 mA (potentiel de cathode : -0,05 V/(Ag/AgCl)) pour les margines réelles, enregistrant la plus grande efficacité d'électrosorption de 72% et de 68%, respectivement. L'effet du pKa des composés phénoliques a ensuite été étudié. L'efficacité d'électrosorption ne dépendait pas seulement du pKa vis-à-vis du pH de la solution, mais également de la taille des molécules adsorbées par rapport à la distribution de la taille des pores du CAG.

D'autre part, la méthode électrochimique a été testée pour récupérer les composés phénoliques de l'électrode en CAG en inversant la polarité. Le pourcentage de composés phénoliques récupérés était de 34,5% en conditions optimales, c'est-à-dire avec 0,1 g L^{-1} de KCl et une intensité du courant de 10 mA pour une durée maximale de 120 min sur un seul cycle.

Bien que l'électrosorption puisse être utilisée comme une technique de séparation, la combinaison de l'électrosorption avec un procédé de dégradation pourrait être une stratégie efficace pour le traitement des margines. Après des tests d'électro-oxydation en sortie de l'électrosorption de l'effluent, l'efficacité d'élimination de la DCO était de 92% après filtration préalable (≈ 10 μm) de l'effluent.

Conclusions et perspectives

L'objectif de ce travail était de réaliser un cycle complet de traitement des déchets d'extraction d'huile d'olive dans lequel le grignon d'olive est d'abord transformé en un adsorbant hautement poreux, puis en une électrode poreuse qui peut ensuite être utilisée pour le traitement des margines par adsorption ou électrosorption. Les résultats du travail effectué ont montré que les deux technologies explorées présentaient une capacité d'élimination élevée des composés phénoliques des margines. L'électrosorption a permis d'améliorer la capacité d'adsorption des billes composites de 123 à 170 mg g^{-1} et le taux d'éliminations des composés phénoliques de 66 à 74% pour le CAG. Par ailleurs, l'électrosorption de composés organiques

a pu faire ses preuves pour la première fois avec des eaux usées réelles. La combinaison de l'électrosorption avec un procédé de dégradation parait être une stratégie prometteuse pour le traitement des margines, mais nécessite encore des ajustements. De plus, certains aspects doivent être intégrés pour valider ces procédés et leurs usages pour le traitement des margines :

- Il faudrait tester d'autres activateurs chimiques plus puissants afin d'éviter la carbonisation pour produire un charbon actif encore plus efficace, c'est-à-dire moins cher, plus rigide, et contenant plus de mésopores et de micropores ; l'activation thermique pourrait aussi être tentée en absence d'oxygène pour éviter la perte en carbone,
- La sélectivité des composés organiques vis-à-vis des technologies de séparation pourrait être étudiée de manière plus détaillée, en développant des protocoles analytiques suffisamment élaborés. Cela permettrait de distinguer les différents types de composés phénoliques (et organiques de manière générale) présents dans des matrices complexes comme les effluents réels, avant, pendant et après adsorption/électrosorption et désorption/électrodésorption,
- Le traitement des margines résiduelles par électro-oxydation pourrait être optimisé après avoir bien identifié les problèmes liés à l'encrassement de l'anode,
- L'efficacité des divers traitements (adsorption / désorption, électrosorption / électrodésorption, électrooxydation) doit être testée sur des procédés à l'échelle pilote puis industrielle ; l'optimisation doit également se faire à plus grande échelle pour ensuite estimer les coûts qui seront plus représentatifs avec des conditions réelles ; cela permettra également de pouvoir mieux comparer l'efficacité de ces technologies par rapport à d'autres procédés existants.

Références

Achak, M. (2016). Essais de traitement des rejets liquides issus d'une huilerie d'olive moderne (margines) par differents procédés : coagulation-floculation, adsorption, infiltration-percolation, phyto-epuration. Thèse de Doctorat, Université Cadi Ayyad, faculté des sciences Semlalia, Marrakech.

Annab, H., Fiol, N., Villaescusa, I., Essamri, A. (2019) A proposal for the sustainable treatment and valorisation of olive mill wastes. Journal of Environmental Chemical Engineering, 7, 102803.

Aziz, F., El Achaby, M., Lissaneddine, A., Aziz, K., Ouazzani, N., Mamouni R., Mandi L., (2019) Composites with alginate beads: A novel design of nano-adsorbents impregnation for large-scale continuous flow wastewater treatment pilots, Saudi Journal of Biological Sciences, 27(10), 2499-2508.

Aziz, F., Mamoun M., Ouazzani N., Uheida A., Mandi, L. (2017) Composites Nanofibers of Polyacrylonitrile/Natural Clay for Decontamination of Waters Containing Pb(II), Cu(II), Zn(II) and Pesticides. Separation Science and Technology, 52, 58-70.

Bampalioutas, K., Vlysidis, A., Lyberatos, G., Vlyssides, A. (2019) Detoxification and methane production kinetics from three-phase olive mill wastewater using Fenton's reagent followed by anaerobic digestion. Journal of Chemical Technology & Biotechnology, 94, 265-275.

Barhoumi, A., Ncib, S., Chibani, A., Brahmi, K., Bouguerra, W., Elaloui, E. (2019) High-rate humic acid removal from cellulose and paper industry wastewater by combining electrocoagulation process with adsorption onto granular activated carbon. Ind. Crops Prod.140, 111715.

Bayram, E., Kizil, Ç., & Ayranci, E. (2018) Flow-through electrosorption process for removal of 2,4-D pesticide from aqueous solutions onto activated carbon cloth fixed-bed electrodes. Water Science and Technology, 77(3), 848–854.

Bressan, M., Liberatore, L., d'Alessandro, N., Tonucci, L., Belli, C., Ranalli G. (2004) Improved combined chemical and biological treatments of olive oil mill wastewaters, J. Agric. Food Chem., 52, 1228-1233.

Cai, Z., Deng, X., Wang, Q., Lai, J., Xie, H., Chen, Y., Huang, B., Lin, G. (2020) Core-shell granular activated carbon and its adsorption of trypan blue. J. Clean. Prod. 242, 118496.

Chatterjee, A., S. Schiewer (2014) Effect of competing cations (Pb, Cd, Zn, and Ca) in fixed-bed column biosorption and desorption from citrus peels. Water, Air & Soil Pollution 225 (2), 1-13.

Chkirida, S., Zari, N., Achour, R., Hassoune, H., Lachehab, A., Qaiss, A. el kacem, Bouhfid, R. (2021) Highly synergic adsorption/photocatalytic efficiency of Alginate/Bentonite impregnated TiO_2 beads for wastewater treatment. J. Photochem. Photobiol. A Chem. 412, 113215.

Díaz-Blancas, V., Ocampo-Pérez, R., Leyva-Ramos, R., Alonso-Dávila, P.A., Moral-Rodríguez, A.I. (2018) 3D modeling of the overall adsorption rate of metronidazole on granular activated carbon at low and high concentrations in aqueous solution. Chem. Eng. J. 349, 82–91.

Eeshwarasinghe, D., Loganathan, P., Vigneswaran, S. (2019) Simultaneous removal of polycyclic aromatic hydrocarbons and heavy metals from water using granular activated carbon. Chemosphere 223, 616–627.

Franca, A.S.; L.S. Oliveira, Fixed-Bed Adsorption Studies. In: Sorption Processes and Pollution. Ed.: Presses Universitaires de Franche-Comté, chapitre 3, p. 79-106, 2010.

Girijan, S., Kumar, M., Gomber, S. (2021) Starch and powdered activated carbon amended alginate-biomass beads for metronidazole and bulk organic matter removal: Synthesis, optimization, reaction kinetics and reusability. J. Environ. Chem. Eng. 9, 106102.

Gupta A, Sankararamakrishnan, N. (2010) Column studies on the evaluation of novel spacer granules for the removal of arsenite and arsenate from contaminated water. Bioresour. Technol 101, 2173–2179.

Khan, A.S., Ibrahim, T.H., Khamis, M.I., Nancarrow, P., Iqbal, J., Al Nashef, I., Jabbar, N.A., Hassan, M.F., Mjalli, F.S. (2021) Preparation of sustainable activated carbon-alginate beads impregnated with ionic liquid for phenol decontamination. J. Clean. Prod. 128899.

Kilic, M. Y., Abdelraheem, W. H., He, X., Kestioglu, K., Dionysiou, D. D. (2019) Photochemical treatment of tyrosol, a model phenolic compound present in olive mill wastewater, by hydroxyl and sulfate radical-based advanced oxidation processes (AOPs). Journal of Hazardous Materials, 367, 734-742.

Li, W., Yan, J., Yan, Z., Song, Y., Jiao, W., Qi, G., Liu, Y. (2018) Adsorption of phenol by activated carbon in rotating packed bed: Experiment and modeling. Applied Thermal Engineering, 142, 760–766.

Łosiewicz, B., Birry, L., Lasia, A. (2007) Effect of adsorbed carbon monoxide on the kinetics of hydrogen electrosorption into palladium. Journal of Electroanalytical Chemistry, 611(1-2), 26–34.

McKay, G. Use of Adsorbents for the Removal of Pollutants from Wastewaters. Ed.: CRC Press, Boca Raton, USA, 186 p., 1996.

Mousset, E., Wang, Z., Hammaker, J., Lefebvre, O., 2016a. Physico-chemical properties of pristine graphene and its performance as electrode material for electro-Fenton treatment of wastewater. Electrochim. Acta 214, 217–230.

Mousset, E., Wang, Z., Hammaker, J., Lefebvre, O., 2016b. Physico-chemical properties of pristine graphene and its performance as electrode material for electro-Fenton treatment of wastewater. Electrochim. Acta 214, 217–230.

Nainamalai, M., Palani, M., Soundarajan, B., Allwin, A. E. (2018) Decolorization of synthetic dye wastewater using packed bed electro-adsorption column. Chemical Engineering and Processing - Process Intensification, 130, 160–168.

Paradas E.G, Sanchez M.V., Cicciana M.S., Sanchez J.C, Perez M.F. (1993) Removal of 3—(3,4—dichlorophenyl)—1, 1 dimethylurea from aqueous solution by natural and activated bentoniteChem. Technol. Biotechnol., 56, 67-71.

Selvaraj, H., Aravind, P., Sundaram, M. (2018) Four compartment mono selective electrodialysis for separation of sodium formate from industry wastewater. Chemical Engineering Journal, 333, 162-169.

Sudaryanto, Y., Hartono, S. B., Irawaty, W., Hindarso, H., Ismadji, S. (2006) High surface area activated carbon prepared from cassava peel by chemical activation. Bioresource Technology, 97(5), 734–739.

Sun, M. L., Meunier, F., Adsorption : aspects théoriques. Techniques de l'ingénieur, J 2 730, 2007.

Xu, S., Jin, Y., Li, R., Shan, M., Zhang, Y. (2022) Amidoxime modified polymers of intrinsic microporosity/alginate composite hydrogel beads for efficient adsorption of cationic dyes from aqueous solution. J. Colloid Interface Sci. 607 890-899.

Zhang, L.M., D.Q. Chen, (2002) An investigation of adsorption of lead (II) and copper (II) ions by water-insoluble starch graft copolymers. Colloids and Surfaces A: Physicochemical and Engineering Aspects 205, 231-236.

Table of Contents

GENERAL INTRODUCTION **1**

REFERENCES **6**

PART I: BIBLIOGRAPHY **8**

1. Adsorption **9**

1.1. Definition and types of adsorption 9

1.2. Adsorption of organic pollutants 12

1.3. Current stage and future prospects 14

2. Electrosorption **15**

2.1. Electrosorption: background and principle 15

2.2. Influence of the main parameters 20

2.3. Reactor design 46

2.4. Factors influencing the electrodesorption step 52

2.5. Long-term efficiency of electrosorption 53

2.6. Modeling 54

2.7. Current developments and future prospects 59

References **65**

PART II: MATERIAL AND METHODS **79**

1. Adsorption **80**

1.1. Sample collection and characterization 80

1.2. Preparation of activated carbon 81

1.3. Preparation of the beads 81

1.4. Characterization of beads and GAC 82

1.5. Stirred batch and column sorption experiments 83

1.6. Batch and fixed-bed column data analysis 85

1.7. Analytical methods 88

2. Electrosorption **89**

2.1. Effluents preparation and characterization 89

2.2. Preparation and characterization of the 3D porous electrode 89

2.3. Electrochemical setup and procedure 90

2.4. Electrochemical regeneration of the GAC electrode 93

2.5. Electrochemical degradation of OMWW 94

References **96**

PART III: RESULTS AND DISCUSSIONS **98**

CHAPTER I: COMPOSITE BEADS **99**

I. Performance and dynamic modeling of a continuously operated pomace olive packed-bed for olive mill wastewater treatment and phenol recovery 100
1. Introduction 100
2. Results and discussion 101
2.1. Physicochemical properties of the effluent 101
2.2. Characterization of the adsorbent 103
2.3. Adsorption efficiency 107
3. Conclusions 122
References 123
II. Electrosorption of phenolic compounds from olive mill wastewater: mass transport consideration under transient regime through alginate-activated carbon fixed-bed electrode 129
1. Introduction 129
2. Modeling 130
3. Results and discussion 131
3.1. Electrochemical characterization of the 3D porous electrodes 131
3.2. Electrosorption efficiency 134
4. Conclusions 147
References 148
CHAPTER II: GRANULAR ACTIVATED CARBON 153
I. Granular activated carbon based on pomace olive for olive mill wastewater treatment and phenol recovery 154
1. Introduction 154
2. Results and discussion 154
2.1. Physicochemical properties of effluent 154
2.2. Preparation and characterization of GAC 155
2.3. Adsorption efficiency 159
2.3.1. Adsorption equilibrium study 159
2.3.2. Modeling of adsorption kinetics 161
2.3.3. Effect of pH 162
2.3.4. Effect of temperature 163
2.3.5. Fixed-bed column 164
2.4. Desorption 167
3. Conclusions 169
References 170
II. Electrosorption with bio-sourced granular activated carbon electrode for phenols recovery and combination with electrooxidation for residual olive mill wastewater treatment 175
1. Introduction 175
2. Results and discussion 176
2.1. Characterization of GAC 176

2.1.1. Influence of electrochemical conditioning on GAC characteristics 176
2.1.2. Electrochemical characterization of the conditioned GAC 179
2.2. Electrosorption 182
2.2.1. Phenol electrosorption 182
2.2.2. Effect of phenolic compounds properties 186
2.2.3. OMWW electrosorption 188
2.3. Electrochemical regeneration of the GAC electrode 191
2.4. Electrochemical degradation of OMWW 194
3. Conclusions 195
References 197
GENERAL CONCLUSION AND PERSPECTIVES 202

List of Figures

Fig. 1. The innovative integrated approach of the thesis. 3
Fig. 2. Some basic terms used in adsorption science and technology (Tran et al., 2017). 10
Fig. 3. Schematic representation of the adsorption processes (Peng & Guo, 2020). 11
Fig. 4. Schematic representation of the physical adsorption and chemical adsorption (Cuong, 2020). 12
Fig. 5. Schematic representation of the EDL at positively charged electrode materials in the presence of anions, cations and solvent. 17
Fig. 6. Schematic diagram illustrating the principle of electrosorption, including anion, cation and uncharged compounds, as well as transport phenomena (δ_a and δ_c: diffusion layer thickness at the anode and cathode, respectively). 19
Fig. 7. (a) Electrode materials used in the literature, (b) SEM image of ACF (Han et al., 2006b), (c) SEM image of the prGO/SWCNT film (Yue et al., 2019). 30
Fig. 8. (a) Range of the specific surface area of the electrode implemented for organics electrosorption in literature, (b) S_{BET} and V_{me} evolutions as a function of modified (AC-NA, AC-Am, AC-HT) and AC-NM (Biniak et al., 2013), (c) EDL drawings representing solvated ions within different negatively charged pore sizes in carbon material: higher than 2 nm (A), between 1 and 2 nm (B) and smaller than 1 nm (Chmiola et al., 2006), (d) Schematic diagrams of a positively charged porous carbon material and the associated model of the EDL: sandwich-type model for micropores, electric double-cylinder model for mesopores, planar model for macropores (Huang et al., 2008; Feng et al., 2010; Dai et al., 2020). 33
Fig. 9. (a) Electrical conductivity of rGO, prGO and prGO/SWCNT materials (b) Surface wettability of rGO, prGO and prGO/SWCNT materials (Yue et al., 2019b). 34
Fig. 10. (a) Occurrence percentages of electrode polarity configurations tested for electrosorption in the literature, (b) effect of the working electrode potential on AO7 electrosorption (Han et al., 2008). 38
Fig. 11. Effect of (a) the initial concentration of the electrolyte on aniline electrosorption in the Na_2SO_4 electrolyte (Han et al., 2006a), (b) pH on the aniline electrosorption (Han et al., 2006a) (c) temperature on the phenol electrosorption (Han et al., 2006b). 39
Fig. 12. (a) Type of effluent studied in the literature, i.e., artificial or real contamination and the presence of either aromatic or aliphatic compounds during electrosorption processes, (b) effect of acid red 88, orange II, and MB co-sorption (Sun et al., 2016), (c) schematic representation of MB

molecule orientation on the prGO/SWCNT surface (Yue et al., 2019), (d) influence of the initial concentration on MB electrosorption (Nainamalai et al., 2018), (e) overscreening versus crowding models of EDL in the presence of concentrated electrolyte (e.g., ionic liquids) (Bazant et al., 2011), (f) impact of the flow rate on 2,4-dichlorophenoxyacetic acid electrosorption (Bayram et al., 2018). 45
Fig. 13. Occurrence frequency of different electrosorption reactor designs found in the literature. 47
Fig. 14. Scheme of the main electrosorption reactor designs applied in the literature: STR (a), flow-by (b) and flow-through (c) parallel-plate cells, fixed-bed reactor (d, e) and fluidized-bed reactor (f, g) arranged in co-current (d, f) and counter-current (e, g) configurations. 50
Fig. 15. General overview of the main parameters and phenomena involved in the electrosorption efficiency associated with a modeling approach. 61
Fig. 16. Images of modern (a) and traditional (b) oil mills, OMWW (c) and olive pomace (d)... 80
Fig. 17. Schematic representation of the SA-AC beads preparation. 82
Fig. 18. Fixed-bed adsorption setup. 84
Fig. 19. Fixed-bed electrosorption image setup. 91
Fig. 20. Fixed-bed electrosorption schematic setup. 92
Fig. 21. Scheme of the fixed-bed electrosorption setup. 93
Fig. 22. An exploded view of the parallel-plate electrochemical reactor. A: anode in BDD, B: spacer, C: cathode in stainless steel. 95
Fig. 23. Chromatographic spectrum (HPLC) of the used OMWW. 103
Fig. 24. FTIR spectra of AC (a), SA-AC beads before (b) and after (c) adsorption. 104
Fig. 25. SEM of AC (a) and SA-AC beads (b). 105
Fig. 26. EDS spectra of AC (a) and SA-AC beads (b). 106
Fig. 27. Effect of contact time (a) on PCs removal by SA-AC beads (Conditions: 5 g of the adsorbent, 4000 mg L^{-1} of PCs, 540 min contact time under optimum conditions of other variables), Adsorption isotherm (b): (c) Langmuir and (d) Freundlich (PCs concentration, 20 – 4000 mg L^{-1}; volume of OMWW, 5 mL; temperature, 19°C; pH = 4.0; and contact time, 24 h). 110
Fig. 28. Adsorption kinetics: pseudo-first-order (a) and pseudo-second-order (b) kinetic models of PCs adsorption onto SA-AC beads. 113
Fig. 29. Variation of the adsorption capacity of beads with pH (at 19 °C; adsorbent = 5 g; C_0 = 4,000 mg L^{-1}) (a) *Kc* as function of *1/T* (R^2 = 0.959) (b). 115

Fig. 30. Experimental and predicted breakthrough curves for PCs adsorption onto the SA-AC beads. 117
Fig. 31. Chromatograms(HPLC) of OMWW before (a) and after (b) treatment. 119
Fig. 32. Electrochemical properties of the prepared SA-AC beads electrode using CV (a), LSV (b) and EIS (c). 133
Fig. 33. Scheme of the EEC model integrated into the 3D porous electrodes. 134
Fig. 34. Effect of the presence of iron (100 % w/v) or calcium (100% w/v) in the beads preparation: on the electrosorption efficiency of phenol (a) and on electrode conductivity estimated from the Nyquist plot (b). Operating conditions: anode: graphite rod, cathode: graphite rod and 35 g SA-1% w/v AC beads, cathode potential: -1.2 V/(Ag/AgCl), electrolyte: 6 g L^{-1} KCl, pH 4 and 4 g L^{-1} phenol, flow rate: 10 mL min^{-1}, m/V = 0.35 g mL^{-1}. 136
Fig. 35. Effect of AC percentage (% w/v) on: the evolution of electrosorption capacity of phenol (a), the mass transport (b) and internal ohmic resistance (c). Operating conditions: anode: graphite rod, cathode: graphite rod and 35 g SA (100% w/v Fe)-AC beads, cathode potential: -1.2 V/(Ag/AgCl), electrolyte: 6 g L^{-1} KCl, pH 4 and 4 g L^{-1} phenol, flow rate: 10 mL min^{-1}, m/V = 0.35 g mL^{-1}. 138
Fig. 36. Mechanism of phenol electrosorption in SA-AC beads with increasing AC content. 140
Fig. 37. Effect of E_{cat} (V/(Ag/AgCl)) considering the contact time (a) and the specific charge (b) on the electrosorption of phenol. Operating conditions: anode: graphite rod, cathode: graphite rod and 35 g SA (100% w/v Fe)-1% w/v AC beads, electrolyte: 6 g L^{-1} KCl, pH 4 and 4 g L^{-1} phenol, flow rate: 10 mL min^{-1}, m/V = 0.35 g mL^{-1}. 142
Fig. 38. Effect of contact time on the electrosorption of PCs from real OMWW at optimal operating conditions. Operating conditions: anode: graphite rod, cathode: graphite rod and 35 g SA (100% w/v Fe)-1% w/v AC beads, cathode potential: -1.1 V/(Ag/AgCl), flow rate: 10 mL min^{-1}, m/V ratio = 0.35 g mL^{-1} 144
Fig. 39. Experimental (symbol) versus theoretical correlations (continuous line) as a function of $t^{1/2}$ in simulated OMWW as function of AC content (a) and of PCs in real OMWW (b), effect of the percentage of AC on the diffusion coefficient (c). 146
Fig. 40. Effect of the mass ratio of activator / precursor on the adsorption of phenol in batch. Phenol concentration = 4,000 mg L^{-1}, pH = 4, stirring = 200 rpm^{-1}. 156
Fig. 41. FTIR spectra of GAC. 157
Fig. 42. SEM spectra of GAC at different magnification. 158

Fig. 43. Effect of the initial concentration on the adsorption of PCs (a), adsorption isotherm: (b) Langmuir and (c) Freundlich. Initial concentration, 20-4,000 mg L^{-1}; volume of OMWW, 5 mL; temperature, 19°C; pH=4; and contact time, 24h. 160
Fig. 44. Effect of the contact time on the adsorption of PCs (a), kinetic adsorption models: pseudo-first-order (b) and pseudo-second-order (c). Initial concentration, 4,000 mg L^{-1}; volume of OMWW, 5 mL; temperature, 19°C; pH=4; and contact time, 480 min). 162
Fig. 45. Variation of the adsorption capacity of GAC with pH (at 19 °C; adsorbent = 5 g; C_0 = 4,000 mg L^{-1}). 163
Fig. 46. Plot of $Ln(K_c)$ as a function of $1/T$ (R^2 = 0.97). 164
Fig. 47. Effects of operating parameters on breakthrough curves: (a) effect of flowrate and (b) effect of bed height. 166
Fig. 48. Effects of different solvents on PCs desorption efficiency. 168
Fig. 49. Fraction of desorbed PCs from GAC by HCl (0.05 M). 169
Fig. 50. SEM images: (a) GAC before conditioning, (b) GAC after conditioning. 177
Fig. 51. Electrosorption of phenol into GAC before conditioning and GAC after conditioning.Operating conditions: anode: platinum wire, cathode: graphite rod and 10 g of GAC, electrolyte: 6 g L^{-1} KCl, pH 4 and 4 g L^{-1} phenol, flow rate: 10 mL min^{-1}, m/V = 0.1 g mL^{-1} 179
Fig. 52. Electrochemical properties of GAC electrode using CV (a), LSV (b) and EIS (c). 181
Fig. 53. Scheme of the EEC model integrated into the GAC porous electrodes. 182
Fig. 54. Effect of the current intensity considering the contact time (a) and the specific charge (b) on the electrosorption of phenol. Operating conditions: cathode: platinum wire, anode: graphite rod and 10 g of GAC, electrolyte: 6 g L^{-1} KCl, pH 4 and 4 g L^{-1} phenol, flow rate: 10 mL min^{-1}, m/V = 0.1 g mL^{-1}. 183
Fig. 55. Effect of the current intensity considering the contact time (a) and the specific charge (b) on the electrosorption of phenol. Operating conditions: anode: platinum wire, cathode: graphite rod and 10 g of GAC, electrolyte: 6 g L^{-1} KCl, pH 4 and 4 g L^{-1} phenol, flow rate: 10 mL min^{-1}, m/V = 0.1 g mL^{-1}. 185
Fig. 56. SEM images conditioned GAC cathode after 8 h of electrosorption at 1 mA. 186
Fig. 57. Effect of the kinds of PCs on the electrosorption at cathode. Operating conditions: anode: platinum wire, cathode: graphite rod and 10 g of GAC, electrolyte: 6 g L^{-1} KCl, pH 4 and PC, current intensity: 1 mA, flow rate: 10 mL min^{-1}, m/V = 0.1 g mL^{-1}. 188

Fig. 58. Effect of the current intensity considering the contact time (a) the specific charge (b) on the electrosorption of PCs from real OMWW and internal resistance (c) at optimal operating conditions. Operating conditions: anode: platinum wire, cathode: graphite rod and 10 g of GAC, flow rate: 10 mL min^{-1}, m/V = 0.1 g mL^{-1}. 190
Fig. 59. Effect of the current intensity on the electro-desorption of PCs from GAC. Operating conditions: cathode: platinum wire, anode: graphite rod and 10 g of GAC, electrolyte: 0.1 g L^{-1} KCl, flow rate: 10 mL min^{-1}, m/V = 0.1 g mL^{-1}. 192
Fig. 60. Pictures about three successive electro-desorption cycles of PCs from GAC electrode. 193
Fig. 61. Scaling on BDD anode after electrooxidation experiments of OMWW. 195

List of Tables

Table 1. Main studies performed on the electrosorption of organic compounds reviewed in the literature. 21
Table 2. Optimal initial solution pH during the electrosorption of selected pollutants. 41
Table 3. Advantages and drawbacks of the different types of reactor designs implemented for the electrosorption of organic compounds. 51
Table 4. Successive electrosorption cycle studies with organic compounds reported in the literature. 54
Table 5. Main dimensionless numbers involved in the literature about the electrosorption. 58
Table 6. Summary of the main emerging processes combinations with electrosorption applied in treatment of organic pollutants. 63
Table 7. Standard methods for determining physicochemical parameters. 81
Table 8. Physicochemical parameters of the OMWW. 102
Table 9. Textural characteristics for AC and SA-AC beads. 107
Table 10. Isotherm parameters of PCs adsorption onto the SA-AC beads (Conditions: 5 g of the adsorbent, 20 – 4,000 mg L^{-1} of PCs, pH = 4, contact time 24 h). 108
Table 11. Kinetic parameters of PCs adsorption onto SA-AC beads (Conditions: 5 g of the adsorbent, 4,000 mg $L^{-1}$of PCs, 540 min contact time under optimum conditions of other variables). 112
Table 12. Thermodynamic parameters of the adsorption process of PCs on beads at various temperatures. 115
Table 13. Parameters of breakthrough curves of the packed bed column for PCs adsorption onto the SA-AC beads. 118
Table 14. Physicochemical parameters of the OMWW before and after adsorption. 120
Table 15. Parameters of Yoon-Nelson and Thomas models for the adsorption of PCs by SA-AC in a fixed-bed column. 121
Table 16. Physicochemical parameters of OMWW. 155
Table 17. EDS of GAC. 159
Table 18. Isotherm parameters of PCs adsorption onto the GAC (Conditions: 5 g of the adsorbent, 20-5,000 mg $L^{-1}$of PCs, pH=4, contact time 24h). 160
Table 19. Kinetic parameters of PCs adsorption onto GAC (Conditions: 5 g of the adsorbent, 4,000 mg L^{-1} of PCs, 480 min contact time under optimum conditions of other variables). 162

Table 20. Thermodynamic parameters of the adsorption process of PCs on GAC at various temperatures. 164
Table 21. Thomas model parameters for PCs adsorption into GAC in a fixed-bed column at different conditions using linear regression analysis. 167
Table 22. Yoon–Nelson model parameters for PCs adsorption into GAC in a fixed-bed column at different conditions using linear regression analysis. 167
Table 23. EDS of GAC before and after conditioning. 178
Table 24. EDS of conditioned GAC cathode after electrosorption at 1 mA for 8 h. 186
Table 25. OMWW characterization before and after electrochemical degradation. 195

List of abbreviations and symbols

Abbreviation	Definition
3D	three-dimensional
AC	activated carbon
AC-Am	ammonia-treated
ACC	activated carbon cloth
ACCO	oxidized activated carbon cloth
ACE	activated carbon electrode
ACF	activated carbon fibers
AC-HT	annealed activated carbon
AC-NA	nitric acid oxidized activated carbon
AC-NM	non-modified activated carbon
AO7	acid orange 7
AO8	acid orange 8
AR151	acid red 151
AY14	acid yellow 14
BA	benzoic acid
CB-W	carbon black
CFP	carbon fiber paper
CNT-c	multiwalled carbon nanotubes - short carboxyl
CNT-h	multiwalled carbon nanotubes - short hydroxyl
CNTs	carbon nanotubes
COD	chemical oxygen demand
CV	cyclic voltammetry
DFT	density functional theory
EDL	electric double layer
EEC	equivalent electrical circuit
EIS	electrochemical impedance spectroscopy
GAC	granular activated carbon
IHP	inner Helmholtz plane
KKT	Kramers-Kronig transform
LSV	linear sweep voltammetry
MAE	mean absolute error
MB	methylene blue
MSE	mercury/mercurous sulfate electrode
MW	molar weight
MWCNTs	multiwalled carbon nanotubes
NA	nicotinic acid
NHE	normal hydrogen electrode
NMO	$Na_{0.7}MnO_2$
OC	open circuit
OMWW	olive mill wastewater
OHP	outer Helmholtz plane
PCs	phenolic compounds
PrGO	porous reduced graphene oxide
RE	regeneration efficiency
Rga	reduced graphene oxide aerogel
rGA-Cu	Cu nanoparticles loaded rGA
rGA-F	F-doped rGA
rGA-F/Cu	F and Cu nanoparticles modified rGA

Rgo	reduced graphene oxide
RHE	reversible hydrogen electrode
RMSE	root-mean-square error
SCE	saturated calomel electrode
SEM	scanning electron microscopy
STR	stirred tank reactor
SWCNTs	single-walled carbon nanotubes

Symbol	Definition
$\%R$	total PCs removal efficiency (%)
C_{in}	targeted compound concentration in the inlet flow
C_{out}	targeted compound concentration in the outlet flow
d_p	particle diameter
q_A	electrosorption capacity
q_D	electrodesorption capacity
y_i	model value
y_i'	experimental value
A	cross-sectional area
a	interfacial area per unit void volume
a_0	effective radius of the counterions
Bi_m	mass transfer Biot number
C	differential capacitance
C_0	initial concentration of the pollutant
C_{DL}	specific double layer capacitance
C_e	equilibrium concentration of the pollutant
C_{GAC}	internal capacitance of GAC
C_R	concentration of PCs removal (mg L^{-1})
C_{st}	sandwich-type capacitance for micropores
D	diffusion coefficient of the targeted compound
d	electrode thickness
D_e	effective diffusivity
d_{eff}	effective separation between the electrode surface and the counterions
E_{an}	anode potential
E_{cat}	cathode potential
G	dimensionless time constant representing competition between electrical potential wave and sorption wave
H	bed height
I_0	exchange current intensity
J	current density
K	number of iterated values
k_1	pseudo-first-order rate constants
k_2	pseudo-second-order rate constants
K_c	thermodynamic distribution coefficient
k_f	external mass transfer coefficient
K_f	Freundlich constant that presents the adsorption capacity of the adsorbent
K_L	Langmuir constant related to the energy of adsorption (L g^{-1})
k_{TH}	Thomas rate constant, (mL min^{-1} mg^{-1})
k_{YN}	rate constant that is related to the diffusion characteristics of the mass transfer zone (min^{-1}).
L	characteristic length
L_0	distance between two parallel electrodes having the same polarity
M	mass of the working electrode

M	total amount of PCs sent to the column (g)
m_{total}	amount of PCs sent to the column (g)
N	constant that presents the greatness of the relationship between PCs and SA-AC beads or GAC.
q_e	amounts of PCs adsorption onto SA-AC beads or GAC at equilibrium
$q_{e(calc)}$	Values of amounts using the pseudo-second-order kinetic model experimental
$q_{e(exp)}$	Values of amounts using the experimental data
q_m	maximum PCs adsorption capacity (mg g^{-1})
q_t	amounts of PCs adsorption onto SA-AC beads or GAC time *t*
q_{total}	total mass of PCs adsorbed
Q_V	inlet flow rate
R_1	outer radii of the cylinder
R_2	inner radii of the cylinder
R_{CT}	charge transfer resistance
Re	Reynolds number
R_f	faradaic resistance of the electrochemical reaction
R_{GAC}	internal resistance of GAC
R_s	difference in the resistance of the solution between two points of interest in the system
R_{Sol}	resistance of the bulk electrolyte
S_{BET}	specific surface area estimated by the Brunauer-Emmett-Teller method
Sc	Schmidt number
Sh	Sherwood number
Sr	scan rate
T	dimensionless time
T	reaction time
t_{dl}	double layer charging time
t_{sc}	scan time
t_{st}	stoichiometric time of sorption
t_{t0}	turnover time
t_{total}	total time (min)
U	linear velocity of the liquid through the void space of the adsorbent
V	volume of solution
V_{ef}	volume of the effluent
V_{me}	volume of mesopore
W	bed width
Wa	Wagner number

Greek letters

δ_a	diffusion layer thickness at anode
δ_c	diffusion layer thickness at cathode
ΔE	potential difference
ΔG	Gibbs free energy of adsorption
ΔH	enthalpy of adsorption
ΔS	entropy of adsorption
ε_B	bed porosity
η	Overpotential
K	effective electrolyte conductivity
τ	time required for 50% adsorbate breakthrough
ν	kinematic viscosity of the solution
ρ_B	bed density
σ	electrical conductivity of the porous material
χ^2	chi-squared residue

General Introduction

Water is an essential element for the life existence. Its role is fundamental for the economic development of human civilization, given its use in many sectors, including industry and agriculture. However, this vital resource is well known for being easily contaminated. Hence, there is the need to improve effective means for its protection against pollution.

In recent decades, the increasing industrial expansion and domestic activities haveproduced significant volumes of wastewater containing undesirable toxic contaminants (e.g., fine suspended solids, metals, dissolved organic and inorganic compounds, and other impurities). Water pollution is therefore becoming a serious concern in the environmental field (Crini et al., 2019; Crini & Lichtfouse, 2019; Bagheri et al., 2020; Li et al., 2020), and the demand for freshwater represents one of the most critical global challenges of the 21st century (Zhang et al., 2018). The United Nations Educational, Scientific and Cultural Organization (UNESCO) approximates that nearly over two billion people live in countries experiencing high water stress, which tends to be globalized (UNESCO, 2019). In addition, numerous studies of industrial wastewater treatment have been reported among the olive mill wastewater (OMWW) effluents, which is a liquid effluent generated during olive oil extraction (Al-Bsoul et al., 2020; Amine et al., 2020; Enaime et al., 2020; Ntaikou et al., 2020; Haddad et al., 2021; Soria & Madeira, 2021). More than 30×10^6 m^3 of OMWW are produced annually by Mediterranean countries (Al-Bsoul et al., 2020). OMWW is an environmentally critical effluent due to its high complexity and its wide variety of pollutants (Amine et al., 2020). Additionally, their acidic pH, high electrical conductivity, high concentration of total solids, high chemical oxygen demand (COD 60-185 g L^{-1}), low ratio of biochemical oxygen demand after 5 days (BOD_5) over COD (0.23-0.40) and high polyphenols content (up to 8 g L^{-1}) could noticeably affect the soil and underground water quality (Achak, 2008; Al-Bsoul et al., 2020; Haddad et al., 2021; Soria & Madeira, 2021). In particular, phenolic compounds (PCs) create a major environmental issue in the main olive-producing countries due to the significant alteration of microbial activities in the water and soil ecosystems (Haddad et al., 2021). However, the PCs also represent added-value molecules that could be recovered for subsequent valorization in the pharmaceutical, cosmetic and food industries (Annab et al., 2019). They have strong antioxidant, anti-inflammatory and antimicrobial properties, and several good health effects have been attributed to consuming food rich in polyphenols (Annab et al., 2019). Thus, there is the need to propose combined

technologies that are able to recover these compounds from the wastewater while eliminating the remaining organic compounds in solution (Kilic et al., 2019; El Ghadraoui et al., 2020; Elmansour et al., 2020).

Many processes have recently been investigated to recover PCs from OMWW, such as physical, thermal, physicochemical and biological technologies (Rahmanian et al., 2013). Azzam and Hazaimeh (2021) used liquid-liquid extraction to recover PCs from OMWW using ethyl acetate as a solvent. Zagklis et al. (2015) used resin adsorption/desorption to recover hydroxytyrosol from OMWW and Achak et al. (2009) used adsorption followed by desorption for the recovery of total PCs from OMWW using banana peel as a biosorbent. Among these processes, adsorption is the most widely used and effective technique to separate organic pollutants from wastewater (Sun et al., 2019). In recent years, many adsorbents, such as activated carbons (AC), have been used to eliminate PCs (Annab et al., 2019). AC is commonly used because of its microporous texture, high surface reactivity, consistency in pore size distribution, a wide spectrum of functional surface groups, and thermal steadiness (Baçaoui et al., 1998; Baçaoui et al., 2001; Shim et al., 2019). Moreover, electrosorption offers several advantages compared to adsorption, such as high removal efficiency (i.e., a high adsorption capacity), fast adsorption kinetics, and the possibility to control the selectivity and the sorption/desorption steps (Han et al., 2006a; Rong & Xien, 2009; Gao et al., 2017). It is particularly suitable for removing charged and/or polar pollutants by polarizing high surface area electrodes at a given electric current or potential (Bayram et al., 2018; Nainamalai et al., 2018). Furthermore, the hypersaline characteristic of OMWW makes those effluents good candidates for electrochemical processes by avoiding high internal ohmic resistance. Nevertheless, the lack of experimental data obtained with real effluents is a handicap for validating adsorption models and improving system performance. This is also necessary for a thorough understanding of the interactions at the sorbent/solution interface. Moreover, the experimental data, as well as their adequate interpretation, are required for the synthesis of new and better performing bio-sourced materials.

In this context, the main objective of this thesis is to propose an integrated approach of waste management of the olive industry, valorizing their solid waste in the treatment of their liquid waste, as presented in Fig. 1.

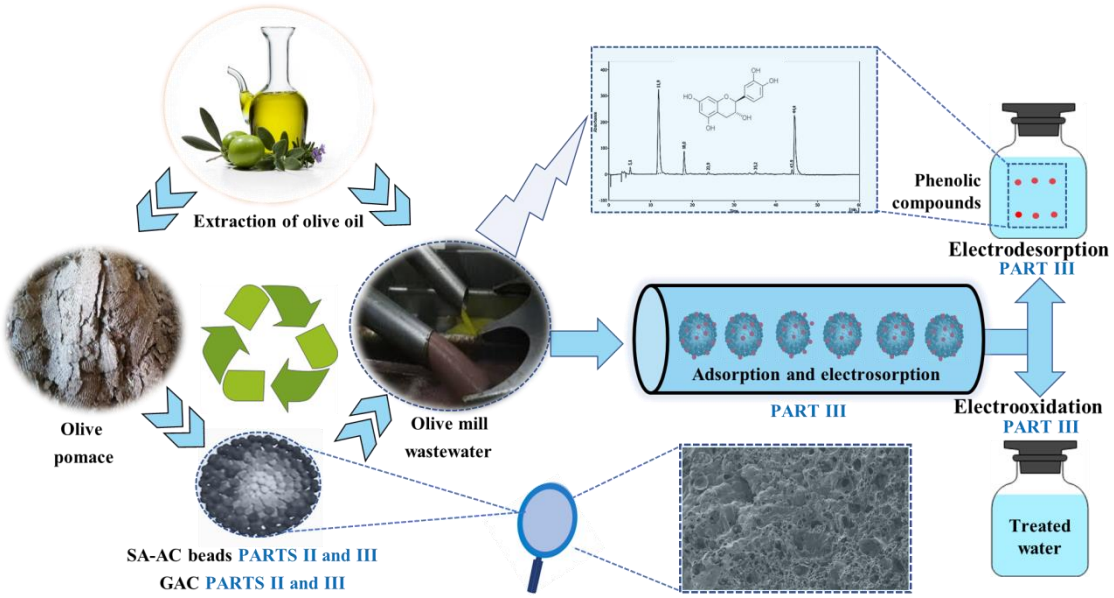

Fig. 1. The innovative integrated approach of the thesis.

The olive pomace waste generated during the olive oil production process is reused as bio-adsorbent (i.e., powdered AC within composite alginate beads or granular AC (GAC)) in either adsorption or electrosorption for PCs recovery from OMWW. The remaining organic compounds in OMWW are then proposed to be eliminated by advanced electrooxidation treatment, while the adsorbent is regenerated by chemical or electrochemical methods. A systematic approach has been adopted by increasing the degree of complexity of the effluent until studies with real OMWW. Emphasis improves the knowledge of adsorption and electrosorption mechanisms of PCs removal from OMWW, through the proposition of new models compared with consistent experimental data. Particular attention has been given to the influence of mass transport and PCs physico-chemical properties on the efficiency of adsorption and electrosorption. These considerations have been taken into account in the models for a better prediction of the system evolution as a function of time. This research work has been performed in the framework of a cotutelle agreement between Cadi Ayyad University and Lorraine University, under the Partenariat Hubert Curien (PHC) Toubkal/19/84 project (Campus France: 41525VG). The formulation of the adsorbents as well as adsorption and desorption tests were carried out in Morocco (National Center for Research and Studies on Water and Energy (CNEREE) and Laboratory of Water, Biodiversity, and Climate Change, Faculty of Sciences Semlalia), while the 3D electrode conception along with electrosorption, electro-desorption and electro-oxidation experiments were performed in France (Laboratoire Réactions et Génie des Procédés (LRGP)).

The structure of the thesis is illustrated in Fig. 1, and the related content of each part is summarized herein after:

- The first part includes a state-of-the-art section about both adsorption and electrosorption. It begins by exposing the background and principles of adsorption and electrosorption technologies. The influence of parameters, such as electrode materials, current density, physico-chemistry of electrolytes and reactor design, is then addressed. Next, identifying of the main influencing factors combined with electrosorption modeling allows the design strategies for implementing porous electrodes to be defined. Finally, future directions for electrosorption processes are presented, which bring new opportunities for their optimization and future development as proposed in this thesis.

- The second part offers a description of the experimental approach. It starts with the location of OMWW used and the different techniques employed to determine the physicochemical properties of OMWW. Then, the preparation of the adsorbents and porous electrodes based on olive pomace has been described, along with their physicochemical and electrochemical characterization. Finally, an overview of the experimental setup of adsorption and electrosorption of PCs was made, along with the different analytical techniques for effluent characterization.

- The third part is about the results and discussion. It is divided into two chapters:

  - The first chapter is devoted to composite beads experiments and is divided into two sub-chapters:

    - The first sub-chapter presents a study about the PCs adsorption onto composite beads. The olive pomace is first converted into a highly porous AC and then a composite bead using alginate (SA-AC beads). It can be subsequently used for the treatment of OMWW by adsorption. The kinetics, mechanism and adsorption characteristics of PCs adsorption were investigated. The experiments were carried out under different operational conditions (time, concentration, pH, temperature) to determine the adsorbent behavior in stirred batch and fixed-bed reactors. PCs recovery and the process reusability of SA-AC beads were carried out in fixed-bed reactors.

    - The second sub-chapter is devoted to the PCs electrosorption with SA-AC beads as a three-dimensional (3D) electrode. Novel theoretical models are proposed to

predict the kinetic evolution of electrosorption of organic compounds in simulated and real effluents, considering the mass transport and difference of acid dissociation constants (pKa) of the PCs.

- The second chapter exposes the results obtained with GAC and is splitted into two sub-chapters:
  - The first sub-chapter deals with a study on the PCs adsorption onto GACs in batch and continuous column setup. Several parameters are investigated such as the kinetics of equilibrium, the effect of pH, and the initial concentration on adsorption efficiency. The effects of bed depth and flow rate on PCs removal from real OMWW are also studied.
  - The second sub-chapter depicts a study on the PCs electrosorption with GAC packed-bed electrodes. The electrosorption efficiency of multiple PCs in synthetic and actual OMWW is first studied. The electrochemical regeneration of the GAC electrodes, as well as the electrochemical degradation of OMWW, is then carried out.

References

Achak, M., Hafidi, A., Ouazzani, N., Sayadi, S., Mandi, L., 2009. Low cost biosorbent "banana peel" for the removal of phenolic compounds from olive mill wastewater: Kinetic and equilibrium studies. J. Hazard. Mater. 166, 117–125. https://doi.org/10.1016/j.jhazmat.2008.11.036

Achak, M., Ouazzani, N., Yaacoubi, A., & Mandi, L., 2008. Caractérisation des margines issues d'une huilerie moderne et essais de leur traitement par coagulation-floculation par la chaux et le sulfate d'aluminium. Revue des sciences de l'eau/Journal of Water Science, 21(1), 53-67.

Al-Bsoul, A., Al-shannag, M., Tawalbeh, M., Al-taani, A.A., Lafi, W.K., Al-othman, A., Alsheyab, M., 2020. Optimal conditions for olive mill wastewater treatment using ultrasound and advanced oxidation processes. Sci. Total Environ. 700, 134576. https://doi.org/10.1016/j.scitotenv.2019.134576

Amine, A., Jeguirim, M., Kinigopoulou, V., Doulgeris, C., Goddard, M., Jellali, S., Matei, C., 2020. Olive mill wastewater: From a pollutant to green fuels , agricultural and water source and bio-fertilizer – Hydrothermal carbonization. Sci. Total Environ. 733, 139314. https://doi.org/10.1016/j.scitotenv.2020.139314

Annab, H., Fiol, N., Villaescusa, I., Essamri, A., 2019. Journal of Environmental Chemical Engineering A proposal for the sustainable treatment and valorisation of olive mill wastes. J. Environ. Chem. Eng. 7, 102803. https://doi.org/10.1016/j.jece.2018.11.047

Baçaoui, A., Yaacoubi, A., Dahbi, A., Bennouna, C., Luu, R. P. T., Maldonado-Hodar, F. Rivera-Utrilla J., J., Moreno-Castilla, C., 2001. Optimization of conditions for the preparation of activated carbons from olive-waste cakes. Carbon, 39(3), 425-432.

Baçaoui, A., Yaacoubi, A., Dahbi, A., Bennouna, C., Ayele, J., & Mazet, M., 1998. Activated Carbon Production from Moroccan Olive Wastes - Influence of Some Factors. Environmental Technology, 19(12), 1203–1212.

Bagheri, H., Fakhri, H., Ghahremani, R., Karimi, M., Madrakian, T., Afkhami, A., 2020. Nanomaterial-based adsorbents for wastewater treatment, Smart nanocontainers. Elsevier Inc. https://doi.org/10.1016/b978-0-12-816770-0.00028-9

Bayram, E., Kizil, Ç., Ayranci, E., 2018. Flow-through electrosorption process for removal of 2,4-D pesticide from aqueous solutions onto activated carbon cloth fixed-bed electrodes. Water Sci. Technol. 77, 848–854. https://doi.org/10.2166/wst.2017.598

Crini, G., Lichtfouse, E., 2019. Advantages and disadvantages of techniques used for wastewater treatment. Environ. Chem. Lett. 17, 145–155. https://doi.org/10.1007/s10311-018-0785-9

Crini, G., Lichtfouse, E., Wilson, L.D., Morin-Crini, N., 2019. Conventional and non-conventional adsorbents for wastewater treatment. Environ. Chem. Lett. 17, 195–213. https://doi.org/10.1007/s10311-018-0786-8

El Ghadraoui, A., Ouazzani, N., Ahmali, A., El Mansour, T.E.H., Aziz, F., Hejjaj, A., Del Bubba, M., Mandi, L., 2020. Treatment of olive mill and municipal wastewater mixture by pilot scale vertical flow constructed wetland. Desalin. Water Treat. 198, 126–139. https://doi.org/10.5004/dwt.2020.26009

Elmansour, T.E., Mandi, L., Ahmali, A., Elghadraoui, A., Aziz, F., Hejjaj, A., Del Bubba, M., Ouazzani, N., 2020. Effect of polyphenols on activated sludge biomass during the treatment of highly diluted olive mill wastewaters: biomass dynamics and purifying performances. Water Sci. Technol. 82, 1416–1429. https://doi.org/10.2166/wst.2020.423

Enaime, G., Baçaoui, A., Yaacoubi, A., Belaqziz, M., Wichern, M., & Lübken, M. (2020). Phytotoxicity assessment of olive mill wastewater treated by different technologies: effect

on seed germination of maize and tomato. Environmental Science and Pollution Research. doi:10.1007/s11356-019-06672-z

Gao, T., Li, H., Zhou, F., Gao, M., Liang, S., Luo, M., 2017. Mesoporous carbon derived from ZIF-8 for high efficient electrosorption. Desalination 451, 133–138. https://doi.org/10.1016/j.desal.2017.06.021

Haddad, K., Jeguirim, M., Jellali, S., Thevenin, N., Ruidavets, L., Limousy, L., 2021. Biochar production from Cypress sawdust and olive mill wastewater: Agronomic approach. Sci. Total Environ. 752, 141713. https://doi.org/10.1016/j.scitotenv.2020.141713

Han, Y., Quan, X., Chen, S., Zhao, H., Cui, C., Zhao, Y., 2006. Electrochemically enhanced adsorption of aniline on activated carbon fibers. Sep. Purif. Technol. 50, 365–372. https://doi.org/10.1016/j.seppur.2005.12.011

Kilic, M.Y., Abdelraheem, W.H., He, X., Kestioglu, K., Dionysiou, D.D., 2019. Photochemical treatment of tyrosol, a model phenolic compound present in olive mill wastewater, by hydroxyl and sulfate radical-based advanced oxidation processes (AOPs). J. Hazard. Mater. 367, 734–742. https://doi.org/10.1016/j.jhazmat.2018.06.062

Li, Z., Shen, C., Liu, Y., Ma, C., Li, F., Yang, B., Huang, M., Wang, Z., Dong, L., Wolfgang, S., 2020. Carbon nanotube filter functionalized with iron oxychloride for flow-through electro-Fenton. Appl. Catal. B Environ. 260, 118204. https://doi.org/10.1016/j.apcatb.2019.118204

Nainamalai, M., Palani, M., Soundarajan, B., Allwin, A.E., 2018. Decolorization of synthetic dye wastewater using packed bed electro-adsorption column. Chem. Eng. Process. - Process Intensif. 130, 160–168. https://doi.org/10.1016/j.cep.2018.06.013

Ntaikou, I., Antonopoulou, G., Vayenas, D., Lyberatos, G., 2020. Assessment of electrocoagulation as a pretreatment method of olive mill wastewater towards alternative processes for biofuels production. Renew. energy 154, 1252–1262. https://doi.org/10.1016/j.renene.2020.03.108

Rong, C., Xien, H., 2009. Reversible electrosorption of thiocyanate anions by active carbon felt. Sep. Sci. Technol. 44, 3984–3999. https://doi.org/10.1080/01496390903182453

Shim, J., Kumar, M., Goswami, R., Mazumder, P., Oh, B.T., Shea, P.J., 2019. Removal of p-cresol and tylosin from water using a novel composite of alginate, recycled MnO2 and activated carbon. J. Hazard. Mater. 364, 419–428. https://doi.org/10.1016/j.jhazmat.2018.09.065

Soria, M.A., Madeira, L.M., 2021. Screening of commercial catalysts for steam reforming of olive mill wastewater. Renew. energy 169, 765-779. https://doi.org/10.1016/j.renene.2020.12.139

Sun, J., Liu, X., Zhang, F., Zhou, J., Wu, J., Alsaedi, A., Hayat, T., Li, J., 2019. Insight into the mechanism of adsorption of phenol and resorcinol on activated carbons with different oxidation degrees. Colloids Surfaces A Physicochem. Eng. Asp. 563, 22–30. https://doi.org/10.1016/j.colsurfa.2018.11.042

UNESCO, 2019. The United Nations world water development report 2019: leaving no one behind. UN Educ. Sci. Cult. Organ.

Zagklis, D.P., Vavouraki, A.I., Kornaros, M.E., Paraskeva, C.A., 2015. Purification of olive mill wastewater phenols through membrane filtration and resin adsorption/desorption. J. Hazard. Mater. 285, 69–76. https://doi.org/10.1016/j.jhazmat.2014.11.038

Zhang, C., He, D., Ma, J., Tang, W., Waite, T.D., 2018. Faradaic reactions in capacitive deionization (CDI) - Problems and possibilities: A review 128, 314–330. https://doi.org/10.1016/j.watres.2017.10.024

Part I: Bibliography

1. Adsorption

1.1.Definition and types of adsorption

Adsorption is a well-known surface phenomenon by which molecules of gas or liquids attach themselves to the solid surfaces of adsorbents according to various more or less intense processes (El-Naas & Alhaija, 2013; Zheng et al., 2021). The adsorbed molecules are called adsorbate, and the solid onto which the molecules are adsorbed is generally called adsorbent (Cuong, 2020). Some basic adsorption terms are schematized in Fig. 2 to better understand the technical terms used in the adsorption process (Tran et al., 2017).

Adsorption is a spontaneous phenomenon that occurs as soon as a solid surface comes into contact with a gas or a liquid, based on the difference in affinity of an adsorbent for the constituents of a mixture (Sarkar & Paul, 2016). This results in a difference in adsorbed amounts of the constituents at equilibrium. However, the difference in adsorption rate can also be exploited to separate the constituents of a mixture having similar adsorbed amounts at equilibrium (Feng et al., 2021). The reverse phenomenon by which molecules break off is desorption.

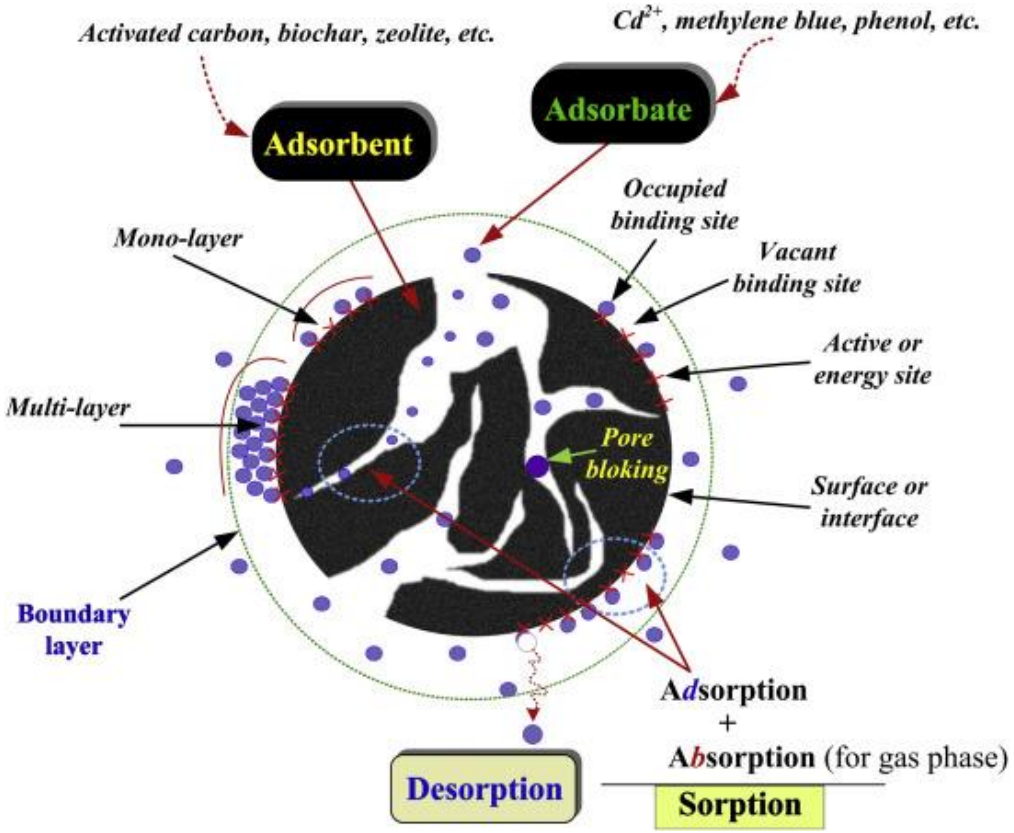

Fig. 2. Some basic terms used in adsorption science and technology (Tran et al., 2017).

The adsorption mechanism of pollutants onto the surface of solids generally occurs through four successive phenomena (Fig. 3) (Peng & Guo, 2020):

- Bulk transport, which corresponds to the transport of contaminants in the solution phase,
- Film transport, which corresponds to the transport of contaminant from the bulk liquid phase to the adsorbent's external surface through a hydrodynamic boundary layer or film,
- Intraparticle transport, which corresponds to the diffusion of the contaminant from the vicinity of the adsorbent into the pores of the adsorbent,
- Adsorption, which corresponds to the attachment of contaminant molecules to the surface of the solid.

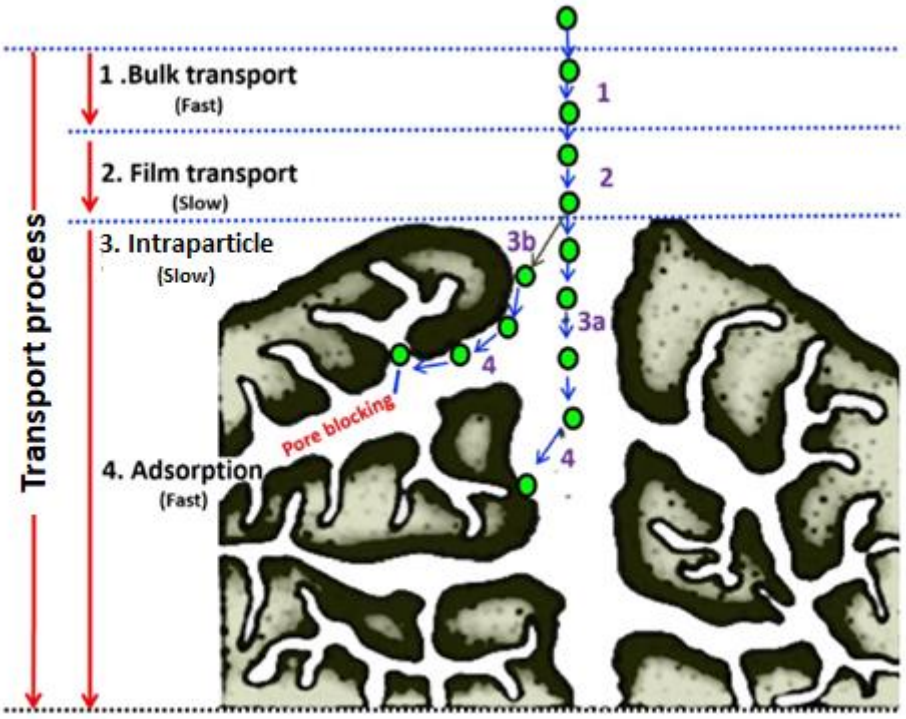

Fig. 3. Schematic representation of the adsorption processes (Peng & Guo, 2020).

The nature of the bonds, as well as the amount of energy, exchanged during the retention of a molecule on the surface of a solid allow distinguishing two types of adsorption (Fig. 4) (Sarkar & Paul, 2016; Cuong, 2020):

- Physical adsorption, also called physisorption, is due to electrostatic forces between the solute and the solid surface; it is characterized by low binding energy (< 40 kJ.mol^{-1}) and corresponds to the establishment of Van der Waals type bonds. As a result, the retention time of the adsorbed substance is short and the adsorbent surface can be covered with multiple molecular layers of the adsorbed product. Furthermore, this adsorption type is reversible and exothermic (Basuki et al., 2019; Cuong, 2020).

- Chemical adsorption, also called chemisorption, involves covalent or hydrogen-like chemical bonds between the adsorbate and the adsorbent molecule; it involves high energy (> 40 kJ mol^{-1}). The retention time is long and only the first layer linked to the adsorbent surface is chemisorbed; if they exist, the additional layers are retained by physisorption. Unlike physical adsorption, chemisorption is irreversible as high energies are involved (Basuki et al., 2019; Cuong, 2020).

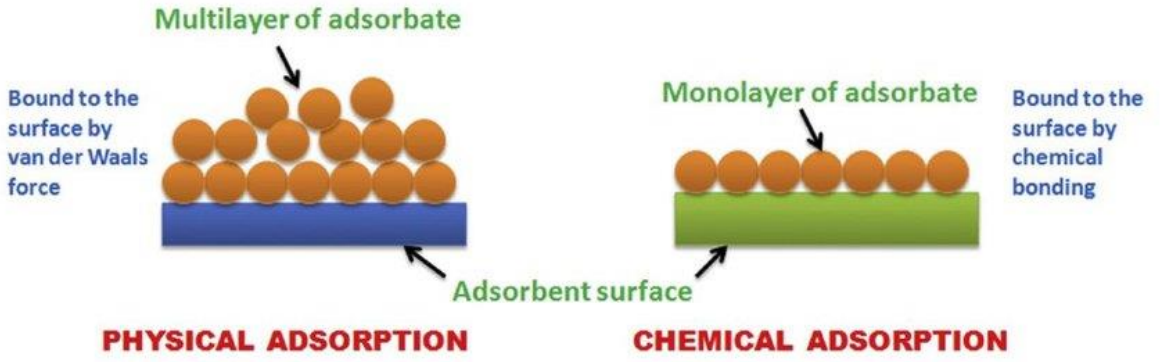

Fig. 4. Schematic representation of the physical adsorption and chemical adsorption (Cuong, 2020).

1.2.Adsorption of organic pollutants

Green approaches have become a trend to solve ongoing aquatic environmental problems in a condition that they fully satisfy the three pillars of sustainability: environmental and social protection as well as economic prosperity (Chkirida et al., 2021).

The reactor design is one of the parameters that can address this issue. A column adsorption device is a practical and simple setup that reduces the costs and energy needed for water treatment by exploiting the concentration gradient between the adsorbent and pollutants. This permits the production of high-quality treated effluents with a minimum pollutant concentration on an ongoing basis (Basu et al., 2019; Aziz et al., 2020). The main advantage of the column setup is that it can handle large volumes of contaminated effluents requiring a very short contact time between the adsorbent and the pollutants (Aziz et al., 2020). Nonetheless, this operation at the real scale requires granular materials of controlled size (Basu et al., 2019; Aziz et al., 2020).

Various bio-sourced and granular materials have been employed for adsorption technologies. Alginate acts as an embedding medium to assist the preparation of easy separating and recycling adsorbents (Xu et al., 2021). Many researchers use beads with alginate coatings on several kinds of adsorbent materials or functionalize them to be more efficient and test the obtained composites to remove organic pollutants in wastewater. Among the composite beads used in the literature, we find amidoxime modified polymers of intrinsic microporosity/alginate composite hydrogel beads for removal of malachite green (Xu et al., 2021), AC-alginate beads for phenol removal (Khan et al., 2021), starch and powdered AC amended alginate-biomass beads for removal of metronidazole and organic matter from

synthetic wastewater (Girijan et al., 2021) as well as alginate/bentonite impregnated TiO_2 beads for removal of methylene blue (Chkirida et al., 2021).

Xu et al. (2021) investigated the amidoxime modified polymers of intrinsic microporosity/alginate composite hydrogel beads to remove malachite green. The adsorption capacity increased with the increase of contact time, temperature and initial concentration of malachite green, and decreased with the increase of the adsorbent dose. Isotherm data were well described by both Freundlich isotherm and Langmuir isotherm models, and pseudo-second-order could fit the adsorption kinetics. The composite beads demonstrated outstanding regeneration properties for malachite green adsorption and they can maintain more than 90% of their original adsorption capacity after ten adsorption/regeneration cycles. Alternatively, Khan et al. (2021) studied the phenol adsorption into AC-alginate beads. The maximum adsorption capacity of composite beads for phenol was 78 mg g^{-1}. The kinetic study concluded that phenol adsorption on composite beads followed a pseudo-second-order kinetic model. The adsorption of phenol on composite beads fitted well to both the Freundlich and Langmuir isotherms. The synthesized composite beads were easily recycled and reused for phenol adsorption. The adsorption of organic pollutants from aqueous solution into composite beads occurred in two successive steps, i.e., film adsorption followed by intraparticle diffusion, as demonstrated by the intra-particle diffusion model. The high adsorption capacity, exceptional regeneration capacity, as well as simple preparation method make composite beads a promising adsorbent for the selective removal of organic pollutants in wastewater treatment applications.

Recently, GAC was used as adsorbent due to its high surface area and high affinity towards the removal of organic pollutants in wastewater (Fazal et al., 2020), such as humic acid (Barhoumi et al., 2019), trypan blue (Cai et al., 2020), naphthenic acids (Islam et al., 2018), metronidazole (Díaz-Blancas et al., 2018), acenaphthylene and phenanthrene (Eeshwarasinghe et al., 2019) as well as organic micropollutants (Jamil et al., 2019; Jaria et al., 2019; Piai et al., 2019; Golovko et al., 2020). Cai et al. (2020) investigated the removal of trypan blue by adsorption. The authors used core-shell GAC with a specific surface area of 1,128 m^2 g^{-1} and an abrasive resistance of 99%. The removal efficiency of trypan blue was 116 mg g^{-1} under the optimal conditions. Islam et al. (2018) studied the adsorption of naphthenic acids. The results indicated that the pseudo-second-order controlled the adsorption kinetics of naphthenic acids to GACand intraparticle diffusion models and the maximum

adsorption capacities obtained from Langmuir adsorption isotherm was 60 mg g^{-1}. In addition, the adsorption rate of acenaphthylene and phenanthrene on GAC was also studied by Eeshwarasinghe et al. (2019). The adsorption kinetics indicated that intraparticle diffusion was the main limiting phenomenon with acenaphthylene and phenanthrene adsorptions into the mesopores and micropores of the GAC. The Langmuir adsorption capacities of acenaphthylene (0.31–2.63 mg g^{-1}) and phenanthrene (0.74–7.36 mg g^{-1}) on GAC decreased with increased heavy metals concentration. To conclude, the GAC adsorbent had a high specific surface area and a higher abrasion resistance compared to composite beads. The adsorption kinetics of organic pollutants into GAC followed a pseudo-second-order model and an intraparticle diffusion model, i.e., the adsorption was mainly controlled by chemisorption and diffusion. The main adsorption isotherm model of organic pollutants into GAC was the Langmuir adsorption model. Thus, composite beads and GAC have shown great potential in environmental remediation applications due to their unique characteristics (granular form, porous morphology and high surface area) and their high adsorption affinity with various organic pollutants.

Further studies could be useful for modeling, designing and optimizing adsorption technologies for organic pollutants recovery and evaluating the performance of new bio-adsorbents as exposed in the following sub-section.

1.3.Current stage and future prospects

Although a significant number of research articles have been published on the adsorption of organic compounds onto composite beads and GAC, there are still numerous gaps that need particular attention. The following facts can be considered, but not restricted to, for future research, including in this PhD thesis:

- Research on the selectivity of adsorption and desorption is very important especially for high-value organic compounds (for example, PCs),
- Little work is done on the use of recycling materials as adsorbents to remove organic compounds. This could have potential for future research,
- More effective, reusable and eco-friendly materials should be developed, and tested with real effluents,

- The possibility of combining adsorption technology based on GAC or beads with other separation technologies (such as electrochemical processes) could also be explored,
- Most papers described herein involved adsorption of organic compounds by batch mode and column study; however, only a few researchers dealt with a pilot or industrial scale. The scale-up methodology should be used and the optimization tested at a larger scale for a better evaluation of the cost efficiency of the technology developed.

2. Electrosorption

2.1.Electrosorption: background and principle

2.1.1. General background

Electrosorption results from the concomitant development of porous electrode materials and electric double layer (EDL) theory.

This is missed most of the time in the literature, but the first hybrid electrochemical method combined with a separation technique using a porous electrode material was proposed as early as the late 19th century (1893) by Paul Léon Hulin, who referred to it as the "electroly-filtration" process (Hulin, 1893; Cœuret, 1993). Afterward, Butler and Armstrong measured hydrogen adsorption on solid metal electrodes in 1933 by applying anodic galvanostatic transients (Butler & Armstrong, 1933; Gileadi et al., 1968). Grahame then studied the potential controlled adsorption of n-octanol in 1946. This was followed by developing electrosorption of neutral organic molecules in 1965 (Brummer et al., 1965). During the end of the 1960s and the beginning of the 1970s, granular electrodes were developed (Coeuret, 2003). Johnson and Newman introduced a porous AC bed for desalination applications (Johnson & Newman, 1971). From the middle of the 1970s, expanded metal electrodes have aroused particular attention for their easy fabrication and implementation at the industrial scale (Cœuret & Legrand, 1985; Coeuret, 2003). Metal foam electrodes emerged in the 1980s due to their much higher specific surface area, which is particularly efficient for electrosorption in diluted media (Marracino et al., 1987). Still aimed at increasing the surface area of electrodes, nanostructured materials emerged in the 2000s, such as carbon nanotubes (CNTs) and graphene (Chabot et al., 2014; Le et al., 2019; Du et al., 2021). Metal-organic framework (MOF)-based materials have been proposed more recently

for electrosorption due to their exceptional surface area with controllable porosity (Chang et al., 2015).

In the meantime, the understanding of the EDL mechanism aroused specific attention within the electrochemistry community. It began with studies about the potential drops at the electrode/electrolyte interface and the so-called "Volta problem". Many known scientists have attempted to explain this phenomenon, such as Volta, Nernst, Ostwald, Planck, Langmuir and Lorenz (Damaskin & Petrii, 2011). Several EDL theories have been developed (Pilon et al., 2015), mainly through phenomenological models that could be supported by experimental data obtained by two kinds of electrochemical techniques: (i) electrocapillary curves, first developed by Lippmann (Lippmann, 1875) and (ii) EDL differential capacitance plots, first proposed by Varley (Varley, 1871). Helmholtz was the first to formalize the EDL concept in 1879 (Helmholtz, 1879), suggesting the existence of a compact layer made of a monolayer of counterions inducing a linear decrease in the potential in the vicinity of an oppositely charged conductive surface (Helmholtz, 1879). In contrast to the assumption of a continuous distribution of ions in the electrolyte upon the Poisson-Boltzmann relation at thermodynamic equilibrium, Gouy (Gouy, 1910) and Chapman (Chapman, 1913) proposed an alternative in the 1910s, introducing the existence of a diffuse double layer, which induces a nonlinear decrease in the potential in the vicinity of the electrode. The Gouy-Chapman approach was still not convincing at the closest distance of the electrode. The ions concentration was overestimated at the electrode surface because the ions were taken as point charges instead of finite size. Thus, in 1924 Stern proposed juxtaposing both the Helmholtz and Gouy-Chapman models (Stern, 1924), in which the EDL is composed of a compact layer close to the surface of the electrode and a diffuse layer in the outer region. In 1947, Grahame proposed dividing the compact layer (i.e., Stern layer) into the inner Helmholtz plane (IHP) and the outer Helmholtz plane (OHP). The IHP consists of a layer of ions and solvent adsorbed by covalent bonds and/or van der Waals forces on the interface. In the OHP, ions are driven by electromigration effects to produce an ionic environment (Grahame, 1947). Figure 1 schematizes the EDL considering the so-called Gouy-Chapman-Stern model, including IHP and OHP (Helmholtz, 1879; Gouy, 1910; Chapman, 1913; Stern, 1924; Grahame, 1947). This polarized interface induces a capacitance whose values usually range between a few $\mu F\ cm^{-2}$ to several tens of $\mu F\ cm^{-2}$ (Simon & Gogotsi, 2008).

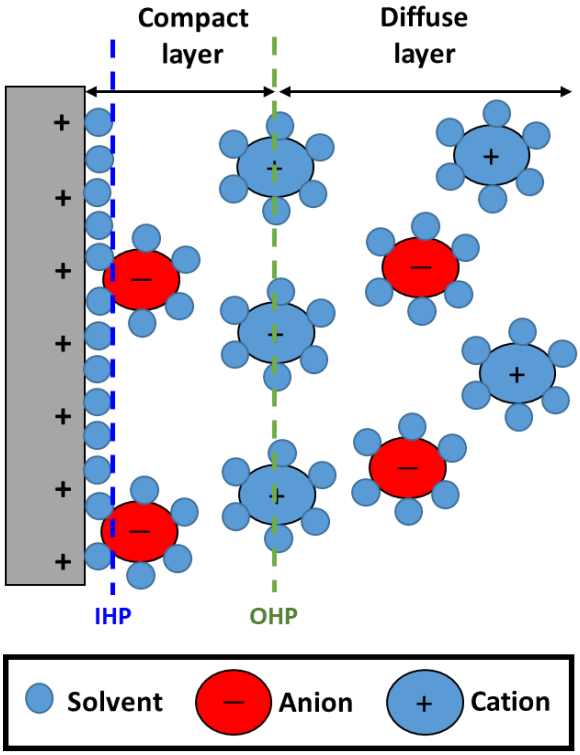

Fig. 5. Schematic representation of the EDL at positively charged electrode materials in the presence of anions, cations and solvent.

2.1.2. Principle

Electrosorption is a heterogeneous process defined as the species adsorption induced by electric current or a polarization potential on the surface of a conductive material without involving faradaic reactions, i.e., without electron transfer reactions (Fig. 6) (Frumkin et al., 1974; Gerçel, 2016). The electrosorption efficiency is usually quantified by estimating the equilibrium electrosorption capacity (q_A in mg g^{-1}), according to Eq. 1 (Li et al., 2016):

$$q_A = \frac{(C_0 - C_e)\,V}{m} \qquad (1)$$

where C_0 and C_e are the initial and equilibrium concentrations of the pollutant, respectively (g L^{-1}), V is the volume of the solution (L), and m is the mass of the working electrode (g).

The higher the electrosorption capacity is, the higher the electrosorption efficiency is (Alencherry et al., 2017).

The electric potential or current is the third driving force of the electrosorption phenomenon and ion exchange mechanism (Jung et al., 2005). The transport steps remain essential in the process efficiency (Schultze & Vetter, 1973; Vetter & Schultze, 1974).

Diffusion (i.e., species subjected to a concentration gradient in the vicinity of the electrode), electromigration (i.e., ions subjected to a gradient of the electrostatic potential) and convection (i.e., global fluid movement in bulk) phenomena can occur in the electrochemical reactor, which has been formalized by the Nernst-Planck equation (Bard & Faulkner, 2001). Most of the time, organic species' diffusion and/or electromigration in diluted media are limited steps before subsequent electrosorption (Panizza et al., 2001; Coeuret, 2003; Mousset, et al., 2019; Adnan et al., 2021a; Alagesan et al., 2021). Electromigration represents an interesting feature when organic ionic species are present in a solution since it can facilitate their selective transport toward the oppositely charged electrode for electrosorption. Nevertheless, the electrosorption of uncharged organic compounds remains feasible by following replacement reactions at an equivalent volume between water molecules adsorbed on the electrode and the organic compound (Gileadi, 1966a).

Apart from transport phenomena, the behavior at the electrode/electrolyte interface is another important concern for efficient electrosorption. This can be characterized by the EDL, which usually needs to be maximized. EDLs have been shown to depend on electrode material properties (i.e., electronic structure of the metal surface, electrode surface roughness, porosity and pore size distribution), interelectrode distances and electrolyte characteristics (i.e., electrolyte concentration, viscosity and polarity, distribution of ions and solvent molecules) (Trasatti, 1992; Schmickler, 1996; Conway, 1999; Yan et al., 2017; Oleinick et al., 2019). The influence of parameters on the organic electrosorption efficiency is discussed in more detail in section 2.2 of part I.

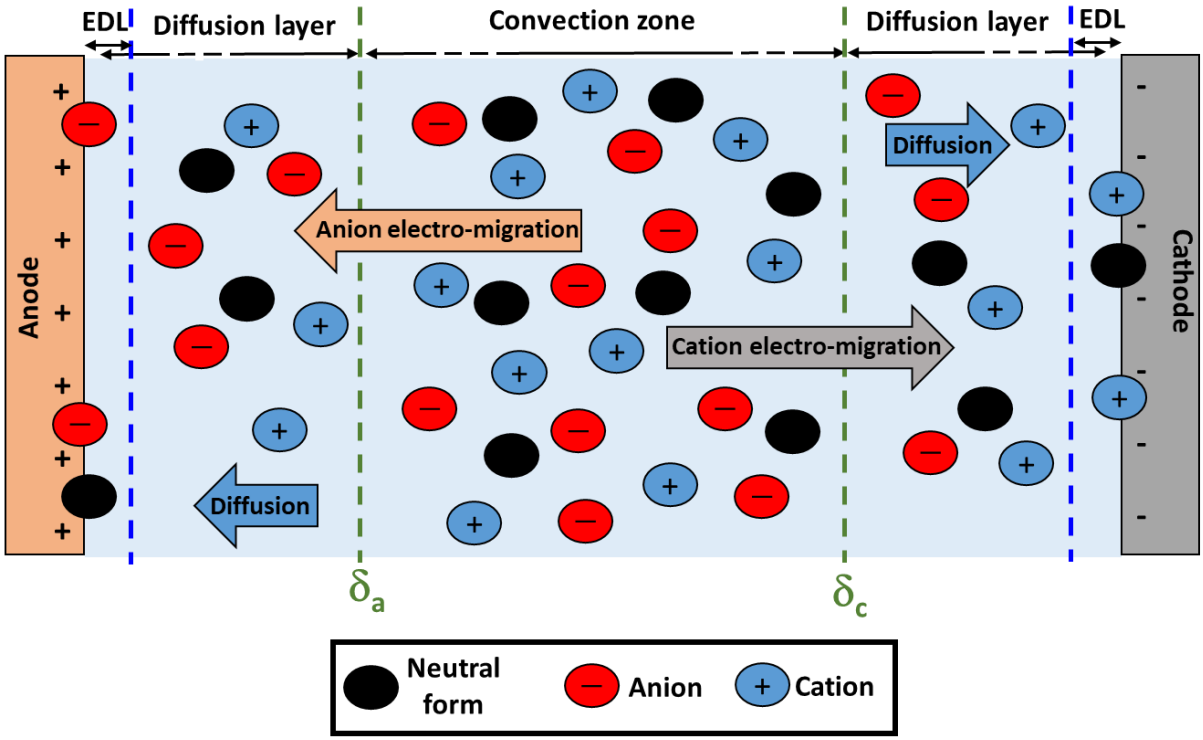

Fig. 6. Schematic diagram illustrating the principle of electrosorption, including anion, cation and uncharged compounds, as well as transport phenomena (δ_a and δ_c: diffusion layer thickness at the anode and cathode, respectively).

2.2.Influence of the main parameters

The effect of the main parameters (i.e., the properties of the electrode materials, the experimental conditions (applied electrode potential, pH, concentration, electric conductivity, residence time, flow rate) and the reactor design) on the electrosorption/desorption kinetics and capacity have been reviewed in detail. The main research articles dealing with the electrosorption of organic compounds in the literature are listed in Table 1.

Table 1. Main studies performed on the electrosorption of organic compounds reviewed in the literature.

Working electrode	Specific surface area	Reactor design	Organic pollutant (concentration)	Electrolyte (concentration)	Current intensity/Electrode potential	Studied parameters	Maximum electrosorption capacity	Reference
Granular activated carbon (GAC)	1,180 $m^2 g^{-1}$	Fixed-bed reactor	Metribuzin (50,150, 300 and 450 mg L^{-1})	KCl (3 mol L^{-1})	−0.050 V/SCE	Electrode potential, flow rate and initial concentration of pollutant	22 mg g^{-1}	(Kitous et al., 2009)
GAC	950 $m^2 g^{-1}$	Fixed-bed reactor	Naphthalenesulfonic acid, benzyl alcohol, naphthoic acid, methylquinolinium chloride (2 mg L^{-1})	KCl (0.1 mol L^{-1})	0.60 V/(Ag/saturated KCl)	Initial concentration of pollutant and pH of the initial solution	100 mg g^{-1}	(Bán et al., 1998)
GAC	-	Fixed-bed reactor	Benzene (1 mmol L^{-1})	KCl (0.2 mol L^{-1})	-2 and 2 V/SCE	Electrode potential	-	(Plaisance et al., 1996)
GAC	1,100 $m^2 g^{-1}$	Fixed-bed reactor	Ethylenediamine (500 mg L^{-1})	NaCl (20 wt. %) and $NaHCO_3$ (0.025 mol L^{-1})	0 to -1 V/SCE	Initial concentration of pollutant and electrode potential	-	(Eisinger & Keller, 1990)
GAC and platinum wire	-	Fixed-bed reactor	Chloroform (2.5-10 mmol L^{-1})	KNO_3 (0.1 mol L^{-1})	0, 1, 2 and 2.5 V/SCE	Electrode potential	-	(Hazourli et al., 1996a)
GAC and activated carbon electrode (ACE)	GAC: 1,062 $m^2 g^{-1}$ ACE: 862 $m^2 g^{-1}$	Flow-through parallel-plate cell	Benzoic acid (BA) and nicotinic acid (NA) (1 mmol L^{-1})	Na_2SO_4 (0.1 mol L^{-1})	0.5, 1.5 and 2 V/(Ag/AgCl)	Time, flow rate and electrode potential	-	(Bayram, 2016)
Activated carbon cloth (ACC)	1,870 $m^2 g^{-1}$	Flow-through parallel-	BA (0.22 mmol L^{-1})	Na_2SO_4 (0.01 mol L^{-1})	0.60 V/(Ag/AgCl)	Flow rate, electrode potential and pH of initial solution	180 mg g^{-1}	(Bayram & Ayranci, 2012b)

		plate cell						
ACC	ACC:926 $m^2 g^{-1}$ ACCO: 960 $m^2 g^{-1}$	Flow-through parallel-plate cell	Bentazone (20 mg L^{-1})	Na_2SO_4 (0.01 mol L^{-1})	5 mA	Time, initial concentration of pollutant, pH of the initial solution	ACC: 127 mg g^{-1} ACCO: 57 mg g^{-1}	(Ania & Béguin, 2007)
ACC	1,870 $m^2 g^{-1}$	STR	Acid orange 8 (AO8), acid yellow 14 (AY14), and acid red 151 (AR151) (0.05 mmol L^{-1})	Na_2SO_5 (0.1 mol L^{-1})	1 V/(Ag/AgCl)	Time and initial concentration of pollutant	AO8: 20 mg g^{-1} AY14: 25 mg g^{-1} AR151: 24 mg g^{-1}	(Sahin et al., 2020)
ACC	1,870 $m^2 g^{-1}$	Flow-through parallel-plate cell	2,4-dichlorofenoxy-acetic acid (0.2 mmol L^{-1})	Na_2SO_4 (0.01 mol L^{-1})	0.90 V/(Ag/AgCl)	Flow rate, electrode potential, and electrolyte concentration	729 mg g^{-1}	(Bayram et al., 2018)
ACC	1,186 $m^2 g^{-1}$	Flow-through parallel-plate cell	Mercury (II) acetate	NaCl (0.01 mol L^{-1})	−1 V/SCE	Flow rate, initial concentration of pollutant, electrode potential and pH of the initial solution	637 mg g^{-1}	(Jayson et al., 1987)
ACC	596 $m^2 g^{-1}$	Fluidized-bed reactor	8-quinolinecarboxylic acid (50 mg L^{-1})	Na_2SO_4 (0.5 mol L^{-1})	3 V (cell potential)	Time and cell potential	24 mg g^{-1}	(López-Bernabeu et al., 2016)
ACC	2,500 $m^2 g^{-1}$	Flow-through parallel-plate cell	Aniline and pyridine	$LiClO_4$ (0.1 mol L^{-1})	0.1, 0.2 and 0.4 V/(Ag/AgO)	Electrode potential	-	(Niu & Conway, 2003)
AC bed and platinum wire	-	Fixed-bed reactor	Phenol (0 to 100 mg L^{-1})	Na_2SO_4 (0.5 mol L^{-1})	- 0.60 V/SCE	Time, initial concentration of the pollutant and electrode potential	-	(McGuire et al., 1985)

Powdered carbon bed	AC-NM: 1,390 m^2 g^{-1} AC-NA: 1,296 m^2 g^{-1} AC-Am: 1,212 m^2 g^{-1} AC-HT:363 m^2 g^{-1} CB-W: 227 m^2 g^{-1} CNT-h: 156 m^2 g^{-1} CNT-c: 209 m^2 g^{-1}	Fixed-bed reactor	4-chlorophenols (10, 25, 50 mmol L^{-1})	Na_2SO_4 (0.1 mol L^{-1})	0.4 V/SCE	Electrode potential and initial concentration of the pollutant	-	(Biniak et al., 2013)
AC	678 m^2 g^{-1}	Fluidized-bed reactor	Burdem orange II (30 and 100 mg L^{-1})	Na_2SO_4 and $NaNO_3$ (5 mg L^{-1})	50, 75 and 100 V (cell potential)	pH of the initial solution, initial concentration of pollutant, flow rate, cell potential, and electrolyte concentration	179 mg g^{-1}	(Gerçel, 2016)
AC –perlite mixture (8:1)	-	Fixed-bed reactor	Acilan blau dye (30, 40 and 100 mg L^{-1})	NaCl (0.1 and 0.3 mol L^{-1})	5, 10, 15 and 20 V (cell potential)	Initial concentration of the pollutant, bed height, cell potential, flow rate, and electrolyte concentration	17 mg g^{-1}	(Koparal et al., 2002)
Carbon bed and the platinum mesh screen	1,010 m^2 g^{-1}	Fixed-bed reactor	Pentanol and heptanol (0.01, 0.02, 0.1 mol L^{-1})	Na_2SO_4 (1 mol L^{-1}))	-0.65 V to -0.20 V/(Hg/Hg_2SO_4 in 1 M H_2S0_4)	Electrode potential and initial concentration of the pollutant	-	(Zabasajja & Savinell, 1989)
Graphite powder	0.048 m^2 g^{-1}	Fixed-bed reactor	β-naphthol (1 mmol L^{-1})	K_2SO_4 (0.5 mol L^{-1})	-0.17, -0.27, -0.50, -0.76, -1.12 and -1.44 V/MSE	Time, initial concentration of the pollutant and electrode potential	-	(Eisinger & Alkire, 1980)
Porous Vycor glass tubing packed with graphite particles	-	Fixed-bed reactor	Quinones (0.1 mmol L^{-1})	KCl (0.1 mol L^{-1})	1 V/(Ag/AgCl)	Initial concentration of the pollutant and cell potential	-	(Strohl & Dunlap, 1972)

Activated carbon fibers (ACF)	1,335 $m^2 g^{-1}$	STR	Phenol (0.4, 1, and 2 mmol L^{-1})	Na_2SO_4 (0.001, 0.01, and 0.1 mol L^{-1})	0.70 V/SCE	Electrode potential, initial concentration of the pollutant, temperature and electrolyte concentration	350 mg g^{-1}	(Han et al., 2006b)
ACF	1,335 $m^2 g^{-1}$	STR	Aniline (2 mmol L^{-1})	Na_2SO_4 (0.01 mol L^{-1})	0.60 V/SCE	Electrode potential, electrolyte concentration, temperature and pH of the initial solution	316 mg g^{-1}	(Han et al., 2006a)
ACF connected by platinum wire	1,335 $m^2 g^{-1}$	STR	Acid orange 7 (AO7) (1 mmol L^{-1})	Na_2SO_4 (0.01 mol L^{-1})	0.60 V/SCE	Time, electrode potential and initial concentration of the pollutant	-	(Han et al., 2008)
ACF	-	STR	Aniline (0.05 mg L^{-1})	Na_2SO_4 (0.01 mol L^{-1})	0.20 to 0.40 V/SCE	Electrolyte concentration, temperature and pH of the initial solution	-	(Chai et al., 2007)
AC felt	27 $m^2 g^{-1}$	Flow-through parallel-plate cell	Thiocyanate anions (0.1-0.6 mmol L^{-1})	H_2SO_4 (0.5 mol L^{-1})	0.5, 0.8, and 1.2 mA	Electrode potential and pH of the initial solution	4 mg g^{-1}	(Rong & Xien, 2005)
AC felt and Pt wire	1,367 $m^2 g^{-1}$	Flow-through parallel-plate cell	Thiocyanate (0.1-0.2 mmol L^{-1})	HNO_3 or NaOH (0.01 mol L^{-1})	0.5 to 1.2 mA	pH of the initial solution, electrode polarization and current intensity	-	(Rong & Xien, 2009)

Carbon-felt attached to a short Pt wire.	2,500 $m^2 g^{-1}$	Flow-through parallel-plate cell	Phenol, phenoxide and chlorophenols (1 mmol L^{-1})	H_2SO_4 (0.01 mol L^{-1})	0.6 mA	Time	-	(Ayranci & Conway, 2001)
Carbonaceous aerogel honeycomb monolith	393 $m^2 g^{-1}$	STR	Diclofenac (150, 300, 600 and 1000 mg L^{-1})	Na^2SO_4 (0.005, 0.01 and 0.02 mol L^{-1})	0.7, 0.9 and 1.1 V (cell potential)	Electrode gap, electrode potential and initial concentration of the electrolyte	120 mg g^{-1}	(Pazos et al., 2021)
Graphene aerogel	211 $m^2 g^{-1}$	STR	Acid red 88, orange II, and MB (0.04–0.2 mmol L^{-1})	Na_2SO_4 and NaOH (1 mol L^{-1})	0.6 V	Time, electrode potential and pollutant concentration	acid red 88: 481 mg g^{-1} orange II: 223 mg g^{-1} MB: 191 mg g^{-1}	(Sun et al., 2016a)
Porous reduced graphene oxide (prGO)/single-walled carbon nanotubes (SWCNTs)	94 $m^2 g^{-1}$	STR	Methylene blue (MB) (10−600 mg L^{-1})	Na_2SO_4 (0.01 mol L^{-1})	−1.2 V/(Ag/AgCl)	Time and initial concentration of the pollutant	13 g g^{-1}	(Yue et al., 2019a)
Graphene oxide aerogel loaded with Cu nanoparticles and fluorine	GO: 286.75 $m^2 g^{-1}$ rGA:188.92 $m^2 g^{-1}$ F-rGA: 203. $m^2 g^{-1}$ Cu-rGA: 151.65 $m^2 g^{-1}$ Cu/F-rGA: 133.49 $m^2 g^{-1}$	STR	Perfluorooctanoic acid (1 mg L^{-1})	Na^2SO_4 (1-20 mmol L^{-1})	0 to + 1.6 V/(Ag/AgCl)	pH, temperature, electrode potential and initial concentration of the electrolyte	rGA:6.05 mg g^{-1} rGA-F: 8.43 mg g^{-1} rGA-Cu: 16.47 mg g^{-1} rGA-Cu/F: 25.93 mg g^{-1}	(Liu et al., 2021)
Porous MXene/single-walled carbon nanotubes	42.89 $m^2 g^{-1}$	STR	MB and methyl orange (30–1000 mg L^{-1})	Phosphate buffer solution (0.01 mol L^{-1})	−2.4 V, −1.2 V, −0.6 V and 0 V/(Ag/AgCl)	Electrode potential, initial concentration of the pollutant and time	28.4 g g^{-1}	(Yao et al., 2021)

Glassy carbon	-	Fixed-bed reactor	B-naphthol (0.02 mmol L^{-1})	K_2SO_4 (0.5 or 0.2 mol L^{-1})	-0.26 V/MSE	Time and initial concentration of the pollutant	-	(Eisinger, 1983)
AC and two copper circular plates	-	Fixed-bed reactor	MB (1, 10 and 15 mg L^{-1})	-	5 V (cell potential)	Bed height, flow rate and initial concentration of the pollutant	81 mg g^{-1}	(Nainamalai et al., 2018)
Pt small spherical of Pt	-	STR	Benzene (2×10^{-6} - 4×10^{-4} mol L^{-1})	-	0.4-0.5 V/RHE	Electrode potential, temperature	-	(Gileadi et al., 1968)
Platinum-plated gold	-	STR	Benzene (2×10^{-6} - 4×10^{-4} mol L^{-1})	H_2SO_4 and H_3PO_4 (1 N)	0.4-0.5 V/NHE	Electrode potential, pH of the initial solution, and time	-	(Heiland et al., 1966)
Platinum-plated gold	-	STR	Ethylene	H_2SO_4 (1 N)	0.4-0.46 V/MSE	Electrode potential, initial concentration of the pollutant and temperature	-	(Gileadi et al., 1965)
Stainless steel wire coated with monolithic porous polymer micro-column	-	STR	Cresol red (5 mg L^{-1})	NaCl (0.005, 0.5 and 0.1 mg L^{-1})	0.3 mA	Cell potential, extraction and desorption time, pH of the initial solution and ionic strength	-	(Wang et al., 2012)

Redox polymer polyvinylferrocene /conducting polymer polypyrrole doped with a large anionic surfactant	-	Flow-through parallel-plate cell	Benzoate (0.25 mmol L^{-1})	$NaClO_4$ (12.5 mol L^{-1})	0.35 V and −0.1 V/(Ag/AgCl)	Electrode potential	-	(He et al., 2020)

Abbreviations: AC: activated carbon; AC-Am: ammonia-treated activated carbon; ACC: activated carbon cloth; ACCO: activated carbon cloth oxidized; ACE: activated carbon electrode; ACF: activated carbon fibers; AC-HT: annealed activated carbon; AC-NA: nitric acid oxidized activated carbon; AC-NM: nonmodified activated carbon; AO7: acid orange 7; AO8: acid orange 8; AR151: acid red 151; AY14: acid yellow 14; BA: benzoic acid; CB-W: carbon black; CFP: carbon fiber paper; CNT-c: multiwalled carbon nanotubes - short carboxyl; CNT-h: multiwalled carbon nanotubes - short hydroxyl; MB: methylene blue; MSE: mercury/mercurous sulfate electrode; NA: nicotinic acid; NHE: normal hydrogen electrode; NMO: $Na_{0.7}MnO_2$; prGO: porous reduced graphene oxide; RHE: reversible hydrogen electrode; rGA: reduced graphene oxide aerogel; rGA-Cu: Cu nanoparticles loaded rGA; rGA-F: F-doped reduced graphene oxide aerogel; rGA-Cu/F: F and Cu nanoparticles modified rGA; SCE: saturated calomel electrode; STR: stirred tank reactor; SWCNTs: single-walled carbon nanotubes.

2.2.1. Electrode materials

The electrosorption efficiency partly depends on the nature of the electrode materials and their characteristics, i.e., specific surface area, porosity, conductivity, surface functions and surface wettability.

2.2.1.1. Nature and surface morphology of the electrode materials

Various electrode materials have been employed for electrosorption technologies, and Fig. 7a shows the occurrence frequency regarding the electrode materials used in the literature (Table 1). These materials are proposed for classification into the following categories (percentage of occurrence in brackets): carbon-based electrodes (85%), metal-based electrodes (9%) and polymer/resin-based electrodes (6%). Under the carbon electrodes, the following subcategories can be found: carbon-based composites (19%), GAC (32%), carbon cloth (19%), carbon fiber (7%), carbon felt (7%), graphite (13%) and graphene (3%).

Metal-based materials have barely been studied in the literature (Fig. 7a), probably due to their usually high cost compared to carbon materials and their lower flexibility in shape, surface area and porosity. The crystallographic orientation of the single-crystal planes (Lust, 1997) and the electronic structure of the metal surface impact the EDL, and therefore the electrosorption efficiency (Schmickler, 1996). It has been further demonstrated that the dipole orientation of water, often used as a solvent, can be impacted by the surface chemistry of metal-based materials (Conway, 1999). In addition, the point of zero charges of metals influences the specific orientation of H_2O molecules, which then impacts H_2O adsorbability (Trasatti, 1972). Therefore, the adsorbability of solvated ions on metals is also impacted, along with their electrosorption efficiency.

In contrast, it is obvious that carbon represents the majority of electrode materials used in the literature (Fig. 7a). Despite their availability and low prices, this enthusiasm toward carbon materials can be explained by their adequate properties for electrosorption, which are discussed more in detail in sections 2.2.1.2 to 2.2.1.5 of part I. Among their important characteristics, they have a particularly high surface area, high porosity, high electrical conductivity and high electrochemical stability, especially for cathodic reduction (Frackowiak, 2001; Hou et al., 2012). Graphene has notably attracted attention as an emerging two-dimensional material composed of sp^2-hybridized carbon atoms arranged in a honeycomb

structure, and its characteristics have benefited environmental electrochemistry (Geim & Novoselov, 2007; Le et al., 2015; Mousset et al., 2016a, 2016b; Mousset et al., 2017; Le et al., 2019; Du et al., 2021).

The surface morphology of electrode materials is often inspected using microscope devices as a qualitative approach to roughly evaluate the adsorption ability. Microscopic views obtained via scanning electron microscopy (SEM) are displayed in Figs. 7b and 7c for activated carbon fiber (ACF) (Han et al., 2006b) and single-walled carbon nanotube (SWCNT) films (Yue et al., 2019b), respectively. Fig. 7b depicts the fine structure of ACF, which involves numerous uniform open pores on the surface (Han et al., 2006b), while the SEM image of the prGO/SWCNT film displays a rough surface and corrugated structures, which should provide a large accessible surface area (Fig. 7c) (Yue et al., 2019b).

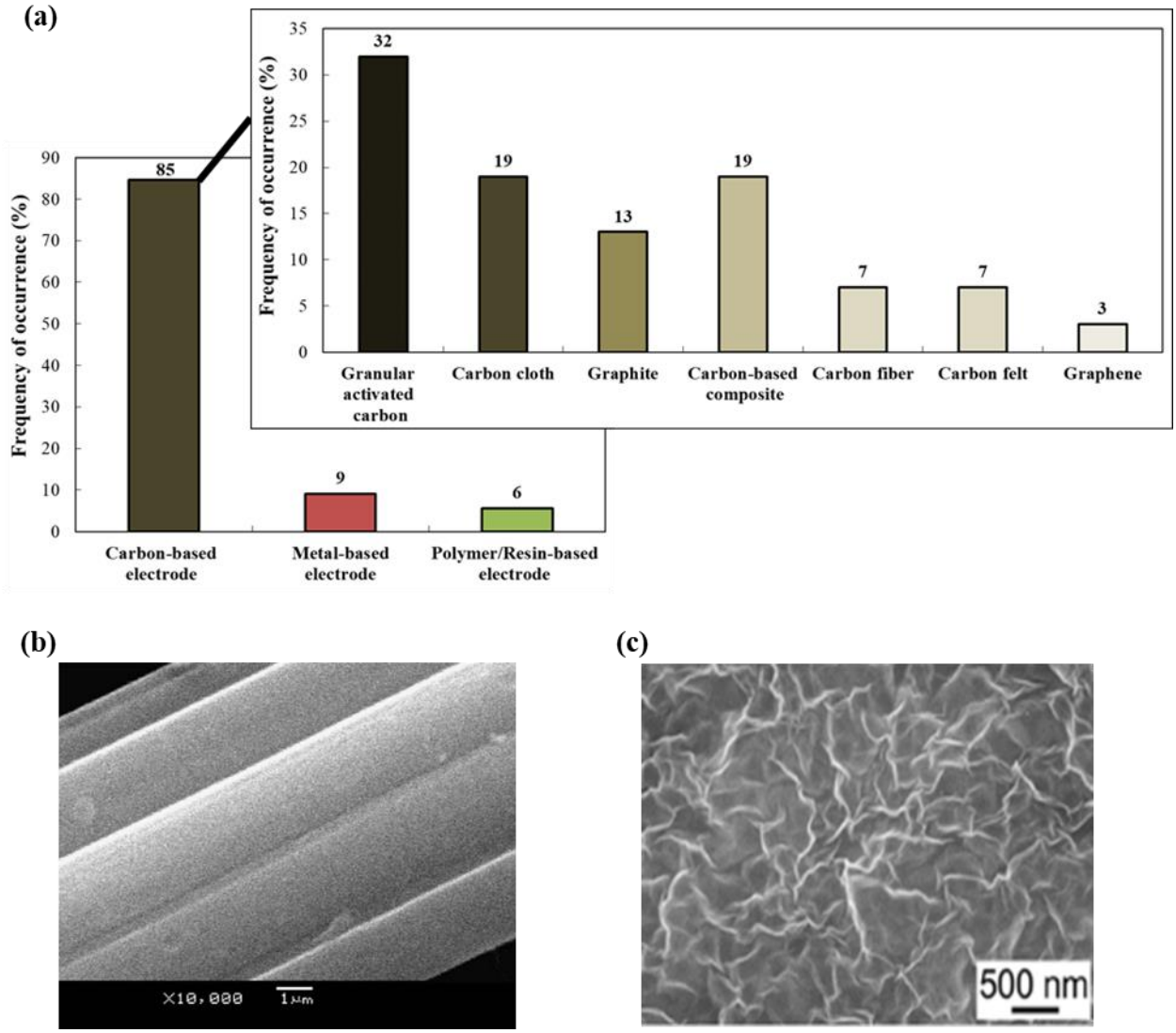

Fig. 7. (a) Electrode materials used in the literature, (b) SEM image of ACF (Han et al., 2006b), (c) SEM image of the prGO/SWCNT film (Yue et al., 2019).

2.2.1.2. Specific surface area, porosity, and roughness

A large surface area and an optimal pore size distribution of the electrode are essential requirements for reaching a high electrosorption capacity. In addition, they result in a high capability for charge accumulation at the active sites of the electrode/electrolyte interface (Zaharaddeen et al., 2016). From Fig. 8a, it can be seen that the specific surface area of the electrode used in the literature reached 2000 m^2 g^{-1}, while a majority of articles (36%) applied materials with specific surface areas within the range of 0-500 m^2 g^{-1} (Table 1).

One of the most common methods employed to modify the surface area and pore size distribution of carbon materials is their activation via chemical and/or thermal treatment. The

electrosorption of 4-chlorophenol was studied by testing AC with different treatments, i.e., nonmodified AC (AC-NM), AC oxidation with nitric acid (AC-NA), AC treated with ammonia (AC-Am), and annealed AC (AC-HT) (Fig. 8b) (Biniak et al., 2013). The results highlighted a decrease in the specific surface area (S_{BET}) estimated by the well-known Brunauer-Emmett-Teller method when the AC was modified. Additionally, the total volume of mesopores (V_{me}) increased with the chemical treatment (AC-NA and AC-Am) (Fig. 8b), while the electrosorption efficiencies were better with these materials. It is important to note that increasing the surface area of materials does not systematically lead to a higher electrosorption efficiency, unlike many studies intend to show. Therefore, the distribution of pores remains an essential factor to consider, along with the specific surface area. The pore size has previously been shown to induce a change in the EDL. Fig. 8c depicts the EDL within different pore sizes of the carbon material, i.e., higher than 2 nm, between 1 and 2 nm and smaller than 1 nm. It has been emphasized that the existence of an optimal pore size gives an optimal capacitance when the pore size is close to the ion size (Largeot et al., 2008). This feature further highlights the impact of microporosity on the EDL and electrosorption efficiency. Due to these differences in the behavior of EDLs in porous materials, a multiscale model has been proposed according to the pore size for better accuracy of capacitance prediction: a sandwich-type model for micropores (< 2 nm), an electric double-cylinder model for mesopores (2-50 nm)), and a planar model for macropores (> 50 nm) (Fig. 8d) (Huang et al., 2008; Feng et al., 2010; Dai et al., 2020).

A more recent approach for modifying the material properties involves carbonaceous nanostructured materials, such as graphene and/or carbon nanotubes (CNTs). A comparison between the specific surface area and porosity of three graphene-based materials, namely, prGO/SWCNTs, prGO and reduced graphene oxide (rGO), used for MB electrosorption has been performed (Yue et al., 2019b). The specific surface areas of rGO (5.5 m^2 g^{-1}) and prGO (29 m^2 g^{-1}) were much smaller than that of prGO/SWCNT (94 m^2 g^{-1}), and the same trend was obtained for the total pore volume. The prGO/SWCNT electrode material depicted a higher electrosorption capacity (13 g^{-1}). The increase in the specific surface area and total porosity could have explained the higher electrosorption capacity (Yue et al., 2019b).

In addition, many electrode materials used in electrosorption can be considered to have a nonidealized electrode geometry, which then affects the EDL and consequently the electrosorption efficiency (Fan et al., 2014). For example, curvature effects are frequently

encountered in cylindrical shapes (e.g., CNTs) and porous materials, which breaks with the linearity of models developed for planar electrode systems (Henstridge et al., 2010; Lian et al., 2016). Moreover, differences have been predicted by using density functional theory (DFT) between concave and convex shapes. Concave induces a lower curvature effect than convex interfaces, leading to higher capacitances in the latter (Lian et al., 2016), and better electrosorption.

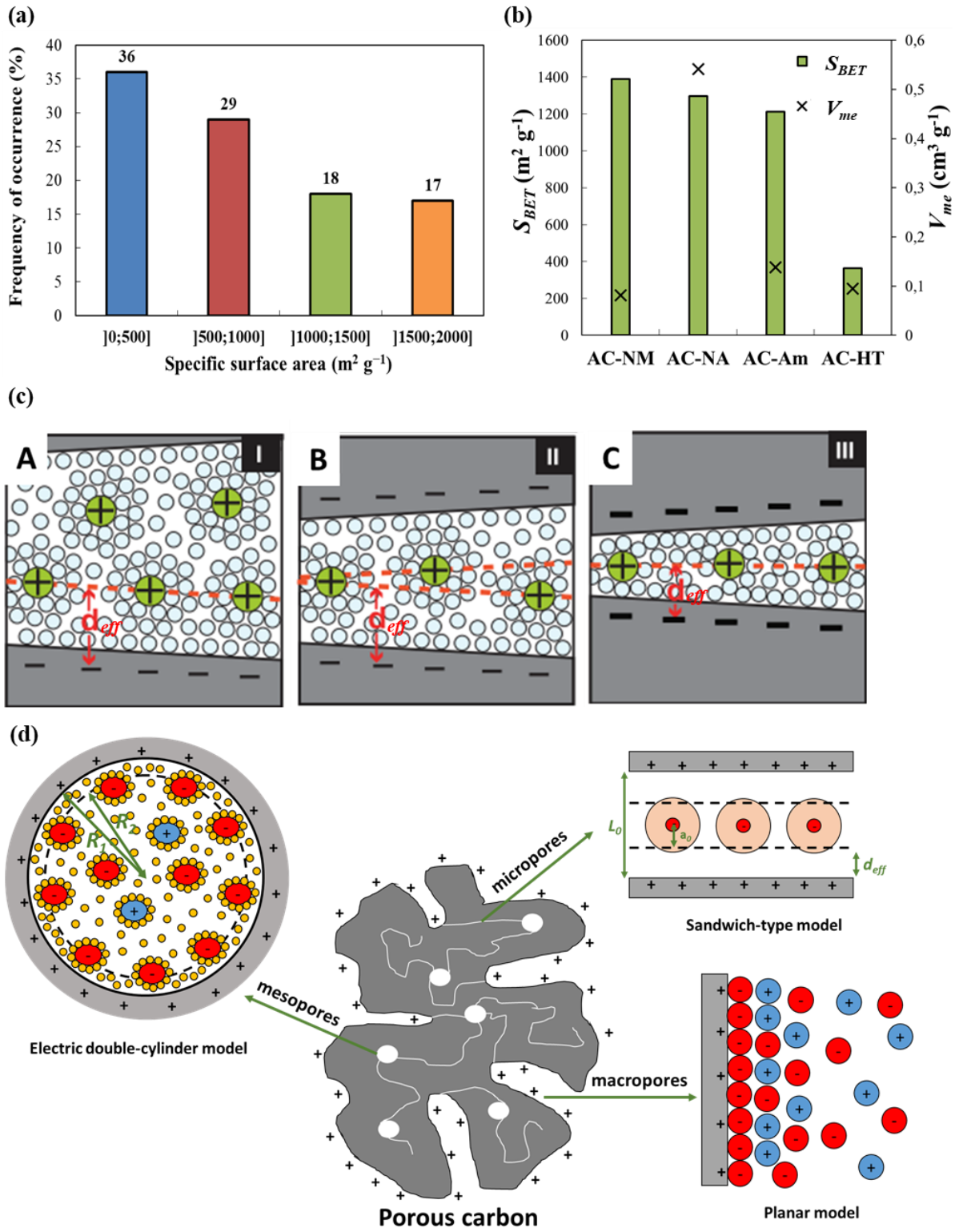

Fig. 8. (a) Range of the specific surface area of the electrode implemented for organics electrosorption in literature, (b) S_{BET} and V_{me} evolutions as a function of modified (AC-NA, AC-Am, AC-HT) and AC-NM (Biniak et al., 2013), (c) EDL drawings representing solvated ions within different negatively charged pore sizes in carbon material: higher than 2 nm (A), between 1 and 2 nm (B) and smaller than 1 nm (Chmiola et al., 2006), (d) Schematic

diagrams of a positively charged porous carbon material and the associated model of the EDL: sandwich-type model for micropores, electric double-cylinder model for mesopores, planar model for macropores (Huang et al., 2008; Feng et al., 2010; Dai et al., 2020).

2.2.1.3. Material conductivity

It is well known that the electrical conductivity of electrode materials increases the rate of electron transfer at the material/electrolyte interface (Du et al., 2021). The effect of electrical conductivity on electrosorption efficiency has been particularly emphasized. It has been shown that the higher electrosorption capacity obtained with prGO/SWCNTs compared to prGO and rGO was partly related to the electrical conductivity of prGO/SWCNTs (74 S cm^{-1}), which was far larger than that of prGO (20 S cm^{-1}) and rGO (30 S cm^{-1}) (Fig. 9a) (Yue et al., 2019b). The electrical conductivity increased with the introduction of SWCNTs in the samples. Other authors have also reported the positive effect of increasing the electrical conductivity on the kinetics and capacity of electrosorption (Alencherry et al., 2017).

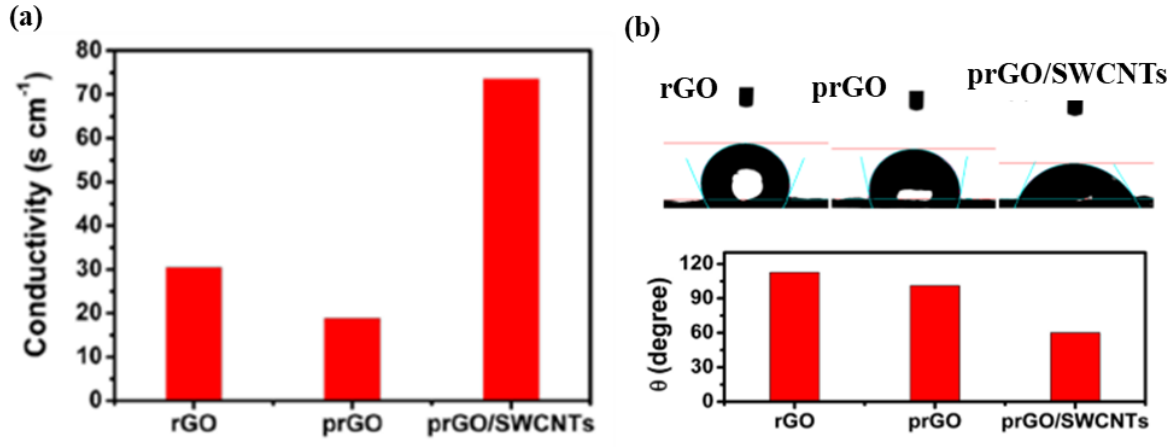

Fig. 9. (a) Electrical conductivity of rGO, prGO and prGO/SWCNT materials, (b) Surface wettability of rGO, prGO and prGO/SWCNT materials (Yue et al., 2019b).

2.2.1.4. Surface functions

The type of surface function on the porous electrode can affect the electrosorption process. A comparison of electrosorption efficiencies using AC with different surface functions (Biniak et al., 2013) has been reported. AC-Am produced basic nitrogen-containing functional groups on the surface, while AC-NA increased the number of acidic oxygen functional groups bound to the surface. The more acidic the carbon surface, the more oxygen bound to it and the lower the efficiency of 4-chlorophenol electrosorption (Biniak et al.,

2013). In another study, incorporating spherical polystyrene and SWCNTs into graphene oxide (prGO/SWCNTs) led to a higher electrosorption capacity than that of rGO and porous rGO films (Yue et al., 2019b). Spherical polystyrene generated 3D macropores, while SWCNTs created efficient pathways for the transfer of ions and electrons.

2.2.1.5. Surface wettability

The surface wettability of the electrode is a parameter that can be obtained by measuring the contact angle. If the contact angle is greater than 90°, the electrode is hydrophobic; while it is less than 90°, itis considered hydrophilic (Yue et al., 2019b). This factor has barely been quantified in electrosorption studies, although it has been established that poor wettability generally hampers ion (hydrophilic) transport within the electrode's pores. This is unfavorable for the electrosorption process (Chang et al., 2014). Nevertheless, a recent study stated the influence of the wettability of three graphene-based materials (prGO/SWCNTs, rGO and prGO) on MB electrosorption (Yue et al., 2019b). The surface wettabilities were 60°, 113° and 101° for prGO/SWCNTs, rGO and prGO, respectively (Fig. 9b) (Yue et al., 2019b). The prGO/SWCNTs showed higher hydrophilicity, and the electrosorption capacity (up to 13 g g^{-1}) was higher than that of the two other materials. The introduction of SWCNTs improved the hydrophilicity of the prGO/SWCNTs. Therefore, the surface wettability also influences the electrosorption capacity of organic compounds, and should not be neglected in investigation studies.

2.2.1.6. Applied electrode potential/current density and electrode polarity

The electrode polarity related to the applied current intensity sign is known to influence the electrosorption capacity of the porous surface, while the electrosorption rate can be increased. According to the reviewed papers (Table 1), the occurrence percentages of electrode polarity configurations tested for electrosorption are as follows: cathode (23%), anode (41%) and both polarities (i.e., cathode and anode) (36%) (Fig. 10a). Most of the time, the electrode polarity can induce electromigration effects that need to be considered according to the charge in the targeted compounds. Since many organic compounds are negatively charged, the reason why more electrosorption studies have been performed with a positively charged anode material could be explained (Fig. 10a). For instance, the electrode polarity was studied using metal wire coated with an epoxy resin-based polymer as the working electrode

and platinum wire as the counter electrode for cresol red electrosorption (Wang et al., 2012). The results showed that anodic polarization enhanced the efficiency compared to cathodic polarization. This was explained by the orderly migration of the negatively charged cresol red molecules with the sulfonic group on the benzene ring toward the positively charged wire anode. In contrast, the same charge between the compound and the cathode material limited their interaction (Wang et al., 2012). Similarly, anodic polarization increased the amount of phenol adsorbed on AC, while cathodic polarization decreased it (McGuire et al., 1985). In contrast, the cathodic polarization remarkably increased the thiocyanate anion electrosorption on the AC compared to anodic polarization (Rong & Xien, 2005), ascribed to coulomb interactions. In addition, the cathodic electrosorption of 8-quinolinecarboxylic acid on ACC resulted in higher removal efficiencies (96%) than anodic electrosorption (84%) (López-Bernabeu et al., 2016). These differences in behavior were due to the occurrence of a faradaic reaction at the Ti-Pt anode, while the cloth was the cathode. In this configuration, the anodic oxidation of 8-quinolinecarboxylic acid and its subsequent byproducts could be implemented, which enhanced the removal efficiency of the targeted compound (López-Bernabeu et al., 2016). In contrast, organic compounds were not oxidized when the AC tissue was used as the anode, and only electrosorption could occur.

The faradaic reactions are considered to be competitive when only electrosorption is desired. Their occurrence is directly related to the applied electrode potential value, which is the driving force that permits modification of the adsorption equilibrium by introducing a difference in the potential at the electrode/electrolyte interface. This potential is linked with the applied current density through the Butler-Volmer equation (Lord et al., 2012). These reactions are involved at either anodic potentials that are too high or cathodic potentials that are too low, and some of them have recently been reviewed (Zhang et al., 2018) and schematized (Holubowitch et al., 2017). Water oxidation into oxygen (O_2) and water reduction into hydrogen (H_2) are the two most famous faradaic equations that can occur in aqueous media. There can be other parasitic reactions according to the electrode material used and/or the composition of the electrolyte. For instance, if a carbon material is used as an anode, it can be easily oxidized (E^0 = 0.21 V/standard hydrogen electrode). This can be an issue because most of the porous electrodes employed are based on a carbon material (Fig. 7a), knowing that anodic polarization is the most experimented upon (Fig. 10a). Therefore, caution should be taken in applied operating conditions if porous carbon anodes are

implemented to avoid corrosion. Moreover, undesirable nitrogenous and/or chlorinated oxyanions (NO_2^-, NO_3^-, ClOH, ClO_3^-) can be initially generated at a sufficiently high anodic potential in the presence of nitrogenous species and/or chloride ions (Brito et al., 2015; Mousset et al., 2018; Mousset et al., 2020a). When a high O_2 overvoltage anode is employed, such as boron-doped diamond (BDD), to cite the most frequently studied anode, perchlorate (ClO_4^-) can even be produced (Bergmann et al., 2009). Often missing in the literature and especially in reviews dealing with faradaic reactions involved in capacitive deionization (Zhang et al., 2018): the local alkalization at the cathode from O_2 reduction and H_2O reduction reactions should not be overlooked. Under this condition, magnesium, calcium and/or carbonate are present in solution, which is the case in many actual aqueous effluents (Belarbi et al., 2016; Adnan et al., 2021a), and electroprecipitation phenomena can occur by forming $Mg(OH)_2$ and/or $CaCO_3$ at the cathode surface (Belarbi et al., 2016; Adnan et al., 2021a). These deposits then progressively passivate the cathode and hamper electrolysis.

Thus, faradaic reactions can be avoided if a sufficiently short potential window is applied, whose range can be verified by a voltammetric analysis. This is a further advantage in terms ofenergy consumption because the cell potential remains low. In this capacitive voltage range, it has been shown that an increase in the applied potential from the open circuit (OC) to 600 mV involved increases in the rate and capacity of AO7 electrosorption into ACF (OC: 1.12 mmol g^{-1}, 200 mV: 1.17 mmol g^{-1}, 400 mV: 1.39 mmol g^{-1}, and 600 mV: 1.84 mmol g^{-1})) (Fig. 10b) (Han et al., 2008). Similarly, an intensification of polarization caused an increase in the percentage of BA electrosorption onto ACC (OC: 52%, -200 mV: 50%, -600 mV: 44%, -900 mV: 15%, +200 mV: 72%, +600 mV: 75%, +900 mV: 74%). This was explained by an amplification of the electrostatic interaction between the ACC surface (positively charged) and benzoate anion (negatively charged) with rising potentials (Bayram & Ayranci, 2012a).

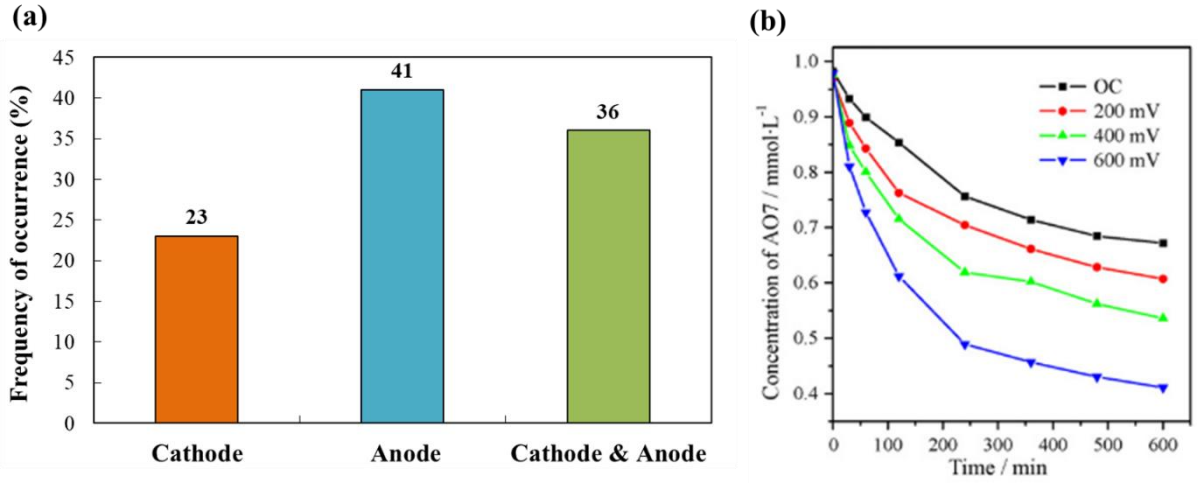

Fig. 10. (a) Occurrence percentages of electrode polarity configurations tested for electrosorption in the literature, (b) effect of the working electrode potential on AO7 electrosorption (Han et al., 2008).

2.2.2. Physico-chemistry of the electrolyte solutions

2.2.2.1 Type and concentration of the inorganic electrolyte

In most synthetic solution studies, an inorganic supporting electrolyte is added to increase the electrical conductivity of the wastewater to be treated (Koparal et al., 2002; Han et al., 2006b; Gerçel, 2016). Although electrolytes should not be added in the context of wastewater depollution to avoid external contamination, studies in their presence have emphasized the antagonist role of the electrosorption efficiency in organics according to their types and concentrations.

It has been highlighted that the equilibrium electrosorption capacity of phenol on ACF was reduced, whereas the electrosorption rate was enhanced with increased sodium sulfate (Na_2SO_4) electrolyte concentration from 1 to 100 mM (Han et al., 2006b). In addition, Na_2SO_4 increased the solution conductivity, which contributed to an increase in ion transport. However, the adsorption sites for phenol on the surface of the adsorbent were occupied by the competitive electrosorption of the Na_2SO_4 electrolyte (Han et al., 2006b). Similar results have been obtained in other studies involving the electrosorption of aniline on ACF in Na_2SO_4 electrolyte (Fig. 11a) (Han et al., 2006a), of 2,4-dichlorofenoxyacetic acid on ACC in Na_2SO_4 electrolyte (Bayram et al., 2018), and of acilan blau dye on AC-perlite mixtures in sodium chloride (NaCl) electrolyte (Han et al., 2006b). This trend was confirmed by the study of 1-adamantanol in the presence of halide (F^-, Cl^-, Br^-)-based electrolytes. This further

emphasized the decrease in the organic adsorption when the electrolyte concentrations increased from 5 to 100 mM, regardless of the types of halide anions (Stenina et al., 2001). It was thus reported that organic-inorganic attraction could occur during concurrent adsorption, which the strong hydrogen bonds could explain between the OH^- group of the organic compound and the halide anions.

The effect of the electrolyte type on the electrosorption efficiency was more emphasized by Gerçel (2016), who compared two different electrolytes, either sodium nitrate ($NaNO_3$) or Na_2SO_4, for the electrosorption of burdem orange II textile dye by using AC prepared from a waste material. The highest dye removals of 95% and 88% were achieved with 0.2 M Na_2SO_4 and 0.2 M $NaNO_3$, respectively. The differences in removal percentages could be attributed to the different hydrated radii and valences of the electrolyte, regardless of the initial solution concentration (Gerçel, 2016).

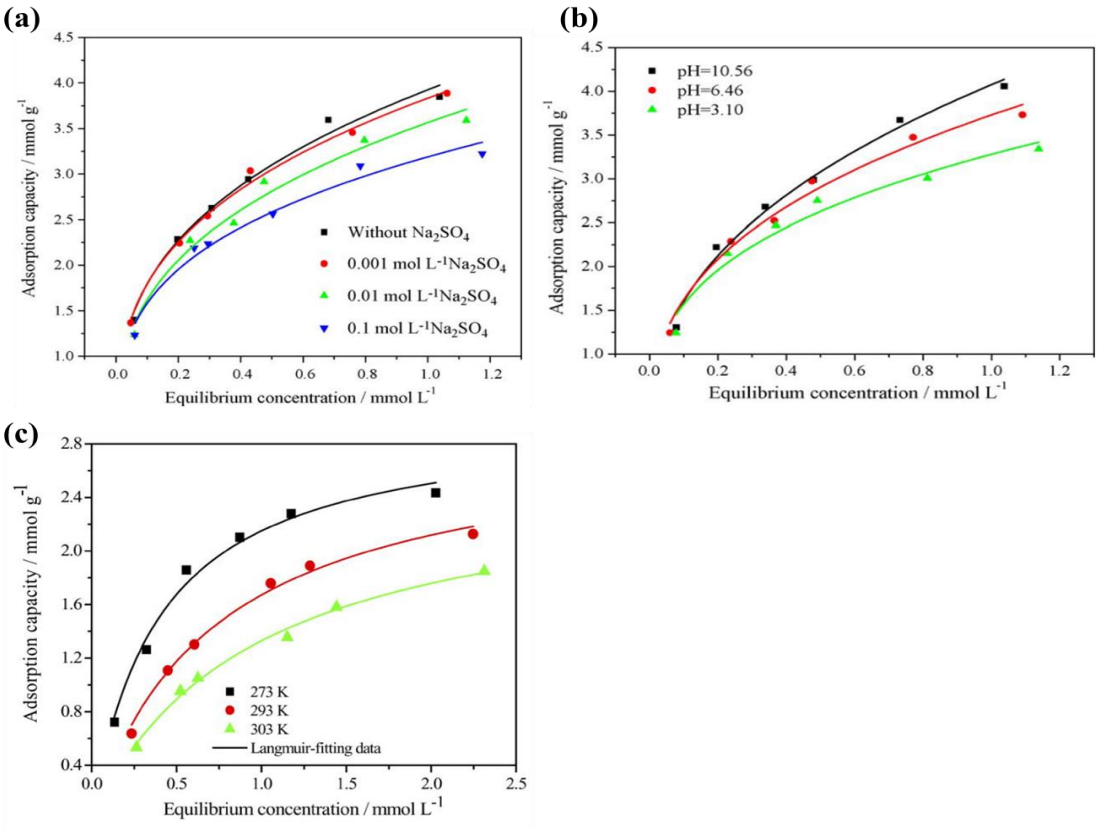

Fig. 11. Effect of (a) the initial concentration of the electrolyte on aniline electrosorption in the Na_2SO_4 electrolyte (Han et al., 2006a), (b) pH on the aniline electrosorption (Han et al., 2006a) (c) temperature on the phenol electrosorption (Han et al., 2006b).

2.2.2.2 pH

The initial pH of the electrolyte solution is an important factor since it can influence the ionization state of the outer electrode surface and the surface electrical charge characteristics of pollutants, as well as the electrosorption mechanism. Therefore, it also influences the electrosorption capacity of the organic compounds.

Table 3 summarizes the optimum pH for various organic pollutants whose acid dissociation constants (pKa) have been reported. The effect of pH within the range of 4 to 12 on the electrosorption capacity of cresol red using electrodes made of stainless steel wire coated with a nonconductive polymer was studied (Wang et al., 2012). Compound electrosorption was optimal at pH 6.0 due to the respective protonation and deprotonation of cresol red in acidic and basic media considering its pKa values of 0.5 (pKa_1) and 8.5 (pKa_2). Protonation in a strong acid medium would lead to the molecular ionization of cresol red, which explains the weak electrosorption in acidic media. Conversely, deprotonation would lead to the electrosorption of cresol red anions. The influence of the initial pH values covering a range from 3.1 to 10.6 on aniline (pKa = 4.6) electrosorption on ACF was also investigated (Han et al., 2006a). The electrosorption capacity of aniline rose with an increasing pH, as shown in Fig. 11b. This was attributed to the electrostatic interaction caused by protonation or deprotonation according to the pH changes, but could also be due to the electron donor ability of the amino group that increased in a basic solution. Similar results have been obtained in other studies regarding the electrosorption of aniline (Chai et al., 2007) and mercury (II) acetate (Jayson et al., 1987).

In contrast, the electrosorption capacity decreased with an increasing pH from 4 to 12 when bentazone (pKa = 3.3) was removed from aqueous solutions using an ACC electrode (Ania & Béguin, 2007). This trend was due to the pH dependence of the charges on the carbon cloth surface and the bentazone ionization. At an acidic pH, the bentazone is mainly nondissociated, and all acidic groups are protonated (neutralization of the negative charges), which minimizes the repulsive electrostatic interactions, and the electrosorption is improved. At a higher pH, the anionic form predominates in the solution, which implies a weaker interaction of the carbon cloth surface with deprotonated bentazone than with its neutral form. Similarly, the electrosorption of BA was lower at a basic pH than at an acidic pH, which was ascribed to the competition between the benzoate (formed at basic pH) and OH^- anions for the

positively charged ACC anode material (Bayram & Ayranci, 2012b). A similar trend was obtained with the electrosorption of thiocyanate (pKa = 0.5) (Rong & Xien, 2005, 2009), benzene (pKa = 43) (Heiland et al., 1966), naphthalene sulfonic acid (pKa = 0.2), benzyl alcohol (pKa = 15.4), naphthoic acid (pKa = 4.2), methylquinolinium chloride (Bán et al., 1998) and burdem orange II (pKa = 11.4) (Gerçel, 2016) (Table 2).

Table 2. Optimal initial solution pH during the electrosorption of selected pollutants.

Pollutant	pH range	Optimum pH	pKa	Reference
Cresol red	4.0 – 12.0	6.0	$pKa_1 = 0.5$; $pKa_2 = 8.5$	(Wang et al., 2012)
Bentazone	2.0 – 7.0	2.0	3.3	(Ania & Béguin, 2007)
Aniline	3.1 – 10.6	10.6	4.6	(Han et al., 2006a)
Thiocyanate	0 – 11.0	3.0	0.5	(Rong & Xien, 2005)
Burden orange II	2.0 – 6.5	2.0	11.4	(Gerçel, 2016)
BA	2.93 – 10.54	4.28	4.2	(Bayram & Ayranci, 2012b)
Phthalic acid		3.98	$pKa_1 = 2.92$; $pKa_2 = 5.41$	
NA		3.62	$pKa_1 = 2.05$; $pKa_2 = 5.81$	
Benzene	0.5 – 11.0	0.5	43	(Heiland et al., 1966)

2.2.2.3 Temperature

Generally, the temperature affects the electrosorption capacity. Many different enthalpies of adsorption (ΔH) values have been presented in the literature that attests to the variabilities of thermodynamic processes and the influence of temperature. For example, ethylene electrosorption on platinum was studied at temperatures varying from 303 to 343 K (Gileadi et al., 1965). The equilibrium adsorption constant was essentially independent of the temperature; consequently, ΔH equaled 0. In contrast, the electrosorption of phenol on ACF at three temperatures, 273, 293, and 303 K, was temperature-dependent (Fig. 11c) (Han et al., 2006b). The electrosorption process was more favorable at lower temperatures, and ΔH was negative, which showed that phenol was exothermally adsorbed by ACF. This further highlights that electrostatic interactions and dipole-dipole interactions might be the main adsorption mechanism for phenol electrosorption on ACF (Han et al., 2006b). The temperature also affected aniline electrosorption on the ACF electrolyte temperature varying

from 293 to 343 K (Chai et al., 2007). The electrosorption efficiency increased with an increasing temperature until reaching a peak at 313 K and then gradually decreased. This was due to the increase in the diffusion rate of aniline through the static aqueous layer at the fiber/solution interface. At temperatures higher than the optimal value, the efficiency did not increase since aniline electrosorption was an exothermic process (Chai et al., 2007). Another study varied the temperature of the electrolyte from 283 to 323 K for butanol and 1-oxyadamantane electrosorption (Stenina et al., 2009). An increase in the temperature led to an increase in the capacitance from 4.9 to 5.5 μF cm^{-2}, resulting in the electrosorption efficiency (Stenina et al., 2009). Thus, the increase in the temperature either decreased or increased the electrosorption capacity, according to the nature of the pollutants and the active sites on the electrodes.

2.2.3. Types of organic pollutants, their co-sorption, and the initial concentration effects

According to the papers reviewed, 92% of the electrosorption studies focused on aromatic compounds, while only 8% focused on aliphatic pollutants (Fig. 12a). Surprisingly, 100% of the articles dealt with artificial contamination. This highlights the crucial need to deal with actual wastewater to consider other matrix effects in the electrosorption efficiency, such as competition with co-sorption, clogging, etc.

In real matrices, the presence of multiple compounds is unavoidable; therefore, co-sorption studies remain essential. Several articles focused on these aspects, but in simulated wastewater. The co-sorption effect in the presence of three organic pollutants (acid red 88, orange II, and MB) on a three-dimensional (3D) graphene aerogel electrode was studied (Sun et al., 2016b). The electrosorption rate of the dyes ranked as follows (with an increasing rate): acid red 88 < orange II < MB (Fig. 12b). This was inversely correlated with the size of the dye molecules (with increasing size): MB < orange II < acid red 88. Thus, smaller molecules would find more pores accessible for electrosorption. The influence of the charge of the dyes must also be considered because it affects the electrostatic force between the adsorbent and the molecules and controls the electrosorption process. For instance, π–π interactions have been shown to play an important role since dyes with more aromatic rings showed stronger interactions with the adsorbent (Sun et al., 2016b). In addition, the charge dipole and dispersion interactions between the adsorbent and the aromatic organic acids have also

depicted an influence on electrosorption. The electrosorptive behavior of aromatic organic acids (i.e., benzoic, phthalic and NA) onto the ACC electrode was further examined (Bayram & Ayranci, 2012b). The rate constants of electrosorption of the acids decreased in the following order: NA > phthalic acid > BA (Bayram & Ayranci, 2012b). A more recent study schematized the material/solution interface in the presence of MB sorption on a prGO/SWCNT surface (Fig. 12c) (Yue et al., 2019b). In the absence of an electric current, i.e., under OC conditions, the dye randomly adsorbed on the material leading to a lower adsorption capacity. In contrast, the positively charged pollutant could adsorb onto the negatively charged material under cathodic polarization, which enhanced the sorption efficiency. The importance of the electrode potential and intermolecular interaction was also emphasized in co-electrosorption studies from Damaskin's group (Damaskin & Baturina, 1999; Stenina et al., 2001; Damaskin & Baturina, 2001a, 2001b; Damaskin et al., 2003; Damaskin, 2008; Damaskin, 2009, 2011). Furthermore, all these trends corroborated the behavior at the electrode/electrolyte interface. The characteristics of anions and cations (e.g., radii, interactions with solvent, charge, etc.) of the electrolyte have been identified as the key role parameters for controlling the distribution and concentrations of ions in EDL, and therefore greatly impact the electrosorption efficiency (Kornyshev, 2007; Waegele et al., 2019).

The influence of the initial concentration of organic compounds on the electrosorption efficiency has been widely reported in the literature, especially in batch mode configurations. The electrosorption efficiency was studied by varying the initial MB concentration from 10 to 600 mg L^{-1} (Yue et al., 2019b). The increase in the pollutant concentration up to 100 mg L^{-1} led to an increase in the electrosorption capacity at a given time and thereafter remained constant at higher initial concentrations. Similarly, in a kinetic study it was observed an increase in the rate of metribuzin electrosorption on GAC with an increase in the initial concentration from 0.23 to 2.1 mmol L^{-1}, leading to a higher capacity at identical times (Kitous et al., 2009). Similar trends have been obtained with the electrosorption of acilan blau dye (Koparal et al., 2002), phenol (Han et al., 2006b), AO7 (Han et al., 2008), β-naphthol (Eisinger & Alkire, 1980), AO8, AY14, AR151 (Sahin et al., 2020), bentazone (Ania & Béguin, 2007), naphthalenesulfonic acid, benzyl alcohol, naphthoic acid, methylquinolinium chloride (Bán et al., 1998) and MB (Fig. 12d) (Nainamalai et al., 2018). These studies were performed in batch mode, meaning that not only the kinetics of

electrosorption were quicker, but also the capacities were higher with an increasing initial concentration. This is formally disclosed with isotherm models discussed in section 2.6.1 of part I. This trend might be explained by the decrease in the driving force of the concentration gradient of pollutants toward the surface of the working electrode during an increase in loading rate (Han et al., 2006b). Moreover, the affinity between the pollutant and the electrode surface was significantly increased by polarization, allowing the enhanced adsorption capacity of pollutants on the electrode (Yue et al., 2019b). Furthermore, different EDL behaviors at high concentrations of organic electrolytes have been highlighted since conventional concepts of EDLs, such as the Gouy-Chapman-Stern representation, remain suitable only for diluted media. In dense mixtures, nonlinear polarization at the interface has been noticed, while a capacitance-voltage dependence was emphasized (Bazant et al., 2011). At a low voltage, a so-called overscreening model is assumed, which is formed by a monolayer of ions and an excess of counterions in the second monolayer (Fig. 12e) (Bazant et al., 2011). In contrast, at a medium voltage, there is a condensed layer formation of counterions, and at even higher voltages, complete lattice saturation is expected (i.e., the formation of two monolayers at the interface), which is defined as the crowding model (Fig. 12e) (Bazant et al., 2011).

From a practical point of view, the continuous mode is preferred, and the variation in the initial concentration will mainly affect the kinetics of electrosorption, while the maximum capacity of the adsorbent can be reached by adapting the contact time. Furthermore, the reactor volume and/or the adsorbent quantity can also be adjusted to reach the maximum electrosorption efficiency, as discussed in section 2.2.4 of part I.

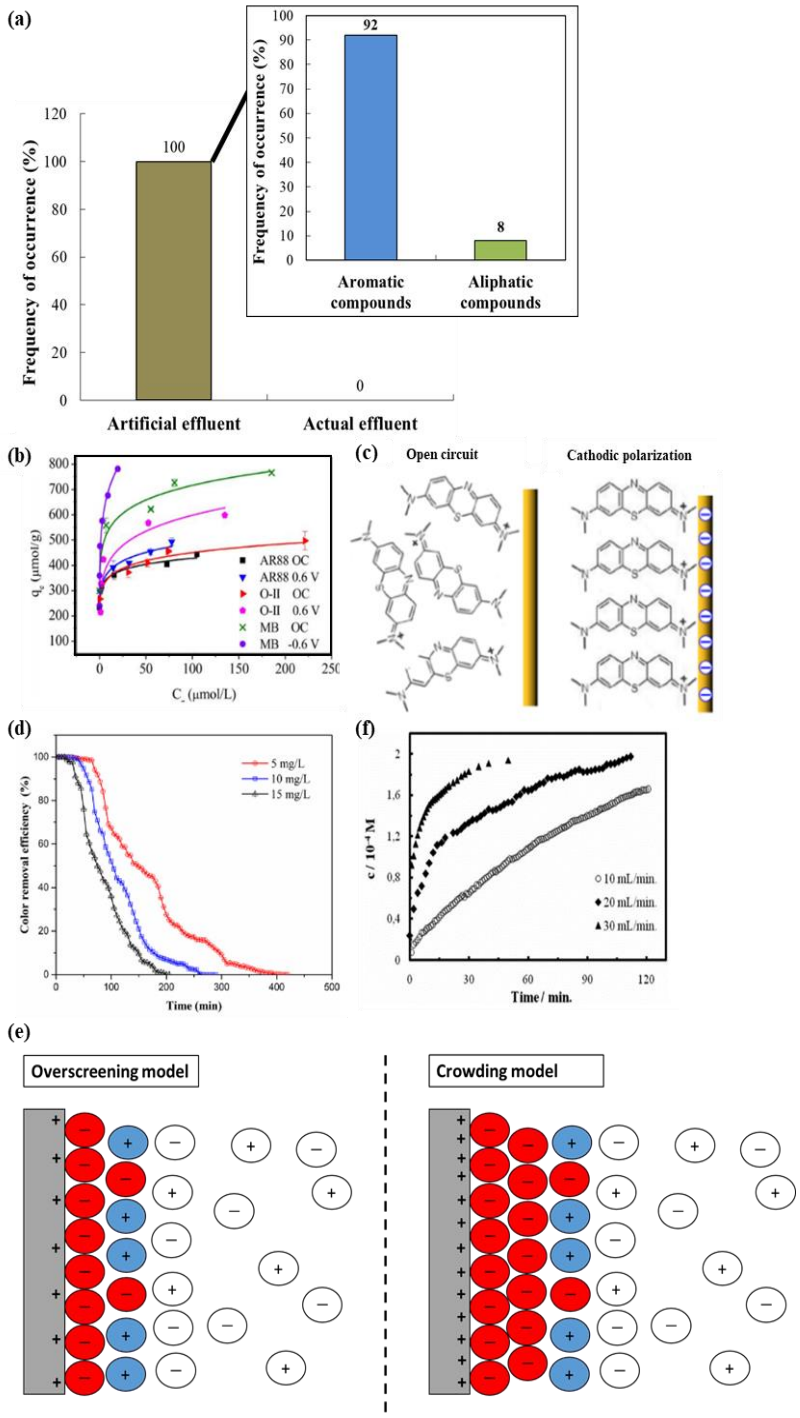

Fig. 12. (a) Type of effluent studied in the literature, i.e., artificial or real contamination and the presence of either aromatic or aliphatic compounds during electrosorption processes, (b) effect of acid red 88, orange II, and MB co-sorption (Sun et al., 2016), (c) schematic representation of MB molecule orientation on the prGO/SWCNT surface (Yue et al., 2019), (d) influence of the initial concentration on MB electrosorption (Nainamalai et al., 2018), (e) overscreening versus crowding models of EDL in the presence of concentrated electrolyte (e.g., ionic liquids) (Bazant et al., 2011), (f) impact of the flow rate on 2,4-dichlorophenoxyacetic acid electrosorption (Bayram et al., 2018).

2.2.4. Residence time, flow rate, reactor volume, and adsorbent load

The electrosorption efficiency is also controlled by the residence time and volume flow rate, which are related to the reactor volume. All previous works reported an enhancement in the electrosorption capacity with an increasing residence time and a decreasing flow rate by maintaining the contact of the pollutants with the active sites of the porous electrode. For example, a decrease in the MB electrosorption onto AC was reported with increased flow rates from 3 to 9 mL min^{-1} (Nainamalai et al., 2018). Similar trends have been observed with 2,4-dichlorophenoxyacetic acid (Fig. 12f) (Bayram et al., 2018), acilan blau dye (Koparal et al., 2002), burden orange II (Gerçel, 2016), BA and NA (Bayram, 2016), metribuzin (Kitous et al., 2009) and BA (Bayram & Ayranci, 2012a) electrosorptions. It was assumed that the EDL thickness at the polarized adsorbent surface decreased with an increasing flow regime (Bayram et al., 2018). Consequently, the specific double-layer capacitance (C_{DL}) value was reduced along with the electrosorption capacity.

The adsorbent load is another way to increase the electrosorption capacity. The influence of the bed heights, and therefore the adsorbent load, on MB electrosorption was studied (Nainamalai et al., 2018). When the bed height increased from 3 to 9 cm, the MB electrosorption capacity increased from 54 mg g^{-1} to 81 mg g^{-1} caused by an increase in the residence time and the accessible binding sites. Similar trends have been obtained with the electrosorption of β-naphthol (Eisinger, 1983) and acilan blau dye (Koparal et al., 2002).

2.3.Reactor design

An ideal reactor design for electrosorption needs to meet the requirements to make full use of the electrode surface area while minimizing the mass transfer limitations and maintaining a homogeneous potential distribution. The typical reactor designs developed in generally applied electrochemistry have been tested for electrosorption (Table 1). They include systems with fixed-bed or fluidized beds, flow-by or flow-through parallel plate cells and stirred tank reactors (STRs). According to the reviewed papers (Table 1), fixed-bed reactors have been more implemented for organic electrosorption (43%), followed by the flow-through parallel-plate cell design (21%) (Fig.13). This could be attributed to their adapted design when porous electrode materials are employed. This then enhances the efficiency by benefitting from the internal surface area.

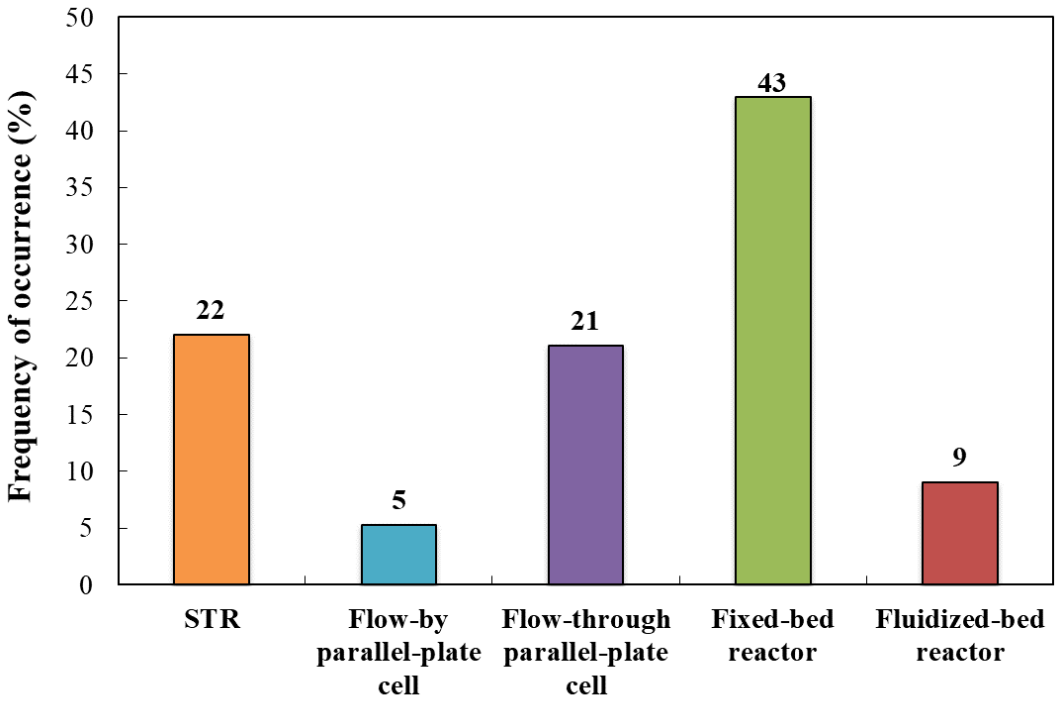

Fig. 13. Occurrence frequency of different electrosorption reactor designs found in the literature.

The reactor design description and their comparison are described as follows, while Table 3 summarizes the advantages and drawbacks of each type of reactor design. Further detailed information regarding the electrochemical reactor design performance for general applications can be found in prominent textbooks in the field (Newman, 1968; Pletcher & Walsh, 1982; Goodridge & Wright, 1983; Cœuret & Storck, 1984).

In STR, the electrode materials are placed in parallel, and the solution is magnetically (lab-scale) or mechanically (pilot-scale) stirred in a tank (Fig. 14a) (Monteil et al., 2019; Mousset & Dionysiou, 2020). The STR configuration was implemented most of the time in batch mode, as opposed to continuous mode. Thus, the STR can be useful for laboratory batch studies, especially for troubleshooting or development works. However, mass transfer is the worst in these systems. This also leads to a higher foot print area due to theelectrode's higher required total surface area. Consequently, an alternative reactor design is preferred for commercial use.

Conventional flow-by and flow-through parallel plate cells have typically been proposed (Figs. 10b and 10c). Two configurations are possible concerning the direction of the effluent flow with respect to the direction of the current flow. In the flow-by cell, the current

and flow of the effluent are perpendicular (Adnan, et al., 2021). The effluent circulates between the electrodes, with a variant with a "channel", similar to a flow-by cell in series, i.e., a succession of cathode and anode materials (Mousset & Dionysiou, 2020). In the flow-through cell, the current and flow of the effluent are parallel, and the effluent flows through the porous electrode. This electrode is considered to be thin, which does not constitute beads or particles, and differentiates the flow-through cell from a "bed reactor". An advantage of parallel-plate cells is that they can be implemented in stacks of cells arranged in series and/or in parallel in order to enhance the conversion yield and/or the treatment capacity, respectively. This is adapted for applications at an industrial scale (Langlois & Cœuret, 1990; Kakhi, 2009). The flow-through cell has a distribution of potentials that tends to be less homogeneous than in the flow-by cell. However, the flow-by cell induces mass transfer limitations compared to the flow-through cell, and has therefore been less implemented for electrosorption purposes (Fig. 13). Another possibility with parallel-plate design is the variation in the inter-electrodes distances that decreases the cell resistance and increases the mass transfer at a shortened gap, and affects the EDL behavior. In more conventional cells, i.e., at millimetric distances, it is considered that an excess charge can occur only at the surface of the material, according to Gauss theory. In nanofluidic thin-film cells, i.e., at nanometric gaps, the assumption of electroneutrality in the double layer may be inappropriate. This is because the OHP in EDL theory becomes highly dynamic due to very high mass transport rates of redox ions (Fan et al., 2014).

In parallel, fixed- and fluidized-bed reactors have been suggested as substitute designs. They consist of systems where the effluent is circulating through a bed constituted by a volume electrode, i.e., a 3D porous polarized material (Figs. 10d-10g). In the fixed-bed reactor, the electrode particles are all in permanent contact, which defines a monopolar connection mode. In this case, the particulate electrodes constitute a single electron-conducting particle that is either completely positively (anode) or negatively (cathode) charged (Goodridge & Wright, 1983). In the fluidized-bed reactor, the electrode particles are not in contact with each other, which leads to a bipolar mode (López-Bernabeu et al., 2016). This means that one side of each particle is positively charged, while the other side of the particle is negatively charged (Goodridge & Wright, 1983). Most of the time, these bed designs are akin to column reactors. Two configurations can be proposed according to the direction of the electric current compared to the hydraulic flow direction. In co-current mode,

they are both parallel (Figs. 10d and 10f), while in counter-current mode, they are perpendicular (Figs. 10e and 10g). The co-current condition is useful for testing different porous materials in lab-scale studies (Coeuret, 2003). However, this configuration has not been adapted for a larger scale because of the low applied flow rate range. In contrast, the counter-current approach is compatible with industrial-scale applications due to the possibility of arrangements in series and parallel (Coeuret, 2003). Additionally, the electrode performance is mainly governed by diffusion polarization in the fixed-bed electrode (Matsuno et al., 1996). This phenomenon is minimized in the fluidized-bed electrode due to the high mass transfer rate induced by the turbulence of the moving particles (Matsuno et al., 1996). However, the fluidized-bed reactor exhibits a number of inherent limitations. The most significant drawback is the range of spatially distributedpotentials within the bed, leading to a high heterogeneity distribution. In addition, the effective resistance of the particle phase in the fluidized-bed electrode was found to be three to four times greater than that of the fixed-bed device (Matsuno et al., 1996). Moreover, the conditions under which the fluidized bed is operated are often unknown (Cheng et al., 2020).

Nevertheless, the fixed-bed presents numerous advantages over other reactor designs, such as very high mass transfer intensification, a high specific area of the working electrode, and feasibility of electrosorption processes for the large-scale plant. This justifies why it has been studied more (Fig. 13).

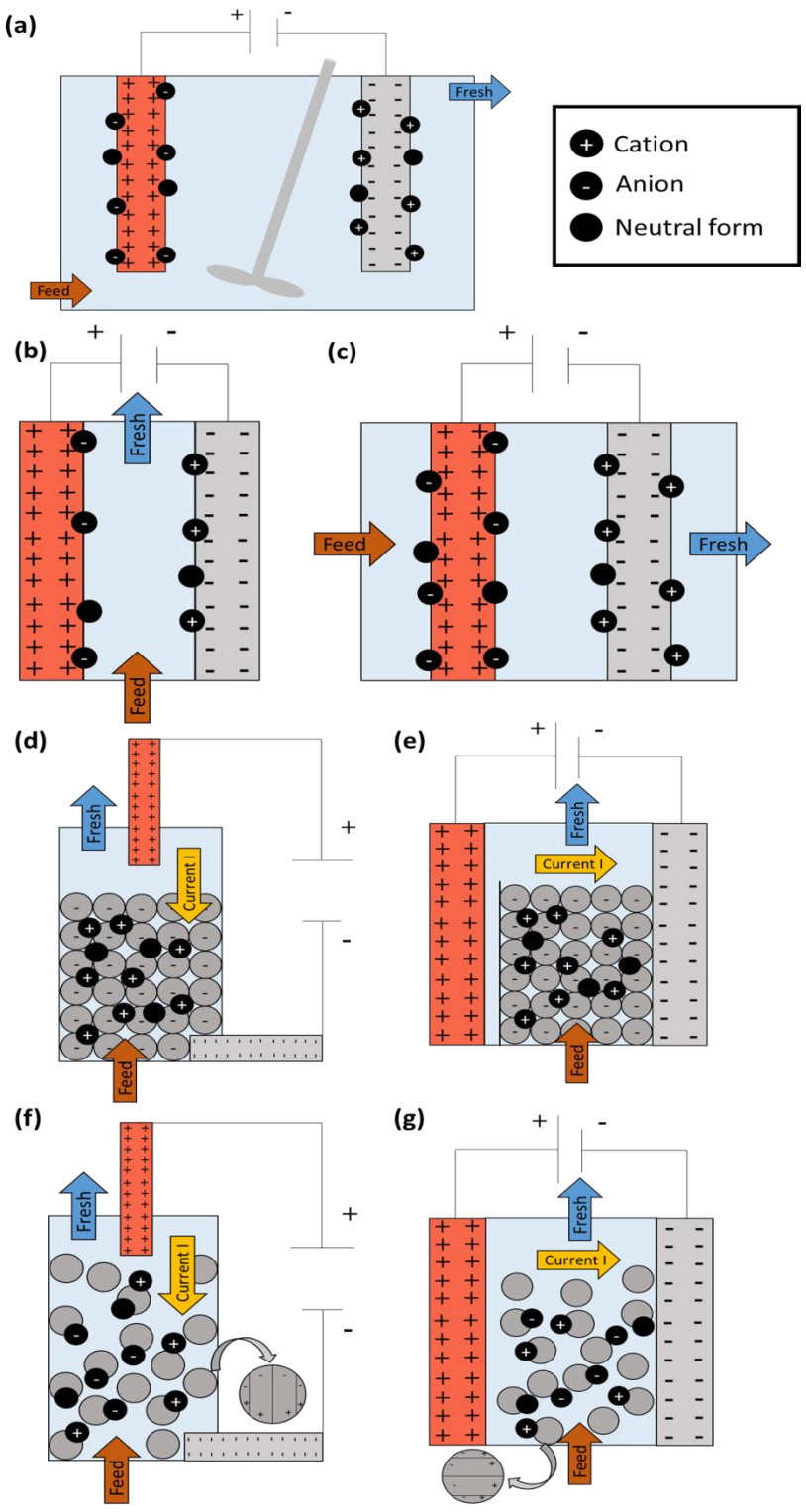

Fig. 14. Scheme of the main electrosorption reactor designs applied in the literature: STR (a), flow-by (b) and flow-through (c) parallel-plate cells, fixed-bed reactor (d, e) and fluidized-bed reactor (f, g) arranged in co-current (d, f) and counter-current (e, g) configurations.

Table 3. Advantages and drawbacks of the different types of reactor designs implemented for the electrosorption of organic compounds.

Reactor design	Advantages	Drawbacks
STR	● Easy to manufacture ● Flexibility to meet different treatment objectives	● Limitations for industrial scale development ● High mass transfer limitations ● Require a higher conductivity of solutions (often needs a supporting electrolyte added) ● High footprint area
Flow-by parallel-plate cell	● Regenerate electrodes ● Offers the operational flexibility of a variable flow rate and conversion ● Easy control of interelectrodes gap ● Industrial scale applicability by implementation in stacks of cells arranged in series and parallel ● Good homogeneity of current and potential distributions	● Mass transfer limitations
Flow-through parallel-plate cell	● Regenerate electrodes ● Enhancement of mass transfer ● Easy control of interelectrodes gap ● Industrial scale applicability by implementation in stacks of cells arranged in series and parallel ● Suitable for effluent with low target compounds concentrations and low electric conductivity	● Low flow rates range ● Clogging effect ● Pressure drop
Fixed-bed reactor	● Enhancement of mass transfer ● Easy operating conditions ● High treatment capacity ● Industrial scale applicability ● High intragranular	● Higher energy requirements ● Clogging effect ● Pressure drop

	electric conductivity ● Suitable for effluent with low target compounds concentrations and low electric conductivity	
Fluidized-bed reactor	● Rapid mixing rate of the bed solids ● Easy operating conditions ● Treatment of municipal and industrial wastewaters with concentrations up to a ppb level ● High treatment capacity ● Industrial scale applicability ● Limit clogging effect	● Higher energy requirements ● Low intra-granular electric conductivity ● High heterogeneity of current and potential distributions ● Low acquisition of knowledge about operating parameters (conductivity, potential, etc.) for kinetic modeling

2.4.Factors influencing the electrodesorption step

An electrodesorption step is required to recover the electrosorbed pollutants for either subsequent degradation or valorization. This further facilitates the regeneration of the porous electrode material for successive electrosorption cycles, as discussed in more detail in section 2.5 of part I (Bain et al., 2010). It consists of reversing the electrode polarity, and the charged contaminants are then released from the interface and diffuse back into the bulk solution (McQuillan et al., 2018).

Electrode polarity and applied current or potential value are the main factors governing the electrodesorption efficiency. For instance, the desorption study of ethylenediamine from AC at a more positive potential (0 V/SCE) than for the electrosorption step (-0.5 V/SCE) provoked significant electrodesorption of the ethylenediamine back into the solution (Eisinger & Keller, 1990). However, the recovery was not complete, as it was approximately 66%, which was attributed to irreversible electrosorption of a fraction of the organic compound on the most active sites. Similarly, thiocyanate anions were desorbed from AC by applying a negative polarization and then neutralizing or basifying the solution pH (Rong & Xien, 2009). Thus, the pH can also play a role in the desorption process according to the pKa of organic compounds. Another parameter that has been shown to influence the desorption efficiency is the solvent. The increase in methyl quinolinium chloride desorption from AC was due not only to the increase in the potential from 0 mV/(Ag/saturated KCl) to 600 mV/(Ag/saturated

KCl), but also to the use of methanol instead of water (Bán et al., 1998). A desorption increase of more than one hundred times was attributed to the use of methanol while keeping the applied potential lower (200 mV instead of 600 mV) (Bán et al., 1998). Methyl quinolinium has a higher affinity toward methanol than water and was preferentially desorbed with the organic solvent. This latter feature might be an approach for subsequent organic compound valorization, but not for their degradation and mineralization, as organic solvents constitute a supplementary source of pollution.

2.5.Long-term efficiency of electrosorption

The regeneration and long-term efficiency of porous electrodes in a given system are also important indicators when evaluating the electrosorption performance of materials and are even more crucial in practical applications in terms of economic viability (Han et al., 2008; Bayram & Ayranci, 2012b; Yue et al., 2019b). Table 4 reports successive electrosorption cycle studies with organic compounds reported in the literature. The electrosorption efficiency decreased by 77% with the ACC electrode after three successive cycles by using a fresh solution at each cycle (Bayram & Ayranci, 2012a). In contrast, the same electrode could maintain efficiency after the same number of cycles by reversing the polarity each time (Bayram & Ayranci, 2012b). Thus, a desorption step seems to be required before any additional electrosorption cycle in order to increase the electrode reusability and its long-term efficiency. Similarly, a 30% decrease in the ACF efficiency was observed for the first three cycles, while the electrosorption capacity remained constant during the seven subsequent cycles (Han et al., 2008). The decrease was associated with the irreversible electrosorbed fraction of organic compounds in the micropores that could not be regenerated. The microporosity of the electrode can therefore be a drawback for compound desorption and full regeneration of the material, although it is an advantage for its electrosorption. In another study, the electrosorption capacity of the prGO/SWCNT film was still as high as 1170 mg g^{-1} (a 3% increase) after ten successive cycles (Yue et al., 2019b). The slight increase in performance could be attributed to enhancingthe wettability and material activation after prolonged electrode polarization.

Table 4. Successive electrosorption cycle studies with organic compounds reported in the literature.

Working electrode	Organic pollutant	Number of successive cycles	Electrosorption capacity	Reference
prGO/SWCNTs film	MB	10	1st cycle: 1133 mg g^{-1} 10th cycle: 1170 mg g^{-1} (3% increase)	(Yue et al., 2019b)
ACF	AO7	10	1st cycle: RE* = 95% 10th cycle: RE* = 70% (26% decrease)	(Han et al., 2008)
ACC	BA, phthalic acid and NA	3	1st cycle: 15 mmol g^{-1} 3rd cycle: 15 mmol g^{-1} (0% decrease)	(Bayram & Ayranci, 2012b)
ACC	BA	4	1st cycle: 77.5 mmol g^{-1} 4th cycle: 5 mmol g^{-1} (93% decrease)	(Bayram & Ayranci, 2012a)

*RE: regeneration efficiency percentage

2.6.Modeling

In addition to the electrosorption parameters, mathematical modeling of the electrosorption process can be an effective tool for understanding the mechanisms involved, optimizing the system, predicting the efficiency, designing the reactor, and increasing the scale via dimensional analysis. Over the years, many electrosorption models have been developed, but these models remain more challenging than those for adsorption reactors due to the involvement of an electric current in the transfer phenomena and reactions. The main models to improve the operating strategies for electrosorption are briefly presented from batch to continuous modes. Dimensionless numbers and scaling considerations are also discussed.

2.6.1 Modeling in batch and continuous modes

Kinetics provides information about the residence time required for the completion of electrosorption. Thus, it constitutes the basis to determine and predict the performance of systems during the optimization step in batch mode and for the subsequent scale-up phase. The kinetic data for electrosorption of many organic species onto carbon electrodes fit quite well with the pseudo-first-order kinetic model (Ayranci & Conway, 2001; Han et al., 2006b; Bayram & Ayranci, 2012a, 2012b). However, since high surface areas of the electrodes (e.g.,

porous carbon materials) are used most of the time in electrosorption, the kinetic rate is often limited by the electric current and not by diffusion. This could explain the good fitting with the pseudo-first-order model (Ayranci & Conway, 2001; Han et al., 2006b; Bayram & Ayranci, 2012a, 2012b).

The electrosorption isotherm remains a typical studied behavior. Numerous propositions have been made to formalize the electrosorption isotherms mathematically. The model that better fits the experimental data obtained in the electrosorption of organic compounds was the Freundlich isotherm (Wang et al., 2012; Biniak et al., 2013; Sahin et al., 2020). It can be explained by organic electrosorption onto carbon electrodes that occurs on a heterogeneous surface with a continuum of electrosorption sites with different ΔH_{ads} values.

Dynamic models, also known as breakthrough curves, have been proposed to explain the design performance and ensure the successful operation of electrosorption in continuous mode. The Adam Boharts, Thomas and Yoon-Nelson models are the main dynamic models tested in the literature regarding the electrosorption of organic compounds (Nainamalai et al., 2018).

2.6.2 Dimensionless numbers and sizing considerations

In general, a dimensional analysis combined with a similarity assessment is commonly used to scale up electrochemical reactors by keeping dimensionless numbers constant for better and faster optimization. Table 5 summarizes the main dimensionless numbers employed in the literature regarding electrosorption processes. Three dimensionless numbers are well known to relate the hydrodynamic conditions by involving the mass-transport coefficient: the Reynolds number (*Re*), the Schmidt number (*Sc*) and the Sherwood number (*Sh*) (Ibl, 1959; Vilar & Cœuret, 1999; Cañizares et al., 2006; López-Bernabeu et al., 2016). The mass transfer Biot number (Bi_m) is an additional number that allows considering the difference between the internal and external mass transfers rates in porous media (López-Bernabeu et al., 2016). Mass transport phenomena are important in terms of the efficiency of electrosorption systems. Numerous correlations, as well as the values of dimensionless numbers, have been proposed in the literature according to the type of electrochemical reactor design and to the operating conditions involved (Newman, 1968; Goodridge & Wright, 1983; Cœuret & Storck, 1984; Pletcher & Walsh, 1993). It is important to note that in a fixed-bed

reactor, the mass transport increases with the length of the bed and decreases with the diameter of the particles from the bed (Storck et al., 1975).

Another valuable parameter is the Wagner number (*Wa*), which represents the ratio between the polarization resistance of the electrode and the ohmic resistance in the electrolyte (Table 5) (Wagner, 1951). It also defines the uniformity of the current density distribution and remains an essential feature when porous electrode materials are implemented (J. S. Newman & Tobias, 1962). It is well established that a drop in the potential is expected in porous polarized materials, which induces a heterogeneous distribution within the electrode. Therefore, a compromise needs to be made between a high surface area electrode for high electrosorption capacity (i.e., a large thickness of material), while keeping the potential distribution as homogeneous as possible for a good selectivity and efficiency (i.e., a small material thickness) (Coeuret, 2003). In practice, it is preferable to implement porous electrode materials with thicknesses in the direction of a current no higher than 0.5-1 cm while maximizing the material length instead of its thickness (Cœuret et al., 1976; Eisinger & Keller, 1990; Coeuret, 2003).

Dimensionless times have also been proposed in the literature, such as *G*, *T* and θ (Chue et al., 1993; Sene et al., 2019). *G* refers to the competition between the electrical potential wave and the sorption wave (Chue et al., 1993), whose value is compared to *T*, which is the reduced time (Chue et al., 1993). When $G<T$, the final potential of the porous material is more rapidly reached than the electrosorption equilibrium, while 90% of the final potential in the electrode is reached at $G = T$ (Chue et al., 1993). At $T>G$, the potential is almost constant in the material, and the concentration of the targeted compound(s) in the effluent begins to decrease. More recently, θ has been suggested as a dimensionless time to define the flow regime, i.e., either the permanent or non-permanent domains (Sene et al., 2019). It allows for estimating the optimal flow rate that will give an optimal charge transfer (Table 5).

Since fixed-bed reactors have been the most widely designed reactors applied in the literature for organic electrosorption (Fig. 13), it is interesting to present a method for scaling estimation. More details can be read in textbooks in the field (Newman, 1968; Pletcher & Walsh, 1982; Goodridge & Wright, 1983; Cœuret & Storck, 1984). A four-time-period method has been proposed to size fixed-bed reactors, namely, the residence time (τ_R) (Eq. 2),

breakthrough time (t_{BT}) (Eq. 3), diffusion time (t_D) (Eq. 4) and t_{dl} (Eq. 5) (Eisinger & Keller, 1990).

$$\tau_R = \frac{\varepsilon_B A d}{Q_V} \quad (2)$$

$$t_{BT} = (q_A - q_D)\rho_B \frac{Ad}{(C_{in} - C_{out})Q_V} \quad (3)$$

$$t_D = \frac{(\frac{d_p}{2})^2}{2D} \quad (4)$$

$$t_{dl} = a\varepsilon_B C d^2 \frac{(\kappa+\sigma)}{\sigma} \quad (5)$$

where ε_B is the bed porosity, d is the electrode thickness (cm), A is the cross-sectional area ($A = H \times W$, where H is the bed height and W is the bed width) (cm^2), q_D is the electrodesorption (at the desorption potential) capacity (mg g^{-1}), ρ_B is the bed density (g of material per cm^{-3} of bed)), C_{in} and C_{out} are the targeted compound concentrations in the inlet and outlet flows, respectively (mg cm^{-3}), Q_V is the inlet flow rate (cm^3 s^{-1}), a is the interfacial area per unit void volume (cm^2 cm^{-3}), C is the differential capacitance (F cm^{-2}), κ and σ are the effective electrolyte conductivity and electrical conductivity of the porous material, respectively ((Ω-cm)$^{-1}$), d_p is the particle diameter (cm), and D is the diffusion coefficient of the targeted compound (cm^2 s^{-1}).

For an optimal sizing, the following criteria must be considered (Eisinger & Keller, 1990):

$$t_{dl} \ll t_{BT} \quad (6)$$

$$t_D < \tau_R \ll t_{BT} \quad (7)$$

Equation 6 allows us to consider the fact that the bed needs to be completely charged at a given potential before reaching the maximum electrosorption capacity (Eisinger & Keller, 1990). Equation 7 avoids being limited by diffusion (Eisinger & Keller, 1990). At a given A and L, the procedure is first to estimate t_{dl} then t_{BT}, followed by the calculation of Q to be implemented (Eisinger & Keller, 1990). From Q, τ_R is evaluated, and the condition from Eq. 7 needs to be then verified (Eisinger & Keller, 1990).

There is a need to consider these dimensionless numbers for scale-up studies with dimensional analysis as this type of consideration is lacking in literature.

Table 5. Main dimensionless numbers involved in the literature about the electrosorption.

Dimensionless number	Equation	Signification
Re	$Re = \frac{u\, d_f}{\nu}$	Ratio between the inertial forces and viscous forces in the liquid. It defines the hydrodynamic regime (laminar or turbulent)
Sc	$Sc = \frac{\nu}{D_m}$	Ratio between the momentum diffusivity and the mass diffusivity. It defines the extension of the diffusion layer
Sh	$Sh = \frac{k_f L}{D}$	Ratio between the convective mass transfer rate and the diffusion rate
Bi_m	$Bi_m = Sh\ \frac{D}{D_e}$	Ratio of the rates of internal to external mass transfers
Wa	$Wa = \frac{\kappa d\eta}{L\, dj}$	Ratio between the polarization resistance of the electrode to ohmic resistance in electrolyte. It defines the uniformity of the current density distribution
G	$G = \frac{t_{dl}}{t_{st}}$	This defines the competition between the electrical potential wave and the sorption wave
T	$T = \frac{t}{t_{st}}$	Reduced time
Θ	$\theta = \frac{t_{sc}}{t_{t0}}$ with $t_{sc} = \frac{\Delta E}{sr}$ and $t_{t0} = \frac{L}{u}$	This defines the different flowing regimes, either the permanent or non-permanent domain

Abbreviations:

u is the linear velocity of the liquid through the void space of the adsorbent (m s^{-1}), $\nu$is the kinematic viscosity of the solution (m^2 s^{-1}), k_f denotes the external mass transfer coefficient (m s^{-1}), *L* is the characteristic length (m), *D* is the molecular diffusivity of the pollutant (m^2 s^{-1}), $D_e$is the effective diffusivity (m^2 s^{-1}), t_{dl} is the double layer charging time (s), $t_{st}$is the stoichiometric time of sorption (s), *t* is the reaction time (s), κ is the effective electrolyte conductivity ($(\Omega\text{-m})^{-1}$), is the overpotential (V), *j* is the current density (A m^{-2}), $t_{sc}$is the scan

time (s), t_{t0} is the turnover time (s), ΔE is the potential difference (V), and *sr* is the scan rate (V s^{-1}).

2.7.Current developments and future prospects

2.7.1 Current challenges to overcome

A general overview of the main factors and phenomena involved in the electrosorption efficiency is proposed and schematized in Fig. 15. This scheme allows for the identification of which parameters affect each phenomenon that then governs the electrosorption efficiency. The importance of the EDL and mass transport is influenced by most of the main parameters. Therefore, future efforts should be made to enhance both EDL and mass transport. The main output and future improvements in the electrosorption process efficiency are addressed as follows and determine part of the orientation of the PhD thesis:

- Electrode material: The high specific surface area of the material is insufficient to obtain a high electrosorption capacity since the pore size also appears to be a crucial parameter. The presence of mesopores tends to improve efficiency. Therefore, the specific surface area and the pore size distribution of materials should be determined before experiments to ensure a maximum electrosorption of the pollutants. Moreover, the material conductivity and wettability should not be neglected in the mechanisms. Material stability and reusability are other essential criteria for long-term use in practical applications. Existing studies lack life span and regeneration tests, which are representative of real conditions.

- Electrode potential and polarity: An optimal electrode potential is required for optimal electrosorption, while values that are too high or too low lead to faradaic reactions that need to be avoided. The electrode polarity plays a role in the electrosorption efficiency according to the types of targeted compounds, but the porous material can be damaged if it does not support either oxidative or reductive potentials. Carbon-based materials have been widely employed in electrosorption, although they can be easily corroded as anodes. Therefore, caution should be taken in the applied conditions to preserve the lifetime of the electrode material.

- Electrolyte concentration and properties: Although an increase in the electrolyte concentration increases the solution conductivity and, therefore the ohmic resistance, co-

sorption with either inorganic or organic compounds occurs. Thus, it can decrease the electrosorption of the targeted compounds as well as the selectivity. In addition, the pKa of organic compounds can influence their electrosorption efficiency and selectivity according to the solution pH. However, there is an important need to operate with more complex matrices until actual wastewater is tested in order to better assess the viability of the technique in experimentalconditions. Moreover, high concentrations of supporting electrolytes have often been added, which should be avoided in wastewater treatment.

- Reactor design: A fixed-bed reactor has been implemented the most extensively, which is ascribed to the high mass transfer, the high specific area of the porous electrode and the scale-up ability. A still pressure drop and clogging effect can occur with this type of reactor. A less conventional design that was recently proposed could also be tested by combining micro-reactors with macro-reactors to avoid these drawbacks (Mousset, 2020). Moreover, an adapted design should be used to operate with low solution conductivity without adding a supporting electrolyte.

- Modeling: Interface phenomena represented by EDL theory is still not well understood under specific conditions (e.g., highly concentrated electrolytes and dense electrolytes). DFT models are gaining an increasing interest. However, their single-use induces scale-level heterogeneity: the atomic level at the electrode surface is considered, while a simple continuum model for the electrolyte is taken into account without considering the discrete form (e.g., dipoles) (Schmickler, 2020). Complete models of the interfaces should describe electrons, solvents, ions and interactions between one another (Schmickler, 2020). Coupling DFT with molecular dynamics (Oleinick et al., 2019) or combining DFT with a reference interaction site model (Schmickler, 2020) have recently been suggested to obtain a complete overview of the mechanisms at the interface. Moreover, kinetic models in either batch or continuous modes should incorporate the matrix effect, the transport phenomena, and the physico-chemical properties of compounds on the electrosorption rates and yields of organics to better understand and predict the efficiency. This will further benefit scale-up studies that include dimensional analysis and a similarity assessment. This is an important tool to reach higher technology readiness level.

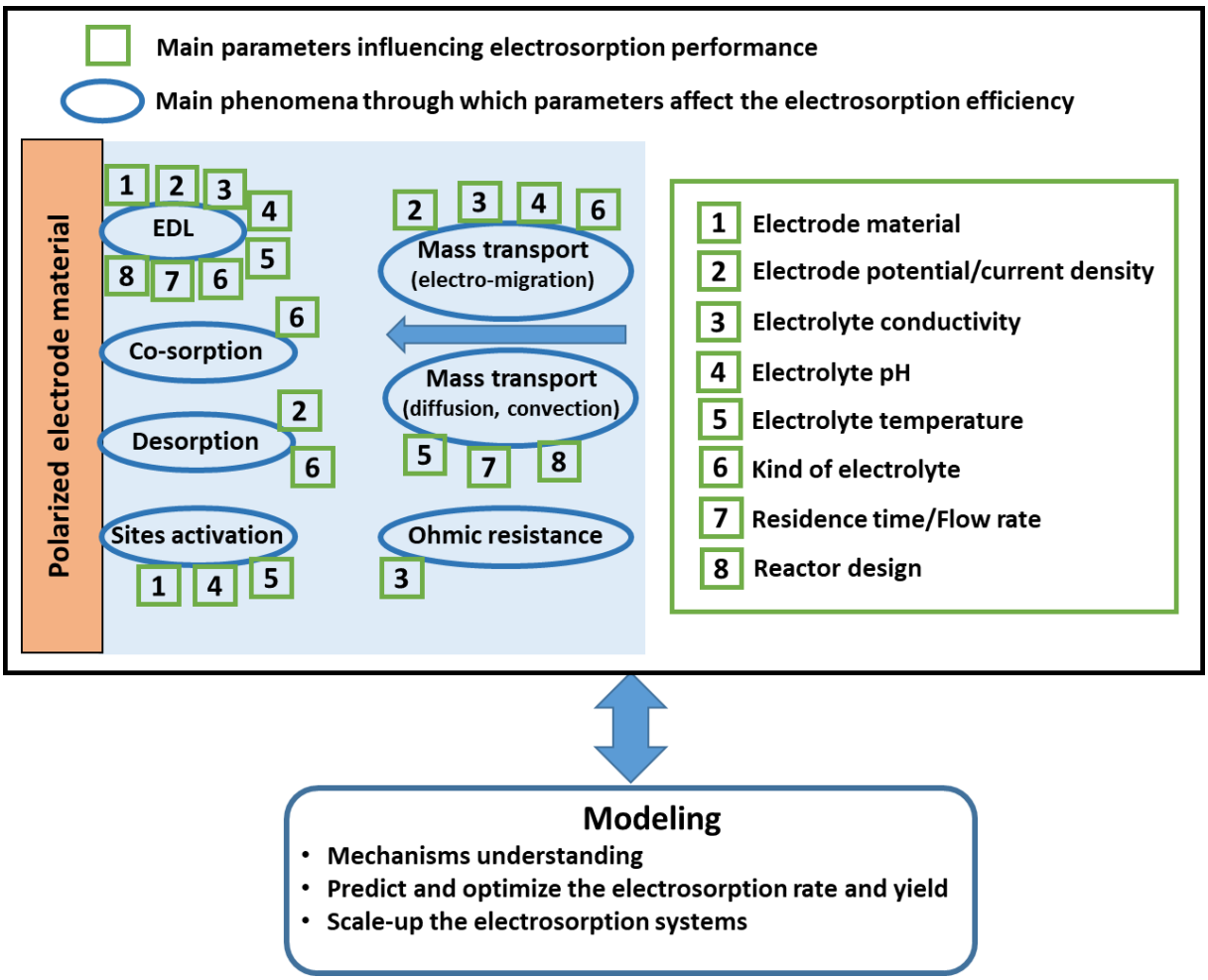

Fig. 15. General overview of the main parameters and phenomena involved in the electrosorption efficiency associated with a modeling approach.

2.7.2 Emerging processes combinations with electrosorption

Electrosorption was initially proposed for separation purposes to remove selected compounds from wastewater, but the treatment strategy could be extended. The recovery of added-value organic compounds in wastewater would be another option after optimizing the electrosorption and electrodesorption conditions for optimal selectivity. An alternative strategy would be to combine electrosorption as a separation technology with a degradation process required for a more integrated treatment of the wastewater. Many researchers studied emerging processes (photocatalytic, electrooxidation, electrically conductive ultrafiltration, electro-Fenton, advanced oxidation processes, electrocatalysis, peroxi-coagulation, solid-phase microextraction,...) combinations with electrosorption using several kinds of electrode materials for the removal of various organic pollutants (Jin et al., 2011a; Wang et al., 2013; Ayoubi-Feiz et al., 2014b, 2014c, 2018a; Chen et al., 2018; Fan et al., 2018a; Nie et al., 2019;

Xu et al., 2019; Mantel et al., 2021; Chai et al., 2021; Yang et al., 2021). Table 6 provides an overview of the main studies in literature illustrating these processes combination. It was noticed that the photoelectrocatalysis had been the most employed process in combination with electrosorption for the removal of nonylphenol (Fan et al., 2018b), alizarin red (Jin et al., 2011a), diazinon (Ayoubi-Feiz et al., 2018a), reactive yellow 39 (Ayoubi-Feiz et al., 2014b) and lanasol red 5B (Ayoubi-Feiz et al., 2014c). Electrooxidation/electroreduction processes have particularly demonstrated a high ability to remove pollutants from wastewater (Martinez-Huitle et al., 2015; Moreira et al., 2017; Mousset et al., 2018; Garcia-Rodriguez et al., 2020; Mousset & Doudrick, 2020; Trellu et al., 2021) by implementing a BDD anode with a high O_2 evolution overvoltage (Mousset et al., 2019; Nidheesh et al., 2019). The degradation and mineralization efficiencies are notably due to the involvement of hydroxyl radicals that have very high reactivity and quasi non-selectivity toward organic compounds (Brillas et al., 2009; Panizza & Cerisola, 2009; Mousset al., 2018). In combination with electrosorption techniques, the global performance is enhanced by maintaining a high degradation yield. For instance, electrooxidation combined with electrosorption was tested in the removal of BA (Chen et al., 2018), acyclovir and phenol (Nie et al., 2019), while the combination with peroxi-coagulation was investigated for the removal of Orange II (Yang et al., 2021). In addition, Chai et al. (2021) investigated the combination of electro-Fenton with electrosorption in removing toluene and trichloromethane (Chai et al., 2021). The authors used a flow-through electro-Fenton treatment (anode: pure iron and cathode: Ti mesh), followed by the electrosorption treatment (anode and cathode were ACF). The removal efficiency is 96% for COD, 98% for NH_3-N, and 46% for salinity under the optimal conditions (voltage intensity of 1.5 V, initial pH of 4, plate spacing of 1 cm, flow rate of 40 mL min^{-1}, H_2O_2 concentration of 50 mM). A similar study was performed by Wang et al. (2013) with imidacloprid. Another advantage of such combinations is the synergy obtained by limiting the amount of potentially formed toxic byproducts (e.g., chlorate and perchlorate), as recently published (Norra & Radjenovic, 2021). Therefore, these combinations seem to offer promising results in the near future for a reliable development at a real scale. This is also the reason why electrooxidation has been proposed in combination with electrosorption in the last chapter of the PhD thesis.

Table 6. Summary of the main emerging processes combinations with electrosorption applied in treatment of organic pollutants.

Combined process with electrosorption	Working electrode	Organic pollutant	Efficiency	Reference
Photoelectrocatalysis	Bi_2WO_6/Carbon aerogel	Nonylphenol	Combined processes: 99%	(Fan et al., 2018a)
Photoelectrocatalysis	Nano N-TiO_2/graphene/titanium grid sheet	Diazinon	Electrosorption: 24% Photocatalytic: 28%	(Ayoubi-Feiz et al., 2018a)
Photoelectrocatalysis	α-Fe_2O_3/TiO_2/AC plate nanocomposite	Reactive yellow 39	Adsorption: 28% Electrosorption: 43% Photocatalytic: 38%	(Ayoubi-Feiz et al., 2014b)
Electro-Fenton	Iron oxide grown AC aerogel	Imidacloprid	Combined processes: 90%	(Wang et al., 2013)
Electro-Fenton	AC felt	Toluene and trichloromethane	Combined process: 96% of COD removal	(Chai et al., 2021)
Electrooxidation	MWCNTs/peroxydisulfate	Acyclovir and phenol	Combined processes: Acyclovir: 97% Phenol: 61%	(Nie et al., 2019)
Electrooxidation	TiO_2-NTs/3D-SnO_2-Sb electrode	BA	Combined processes: 89%	(Chen et al., 2018)
Peroxi-coagulation	ACF and iron sheet	Orange II	Combined processes: Removal efficiency: 93% Removal capacity: 1043 mg g^{-1}	(Yang et al., 2021)

Electrically conductive ultrafiltration	Conductive membrane	River natural organic matter, Hohloh lake natural organic matter, humic acid and brilliant blue ionic dye	Combined processes: River natural organic matter: 70% Hohloh lake natural organic matter: 75% Humic acid: 93% Brilliant blue ionic dye: 99%	(Mantel et al., 2021)
Electrocatalysis	Layer-by-layer CNT/PbO_2	Sodium pentachlorophenate	Combined processes: 74%	(Xu et al., 2019)
Photocatalysis	Nanosized TiO_2/AC plate electrode	Lanasol red 5B	Photocatalytic: 66% Combined processes: 86%	(Ayoubi-Feiz et al., 2014c)
Photocatalysis	TiO_2/carbon aerogel	Alizarin red	Electrosorption: 31% Combined processes: 97%	(Jin et al., 2011a)

References

Adnan, F.H., Mousset, E., Pontvianne, S., Pons, M., 2021a. Mineral cathodic electro-precipitation and its kinetic modelling in thin-film microfluidic reactor during advanced electro-oxidation process. Electrochim. Acta 387, 138487. https://doi.org/10.1016/j.electacta.2021.138487

Adnan, F.H., Pons, M.-N., Mousset, E., 2021b. Mass transport evolution in microfluidic thin film electrochemical reactors: New correlations from millimetric to submillimetric interelectrode distances. Electrochem. commun. 130, 107097. https://doi.org/10.1016/j.elecom.2021.107097

Ahmad, T., Guria, C., Mandal, A., 2020. Journal of water process engineering a review of oily wastewater treatment using ultrafiltration membrane: a parametric study to enhance the membrane performance. J. water Process Eng. 36, 101289. https://doi.org/10.1016/j.jwpe.2020.101289

Alagesan, J., Jaisankar, M., Muthuramalingam, S., Mousset, E., Chellam, P.V., 2021. Influence of number of azo bonds and mass transport limitations towards the elimination capacity of continuous electrochemical process for the removal of textile industrial dyes. Chemosphere 262. https://doi.org/10.1016/j.chemosphere.2020.128381

Alencherry, T., Naveen, A.R., Ghosh, S., Daniel, J., Venkataraghavan, R., 2017. Effect of increasing electrical conductivity and hydrophilicity on the electrosorption capacity of activated carbon electrodes for capacitive deionization. Desalination 415, 14–19. https://doi.org/10.1016/j.desal.2017.04.001

Ania, C.O., Béguin, F., 2007. Mechanism of adsorption and electrosorption of bentazone on activated carbon cloth in aqueous solutions. Water Res. 41, 3372–3380. https://doi.org/10.1016/j.watres.2007.03.031

Ayoubi-Feiz, B., Aber, S., Khataee, A., Alipour, E., 2014a. Electrosorption and photocatalytic one-stage combined process using a new type of nanosized TiO_2/activated charcoal plate electrode. Environ. Sci. Pollut. Res. Int. 21, 8555–64. https://doi.org/10.1007/s11356-014-2777-z

Ayoubi-Feiz, B., Aber, S., Khataee, A., Alipour, E., 2014b. Preparation and application of α-Fe_2O_3/TiO_2/activated charcoal plate nanocomposite as an electrode for electrosorption-assisted visible light photoelectrocatalytic process. J. Mol. Catal. A Chem. 395, 440–448. https://doi.org/10.1016/j.molcata.2014.09.006

Ayoubi-Feiz, B., Mashhadizadeh, M.H., Sheydaei, M., 2018. Preparation of reusable nano N-TiO_2/graphene/titanium grid sheet for electrosorption-assisted visible light photoelectrocatalytic degradation of a pesticide: Effect of parameters and neural network modeling. J. Electroanal. Chem. 823, 713–722. https://doi.org/10.1016/j.jelechem.2018.07.020

Ayranci, E., Conway, B.E., 2001. Removal of phenol, phenoxide and chlorophenols from waste-waters by adsorption and electrosorption at high-area carbon felt electrodes. J. Electroanal. Chem. 513, 100–110.

Aziz, F., Achaby, M. El, Lissaneddine, A., Aziz, K., Ouazzani, N., Mamouni, R., Mandi, L., 2020. Composites with alginate beads: A novel design of nano-adsorbents impregnation for large-scale continuous flow wastewater treatment pilots. Saudi J. Biol. Sci. 27, 2499–2508. https://doi.org/10.1016/j.sjbs.2019.11.019

Bagheri, H., Fakhri, H., Ghahremani, R., Karimi, M., Madrakian, T., Afkhami, A., 2020. Nanomaterial-based adsorbents for wastewater treatment. Smart nanocontainers, Elsevier Inc. 467-485. https://doi.org/10.1016/b978-0-12-816770-0.00028-9

Bain, E.J., Calo, J.M., Spitz-Steinberg, R., Kirchner, J., Axén, J., 2010. Electrosorption/electrodesorption of arsenic on a granular activated carbon in the presence of other heavy metals. Energy and fuels 24, 3415–3421. https://doi.org/10.1021/ef901542q

Bán, A., Schäfer, A., Wendt, H., 1998. Fundamentals of electrosorption on activated carbon for wastewater treatment of industrial effluents. J. Appl. Electrochem. 28, 227–236. https://doi.org/10.1023/A:1003247229049

Bard, A.J., Faulkner, L.R., 2001. Electrochemical methods - fundamentals and applications, 2nd Ed. ed. John Wiley & Sons, Inc. https://doi.org/10.1016/B978-0-12-381373-2.00056-9

Barhoumi, A., Ncib, S., Chibani, A., Brahmi, K., Bouguerra, W., Elaloui, E., 2019. High-rate humic acid removal from cellulose and paper industry wastewater by combining electrocoagulation process with adsorption onto granular activated carbon. Ind. Crops Prod. 140, 111715. https://doi.org/10.1016/j.indcrop.2019.111715

Basu, M., Guha, A.K., Ray, L., 2019. Adsorption of lead on lentil husk in fixed bed column bioreactor. Bioresour. Technol. 283, 86–95. https://doi.org/10.1016/j.biortech.2019.02.133

Basuki, K.T., Hasnowo, L.A., Jamayanti, E., 2019. Adsorption of uranium simulation waste using bentonite: Titanium dioxide. Urania J. Ilm. Daur Bahan Bakar Nukl. 25, 19–31. https://doi.org/10.17146/urania.2019.25.1.4527

Bayram, E., 2016. Electrosoption of aromatic organic acids from aqueous solutions onto granular activated carbon electrodes for water purification. Hacettepe J. Biol. Chem. 3, 273–273. https://doi.org/10.15671/hjbc.20164420570

Bayram, E., Ayranci, E., 2012a. Structural effects on electrosorptive behavior of aromatic organic acids from aqueous solutions onto activated carbon cloth electrode of a flow-through electrolytic cell. J. Electroanal. Chem. 683, 14–20. https://doi.org/10.1016/j.jelechem.2012.07.028

Bayram, E., Ayranci, E., 2012b. Electrosorption based waste water treatment system using activated carbon cloth electrode: Electrosorption of benzoic acid from a flow-through electrolytic cell. Sep. Purif. Technol. 86, 113–118. https://doi.org/10.1016/j.seppur.2011.10.032

Bayram, E., Kizil, Ç., Ayranci, E., 2018. Flow-through electrosorption process for removal of 2,4-D pesticide from aqueous solutions onto activated carbon cloth fixed-bed electrodes. Water Sci. Technol. 77, 848–854. https://doi.org/10.2166/wst.2017.598

Bazant, M.Z., Storey, B.D., Kornyshev, A.A., 2011. Double layer in ionic liquids: Overscreening versus crowding. Phys. Rev. Lett. 106. https://doi.org/10.1103/PhysRevLett.106.046102

Belarbi, Z., Sotta, B., Makhloufi, L., Tribollet, B., Gamby, J., 2016. Modelling of delay effect of calcium carbonate deposition kinetics on rotating disk electrode in the presence of green inhibitor. Electrochim. Acta 189, 118–127. https://doi.org/10.1016/j.electacta.2015.12.089

Bergmann, M.E.H., Rollin, J., Iourtchouk, T., 2009. The occurrence of perchlorate during drinking water electrolysis using BDD anodes. Electrochim. Acta 54, 2102–2107. https://doi.org/10.1016/j.electacta.2008.09.040

Biniak, S., Świątkowski, A., Pakuła, M., Sankowska, M., Kuśmierek, K., Trykowski, G., 2013. Cyclic voltammetric and FTIR studies of powdered carbon electrodes in the electrosorption of 4-chlorophenols from aqueous electrolytes. Carbon 51, 301–312. https://doi.org/10.1016/j.carbon.2012.08.057

Brillas, E., Sirés, I., Oturan, M.A., 2009. Electro-Fenton process and related electrochemical technologies based on Fenton's reaction chemistry. Chem. Rev. 109, 6570–6631. https://doi.org/10.1007/s00894-008-0358-0

Brito, C.D.N., de Araújo, D.M., Martínez-Huitle, C.A., Rodrigo, M.A., 2015. Understanding active chlorine species production using boron doped diamond films with lower and higher sp^3/sp^2 ratio. Electrochem. commun. 55, 34–38. https://doi.org/10.1016/j.elecom.2015.03.013

Brummer, S.B., Ford, J.I., Turner, M.J., 1965. The adsorption and oxidation of hydrocarbons on noble metal electrodes. I. Propane adsorption on smooth platinum electrodes. J. Phys. Chem. 69, 3424–3433. https://doi.org/10.1021/j100894a031

Butler, J.A.., Armstrong, G., 1933. The kinetics of electrode processes. Part II.—Reversible reduction and oxidation processes. Proceeding R. Soc. A 139, 406–416. https://doi.org/10.1524/zpch.1972.80.1_2.110a

Cai, Z., Deng, X., Wang, Q., Lai, J., Xie, H., Chen, Y., Huang, B., Lin, G., 2020. Core-shell granular activated carbon and its adsorption of trypan blue. J. Clean. Prod. 242, 118496. https://doi.org/10.1016/j.jclepro.2019.118496

Cañizares, P., Marcos, I.F. De, Rodrigo, M.A., Lobato, J., 2006. Measurement of mass-transfer coefficients by an electrochemical technique. J. Chem. Educ. 83, 1204–1207. https://doi.org/10.1021/ed083p1204

Chabot, V., Higgins, D., Yu, A., Xiao, X., Chen, Z., Zhang, J., 2014. A review of graphene and graphene oxide sponge: Material synthesis and applications to energy and the environment. Energy Environ. Sci. 7, 1564. https://doi.org/10.1039/c3ee43385d

Chai, X., He, Y., Ying, D., Jia, J., Sun, T., 2007. Electrosorption-enhanced solid-phase microextraction using activated carbon fiber for determination of aniline in water. J. Chromatogr. A 1165, 26–31. https://doi.org/10.1016/j.chroma.2007.07.048

Chai, Y., Qin, P., Wu, Z., Bai, M., Li, W., Pan, J., Cao, R., Chen, A., Jin, D., Peng, C., 2021. A coupled system of flow-through electro-Fenton and electrosorption processes for the efficient treatment of high-salinity organic wastewater. Sep. Purif. Technol. 267, 118683. https://doi.org/10.1016/j.seppur.2021.118683

Chang, L., Li, J., Duan, X., Liu, W., 2015. Porous carbon derived from Metal-Organic Framework (MOF) for capacitive deionization electrode. Electrochim. Acta 176, 956–964. https://doi.org/10.1016/j.electacta.2015.07.130

Chang, L., Zhou, Y., Duan, X., 2014. Kinetics and equilibrium studies on the electrosorption of anions with activated carbon electrodes. Desalin. water Treat. 52, 6549–6555. https://doi.org/10.1080/19443994.2013.816873

Chapman, D.L., 1913. A contribution to the theory of electrocapillary. Philos. Mag. 25, 475–481. https://doi.org/10.1016/0304-3975(85)90090-8

Chen, Y., Tu, Y., Bai, Y., Li, J., Lu, J., 2018. Electrosorption enhanced electrooxidation of a model organic pollutant at 3D SnO_2-Sb electrode in superimposed pulse current mode. Chemosphere 195, 63–69. https://doi.org/10.1016/j.chemosphere.2017.12.074

Cheng, J., Yang, H., Fan, C., Li, R., Yu, X., Li, H., 2020. Review on the applications and development of fluidized bed electrodes. J. solid state Electrochem.

Chkirida, S., Zari, N., Achour, R., Hassoune, H., Lachehab, A., Qaiss, A. El Kacem, Bouhfid, R., 2021. Highly synergic adsorption/photocatalytic efficiency of Alginate/Bentonite impregnated TiO_2 beads for wastewater treatment. J. Photochem. Photobiol. A Chem. 412, 113215. https://doi.org/10.1016/j.jphotochem.2021.113215

Chmiola, J., Yushin, G., Gogotsi, Y., Portet, C., Simon, P., Taberna, P.L., 2006. Anomalous increase in carbon at pore sizes less than 1 nanometer. Science (80-.). 313, 1760–1763.

https://doi.org/10.1126/science.1132195
Chue, K.T., Grévillot, G., Tondeur, D., 1993. Electrosorption an activated carbon bed. Stud. Surf. Sci. Catal. 80, 97–104.
Coeuret, F., 2003. Ingénierie des procédés électrochimiques. Ellipses, Paris (France).
Cœuret, F., 1993. A flow-through porous electrode patented 100 years ago: The Hulin process. J. Appl. Electrochem. 23, 853–855.
Cœuret, F., Hutin, D., Gaunand, A., 1976. Study of the effectiveness of fixed flow-through electrodes. J. Appl. Electrochem. 6, 417–423. https://doi.org/10.1007/BF00616541
Cœuret, F., Legrand, J., 1985. Mass transfer at the electrodes of the "falling-film cell." J. Appl. Electrochem. 15, 181–190.
Cœuret, F., Storck, A., 1984. Eléments de génie électrochimique, 1st Ed. ed. Tec & Doc, Paris (France).
Conway, B.E., 1999. Theoretical treatment and modeling of the double layer at electrode interfaces, in: Electrochemical Supercapacitors. pp. 125–168. https://doi.org/10.1007/978-1-4757-3058-6_7
Crini, G., Lichtfouse, E., 2019. Advantages and disadvantages of techniques used for wastewater treatment. Environ. Chem. Lett. 17, 145–155. https://doi.org/10.1007/s10311-018-0785-9
Crini, G., Lichtfouse, E., Wilson, L.D., Morin-Crini, N., 2019. Conventional and non-conventional adsorbents for wastewater treatment. Environ. Chem. Lett. 17, 195–213. https://doi.org/10.1007/s10311-018-0786-8
Cuong, D.V., 2020. Eco-friendly biochar-based materials in removal of contaminants from aqueous solutions: Fabrication, characterization and applications. https://doi.org/10.6342/NTU202003877
Dai, G., Zhang, L., Liao, Y., Shi, Y., Xie, J., Lei, F., Fan, L., 2020. Multi-scale model for describing the effect of pore structure on carbon-based electric double layer. J. Phys. Chem. C 124, 3952–3961. https://doi.org/10.1021/acs.jpcc.9b10587
Damaskin, B. B., Baturina, O.A., 1999. Co-adsorption of anions and low-adsorbing cations within the Alekseev-Popov-Kolotyrkin model. Russ. J. Electrochem. 35(11), 1182–1185.
Damaskin, B.B., 2011. Modeling of co-adsorption of cations and anions localized in different layers of the dense part of electrical double layer under the conditions of linear charge dependence of the adsorption energy. Russ. J. Electrochem. 47, 988–994. https://doi.org/10.1134/S1023193511090047
Damaskin, B.B., 2009. Mechanism of coadsorption of two organic substances on electrodes at strong attractive interaction between their molecules in the adsorption layer. Russ. J. Electrochem. 45, 241–245. https://doi.org/10.1134/S102319350903001X
Damaskin, B.B., 2008. Modeling of synergism effect at different orientation of co-adsorbing molecules. Russ. J. Electrochem. 44, 1411–1417. https://doi.org/10.1134/S102319350812001X
Damaskin, B. B., Baturina, O.A., 2001. Some anomalies in coadsorption of two organic substances due to differences in molecular interaction of species undergoing coadsorption. Russ. J. Electrochem. 37, 1292–1299. https://doi.org/10.1023/A:1013239813826
Damaskin, B B, Baturina, O.A., 2001a. Simulating coadsorption of surface active anions and organic molecules capable of forming two-dimensional condensed layers on the electrode. Russ. J. Electrochem. 37, 121–126.
Damaskin, B B, Baturina, O.A., 2001b. Simulation of coadsorption of inorganic ions and

organic molecules on electrodes. Russ. J. Electrochem. 37, 73–79.

Damaskin, B.B., Petrii, O.A., 2011. Historical development of theories of the electrochemical double layer. J. solid state Electrochem. 15, 1317–1334. https://doi.org/10.1007/s10008-011-1294-y

Damaskin, B.B., Safonov, V.A., Safonov, N. V, 2003. Adsorption of an organic compound in two different positions: Simulation taking into account all three parameters of intermolecular interaction. Russ. J. Electrochem. 39, 814–819.

Díaz-Blancas, V., Ocampo-Pérez, R., Leyva-Ramos, R., Alonso-Dávila, P.A., Moral-Rodríguez, A.I., 2018. 3D modeling of the overall adsorption rate of metronidazole on granular activated carbon at low and high concentrations in aqueous solution. Chem. Eng. J. 349, 82–91. https://doi.org/10.1016/j.cej.2018.05.076

Du, X., Oturan, M.A., Zhou, M., Belkessa, N., Su, P., Cai, J., Trellu, C., Mousset, E., 2021. Nanostructured electrodes for electrocatalytic advanced oxidation processes: From materials preparation to mechanisms understanding and wastewater treatment applications. Appl. Catal. B Environ. 296, 120332. https://doi.org/10.1016/j.apcatb.2021.120332

Eeshwarasinghe, D., Loganathan, P., Vigneswaran, S., 2019. Simultaneous removal of polycyclic aromatic hydrocarbons and heavy metals from water using granular activated carbon. Chemosphere 223, 616–627. https://doi.org/10.1016/j.chemosphere.2019.02.033

Eisinger, R.S., 1983. Separation by electrosorption of organic compounds in a flow-through porous electrode. J. Electrochem. Soc. 130, 93. https://doi.org/10.1149/1.2119689

Eisinger, R.S., Alkire, R.C., 1980. Electrosorption of b-naphthol on graphite. J Electroanal.Chem. 112, 327–337.

Eisinger, R.S., Keller, G.E., 1990. Electrosorption: A case study on removal of dilute organics from water. Environ. Prog. 9, 235–244. https://doi.org/10.1002/ep.670090418

El-Naas, M.H., Alhaija, M.A., 2013. Modelling of adsorption processes. Math. Model. 579–600.

Fan, L., Liu, Y., Xiong, J., White, H.S., Chen, S., 2014. Electron-transfer kinetics and electric double layer effects in nanometer-wide thin-layer cells. ACS Nano 8, 10426–10436. https://doi.org/10.1021/nn503780b

Fan, Z., Shi, H., Zhao, H., Cai, J., Zhao, G., 2018a. Application of carbon aerogel electrosorption for enhanced Bi2WO6 photoelectrocatalysis and elimination of trace nonylphenol. Carbon N. Y. 126, 279–288. https://doi.org/10.1016/j.carbon.2017.10.009

Feng, C., E, J., Han, W., Deng, Y., Zhang, B., Zhao, X., Han, D., 2021. Key technology and application analysis of zeolite adsorption for energy storage and heat-mass transfer process: A review. Renew. Sustain. Energy Rev. 144, 110954. https://doi.org/10.1016/j.rser.2021.110954

Feng, G., Qiao, R., Huang, J., Sumpter, B.G., Meunier, V., 2010. Ion distribution in electrified micropores and its role in the anomalous enhancement of capacitance. ACS Nano 4, 2382–2390. https://doi.org/10.1021/nn100126w

Folaranmi, G., Bechelany, M., Sistat, P., Cretin, M., Zaviska, F., 2020. Towards electrochemical water desalination techniques: a review on capacitive deionization, membrane capacitive deionization and flow capacitive deionization. Membranes (Basel).

Foo, K.Y., Hameed, B.H., 2009. A short review of activated carbon assisted electrosorption process : An overview , current stage and future prospects. J. Hazard. Mater. 170, 552–559. https://doi.org/10.1016/j.jhazmat.2009.05.057

Frackowiak, E., 2001. Carbon materials for the electrochemical storage of energy in capacitors. Carbon N. Y. 39, 937–950

Frumkin, A., Damaskin, B., Petrii, O., 1974. On the charge transfer in the process of adsorption at the electrode/solution interface. Electroanal. Chem. interfacial Electrochem. 53, 57–65.

Ganzenko, O., Huguenot, D., Hullebusch, E.D. Van, Esposito, G., Oturan, M.A., 2014. Electrochemical advanced oxidation and biological processes for wastewater treatment : a review of the combined approaches. Env. Sci Pollut Res. https://doi.org/10.1007/s11356-014-2770-6

Gao, T., Li, H., Zhou, F., Gao, M., Liang, S., Luo, M., 2017. Mesoporous carbon derived from ZIF-8 for high efficient electrosorption. Desalination 451, 133–138. https://doi.org/10.1016/j.desal.2017.06.021

Garcia-Rodriguez, O., Mousset, E., Olvera-Vargas, H., Lefebvre, O., 2020. Electrochemical treatment of highly concentrated wastewater: A review of experimental and modeling approaches from lab-to full-scale. Crit. Rev. Environ. Sci. Technol. 0, 1–70. https://doi.org/10.1080/10643389.2020.1820428

Geim, A., Novoselov, K., 2007. The rise of graphene. Nat. Mater. 6, 183–191

Gerçel, Ö., 2016. Removal of textile dye from aqueous solution by electrochemical method. Sep. Sci. Technol. 51, 711–717. https://doi.org/10.1080/01496395.2015.1088870

Gileadi, E., 1966. Electrosorption of uncharged molecules on solid electrodes. J. Electroanal. Chem. 11, 137–151. https://doi.org/10.1016/0022-0728(66)80073-6

Gileadi, E., Duić, L., Bockris, J.O.M., 1968. A comparison of radiotracer and electrochemical methods for the measurement of the electrosorption of organic molecules. Electrochim. Acta 13, 1915–1935. https://doi.org/10.1016/0013-4686(68)80103-3

Gileadi, E., Rubin, B.T., Bockris, J.O.M., 1965. Electrosorption of ethylene on platinum as a function of potential, concentration, and temperature. J. Phys. Chem. 69, 3335–3345. https://doi.org/10.1021/j100894a019

Girijan, S., Kumar, M., Gomber, S., 2021. Starch and powdered activated carbon amended alginate-biomass beads for metronidazole and bulk organic matter removal: Synthesis, optimization, reaction kinetics and reusability. J. Environ. Chem. Eng. 9, 106102. https://doi.org/10.1016/j.jece.2021.106102

Golovko, O., Anton, L. de B., Cascone, C., Ahrens, L., Lavonen, E., Köhler, S.J., 2020. Sorption characteristics and removal efficiency of organic micropollutants in drinking water using Granular Activated Carbon (GAC) in pilot-scale and full-scale tests. Water (Switzerland) 12, 1–14. https://doi.org/10.3390/w12072053

Goodridge, F., Wright, A.R., 1983. Porous flow-through and fluidized-bed electrodes. Compr. Treatise Electrochem. 393–443

Gouy, M., 1910. Charge électrique à la surface d'un électrolyte. J. Phys 9, 457–468

Grahame, D.C., 1947. The electrical double layer and the theory of electrocapillarity. Chem. Rev. 41, 441–501. https://doi.org/10.1021/cr60130a002

Grahame, D.C., 1946. Properties of the electrical double layer at a mercury surface. II. the effect of frequency on the capacity and resistance of ideal polarized electrodes. J. Am. Chem. Soc. 68, 301–310. https://doi.org/10.1021/ja01206a045

Han, Y., Quan, X., Chen, S., Zhao, H., Cui, C., Zhao, Y., 2006a. Electrochemically enhanced adsorption of aniline on activated carbon fibers. Sep. Purif. Technol. 50, 365–372. https://doi.org/10.1016/j.seppur.2005.12.011

Han, Y., Quan, X., Chen, S., Zhao, H., Cui, C., Zhao, Y., 2006b. Electrochemically enhanced

adsorption of phenol on activated carbon fibers in basic aqueous solution. J. Colloid Interface Sci. 299, 766–771. https://doi.org/10.1016/j.jcis.2006.03.007

Han, Y., Quan, X., Ruan, X., Zhang, W., 2008. Integrated electrochemically enhanced adsorption with electrochemical regeneration for removal of acid orange 7 using activated carbon fibers. Sep. Purif. Technol. 59, 43–49. https://doi.org/10.1016/j.seppur.2007.05.026

Hazourli, S., Bonnecaze, G., Astruc, M., 1996. Adsorption et electrosorption de composes organiques sur charbon actif en grains partie I - Influence du potentiel imposé et du nombre de cycles adsorption and electrosorption of organic compounds on granular activated carbon part I- Influence of applied. Environ. Technol. 17, 1275–1283. https://doi.org/10.1080/09593330.1996.9618457

He, F., Hemmatifar, A., Bazant, M.Z., Hatton, T.A., 2020. Selective adsorption of organic anions in a flow cell with asymmetric redox active electrodes. Water Res. 182, 115963. https://doi.org/10.1016/j.watres.2020.115963

Heiland, W., Gileadi, E., Bockris, J.O.M., 1966. Kinetic and thermodynamic aspects of the electrosorption of benzene on platinum electrodes. J. Phys. Chem. 70, 1207–1216. https://doi.org/10.1021/j100876a040

Helmholtz, H. von, 1879. Studien über electrische grenzschichten. Ann. der Phys. und chemie 243, 22–382.

Henstridge, M.C., Dickinson, E.J.F., Compton, R.G., 2010. On the estimation of the diffuse double layer of carbon nanotubes using classical theory: Curvature effects on the Gouy-Chapman limit. Chem. Phys. Lett. 485, 167–170. https://doi.org/10.1016/j.cplett.2009.12.034

Holubowitch, N., Omosebi, A., Gao, X., Landon, J., Liu, K., 2017. Quasi-steady-state polarization reveals the interplay of capacitive and faradaic processes in capacitive deionization. ChemElectroChem 4, 2404–2413. https://doi.org/10.1002/celc.201700082

Hou, C.H., Huang, J.F., Lin, H.R., Wang, B.Y., 2012. Preparation of activated carbon sheet electrode assisted electrosorption process. J. Taiwan Inst. Chem. Eng. 43, 473–479. https://doi.org/10.1016/j.jtice.2011.12.003

Huang, J., Sumpter, B.G., Meunier, V., 2008. Theoretical model for nanoporous carbon supercapacitors. Angew. chemie - Int. Ed. 47, 520–524. https://doi.org/10.1002/anie.200703864

Hulin, P.L., 1893. Procédés et appareil électrolytiques pour la séparation immédiate des produits d'électrolyse liquides ou dissous.

Huong Le, T.X., Dumée, L.F., Lacour, S., Rivallin, M., Yi, Z., Kong, L., Bechelany, M., Cretin, M., 2019. Hybrid graphene-decorated metal hollow fibre membrane reactors for efficient electro-Fenton - Filtration co-processes. J. Memb. Sci. 587, 117182. https://doi.org/10.1016/j.memsci.2019.117182

Ibl, N., 1959. The use of dimensionless groups in electrochemistry. Electrochim. Acta 1, 117–129. https://doi.org/10.1016/0013-4686(59)85001-5

Islam, M.S., McPhedran, K.N., Messele, S.A., Liu, Y., Gamal El-Din, M., 2018. Isotherm and kinetic studies on adsorption of oil sands process-affected water organic compounds using granular activated carbon. Chemosphere 202, 716–725. https://doi.org/10.1016/j.chemosphere.2018.03.149

Jamil, S., Loganathan, P., Listowski, A., Kandasamy, J., Khourshed, C., Vigneswaran, S., 2019. Simultaneous removal of natural organic matter and micro-organic pollutants from reverse osmosis concentrate using granular activated carbon. Water Res. 155, 106–114. https://doi.org/10.1016/j.watres.2019.02.016

Jaria, G., Calisto, V., Silva, C.P., Gil, M.V., Otero, M., Esteves, V.I., 2019. Fixed-bed performance of a waste-derived granular activated carbon for the removal of micropollutants from municipal wastewater. Sci. Total Environ. 683, 699–708. https://doi.org/10.1016/j.scitotenv.2019.05.198

Jayson, G.G., Sangster, J.A., Thompson, G., Wilkinson, M.C., 1987. Adsorption and electrosorption of mercury (II) acetate onto activated charcoal cloth from aqueous solution. Carbon N. Y. 25, 523–531. https://doi.org/10.1016/0008-6223(87)90193-X

Jin, Y., Wu, M., Zhao, G., Li, M., 2011. Photocatalysis-enhanced electrosorption process for degradation of high-concentration dye wastewater on TiO_2/carbon aerogel. Chem. Eng. J. 168, 1248–1255. https://doi.org/10.1016/j.cej.2011.02.026

Johnson, A.M., Newman, J., 1971. Desalting by means of porous carbon electrodes. J. Electrochem. Soc. 118, 510. https://doi.org/10.1149/1.2408094

Jung, C., Oh, W., Lee, Y., Park, S., 2005. Electrosorption of U(IV) by electochemically modified activated carbon fibers. Carbon Sci. 6, 25–30.

Kakhi, M., 2009. Classification of the flow regimes in the flow-through cell. Eur. J. Pharm. Sci. 37, 531–544. https://doi.org/10.1016/j.ejps.2009.04.003

Khan, A.S., Ibrahim, T.H., Khamis, M.I., Nancarrow, P., Iqbal, J., AlNashef, I., Jabbar, N.A., Hassan, M.F., Mjalli, F.S., 2021. Preparation of sustainable activated carbon-alginate beads impregnated with ionic liquid for phenol decontamination. J. Clean. Prod. 128899. https://doi.org/10.1016/j.jclepro.2021.128899

Kitous, O., Cheikh, A., Lounici, H., Grib, H., Pauss, A., Mameri, N., 2009. Application of the electrosorption technique to remove Metribuzin pesticide. J. Hazard. Mater. 161, 1035–1039. https://doi.org/10.1016/j.jhazmat.2008.04.091

Koparal, A.S., Yavuz, Y., Bakir Öğütveren, Ü., 2002. Electroadsorption of Acilan Blau dye from textile effluents by using activated carbon-perlite mixtures. Water Environ. Res. 74, 521–525. https://doi.org/10.2175/106143002x140314

Kornyshev, A.A., 2007. Double-layer in ionic liquids: Paradigm change? J. Phys. Chem. B 111, 5545–5557.

Langlois, S., Cœuret, F., 1990. Flow-through and flow-by porous electrodes of nickel foam Part III: theoretical electrode potential distribution in the flow-by configuration. J. Appl. Electrochem. 20, 740–748.

Largeot, C., Portet, C., Chmiola, J., Taberna, P.L., Gogotsi, Y., Simon, P., 2008. Relation between the ion size and pore size for an electric double-layer capacitor. J. Am. Chem. Soc. 130, 2730–2731. https://doi.org/10.1021/ja7106178

Le, T.X.H., Bechelany, M., Lacour, S., Oturan, N., Oturan, M.A., Cretin, M., 2015. High removal efficiency of dye pollutants by electron-Fenton process using a graphene-based cathode. Carbon N. Y. 94, 1003–1011. https://doi.org/10.1016/j.carbon.2015.07.086

Li, Y., Zhang, C., Jiang, Y., Wang, T., Wang, H., 2016. Effects of the hydration ratio on the electrosorption selectivity of ions during capacitive deionization. Desalination 399, 171–177. https://doi.org/10.1016/j.desal.2016.09.011

Li, Z., Shen, C., Liu, Y., Ma, C., Li, F., Yang, B., Huang, M., Wang, Z., Dong, L., Wolfgang, S., 2020. Carbon nanotube filter functionalized with iron oxychloride for flow-through electro-Fenton. Appl. Catal. B Environ. 260, 118204. https://doi.org/10.1016/j.apcatb.2019.118204

Lian, C., Jiang, D.E., Liu, H., Wu, J., 2016. A generic model for electric double layers in porous electrodes. J. Phys. Chem. C 120, 8704–8710. https://doi.org/10.1021/acs.jpcc.6b00964

Lippmann, M.G., 1875. Relations entre les phénomènes électriques et capillaires. Ann.

Chim. Phys. 5, 494–549.
Liu, L., Liu, Y., Che, N., Gao, B., Li, C., 2021. Electrochemical adsorption of perfluorooctanoic acid on a novel reduced graphene oxide aerogel loaded with Cu nanoparticles and fluorine. J. Hazard. Mater. 416, 125866. https://doi.org/10.1016/j.jhazmat.2021.125866
López-Bernabeu, S., Ruiz-Rosas, R., Quijada, C., Montilla, F., Morallón, E., 2016. Enhanced removal of 8-quinolinecarboxylic acid in an activated carbon cloth by electroadsorption in aqueous solution. Chemosphere 144, 982–988. https://doi.org/10.1016/j.chemosphere.2015.09.071
Lord, H.L., Zhan, W., Pawliszyn, J., 2012. Fundamentals and Applications of Needle Trap Devices, Comprehensive Sampling and Sample Preparation: Analytical Techniques for Scientists. Elsevier. https://doi.org/10.1016/B978-0-12-381373-2.10056-0
Lust, E., Jänes, A., Lust, K., Pullerits, R., 1997a. Adsorption of organic compounds and hydrophilicity of bismuth, cadmium and antimony electrodes. J. Electroanal. Chem. 431, 183–201. https://doi.org/10.1016/S0022-0728(97)00150-2
Lust, E., Jänes, A., Lust, K., Väärtnõu, M., 1997b. Electric double layer structure and adsorption of cyclohexanol on single crystal cadmium, antimony and bismuth electrodes. Electrochim. Acta 42, 771–783. https://doi.org/10.1016/s0013-4686(96)00339-8
Mantel, T., Jacki, E., Ernst, M., 2021. Electrosorptive removal of organic water constituents by positively charged electrically conductive UF membranes. Water Res. 201, 117318. https://doi.org/10.1016/j.watres.2021.117318
Marracino, J.M., Cœuret, F., Langlois, S., 1987. A first investigation of flow-through porous electrodes made of metallic felts or foams. Electrochim. Acta 32, 1303–1309. https://doi.org/10.1016/0013-4686(87)85059-4
Martinez-Huitle, C.A., Rodrigo, M.A., Sires, I., Scialdone, O., 2015. Single and coupled electrochemical processes and reactors for the abatement of organic water pollutants: A critical review. Chem. Rev. 115, 13362–13407. https://doi.org/10.1021/acs.chemrev.5b00361
Matsuno, Y., Yoshida, K., Tsutsumi, A., 1996. Electrode electrodes performance of fixed and fluidized bed carbonate. Int. J. Hydrog. energ 21.
McGuire, J., Dwiggins, C.F., Fedkiw, P.S., 1985. The electrosorption of phenol onto activated carbon. J. Appl. Electrochem. 15, 53–62. https://doi.org/10.1007/BF00617740
McQuillan, R. V., Stevens, G.W., Mumford, K.A., 2018. The electrochemical regeneration of granular activated carbons: A review. J. Hazard. Mater. 355, 34–49. https://doi.org/10.1016/j.jhazmat.2018.04.079
Monteil, H., Péchaud, Y., Oturan, N., Oturan, M.A., 2019. A review on efficiency and cost effectiveness of electro- and bio-electro-Fenton processes: Application to the treatment of pharmaceutical pollutants in water. Chem. Eng. J. 376, 1–30. https://doi.org/10.1016/j.cej.2018.07.179
Moreira, F.C., Boaventura, R.A.R., Brillas, E., Vilar, V.J.P., 2017. Electrochemical advanced oxidation processes: A review on their application to synthetic and real wastewaters. Appl. Catal. B Environ. 202, 217–261. https://doi.org/10.1016/j.apcatb.2016.08.037
Mousset, E., 2020. Unprecedented reactive electro-mixing reactor: Towards synergy between micro- and macro-reactors? Electrochem. commun. 118, 106787. https://doi.org/10.1016/j.elecom.2020.106787
Mousset, E., Dionysiou, D.D., 2020a. Photoelectrochemical reactors for treatment of water and wastewater: a review. Environ. Chem. Lett. https://doi.org/10.1007/s10311-020-

01014-9

Mousset, E., Doudrick, K., 2020b. A review of electrochemical reduction processes to treat oxidized contaminants in water. Curr. Opin. Electrochem. 22, 221–227. https://doi.org/10.1016/j.coelec.2020.07.008

Mousset, E., Ko, Z.T., Syafiq, M., Wang, Z., Lefebvre, O., 2016a. Electrocatalytic activity enhancement of a graphene ink-coated carbon cloth cathode for oxidative treatment. Electrochim. Acta. https://doi.org/http://dx.doi.org/10.1016/j.electacta.2016.11.151

Mousset, E., Loh, W.H., Lim, W.S., Jarry, L., Wang, Z., Lefebvre, O., 2021a. Cost comparison of advanced oxidation processes for wastewater treatment using accumulated oxygen-equivalent criteria. Water Res. 200, 117234. https://doi.org/https://doi.org/10.1016/j.electacta.2021.138466

Mousset, E., Oturan, N., Oturan, M.A., 2018a. An unprecedented route of OH radical reactivity evidenced by an electrocatalytical process: Ipso-substitution with perhalogenocarbon compounds. Appl. Catal. B Environ. 226, 135–146. https://doi.org/10.1016/j.apcatb.2017.12.028

Mousset, E., Pechaud, Y., Oturan, N., Oturan, M.A., 2019a. Charge transfer/mass transport competition in advanced hybrid electrocatalytic wastewater treatment: Development of a new current efficiency relation. Appl. Catal. B Environ. 240, 102–111. https://doi.org/10.1016/j.apcatb.2018.08.055

Mousset, E., Pontvianne, S., Pons, M.-N., 2018b. Fate of inorganic nitrogen species under homogeneous Fenton combined with electro-oxidation/reduction treatments in synthetic solutions and reclaimed municipal wastewater. Chemosphere 201, 6–12. https://doi.org/10.1016/j.chemosphere.2018.02.142

Mousset, E., Puce, M., Pons, M.N., 2019b. Advanced electro-oxidation with boron-doped diamond for acetaminophen removal from real wastewater in a microfluidic reactor: Kinetics and mass-transfer studies. ChemElectroChem 6, 2908–2916. https://doi.org/10.1002/celc.201900182

Mousset, E., Quackenbush, L., Schondek, C., Gerardin-Vergne, A., Pontvianne, S., Kmiotek, S., Pons, M.N., 2020. Effect of homogeneous Fenton combined with electron transfer on the fate of inorganic chlorinated species in synthetic and reclaimed municipal wastewater. Electrochim. Acta 334, 135608. https://doi.org/10.1016/j.electacta.2019.135608

Mousset, E., Trellu, C., Olvera-Vargas, H., Pechaud, Y., Fourcade, F., Oturan, M.A., 2021b. Electrochemical technologies coupled with biological treatments. Curr. Opin. Electrochem. 26, 100668. https://doi.org/https://doi.org/10.1016/j.coelec.2020.100668

Mousset, E., Wang, Z., Hammaker, J., Lefebvre, O., 2017. Electrocatalytic phenol degradation by a novel nanostructured carbon fiber brush cathode coated with graphene ink. Electrochim. Acta 258, 607–617. https://doi.org/10.1016/j.electacta.2017.11.104

Mousset, E., Wang, Z., Hammaker, J., Lefebvre, O., 2016b. Physico-chemical properties of pristine graphene and its performance as electrode material for electro-Fenton treatment of wastewater. Electrochim. Acta 214, 217–230. https://doi.org/10.1016/j.electacta.2016.08.002

Mousset, E., Wang, Z., Olvera-Vargas, H., Lefebvre, O., 2018c. Advanced electrocatalytic pre-treatment to improve the biodegradability of real wastewater from the electronics industry — A detailed investigation study. J. Hazard. Mater. 360, 552–559. https://doi.org/10.1016/j.jhazmat.2018.08.023

Nainamalai, M., Palani, M., Soundarajan, B., Allwin, A.E., 2018. Decolorization of synthetic dye wastewater using packed bed electro-adsorption column. Chem. Eng. Process. -

Process Intensif. 130, 160–168. https://doi.org/10.1016/j.cep.2018.06.013

Nan, X., Lavrni, S., Toscano, A., 2020. Potential of constructed wetland treatment systems for agricultural wastewater reuse under the EU framework. J. Environ. Manage. 275. https://doi.org/10.1016/j.jenvman.2020.111219

Newman, J., 1968. Engineering design of electrochemical systems. Ind. Eng. Chem. 60, 12–27. https://doi.org/10.1021/ie50700a005

Newman, J.S., Tobias, C.W., 1962. Theoretical analysis of current distribution in porous electrodes. J. Electrochem. Soc. 109, 1183. https://doi.org/10.1149/1.2425269

Nidheesh, P. V., Divyapriya, G., Oturan, N., Trellu, C., Oturan, M.A., 2019. Environmental applications of boron-doped diamond electrodes: 1. Applications in water and wastewater treatment. ChemElectroChem 6, 1–20. https://doi.org/10.1002/celc.201801876

Nie, C., Dai, Z., Meng, H., Duan, X., Qin, Y., Zhou, Y., Ao, Z., Wang, S., An, T., 2019. Peroxydisulfate activation by positively polarized carbocatalyst for enhanced removal of aqueous organic pollutants. Water Res. 166, 115043. https://doi.org/10.1016/j.watres.2019.115043

Niu, J., Conway, B.E., 2003. Adsorption of organics onto an high-area C-cloth electrode from organic solvents and organic solvent/water mixtures. J. Electroanal. Chem. 546, 59–72. https://doi.org/10.1016/S0022-0728(03)00146-3

Norra, G.F., Radjenovic, J., 2021. Removal of persistent organic contaminants from wastewater using a hybrid electrochemical-granular activated carbon (GAC) system. J. Hazard. Mater. 415, 125557. https://doi.org/10.1016/j.jhazmat.2021.125557

Oleinick, A., Svir, I., Amatore, C., 2019. A few key theoretical issues of importance in modern molecular electrochemistry. Curr. Opin. Electrochem. 13, 33–39. https://doi.org/10.1016/j.coelec.2018.10.008

Oller, I., Malato, S., Sánchez-Pérez, J.A., 2011. Combination of advanced oxidation processes and biological treatments for wastewater decontamination-A review. Sci. Total Environ. 409, 4141–4166. https://doi.org/10.1016/j.scitotenv.2010.08.061

Panizza, M., Cerisola, G., 2009. Direct and mediated anodic oxidation of organic pollutants. Chem. Rev. 109, 6541–6569. https://doi.org/10.1021/cr9001319

Panizza, M., Michaud, P.A., Cerisola, G., Comninellis, C., 2001. Anodic oxidation of 2-naphthol at boron-doped diamond electrodes. J. Electroanal. Chem. 507, 206–214. https://doi.org/10.1016/S0022-0728(01)00398-9

Pazos, M., Rosales, E., Sanrom, M.A., 2021. Electro-reversible adsorption as a versatile tool for the removal of diclofenac from wastewater 280. https://doi.org/10.1016/j.chemosphere.2021.130778

Peng, H., Guo, J., 2020. Removal of chromium from wastewater by membrane filtration, chemical precipitation, ion exchange, adsorption electrocoagulation, electrochemical reduction, electrodialysis, electrodeionization, photocatalysis and nanotechnology: a review. Environ. Chem. Lett. 18, 2055–2068. https://doi.org/10.1007/s10311-020-01058-x

Piai, L., Dykstra, J.E., Adishakti, M.G., Blokland, M., Langenhoff, A.A.M., van der Wal, A., 2019. Diffusion of hydrophilic organic micropollutants in granular activated carbon with different pore sizes. Water Res. 162, 518–527. https://doi.org/10.1016/j.watres.2019.06.012

Pilon, L., Wang, H., D'Entremont, A., 2015. Recent advances in continuum modeling of interfacial and transport phenomena in electric double layer capacitors. J. Electrochem. Soc. 162, A5158–A5178. https://doi.org/10.1149/2.0211505jes

Plaisance, H., Mocho, P., Bonnecaze, G., 1996. Adsorption et electrosorption de benzene sur charbon actif en grains adsorption and electrosorption of benzene on granular activated carbon. Environ. Technol. 17, 1313–1325. https://doi.org/10.1080/09593331708616501

Pletcher, D., Walsh, F.C., 1993. Industrial electrochemistry, Springer netherlands. https://doi.org/10.1007/978-94-011-2154-5

Pletcher, D., Walsh, F.C., 1982. Industrial electrochemistry, 1st Ed. ed. Chapman and Hall, London. https://doi.org/10.1179/bcj.1983.18.2.70

Rezakazemi, M., Maghami, M., Mohammadi, T., 2018. High loaded synthetic hazardous wastewater treatment using lab- scale submerged ceramic membrane bioreactor. Period. Polytech. Chem. Eng. 62, 299–304.

Rizzo, L., Gernjak, W., Krzeminski, P., Malato, S., McArdell, C.S., Perez, J.A.S., Schaar, H., Fatta-Kassinos, D., 2020. Best available technologies and treatment trains to address current challenges in urban wastewater reuse for irrigation of crops in EU countries. Sci. Total Environ. 710, 136312. https://doi.org/10.1016/j.scitotenv.2019.136312

Rong, C., Xien, H., 2009. Reversible electrosorption of thiocyanate anions by active carbon felt. Sep. Sci. Technol. 44, 3984–3999. https://doi.org/10.1080/01496390903182453

Rong, C., Xien, H., 2005. Electrosorption of thiocyanate anions on active carbon felt electrode in dilute solution. J. Colloid Interface Sci. 290, 190–195. https://doi.org/10.1016/j.jcis.2005.04.022

Sahin, E.M., Tongur, T., Ayranci, E., 2020. Removal of azo dyes from aqueous solutions by adsorption and electrosorption as monitored with in-situ UV-visible spectroscopy. Sep. Sci. Technol. 55, 3287–3298. https://doi.org/10.1080/01496395.2019.1676786

Sarkar, A., Paul, B., 2016. The global menace of arsenic and its conventional remediation - A critical review. Chemosphere 158, 37–49. https://doi.org/10.1016/j.chemosphere.2016.05.043

Schmickler, W., 2020. Double layer theory. J. solid state Electrochem. 24, 2175–2176. https://doi.org/10.1007/s10008-020-04597-z

Schmickler, W., 1996. Electronic effects in the electric double layer. Chem. Rev. 96, 3177–3200. https://doi.org/10.1021/cr940408c

Schultze, J.W., Vetter, K.J., 1973. Experimental determination and interpretation of the electrosorption valency gamma. Electroanal. Chem. interfacial Electrochem. 44, 63–81.

Sene, A., Daffos, B., Taberna, P.L., Simon, P., 2019. Characterization of the mass transfer fluxes in a capacitive desalination cell by using $FeIII(CN)_6^{3-}$/$FeII(CN)_6^{4-}$ redox couple as an electrochemical probe. J. Electroanal. Chem. 842, 127–132. https://doi.org/10.1016/j.jelechem.2019.04.060

Simon, P., Gogotsi, Y., 2008. Materials for electrochemical capacitors. Nat. Mater. 7, 845–854.

Stenina, E. V., Sviridova, L.N., Damaskin, B.B., 2009. Comparison of temperature dependences of adsorption parameters for secondary butanol and 1-oxyadamantane at their adsorption on the Hg electrode/aqueous solution interface. Russ. J. Electrochem. 45, 847–854. https://doi.org/10.1134/S1023193509080023

Stenina, E. V, Baturina, O.A., Sviridova, L.N., Damaskin, B.B., 2001. Coadsorption of halide anions and 1-adamantanol molecules on a mercury electrode. Russ. J. Electrochem. 37, 931–938.

Stern, O., 1924. Zur Theorie der Elektrolytischen Doppelschicht. Zeitschrift fur Elektrochemie 30, 508–516.

Storck, A., Vergnes, F., Le Goff, P., 1975. Transfert de matière entre un électrolyte et une paroi cylindrique immergée dans un lit fixe ou fluidisé de grains isolants. Powder

Technol. 12, 215–223.
Strohl, J.H., Dunlap, K.L., 1972. Electrosorption and separation of quinones on a column of graphite particles. Anal. Chem. 44, 2166–2170. https://doi.org/10.1021/ac60321a012
Su, S.X., Hatton, T.A., 2017. As featured in: Electrosorption at functional interfaces : from molecular-level interactions to electrochemical. Phys. Chem. Chem. Phys. 19, 23570–23584. https://doi.org/10.1039/C7CP02822A
Su, S.X., Hatton, T.A., 2016. Electrosorption 1. Kirk-Othmer Encycl. Chem. Technol. 1–11. https://doi.org/10.1002/0471238961.koe00022
Sun, X.-F., Guo, B.-B., He, L., Xia, P.-F., Shu-Guang Wang, 2016. Electrically accelerated removal of organic pollutants by a three-dimensional graphene aaerogel. AIChE J. 59, 215–228. https://doi.org/10.1002/aic
Tran, H.N., You, S.J., Hosseini-Bandegharaei, A., Chao, H.P., 2017. Mistakes and inconsistencies regarding adsorption of contaminants from aqueous solutions: A critical review. Water Res. 120, 88–116. https://doi.org/10.1016/j.watres.2017.04.014
Trasatti, S., 1992. Adsorption of organic substances at electrodes: Recent advances. Electrochim. Acta 37, 2137–2144. https://doi.org/10.1016/0013-4686(92)85104-S
Trasatti, S., 1972. Work function, electronegativity, and electrochemical behaviour of metals. III. Electrolytic hydrogen evolution in acid solutions. J. Electroanal. Chem. 39, 163–184. https://doi.org/10.1016/S0022-0728(72)80485-6
Trellu, C., Olvera Vargas, H., Mousset, E., Oturan, N., Oturan, M.A., 2021. Electrochemical technologies for the treatment of pesticides. Curr. Opin. Electrochem. 26, 100677. https://doi.org/10.1016/j.coelec.2020.100677
UNESCO, 2019. The United Nations world water development report 2019: leaving no one behind. UN Educ. Sci. Cult. Organ.
Vafakhah, S., Beiramzadeh, Z., Saeedikhani, M., Ying, H., 2020. A review on free-standing electrodes for energy-e ff ective desalination: Recent advances and perspectives in capacitive deionization. Desalination 493, 114662. https://doi.org/10.1016/j.desal.2020.114662
Varley, C.F., 1871. Polarization of metallic surfaces in aqueous solutions. On a new method of obtaining electricity from mechanical force, and certain relations between electrostatic induction and the decomposition of water. Philos. Trans. R. Soc. London 161, 129–136. https://doi.org/10.1098/rstl.1871.0008
Vetter, K.J., Schultze, J.W., 1974. General aspects of the electrosorption valency. Electroanal. Chem. Interfacial Electrochem. 53, 67–76.
Vilar, E.O., Cœuret, F., 1999. Détermination électrochimique du nombre de sherwood minimum pour un milieu macro-poreux (fritté - Lit fixe de grains). Can. J. Chem. Eng. 77, 855–862. https://doi.org/10.1002/cjce.5450770510
Volfkovich, Y.M., 2020. Capacitive deionization of water (a review). Russ. J. Electrochem. 56, 18–51. https://doi.org/10.1134/S1023193520010097
Wadhawan, S., Jain, A., Nayyar, J., Kumar, S., 2020. Journal of water process engineering role of nanomaterials as adsorbents in heavy metal ion removal from waste water: a review. J. water Process Eng. 33, 101038. https://doi.org/10.1016/j.jwpe.2019.101038
Waegele, M.M., Gunathunge, C.M., Li, J., Li, X., 2019. How cations affect the electric double layer and the rates and selectivity of electrocatalytic processes. J. Chem. Phys. 151, 1DUMMT. https://doi.org/10.1063/1.5124878
Wagner, C., 1951. Theoretical analysis of the current density distribution in electrolytic cells. J. Electrochem. Soc. 98, 116. https://doi.org/10.1149/1.2778113
Wang, S., Deng, A.N., Wei, J., Guo, Z., Zhang, N., Guo, Z.Y., 2012. Electrosorption-

enhanced micro-column solid-phase extraction of traces of cresol red in water using electrodes of stainless steel wire coated with non-conductive polymer. Adsorpt. Sci. Technol. 30, 241–253. https://doi.org/10.1260/0263-6174.30.3.241

Wang, Yujing, Zhao, H., Chai, S., Wang, Yabo, Zhao, G., Li, D., 2013. Electrosorption enhanced electro-Fenton process for efficient mineralization of imidacloprid based on mixed-valence iron oxide composite cathode at neutral pH. Chem. Eng. J. 223, 524–535. https://doi.org/10.1016/j.cej.2013.03.016

Xu, F., Chang, L., Duan, X., Bai, W., Sui, X., Zhao, X., 2019. A novel layer-by-layer CNT/PbO_2 anode for high-efficiency removal of PCP-Na through combining adsorption/electrosorption and electrocatalysis. Electrochim. Acta 300, 53–66. https://doi.org/10.1016/j.electacta.2019.01.090

Xu, S., Jin, Y., Li, R., Shan, M., Zhang, Y., 2021. Amidoxime modified polymers of intrinsic microporosity/alginate composite hydrogel beads for efficient adsorption of cationic dyes from aqueous solution. J. Colloid Interface Sci. https://doi.org/10.1016/j.jcis.2021.08.157

Yan, J.W., Tian, Z.Q., Mao, B.W., 2017. Molecular-level understanding of electric double layer in ionic liquids. Curr. Opin. Electrochem. 4, 105–111. https://doi.org/10.1016/j.coelec.2017.09.008

Yang, W., Zhou, M., Ma, L., 2021. A continuous flow-through system with integration of electrosorption and peroxi-coagulation for efficient removal of organics. Chemosphere 274, 129983. https://doi.org/10.1016/j.chemosphere.2021.129983

Yao, C., Zhang, W., Xu, L., Cheng, M., Su, Y., Xue, J., Liu, J., 2021. A facile synthesis of porous MXene-based freestanding film and its spectacular electrosorption performance for organic dyes. Sep. Purif. Technol. 263, 118365. https://doi.org/10.1016/j.seppur.2021.118365

Yue, F., Zhang, Q., Xu, L., Zheng, Y., Yao, C., Jia, J., Leng, W., Hou, S., 2019. Porous reduced graphene oxide/single-walled carbon nanotube film as freestanding and flexible electrode materials for electrosorption of organic dye. ACS Appl. nano Mater. 2, 6258–6267. https://doi.org/10.1021/acsanm.9b01236

Zabasajja, J., Savinell, R.F., 1989. Electrosorption of n-alcohols on graphite particles. AIChE J. 35, 755–763. https://doi.org/10.1002/aic.690350507

Zaharaddeen S. Iro, Subramani, C., Dash, S.S., 2016. A brief review on electrode materials for supercapacitor. Int. J. Electrochem. Sci. 11, 10628–10643. https://doi.org/10.20964/2016.12.50

Zhang, C., He, D., Ma, J., Tang, W., Waite, T.D., 2018. Faradaic reactions in capacitive deionization (CDI) - problems and possibilities: A review 128, 314–330. https://doi.org/10.1016/j.watres.2017.10.024

Zhang, W., Liu, N., Cao, Y., Lin, X., Liu, Y., Feng, L., 2017. Superwetting porous materials for wastewater treatment: from immiscible oil / water mixture to emulsion separation. Adv. Mater. interfaces 4(10). https://doi.org/10.1002/admi.201700029

Zheng, Y., Cheng, B., Fan, J., Yu, J., Ho, W., 2021. Review on nickel-based adsorption materials for Congo red. J. Hazard. Mater. 403, 123559. https://doi.org/10.1016/j.jhazmat.2020.123559

Part II: Materials and Methods

1. Adsorption

1.1.Sample collection and characterization

OMWW was sampled from modern and traditional oil mills (Fig. 16.) located in the region of Marrakech in Morocco. The olive oil extraction season was from December to March during 2019/2020 and 2020/2021 campaigns. The collected samples were subjected to various physicochemical analyses according to the analysis methods as indicated in Table 7. The pH, temperature, total dissolved solids, salinity and electrical conductivity, were measured by a Hanna HI 9829 probe (Kallang Road, Singapore). The COD suspended matter and volatile matter in suspension, ammonium, total phosphorus and orthophosphates were analyzed according to AFNOR standards. The PCs were measured using the Folin-Ciocalteu method (Singleton & Rossi, 1965) using caffeic acid as a standard.

Fig. 16. Images of modern (a) and traditional (b) oil mills, OMWW (c) and olive pomace (d).

Table 7. Standard methods for determining physicochemical parameters.

Parameters	Method
pH, temperature, total dissolved solids, salinity, electrical conductivity	Measured by a probe Hanna HI 9829 (Kallang Road, Singapore)
COD	A dichromate open reflux method measures the amount of oxygen required to oxidize the organic matter in the sample by a redox reaction, AFNOR T90-101.
Suspended matter and volatile matter in suspension	Filtration method on filter, AFNOR T90-105.
Nitrite	Colorimetric determination of nitrite ions, AFNOR T90-013.
Ammonium	Ammonium ions react with phenol and hypochlorite. In alkaline medium, the indophenol blue is determined spectrophotometrically, AFNOR T90-015.
Total phosphorus and ortho-phosphates	Spectrometric methods of phosphorus present in water in various forms from concentrations expressed as phosphorus (P), greater than 0.01 mg L^{-1}, AFNOR T90-023
PCs	Folin-Ciocalteu colorimetric method (Singleton & Rossi, 1965) using caffeic acid as standard.

1.2.Preparation of activated carbon

The olive pomace was collected from modern oil mills located in the region of Marrakech in Morocco. It was dried at 105°C overnight and then ground to a coarse aggregate. The activation process was performed using chemical activation. Ten grams of precursor (olive pomace) was physically mixed with 5 M sodium hydroxide (98-100.5% purity, Sigma-Aldrich) at a weight ratio (activator/precursor) of 1:1 for AC powder and 1: 1; 2: 1; 3: 1; 5: 1 for GAC by stirring for 1 h. Then, the material was thoroughly washed and filtered using deionized ultrapure water until a pH of 7.0 was obtained. Finally, the material was placed in a furnace at room temperature. The adsorbent was heated to 700°C with a temperature increase rate of 10°C per minute. The material was then kept in the furnace (SF7/S Stuart, United Kingdom) at 700°C for 30 min.

The GAC obtained with different mass ratios (activator/precursor) was tested as an adsorbent for PC, and the greatest mass ratio (activator/precursor) was determined.

1.3.Preparation of the beads

Composite beads (sodium alginate (SA)-AC) were prepared via the crosslinking process (Fig. 17). The process for preparing the composite beads consisted of first producing

a primary mixture of the hydrogel of sodium alginate (BioChemica) (1%) at 60°C. Next, the AC powder (1%) was added to the alginate hydrogel under constant stirring to prepare a homogeneous dispersion (24 h). In the second step, the secondary mixture was poured dropwise into a crosslinking iron solution at 20 g L^{-1} (iron (III) chloride hexahydrate, 99%, ACROS Organics). Bead solidification was performed for 24 h. Finally, the aggregated SA-AC beads were thoroughly washed with ultrapure water and stored in ultrapure water.

.

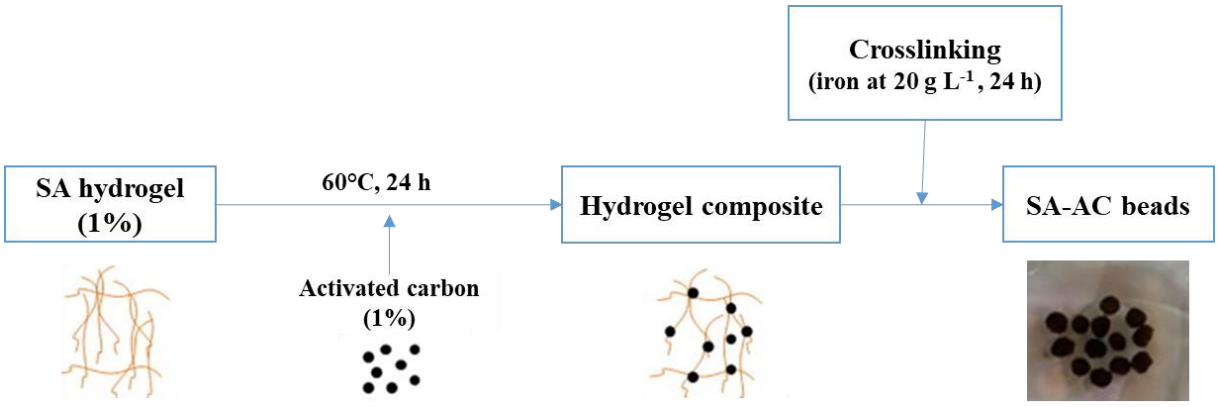

Fig. 17. Schematic representation of the SA-AC beads preparation.

1.4.Characterization of beads and GAC

FTIR was used to assess the functional groups on the surface of the AC, beads and GAC. The FTIR spectra were obtained by ALPHA FT-IR Spectrometer (ALPHA-P, Germany) in the wave number range of 400 to 4,000 cm^{-1}. Each spectrogram consisted of an average of 60 scans.

Morphological examination of the SA-AC beads and GAC was performed using SEM measurements taken with a TESCAN™ VEGA3 scanning electron microscope (Fuveau, France). An EDS analyzer (TEAM™ EDS) enabled the analysis of elements on the micro-scale and element distribution on the SA-AC beads and GAC. In addition, the BET method was used to calculate the specific surface area (S_{BET}) and the total volume (V_T) of AC and SA-AC beads that had been previously outgassed and assessed by nitrogen adsorption at −196°C (via a Micromeritics ASAP 2020 surface analyzer system).

The average pore radius (r^-) was calculated from Eq. 8 (Lawal et al., 2020):

$$r^-(nm) = \frac{2V_T}{S_{BET}} \times 10^3 \quad (8)$$

1.5.Stirred batch and column sorption experiments

1.5.1. SA-AC beads

Batch tests were achieved by adding 5 g of SA-AC beads to a 5 mL OMWW sample for the optimal time in tubes in a rotary mixer under continuous stirring (KS 3000 i control, Germany) at 200 rpm. Isotherm studies were performed on the prepared SA-AC with OMWW of various concentrations (20; 40; 80; 100; 250; 800; 1,000; 1,500; 2,000; 2,500; 3,000; 3,500 and 4,000 mg L^{-1}) for 24 h and at pH 4.0, which corresponds to the pH of the real effluent. In a subset of experiments, the pH of the OMWW solution was adjusted from 4.0 to 10.0 using 1.0 M NaOH or HCl. In the control tests, samples were stirred without SA-AC beads under the same conditions. All experiments were performed at ambient temperature (19 °C) and were performed in duplicate.

The continuous system assays were performed with a column with a 4 cm interior diameter and a height of 30 cm, which was shown in Fig. 18. The SA-AC beads (140 g) were introduced into the column. The OMWW was introduced in ascending flow using a peristaltic pump (Antlia - 3C Dutscher, France) at a constant flow rate of 2 mL min^{-1}. At the outlet of the column, the OMWW was sampled at regular time intervals, and the PC concentration was measured. All tests were carried out in duplicate.

To assess the reusability of this newly generated material, PC desorption from SA-AC beads in the liquid phase was examined in fixed-bed reactors. After the adsorption experiment, the SA-AC beads were rinsed with distilled water three times to eliminate PCs on the surface, targeting the adsorbed fraction. The desorption tests were then performed with ethanol due to the selectivity of this solvent for PCs (Zagklis et al., 2018). Desorption was performed with 5 mL ethanol per g of SA-AC beads. At a constant temperature, ethanol was pumped into the column at a fixed flow rate of 2 mL min^{-1} for 3 h. The PCs concentrations were determined at various time intervals from the beginning of the desorption operation.

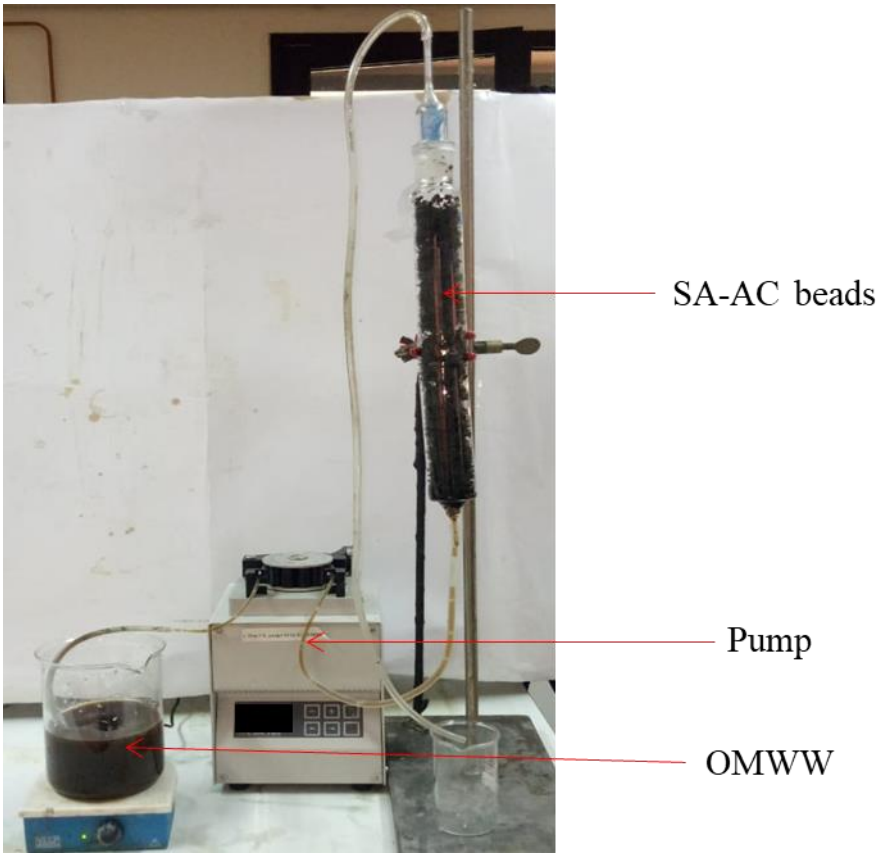

Fig. 18. Fixed-bed adsorption setup.

1.5.2. Granular activated carbon

Batch experiments were performed by adding 5 g of GAC into 5 mL of OMWW sample for an optimized time in tubes under continuous stirring in a rotary mixer (KS 3000 i control, Germany) at 200 rpm. The isotherm studies were done on the prepared GAC with OMWW of various concentrations (20; 50; 100; 250; 1,000; 2,000; 3,000; 4,000 and 5,000 mg L^{-1}) for 24 h and at pH 4, corresponds to the pH of real effluent. In a subset of experiments, the pH of the OMWW solution was adjusted from 2 to 6 using 1.0 M HCl or NaOH. Control tests, in which samples were stirred without GAC, were performed in the same conditions. All experiments were carried out at ambient temperature (between 20 °C and 25 °C) and were performed in duplicate.

A 1 cm diameter and 10, 15 or 20 cm height column filled with GAC (3, 4.5 and 6 g) was used in this study. The OMWW was introduced in ascending flow using a peristaltic pump (Antlia - 3C Dutscher, France), applying a constant flow rate of 0.5, 0.8 or 1.5 mL min^{-}

[1]. The OMWW at the column outlet was collected at regular time intervals, and the PCs' concentrations were measured. All experiments were performed in duplicate.

In order to assess the reusability of GAC, the PCs desorption from the GAC in the liquid phase was examined in batch and fixed-bed reactors. In batch mode, the desorption experiments were carried out with distilled water, ethanol or a mixture of methanol and ethanol (1V/1V) and HCl (0.05 M) due to the selectivity of these solvents for PCs. The desorption experiments were carried out in a fixed-bed device with the most efficient solvent determined in batch. The desorption has been done with 5 mL of solvents per g of GAC. From the start of the desorption process, samples were collected at different time intervals, and the PCs' concentrations were determined.

1.6.Batch and fixed-bed column data analysis

To understand and explain the adsorption process of PCs onto beads and GAC, Langmuir and Freundlich's adsorption isotherm models were presented in this study, according to many references (Badawi et al., 2017; Olusegun et al., 2018; Es-Sahbany et al., 2019). Therefore, these two models are considered compatible with describing the sorption phenomena.

The Langmuir isotherm equation (Eq. 9) shows an adsorption model of a homogeneous system with a single layer and it is expressed as follows (Langmuir, 1916):

$$\frac{C_e}{q_e} = \frac{1}{K_L \times q_m} + \frac{C_e}{q_m} \quad (9)$$

where q_e (mg g^{-1}) is the PCs amount adsorbed at equilibrium, K_L is the Langmuir constant related to the energy of adsorption (L g^{-1}) and q_m (mg g^{-1}) is the maximum PCs adsorption capacity.

The Freundlich adsorption isotherm model is applied for multiple layer adsorption founded on a heterogeneous process. The Freundlich adsorption isotherm equation (Eq. 10) is given as follows (Freundlich, 1906):

$$ln\ q_e = ln\ K_f + \frac{1}{n} \times ln\ C_e \quad (10)$$

where K_f is a Freundlich constant that presents the adsorption capacity of the adsorbent and n is a constant that presents the greatness of the relationship between PCs and SA-AC beads or GAC.

Two kinetic models were investigated to further explain the elimination process of PCs onto SA-AC beads and GAC. The adsorption kinetics data have been compared with the pseudo-first-order and pseudo-second-order rate equations; according to many references, these two models are used to define the sorption mechanisms (Lagergren, 1898; Ho & McKay, 1999) (Eqs. 11 and 12):

$$log\ (q_e - q_t) = log(q_e) - \frac{K_1}{II.303} \times t \quad (11)$$

$$\frac{t}{q_t} = \frac{1}{K_2 \times {q_e}^2} + \frac{t}{q_e}\frac{t}{q_t} = \frac{1}{K_2 {q_e}^2} + \frac{t}{q_e} \quad (12)$$

where q_e and q_t are the amounts of PCs adsorption onto SA-AC beads or GAC at equilibrium and time t, respectively, and k_1 and k_2 are the pseudo-first-order and pseudo-second-order rate constants, respectively.

A temperature study on the adsorption of PCs on alginate beads and GAC at various temperatures (19-35°C) was performed. The thermodynamic parameters, i.e., the Gibbs energy (ΔG in kJ mol^{-1}), standard entropy (ΔS in J mol^{-1} K^{-1}) change, and standard enthalpy (ΔH in kJ mol^{-1}) change, of the adsorption process were calculated from the following equations (Eqs. 13-15) (Li et al., 2019):

$$\Delta G = -R \times T \times ln\ K_c \quad (13)$$

$$\Delta G = \Delta H - T \times \Delta S \quad (14)$$

$$lnK_c = -\frac{\Delta H}{R \times T} + \frac{\Delta S}{R} \quad (15)$$

where K_c is the thermodynamic distribution coefficient calculated using Eq. 16:

$$K_c = \frac{q_e}{C_e} \quad (16)$$

The values of the important design parameters of the breakthrough curves of the column for PCs adsorption onto the SA-AC beads were calculated. The volume of the effluent (V_{ef}) (mL), was calculated using the following equation (Eq. 17):

$$V_{ef} = Q \times t_{total} \quad (17)$$

where t_{total} is the total time (min) and Q_v is the flow rate circulating through the column (mL min^{-1}).

The peak area of the breakthrough curve signifies the total mass of PCs biosorbed, q_{total} (mg), for a specific feed concentration and flow rate and can be calculated by integration as follows (Eq. 18):

$$q_{total} = \frac{Q_v}{1000} \times \int_0^{t_{total}} C_R \times dt \quad (18)$$

where C_R is the concentration of PCs removal (mg L^{-1}).

The total amount of PCs sent to the column (mg) can be determined from Eq. (19):

$$m_{tot} = \frac{C_i \times Q_v \times t_{total}}{1000} \quad (19)$$

The total PC removal efficiency (%) can be determined from the ratio of PCs mass adsorbed (q_{total}) to the total amount of PCs sent to the column (m_{total}) (Eq. 20):

$$\%R = \frac{q_{total}}{m_{total}} \times 100 \quad (20)$$

The amount of PCs adsorbed at equilibrium or adsorption capacity (q_e) (mg of adsorbed PCs/g of SA-AC beads), and the equilibrium PCs concentration (C_e) (mg L^{-1}), can be determined from Eqs. 21 and 22:

$$q_e = \frac{q_{total}}{m} \quad (21)$$

$$C_e = \frac{m_{total} - q_{total}}{V_{ef}} \times 1000 \quad (22)$$

where m_{total} is the amount of PCs sent to the column (g) and V_{ef} (mL) is the volume of the effluent.

The dynamic behavior of the column is approached by the following models: Thomas and Yoon-Nelson.

- Thomas model

The Thomas model is one of the most extensively used breakthrough models in fixed-bed column performance theory. It assumes Langmuir kinetics for adsorption and desorption with no axial dispersion. The model can be presented using Eq. 23 (Thomas, 1944):

$$\frac{C}{C_0} = \frac{1}{1+exp\left(K_{TH}\times q_0\times\frac{m}{Q}-K_{TH}\times C_0\times t\right)} \quad (23)$$

where k_{TH} (mL min^{-1} mg^{-1}) is the Thomas rate constant, q_0 (mg g^{-1}) is the adsorption capacity, m total amount of PCs sent to the column (g), and Q is the flow rate that circulates through the column (mL min^{-1}).

- Yoon-Nelson model

The Yoon-Nelson model (Eq. 24) involves no detailed data about the physical properties of the adsorbent in the fixed-bed column (Yoon & Nelson, 1984):

$$\frac{C}{C_0} = \frac{exp(K_{YN}\times t-\tau\times K_{YN})}{1+exp(K_{YN}\times t-\tau\times K_{YN})} \quad (24)$$

where τ is the time required for 50% adsorbate breakthrough (min) and k_{YN} is a rate constant that is related to the diffusion characteristics of the mass transfer zone (min^{-1}).

The fittings of the models with experimental results were evaluated with the mean absolute error (MAE) and the root-mean-square error (RMSE) as written in Eq. 25 and Eq. 26, respectively:

$$MAE = \frac{\sum_{i=1}^{K}|y_i- y_i'|}{K} \quad (25)$$

$$RMSE = \sqrt{\frac{\sum_{i=1}^{K}(y_i- y_i')^2}{K}} \quad (26)$$

where y_i' the experimental value, y_i the model value and K is the number of iterated values.

The lower the MAE and RMSE value are, the more suitable the model.

1.7.Analytical methods

The phenolic extracts were analyzed by high-performance liquid chromatography (HPLC). A Knauer-HPLC chromatography equipped with a diode array detector was used for processing the data. The column had a reversed-phase polarity (Eurospher II 100-5 C-18, 250×4.6). The mobile phase was a gradient of acetonitrile and bidistilled water acidified to pH 2.6 with O-phosphoric acid. The separation lasted 1 h according to a linear gradient program of acetonitrile/water and was performed at a temperature of 25°C, a pressure of 400 bar and a flow rate of 1 mL min^{-1}.

2. Electrosorption

2.1. Effluents preparation and characterization

The simulated OMWW was prepared using potassium chloride (KCl) (6 g L^{-1}) and phenol (4 g L^{-1}) adjusted to pH 4 using hydrochloric acid (HCl) (Sigma Aldrich, Saint-Quentin-Fallavier, France), which was representative of the average characteristics in actual OMWW (Lissaneddine et al., 2021a). The phenol content was determined by UV-visible spectrophotometry (Shimadzu UV-2600 spectrophotometer) at the maximum absorption wavelength of 269 nm (Adebayo & Areo, 2021). In the case of the influence of the properties of PCs (Part III, sub-chapter II.II), other PCs were studied such as gallic acid (4,000 mg L^{-1}), caffeic acid (500 mg L^{-1}), coumaric acid (500 mg L^{-1}) and quercetin (60 mg L^{-1}), and they were also quantified by UV-visible spectrophotometry.

The real OMWW was collected from modern oil mills located in the region of Marrakech in Morocco during the olive oil extraction season from December to March during the 2019/2020 and 2020/2021 campaigns, during which the main products were PCs (Lissaneddine et al., 2021a). Meta-phosphoric acid, petroleum ether, ethyl acetate and methanol (Sigma Aldrich, Saint-Quentin-Fallavier, France) were employed to measure the total PCs using the Folin-Ciocalteu method (Singleton & Rossi, 1965). All commercially available reagents were used without further purification, while ultrapure water (18.2 mΩ cm) was used in all experiments and analyses (PureLab ELGA Classic, Veolia Water, Antony, France).

2.2.Preparation and characterization of the 3D porous electrode

The porous material (SA-AC beads) was prepared based on AC of olive pomace according to the protocol described in section 1.3 of part II (Lissaneddine, et al., 2021a). Two crosslinking agents (iron and calcium) have been used in beads preparation (100% w/v Fe and 100% w/v Ca). The proportions in weight per volume (% w/v) of AC (0%, 0.5%, 0.75%, 1%, 2%, 3%) have been varied in the SA-AC beads preparation.

The new porous GAC was prepared based on olive pomace according to section 1.2 of part II. An electrochemical condition step has been added to further improve the GAC properties. The GAC was implemented in the setup detailed in section 2.3 of part II. Then an

anodic current of 200 mA (anode potential (E_{an}) = 1.8V/(Ag/AgCl)) was applied for 1 h, while 100 mL of KCl (6 g L^{-1}) was used as electrolyte.

The electrochemical properties of the prepared SA-AC beads and GAC electrode were evaluated using a potentiostat (AMETEK, Massy, France) in a three-electrode system whose design is described in section 2.3 of part II. The SA-AC beads or GAC were employed as a working electrode, a graphite rod (Final Advanced Material, Didenheim, France) or platinum wire (Ögussa, Vienna, Austria) as a counter electrode and Ag/AgCl as a reference electrode. The electroactive surface of the porous material was determined by cyclic voltammetry (CV) with -0.2 to 0.8 V/(Ag/AgCl) of voltage range and 0.01 V s^{-1} as scan rate, followed by the use of the Randles-Sevcik equation to determine the surface from the current intensity peak (Mousset, et al., 2016a). Tafel slopes were obtained from linear sweep voltammetry (LSV) with -2 to 2 V/(Ag/AgCl) of voltage range and 0.01 V s^{-1} as scan rate and were used to calculate the exchange current intensity (I_0) of the 3D porous electrode (Mousset et al., 2016b; Fang et al., 2017; Adnan et al., 2021b). Electrochemical impedance spectroscopy (EIS) using the frequency range from 50,000 to 0.1 Hz with an amplitude of 10 mV have been performed to characterize the working electrode/electrolyte interface using the equivalent electrical circuit (EEC) method (Mousset et al., 2016c). The EIS data were fitted using ZSimpWin data analysis software (AMETEK, Massy, France).

2.3.Electrochemical setup and procedure

2.3.1. SA-AC beads

The performance of electrosorption with SA-AC beads working electrode was tested on a fixed-bed column reactor (Figs. 19 and 20) using a graphite rod (210 mm length, 12 mm diameter) as current collector to connect in a monopolar mode the SA-AC beads (35 g) with the potentiostat. The counter electrode was a graphite rod (100 mm length, 8 mm diameter) and was ascribed to the anode. In all experiments, 100 mL of effluent was introduced in ascending flow using a peristaltic pump (Fisher Scientific, Illkirch-Graffenstaden, France) at a constant flow rate of 10 mL min^{-1}. The cathode potential (E_{cat}) was varied from -0.8 to -1.3 V/(Ag/AgCl) and the open circuit (OC) was tested for a blank experiment in the absence of applied voltage. The electrosorption capacity (q_A in mg g^{-1}) was calculated according to Eq. 1 (Yingzhen Li et al., 2016):

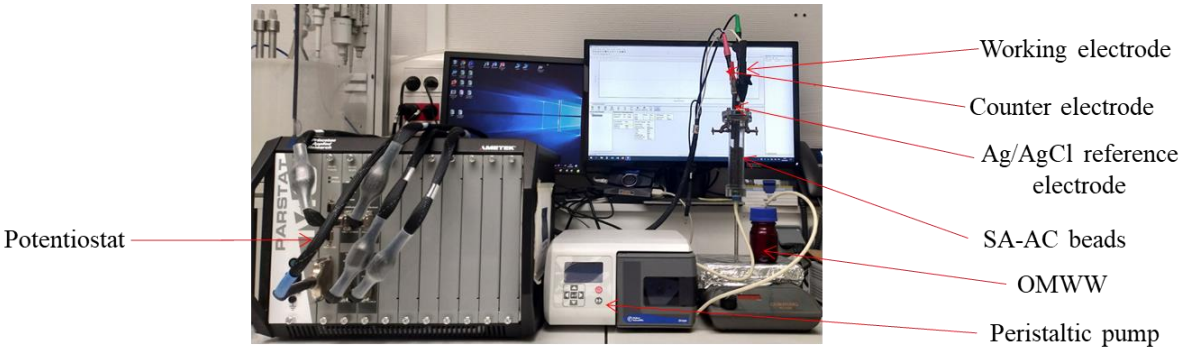

Fig. 19. Fixed-bed electrosorption image setup.

The mass transfer coefficients (k_m) within the column were determined by LSV using the limiting-current technique with solutions containing 0.05 M $K_3Fe(CN)_6$, 0.10 M $K_4Fe(CN)_6$ and 0.50 M Na_2CO_3 (Sigma Aldrich, Saint-Quentin-Fallavier, France) (Selman & Tobias, 1978; Cañizares et al., 2006; Adnan et al., 2021). The internal ohmic resistance were determined according to the Eq. 27 (Miller et al., 2019):

$$\sum R = E_{cell} - |E_C| - |E_A| \quad (27)$$

where ∑R is the ohmic drop, E_{cell} is the cell voltage, $|E_A|$ and $|E_C|$ are the absolute values of anode and cathode potentials, respectively.

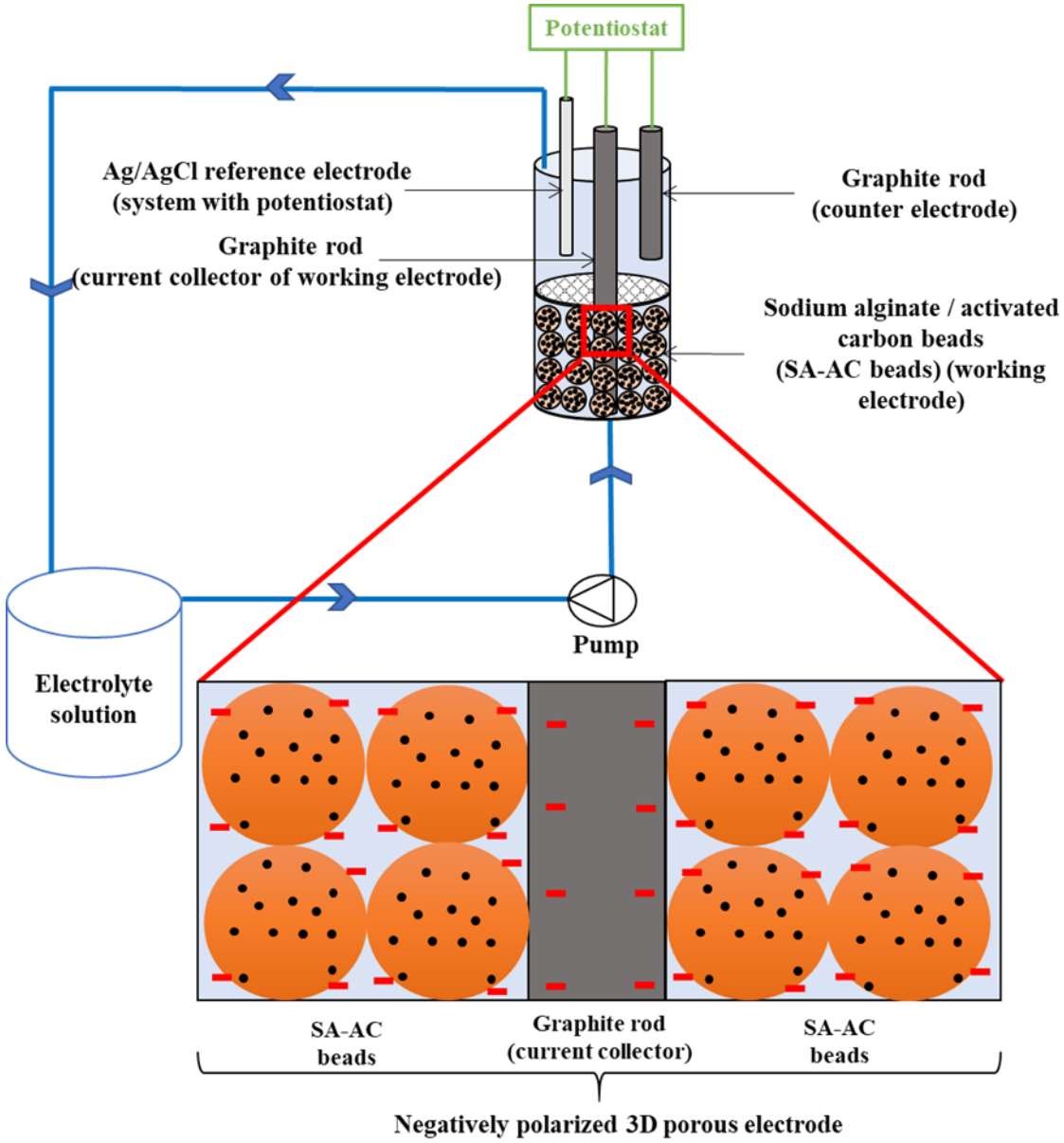

Fig. 20. Fixed-bed electrosorption schematic setup.

2.3.2. Granular activated carbon

The PCs electrosorption tests were performed with a fixed-bed column with a 2.6 cm interior diameter and a height of 15 cm (Fig. 21). This setup is similar to the one employed with alginate beads, except that instead of filling with SA-AC beads it was filed by GAC prepared according to the protocol developed in Part III, Chapter II. 10 g of GAC were introduced into the column connected by graphite rod (210 mm length, 12 mm diameter) as a current collector between the power supply and the porous GAC, considering a monopolar connection mode. The counter electrode was a platinum wire (80 mm length, 1 mm diameter).

The applied current intensities were varied from 1 to 150 mA. In all experiments, 100 mL of effluent was introduced in ascending flow using a peristaltic pump at a constant flow rate of 10 mL min^{-1}. At the column outlet, the effluent was sampled at regular time intervals, and the PCs concentration was measured.

A possible way for quantitative comparison of the extent of electrosorption could be made by calculating the percentage of PCs removed at equilibrium ($\%R_{eq}$), through Eq. 28 (Bayram, 2016):

$$\%R_{eq} = \frac{(C_0 - C_e)}{C_0} \times 100 \quad (28)$$

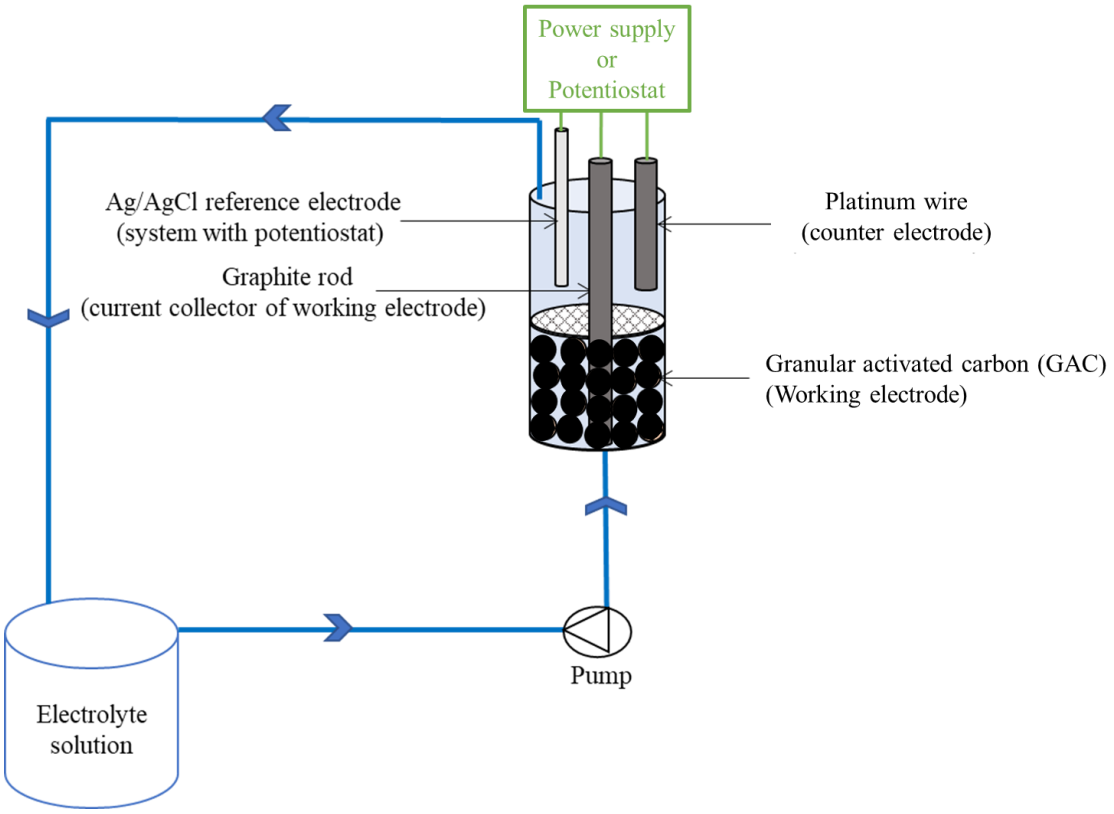

Fig. 21. Scheme of the fixed-bed electrosorption setup.

2.4.Electrochemical regeneration of the GAC electrode

The electrochemical regeneration of GAC was performed with 100 mL KCl (Sigma Aldrich, Saint-Quentin-Fallavier, France) solution (0.1 g L^{-1}) (Hou et al., 2012) using the reactor used for the electrosorption experiment. The regeneration currents were 1 then 10 mA at anodic polarization during 6 h. The regeneration process was evaluated using the percentage of regeneration efficiency (*RE*) (Han et al., 2008):

$$RE = \frac{C_r}{C_e} \times 100 \quad (29)$$

where C_r *is* the adsorptive capacity of regenerated GAC.

2.5.Electrochemical degradation of OMWW

After electrosorption, electro-oxidation was implemented to further treat the organic compounds that remained in the OMWW solution. The anodic oxidation experiments were performed in a cell described elsewhere (Fig. 22) (Adnan et al., 2021a), with a working volume of 94 mL. The cathode used in this work was in stainless steel (Gantois Industries, Saint-Dié-des-Vosges, France) and the anode was a double-sided BDD coated on Niobium (Nb) substrate (DiaCCon, Fürth, Germany). The stainless steel and BDD had an effective surface area of 50 cm^2. A peristaltic pump (Masterflex, Cole-Parmer, Vernon Hills, IL, USA) was used to circulate the OMWW at a constant flow rate of 0.68 L min^{-1}. A non-conductive polytetrafluoroethylene spacer (3 mm) (Bohlender, Grünsfeld, Germany) was placed between the cathode and the anode to avoid contact in-between. The applied current was 1 A. The effluent was sampled before and after electrooxidation, and the COD and PCs concentrations were measured.

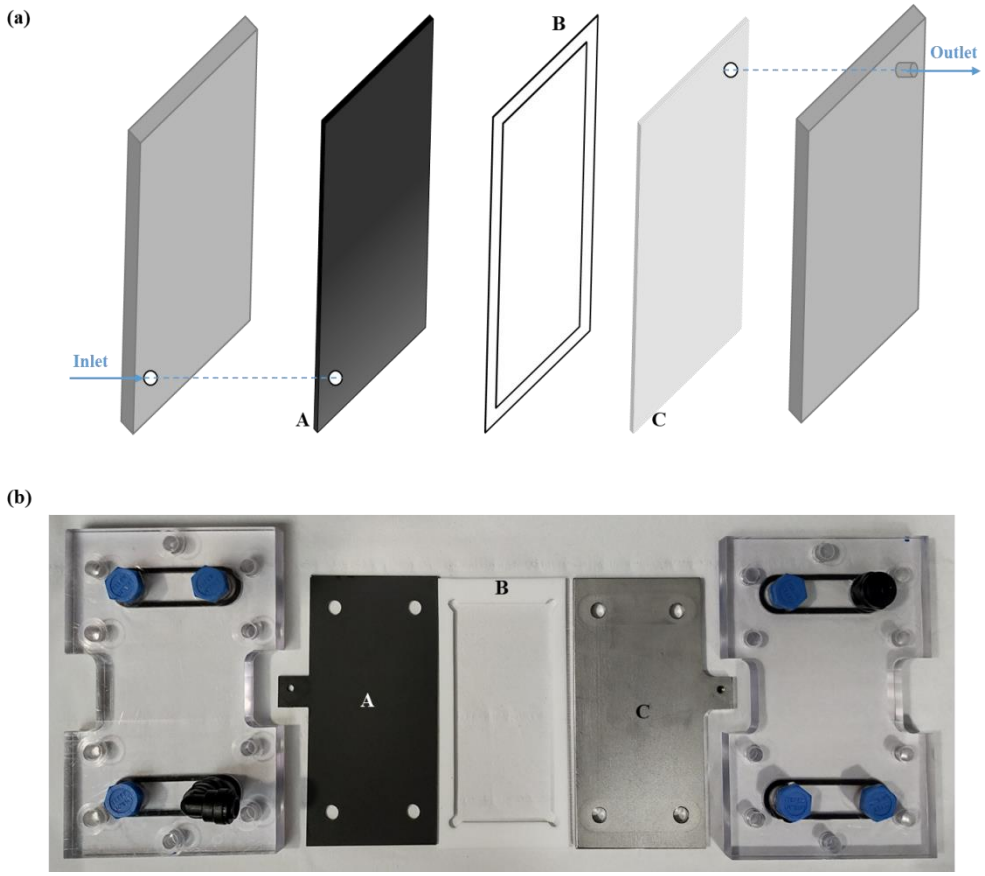

Fig. 22. An exploded view of the parallel-plate electrochemical reactor. A: anode in BDD, B: spacer, C: cathode in stainless steel.

References

Adebayo, M.A., Areo, F.I., 2021. Removal of phenol and 4-nitrophenol from wastewater using a composite prepared from clay and Cocos nucifera shell: Kinetic, equilibrium and thermodynamic studies. Resour. Environ. Sustain. 3, 100020. https://doi.org/10.1016/j.resenv.2021.100020

Adnan, F.H., Mousset, E., Pontvianne, S., Pons, M., 2021a. Mineral cathodic electro-precipitation and its kinetic modelling in thin-film microfluidic reactor during advanced electro-oxidation process. Electrochim. Acta 387, 138487. https://doi.org/10.1016/j.electacta.2021.138487

Adnan, F.H., Pons, M.-N., Mousset, E., 2021b. Mass transport evolution in microfluidic thin film electrochemical reactors: New correlations from millimetric to submillimetric interelectrode distances. Electrochem. commun. 130, 107097. https://doi.org/10.1016/j.elecom.2021.107097

Badawi, M.A., Negm, N.A., Abou Kana, M.T.H., Hefni, H.H., Abdel Moneem, M.M., 2017. Adsorption of aluminum and lead from wastewater by chitosan-tannic acid modified biopolymers: Isotherms, kinetics, thermodynamics and process mechanism. Int. J. Biol. Macromol. 99, 465–476. https://doi.org/10.1016/j.ijbiomac.2017.03.003

Bayram, E., 2016. Electrosoption of aromatic organic acids from aqueous solutions onto granular activated carbon electrodes for water purification. Hacettepe J. Biol. Chem. 3, 273–273. https://doi.org/10.15671/hjbc.20164420570

Cañizares, P., Marcos, I.F. De, Rodrigo, M.A., Lobato, J., 2006. Measurement of mass-transfer coefficients by an electrochemical technique. J. Chem. Educ. 83, 1204–1207. https://doi.org/10.1021/ed083p1204

Es-Sahbany, H., Berradi, M., Nkhili, S., Hsissou, R., Allaoui, M., Loutfi, M., Bassir, D., Belfaquir, M., El Youbi, M.S., 2019. Removal of heavy metals (nickel) contained in wastewater-models by the adsorption technique on natural clay. Mater. Today Proc. 13, 866–875. https://doi.org/10.1016/j.matpr.2019.04.050

Fang, Z., Cao, X., Li, Xuexiao, Wang, H., Li, Xianning, 2017. Electrode and azo dye decolorization performance in microbial-fuel-cell- coupled constructed wetlands with different electrode size during long- term wastewater treatment. Bioresour. Technol. 238, 450–460. https://doi.org/10.1016/j.biortech.2017.04.075

Freundlich, H.M.F., 1906. Über die adsorption in lösungen. Z. Phys. Chem. 57, 385–470.

Han, Y., Quan, X., Ruan, X., Zhang, W., 2008. Integrated electrochemically enhanced adsorption with electrochemical regeneration for removal of acid orange 7 using activated carbon fibers. Sep. Purif. Technol. 59, 43–49. https://doi.org/10.1016/j.seppur.2007.05.026

Ho, Y.S., McKay, G., 1999. Pseudo-second-order model for sorption processes. Process Biochem. 451–465. https://doi.org/10.1021/acs.oprd.7b00090

Lagergren, S. Sven, K., 1898. Vetenskapsakad, Citation review of lagergren kinetic rate equation on adsorption reactions. Handl 24, 1–39.

Langmuir, I., 1916. The constitution and fundamental properties of solids and liquids. Part-I. Solids. J. Am. Chem. Soc. 38, 2221–2295.

Li, Y., Fu, F., Cai, W., Tang, B., 2019. Synergistic effect of mesoporous feroxyhyte nanoparticles and Fe(II) on phosphate immobilization: Adsorption and chemical precipitation. Powder Technol. 345, 786–795. https://doi.org/10.1016/j.powtec.2019.01.075

Li, Y., Zhang, C., Jiang, Y., Wang, T., Wang, H., 2016. Effects of the hydration ratio on the

electrosorption selectivity of ions during capacitive deionization. Desalination 399, 171–177. https://doi.org/10.1016/j.desal.2016.09.011

Lissaneddine, A., Mandi, L., Achaby, M. El, Mousset, E., Eldon, R., Ouazzani, N., Pons, M., Aziz, F., 2021. Performance and dynamic modeling of a continuously operated pomace olive packed bed for olive mill wastewater treatment and phenol recovery. Chemosphere 130797. https://doi.org/10.1016/j.chemosphere.2021.130797

Miller, A., Singh, L., Wang, L., Liu, H., 2019. Linking internal resistance with design and operation decisions in microbial electrolysis cells. Environ. Int. 126, 611–618. https://doi.org/10.1016/j.envint.2019.02.056

Mousset, E., Wang, Z., Hammaker, J., Lefebvre, O., 2016. Physico-chemical properties of pristine graphene and its performance as electrode material for electro-Fenton treatment of wastewater. Electrochim. Acta 214, 217–230. https://doi.org/10.1016/j.electacta.2016.08.002

Olusegun, S.J., de Sousa Lima, L.F., Mohallem, N.D.S., 2018. Enhancement of adsorption capacity of clay through spray drying and surface modification process for wastewater treatment. Chem. Eng. J. 334, 1719–1728. https://doi.org/10.1016/j.cej.2017.11.084

Selman, J.R., Tobias, C.W., 1978. Mass-transfer measurements by the limiting-current technique. Adv. Chem. Eng. 10, 211–318.

Singleton, V. L., & Rossi, J.A., 1965. Colorimetry of total phenolic substances. US Am. Chem. Soc. Symp. Ser. 26, 47–70.

Singleton, V.L., Rossi, J.A., 1965. Colorimetry of total phenolics with phosphomolybdic-phosphotungstic acid reagents. Am. J. Enol. Vitic. 16(3), 144–158.

Thomas, C., 1944. Heterogeneous ion exchange in a flowing system. J. Am. Chem. Soc. 1664–1666.

Yoon, Y.H.E.E., Nelson, J.H., 1984. Application of gas adsorption kinetics I. A theoretical model for respirator cartridge service life. Am. Ind. Hyg. Assoc. J. ISSN 8894, 509–516. https://doi.org/10.1080/15298668491400197

Part III: Results and Discussion

Chapter I: Composite beads

I. Performance and dynamic modeling of a continuously operated pomace olive packed-bed for olive mill wastewater treatment and phenol recovery

1. Introduction

In recent years, many adsorbents, such as AC, have been used to eliminate PCs (Annab et al., 2019). AC is commonly used because of its microporous texture, high surface reactivity, consistency in the distribution of pore size, wide spectrum of functional surface groups and thermal steadiness (Shim et al., 2019).

A column reactor is a practical and simple device that reduces the costs of the energy needed for water treatment by exploiting the concentration gradient between the adsorbent and pollutants, producing high-quality treated effluents with a minimum pollutant concentration on an ongoing basis (Basu et al., 2019). However, due to the small particle size of AC, its application in continuous flow adsorption systems has some disadvantages, such as bed compaction and a high-pressure drop in fixed bed column systems (Aziz et al., 2020). To avoid such drawbacks, the encapsulation of AC in alginate hydrogels is an attractive alternative with high applicability for continuous flow adsorption processes (Aziz et al., 2020; Quesada et al., 2020). Alginate gels are highly permeable due to their porous texture and hydrophilicity, providing important advantages due to their high affinity and adsorption potential for several micropollutants, such as heavy metal ions and dyes (Arenales-Sierra et al., 2019; Quesada et al., 2020). However, the wastewater treatment operation at the real scale requires granular materials of controlled size. Numerous researchers had to generate those materials by encapsulating diverse adsorbents in the alginate composite to improve their potentials (Aziz et al., 2020).

Currently, many researchers use beads with alginate coatings on several kinds of sorbent materials or functionalize them to be more efficient and test the obtained composites for OMWW PCs or synthetic effluent. Duarte et al. (2014) used silica-alginate-fungi biocomposites; Nadavala et al. (2009) investigated chitosan-calcium (CS/Ca) alginate blended beads; Kim et al. (2008) used an alginate-activated carbon (AAC) bead and Jodra and Mijangos (2003) used a calcium alginate-AC composite bead. Although numerous studies exist on applyingof alginate composite beads for the treatment of PCs of OMWW or synthetic

phenol from water, this is the first work on the combined use of olive mill wastes and alginate for the adsorption and recovery of PCs from real OMWW.

In a similar work, Annab et al. (2019) investigated beads based on AC encapsulated in calcium alginate to adsorb polyphenols from OMWW. This work succeeded in attaining a high level of adsorption capacity of their synthesized material for polyphenols. In addition, the activation of the pomace used in this work was accomplished with KOH. Furthermore, these beads were tested under batch and column conditions on only synthetic effluent and OMWW diluted in ultrapure water, i.e., without the high concentrations that are characteristic of real effluents. All these reasons make their results not easily applicable to industrial applications. Therefore, it is suggested in the present work to use raw effluent and AC treated with NaOH before transforming it into beads for the first time and characterizes the PCs adsorbed from OMWW by liquid chromatography.

The objective of this study was to perform a cycle of olive mill waste treatment in which the OP is first converted into a highly porous AC that can be subsequently used for the treatment of OMWW by adsorption. The kinetics, mechanism and adsorption characteristics of PCs adsorption were investigated. The experiments were carried out under different operational conditions (time, concentration, pH, temperature) to determine the adsorbent behavior in stirred batch and fixed-bed reactors. PCs recovery and the process reusability of SA-AC beads were carried out in fixed-bed reactors.

2. Results and discussion

2.1.Physicochemical properties of the effluent

Table 8 presents the physicochemical properties of the studied OMWW. The results showed that OMWW has acidic pH values equal to 4.8 and 4.7 for modern oil mills and traditional oil mills, respectively, due to the presence of organic acids and PCs. The latter constitute a large proportion of OMWW (4 and 10 g L^{-1} for modern oil mills and traditional oil mills, respectively). This high content of PCs leads to the toxicity of this effluent. It is further associated with a high concentration of organic matter, indicated by a very high COD value (110 g-O_2 L^{-1} for traditional oil mills). Furthermore, inorganic loads such as sodium (0.13 g L^{-1}), potassium (5.9 g L^{-1}), calcium (0.24 g L^{-1}) and chloride (3.5 g L^{-1}) are high for modern oil mills. These high organic and inorganic loads can make biological treatment

extremely difficult and justify implementingalternative physicochemical processes such as adsorption. In addition, the concentration of total solids is relatively high (128 g L^{-1}).

Table 8. Physicochemical parameters of the OMWW.

Parameters	Traditional oil mills	Modern oil mills
pH	4.86 ± 0.01	4.7 ± 0.005
Electrical conductivity (mS cm^{-1})	25.0 ± 0.4	23.3 ± 0.02
Total dissolved solids (g L^{-1})	11.5 ± 0.6	12.0 ± 0.07
Salinity (practical salinity unit)	14.0 ± 0.02	14.3 ± 0.01
Total dry matter (g L^{-1})	128 ± 18	105 ± 11
Suspended matter (g L^{-1})	2.6 ± 0.08	2.1 ± 0.06
Alkalinity (mg-$CaCO_3$ L^{-1})	444 ± 32	336 ± 22
COD (g-O_2 L^{-1})	110 ± 8	66 ± 3
Total phosphorus (mg L^{-1})	0.57 ± 0.09	0.53 ± 0.02
Orthophosphate (mg L^{-1})	0.37 ± 0.01	0.30 ± 0.001
Nitrite (mg L^{-1})	0.09 ± 0.01	0.08 ± 0.005
Ammonia nitrogen (mg L^{-1})	2 ± 0.5	2 ± 0.1
Total phenol (g L^{-1})	10.7 ± 0.05	4.7 ± 0.2
Total sugars (g L^{-1})	4.7 ± 0.003	4.5 ± 0.02
Sodium (g L^{-1})	0.13 ± 0.03	0.13 ± 0.01
Potassium (g L^{-1})	5.5 ± 0.05	5.9 ± 0.02
Calcium (g L^{-1})	0.24 ± 0.04	0.24 ± 0.01
Chloride (g L^{-1})	2.4 ± 0.08	3.5 ± 0.03

The analysis of the phenolic composition of this effluent by HPLC (Fig. 23) revealed the presence of a varied phenolic pool composed mainly of gallic acid, tyrosol, ferulic acid, caffeic acid, cinnamic acid, and coumaric acid. Magdich et al. (2012) found protocatechuic acid, tyrosol, benzoic acid, ferulic acid and p-coumaric acid. In addition, Tafesh et al. (2014)

showed the presence of hydroxytyrosol, acetic acid, 3,4-dihydroxyphenyl, tyrosol, protocatechuic acid, vanillic acid, verbascoside, caffeic acid, p-coumaric acid and ferulic acid. However, Leouifoudi et al. (2014) identified tyrosol and hydroxytyrosol as the main PCs in OMWW, which is similar to the results reported by Achak et al. (2009). PCs do not have the same organic functions; therefore, the adsorption mechanism should not be selective for the organic structure of only one type of PC.

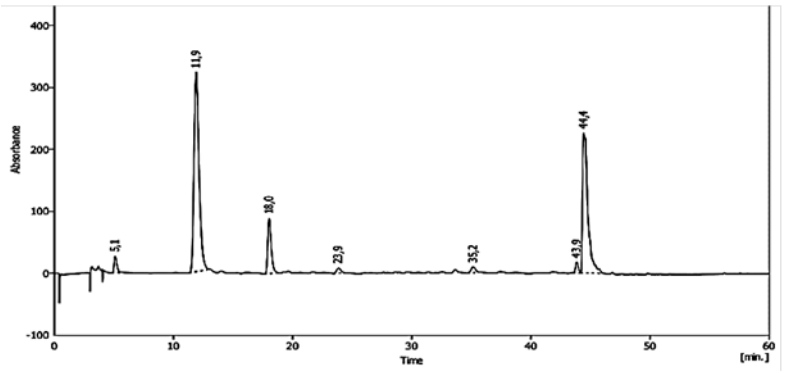

Time (min)	Phenolic compounds
5.1	Gallic acid
11.9	Tyrosol
18.0	Caffeic acid
23.9	Ferulic acid
35.2	Coumaric acid
44.4	Cinnamic acid

Fig. 23. Chromatographic spectrum (HPLC) of the used OMWW.

2.2.Characterization of the adsorbent

FTIR spectra of AC and SA-AC beads before and after adsorption are displayed in Figs. 24a, 24b and 24c. FTIR spectra were obtained in the wavenumber range of 4000 - 400 cm^{-1}. The peaks of the FTIR spectrum of AC (Fig. 24 a) at 3457 cm^{-1} could be the -OH stretching vibration mode of hydroxyl functional groups. The band at approximately 3032 cm^{-1} corresponds to the stretching mode of aromatic unsaturated hydrocarbon groups (Iwanow et al., 2020). The symmetrical stretching vibrations of $-CH_2-$ and -C=O groups are represented by the bands at1435 cm^{-1} and 1683 cm^{-1}, respectively (Wang et al., 2019). In the FTIR spectrum of the SA-AC beads (Fig. 24b), the band at approximately 3308 cm^{-1} corresponds to the hydroxyl group (-OH group). The stretching vibration of the carbonyl (-C=O) group appears at 1590 cm^{-1}; the symmetrical stretching vibration of $-CH_2-$ is located at 1402 cm^{-1} (Allwar et al., 2020). The absorption band at 1037 cm^{-1} is attributed to the bending vibration of the O-H group (Nasrullah et al., 2018). There were no significant differences in FTIR spectra between SA-AC beads after adsorption of PCs and SA-AC beads before adsorption. This result is in accordance with the work previously reported by Shim et al. (2018). These researchers speculated that weak electrostatic interactions and ionic adsorption are prevalent among the studied contaminants and beads.

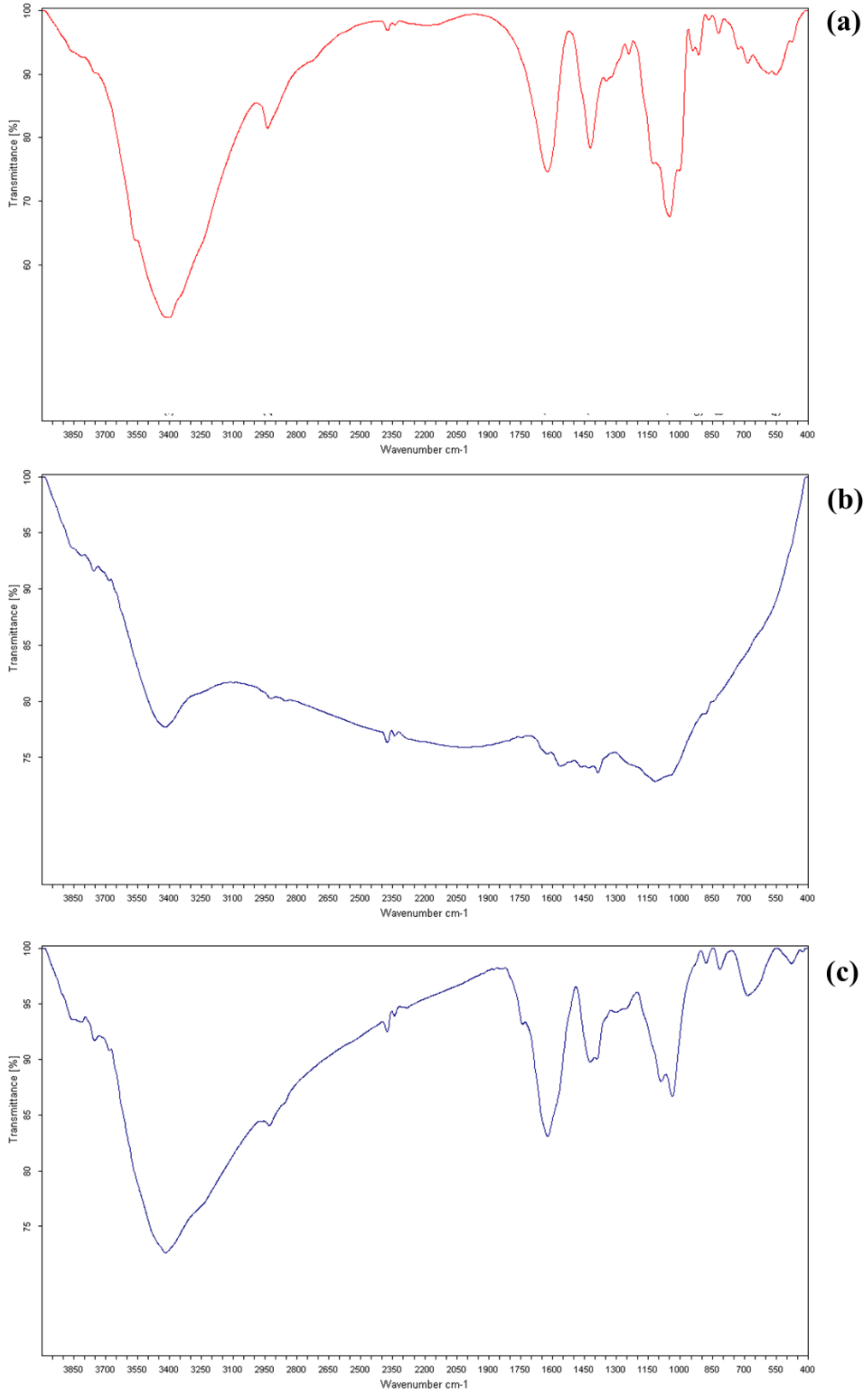

Fig. 24. FTIR spectra of AC (a), SA-AC beads before (b) and after (c) adsorption.

The textural characteristics of AC and SA-AC beads were evaluated by SEM, and images at the same magnifications are shown in Figs. 25a and 25b. In the SEM photograph, the AC surface has a porous morphology caused by the effect of sodium hydroxide as an activating agent at higher temperatures, and the surface of SA-AC beads has a porosity less than that of a pure AC sample. However, SA-AC beads still have a rough and porous surface. Similar texture characteristics were observed by Iqbal et al. (2019), Nasrullah et al. (2018) and Hassan et al. (2014). Nasrullah et al. (2018) and Hassan et al. (2014) used alginate/AC composite beads and AC based on apricot stones, respectively. The SEM of these composite beads shows that the surface of the bead composite has a porosity less than that of pure AC, which is similar to the results of the present study.

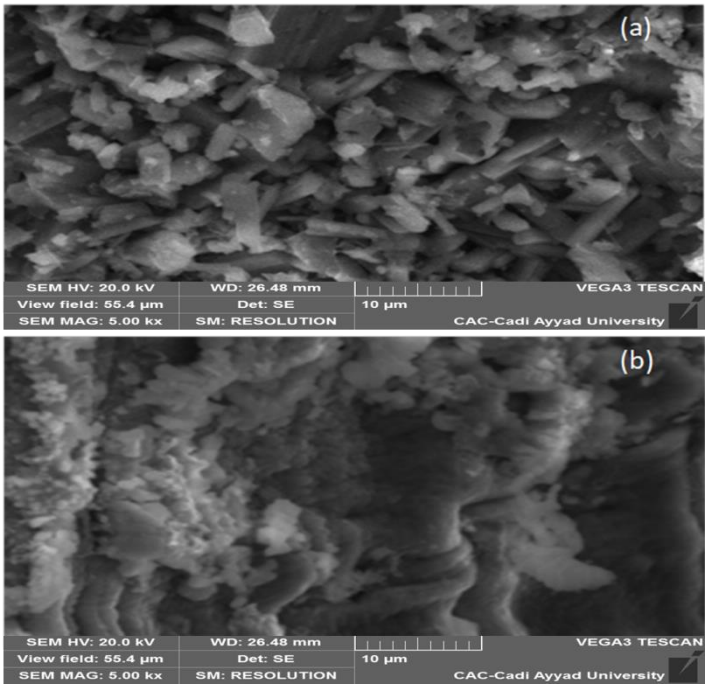

Fig. 25. SEM of AC (a) and SA-AC beads (b).

Figs. 26a and 26b show the EDS spectra of AC and SA-AC beads. EDS analysis revealed the presence of C, O and Na on the AC surface. After crosslinking (Fig. 26b), Fe, Al and Cl appeared on the surface. These results confirm the existence of a crosslinking agent on the bead surface. Iqbal et al. (2019) used nano-zero valent copper and AC on hydroxyapatite-alginate beads and $CaCl_2$ as a crosslinking agent, and EDS analysis showed Ca and Cl elements in the prepared beads. In addition, Huixue et al. (2016) used $CaCl_2$ and $FeCl_3$

solutions to synthesize SA-carboxymethyl cellulose beads and showed that Fe, Ca, and Cl exist on the bead surface and are important for the formation of beads.

The textural characteristics of the raw AC and SA-AC beads are shown in Table 9. The specific surface areas (S_{BET}) of AC and SA-AC were 758 and 523 m^2 g^{-1}, respectively. In addition, the total pore volume (V_T) values were 0.805 cm^3 g^{-1} for AC and 0.308 cm^3 g^{-1} for SA-AC beads, which are almost analogous to those reported by other researchers. Kwak et al. (2018) reported V_T values of 0.710 cm^3 g^{-1} for AC and 0.358 cm^3 g^{-1} for composite beads.

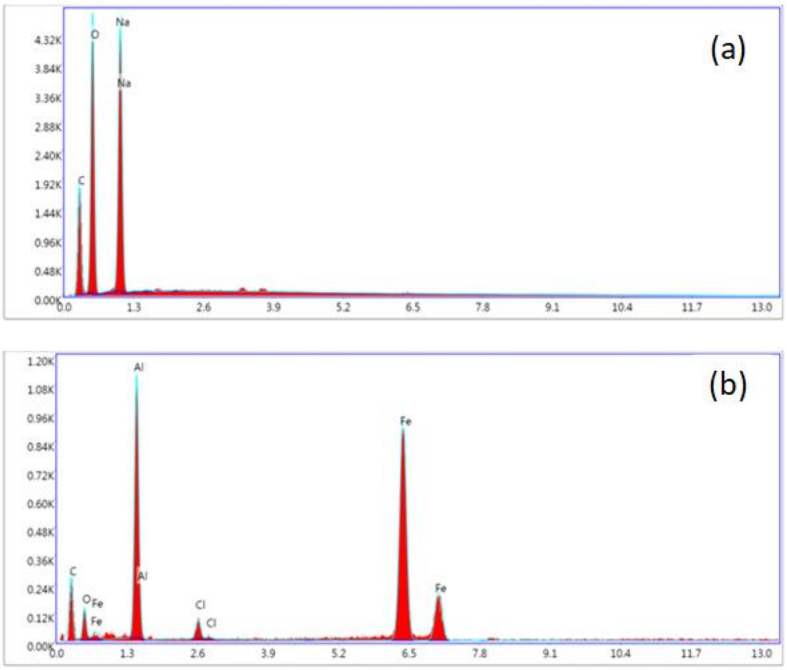

Fig. 26. EDS spectra of AC (a) and SA-AC beads (b).

The average $\bar{r}$ values were 2.124 nm and 1.179 nm for the AC and SA-AC beads, respectively. The decrease in the $\bar{r}$ of AC when mixed with sodium alginate polymer to generate SA-AC beads indicates pore encapsulation by sodium alginate. These results show the feasibility of agglomerating the adsorbent (powder) into the macroparticles (beads), thereby maintaining higher adsorption capacities and avoid clogging problems during continuous column operation. By overcoming the operational problems such as pressure drop and clogging, the process life cycle increases resulting in a decrease in the operational costs. Besides, in order to promote the concept of a circular greeneconomy, it is important to move in the direction of resource recovery rather than following the traditional end of pipe treatment approach. The application of resource-efficient technologies such as adsorption using locally available materials and resource recovery to obtain value-added products (e.g.

phenols) will not only facilitate the removal of harmful contaminants from water or wastewater, but it will also be rewarding economically at the industrial scale (Aziz et al, 2020).

Table 9. Textural characteristics for AC and SA-AC beads.

	S_{BET} (m^2 g^{-1})	V_T (cm^3 g^{-1})	r^- (nm)
AC	758	0.805	2.124
SA-AC	523	0.308	1.179

2.3.Adsorption efficiency

Figure 27a presents the effect of contact time on the removal PCs capacity onto SA-AC beads. The results show that the removal potential increased rapidly at the initial stage until 120 min. Afterward, the PCs adsorption potential did not change meaningfully until equilibrium was reached. Thus, the initial rapid uptake is caused by the existence of a greater number of active sites on the SA-AC beads in the starting stage. After a lapse of time, the accumulation of PCs in the active sites cause the decrease in the adsorption of more compounds (Braghiroli et al., 2018).

2.3.1. Adsorption equilibrium study

The adsorption isotherms were analyzed to describe the PCs distribution between the liquid and solid phases when the adsorption process attained equilibrium (Liu et al., 2019). Figure 27b shows the PCs adsorption isotherms onto SA-AC beads. The amount of adsorbed PCs increased with the PCs concentration in solution until it reached 95 mg g^{-1} at 1,000 mg L^{-1}. The increasing amount of PCs in the solution causes a rise in the mass transfer driving force (Li et al., 2019).

The model-fitting results from the adsorption isotherms are shown in Figs. 27c and 27d and the parameters are provided in Table 10. The Langmuir isotherm provided the highest correlation (R^2 = 0.995) and lowlest RMSE for PCs adsorption, indicating that adsorption sites are assumed to be energetically homogeneous, and significant PCs monolayer coverage on the outer bead surface is formed without any interaction between the PCs (adsorbed molecules) (Mojoudi et al., 2019). Therefore, the monolayer saturation capacity is 114 mg g^{-1}

beyond which no further adsorption can occur. Still, full-scale, supplementary experiments (adsorption kinetics) are needed to predict the adsorption capacity of PCs accurately.

Table 10. Isotherm parameters of PCs adsorption onto the SA-AC beads (Conditions: 5 g of the adsorbent, 20 – 4,000 mg L^{-1} of PCs, pH = 4, contact time 24 h).

Isotherm	**Parameters**	**Value**
Langmuir	Q_m (mg g^{-1})	114
	K_L (L mg^{-1})	15×10^{-3}
	R^2	0.995
	RMSE	1.65×10^{-6}
Freundlich	1/*n*	0.87
	K_F (L mg^{-1})	4.21
	R^2	0.967
	RMSE	174×10^{-6}

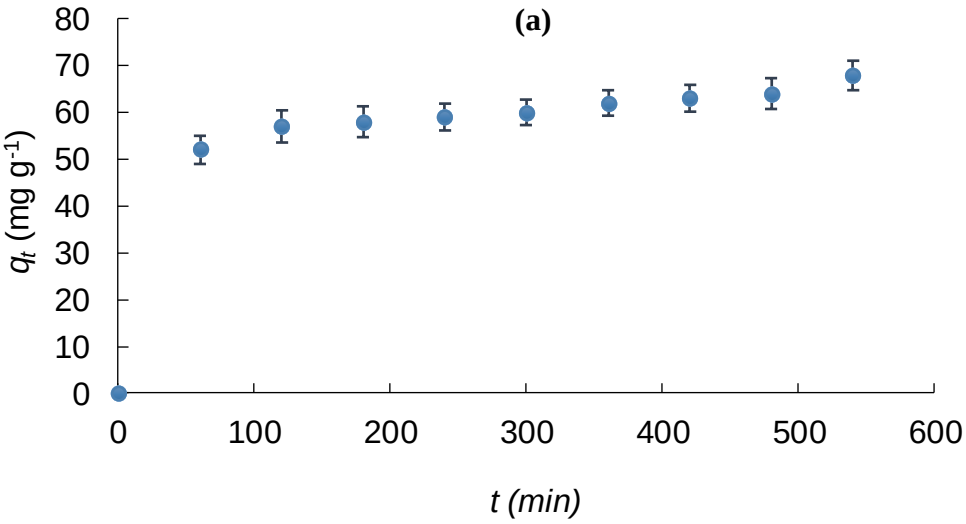
(a)
80
70
60
50
40
30
20
10
0
q_t (mg g^{-1})
0
100
200
300
400
500
600
t (min)

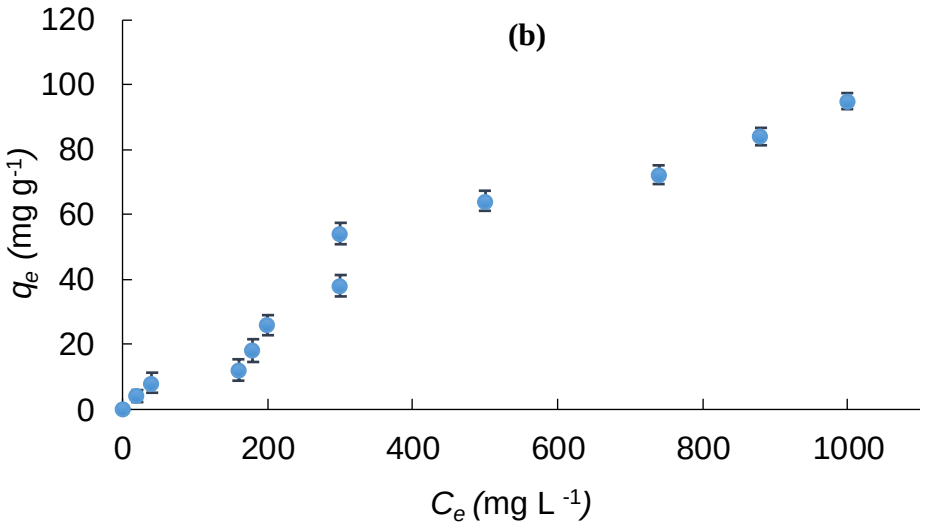
(b)
120
100
80
60
40
20
0
q_e (mg g^{-1})
0
200
400
600
800
1000
C_e (mg L^{-1})

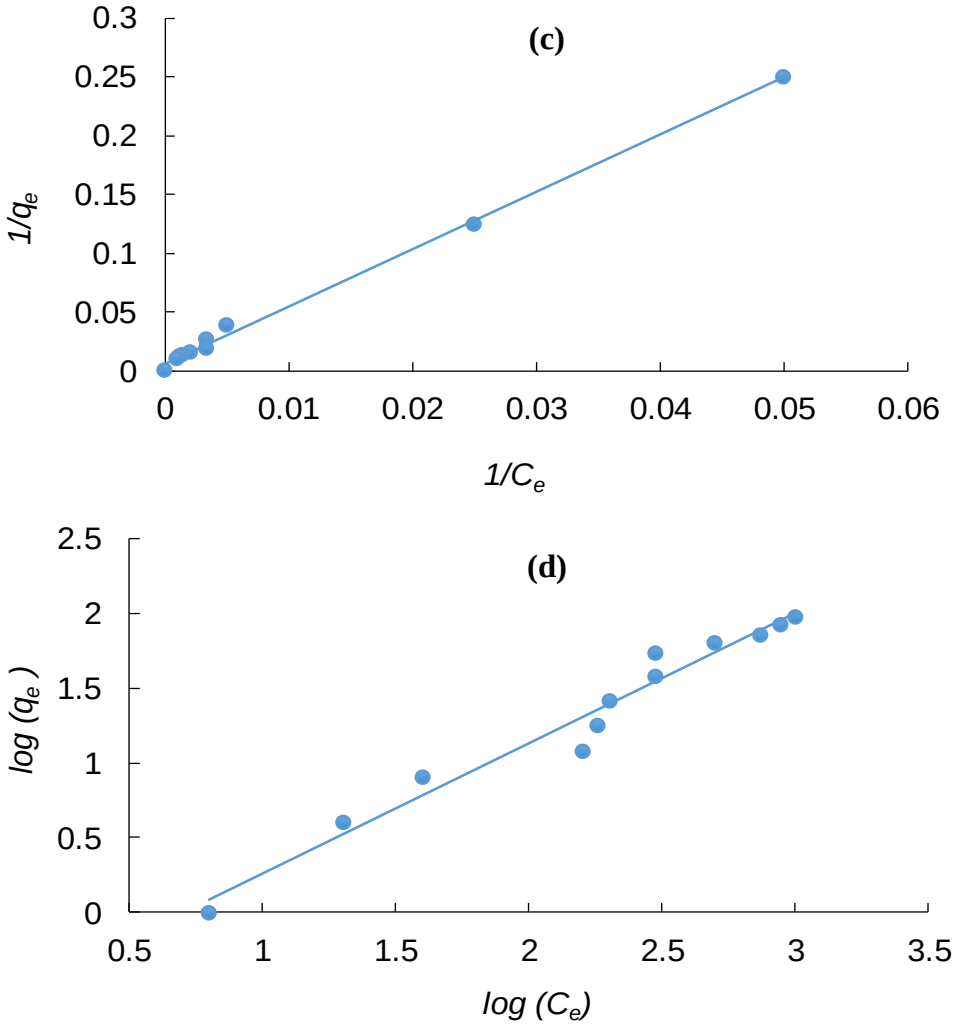

Fig. 27. Effect of contact time (a) on PCs removal by SA-AC beads (Conditions: 5 g of the adsorbent, 4000 mg L^{-1} of PCs, 540 min contact time under optimum conditions of other variables), Adsorption isotherm (b): (c) Langmuir and (d) Freundlich (PCs concentration, 20 – 4000 mg L^{-1}; volume of OMWW, 5 mL; temperature, 19°C; pH = 4.0; and contact time, 24 h).

2.3.2. Modeling of adsorption kinetics

The rate constants and R^2 values were calculated from the linearized plots shown as in Fig. 28 and summarized in Table 11. Considering the reported R^2 and RMSE values, PCs adsorption onto SA-AC beads followed pseudo-second-order kinetics, and the correlation coefficients were higher (0.997) than those of pseudo-first-order kinetics (0.701). The amount of PCs adsorption for pseudo-first-order kinetics was 28 mg g^{-1}, whereas pseudo-second-order kinetics was 68 mg g^{-1}. The calculated $q_{e(calc)}$ values using the pseudo-second-order kinetic model are much closer to the experimental $q_{e(exp)}$values, further suggesting that the adsorption of PCs onto SA-AC beads best fits pseudo-second-order kinetics. This model supposes that PCs adsorption is principally controlled by chemisorption, which includes valency changes through sharing or exchanging electrons between the SA-AC beads and the PCs, and external adsorption occurs more often than micropore adsorption (Abdelhay et al., 2017; Tao et al., 2017). Analogous results have also been reported for biochars prepared from olive oil processing waste, CuO-coated olive cake nanocomposites, granular and powdered AC encapsulated in calcium alginate (beads), and shrimp shell chitin (Annab et al., 2019; Elayadi et al., 2020; El Hanandeh et al., 2020; Yuney et al., 2020).

The SA-AC beads used in the present study for PCs adsorption from a batch test, removed 68 mg g^{-1} PCs, yielded more promising results than other reported adsorbents. In comparison to biochar prepared from olive oil processing waste (51 mg g^{-1}), granular and powdered AC encapsulated in calcium alginate beads (14 and 36 mg g^{-1}, respectively), SA-AC composite beads showed a higher removal capacity. However, in using shrimp shell chitin (1,045 mg g^{-1}), the adsorption potential was higher than that of the adsorbent used in our study because the initial phenol concentration tested was also higher (10-12 g L^{-1}). In addition, information on the kinetics of PCs adsorption is necessary to determine the optimum conditions for full-scale PCs removal procedures.

Table 11. Kinetic parameters of PCs adsorption onto SA-AC beads (Conditions: 5 g of the adsorbent, 4,000 mg $L^{-1}$of PCs, 540 min contact time under optimum conditions of other variables).

Model	Parameters	Value
Pseudo-first-order	k_1 (min^{-1})	41×10^{-3}
	q_e (Calc.) (mg g^{-1})	28
	R^2	0.701
	RMSE	3.90×10^{-4}
Pseudo-second-order	k_2 (min^{-1})	50×10^{-4}
	q_e (Calc.) (mg g^{-1})	68
	R^2	0.997
	RMSE	3.90×10^{-4}

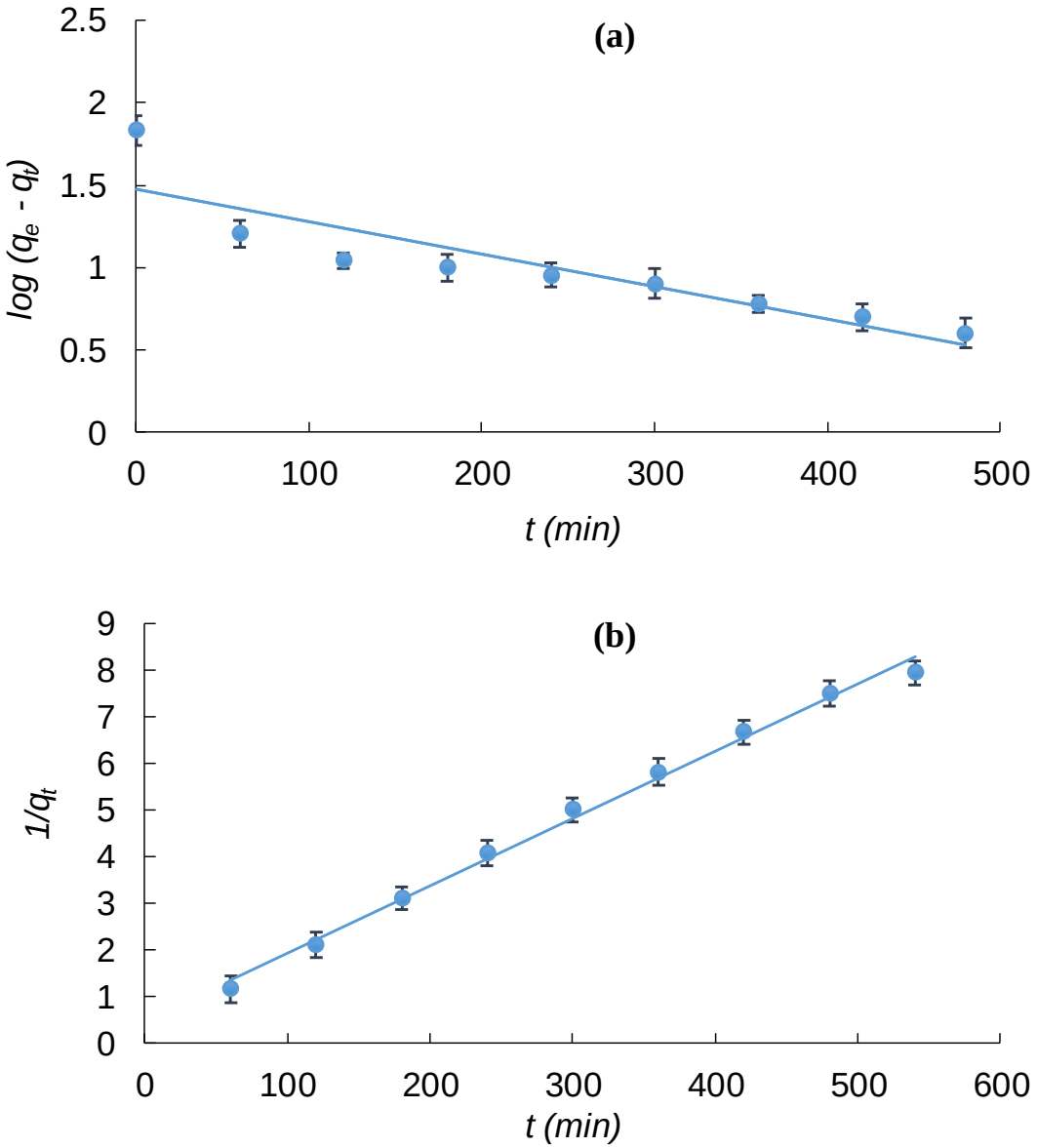

Fig. 28. Adsorption kinetics: pseudo-first-order (a) and pseudo-second-order (b) kinetic models of PCs adsorption onto SA-AC beads.

2.3.3. Effect of pH

The PCs adsorption ability of the SA-AC beads at different pH values is shown in Fig. 29a. The adsorption capacity of PCs declined from 65 to 12 mg g^{-1} as the pH increased from 2 to 10. This is due to the solubility of PCs that increases when the pH values decrease. Thus, there was an inverse relationship between the adsorption and solubility of PCs. However, pH values influenced the augmentation of oxygen-containing functional groups of SA-AC beads, inducing the effects of pH on the zeta potentials of SA-AC beads (Tahermansouri et al., 2015; Sun et al., 2019; Al Bsoul et al., 2020). These authors studied the effect of pH on phenol adsorption using carboxylated multi-walled carbon nanotubes, AC, and Ziziphus leaves, respectively. The same results were also reported for the effect of pH.

The main PCs identified in the effluent are mentioned in Section 2.1 of Part III, sub-chapter I.I. The pKa of PCs varies from ~ 3.0-4.0 to 10.0-11.0, while for most of them it is around 10.0. Thus, the protonated forms of PCs are predominant from acidic to neutral pH. This form is more prone to be adsorbed on SA-AC beads than the unprotonated form. This is one of the possible reasons for an increase in the adsorption capacity when the pH decreases. The adsorption capacity is higher at an acidic pH than at a basic pH, which is advantageous since the pH of real effluent is acidic and thus, pH adjustment would not be required during the treatment. Therefore, in full-scale systems, OMWW can be used directly, which will minimize costs during treatment. Alwan (2008) showed that pH control in industrial wastewater treatment plants affects the treatment efficiency, which subsequently increases the cost of treating the wastewater and meeting regulatory discharge guidelines.

2.3.4. Effect of temperature

The thermodynamic parameters, i.e., ΔG, ΔS and ΔH values, were obtained from the plot of $\ln(K_D)$ versus $1/T$ (Fig. 29b and Table 12). The positive values of ΔH suggest an endothermic reaction. In addition, the value of ΔH was 29 kJ mol^{-1} (higher than 20 kJ mol^{-1}), suggesting that PCs adsorption onto SA-AC beads involves some chemisorption. The ΔG values for different temperatures were found to be negative and decreased as the temperature decreased; the negative values of ΔG (19°C: -255; 25°C: -1,183; 30°C: -1,460; 35°C: -1,946 J mol^{-1}) indicate a spontaneous reaction. On the other hand, the positive value of ΔS (74 J mol^{-1} K^{-1}) corresponds to a dissociative mechanism. Moreover, the positive value of ΔS also

indicates an increased degree of freedom of the PCs in the solution and randomness at the solid/solution interface with some structural variations in the PCs and SA-AC beads during the PCs adsorption process, while the PCs molecules can displace the adsorbed molecules of water (Srivastava et al., 2006; Cheng et al., 2016).

Table 12. Thermodynamic parameters of the adsorption process of PCs on beads at various temperatures.

ΔH (kJ mol^{-1})	ΔS (J mol^{-1} K^{-1})	ΔG (J mol^{-1})			
		19°C	25°C	30°C	35°C
29	74	-255	-1,183	-1,460	-1,946

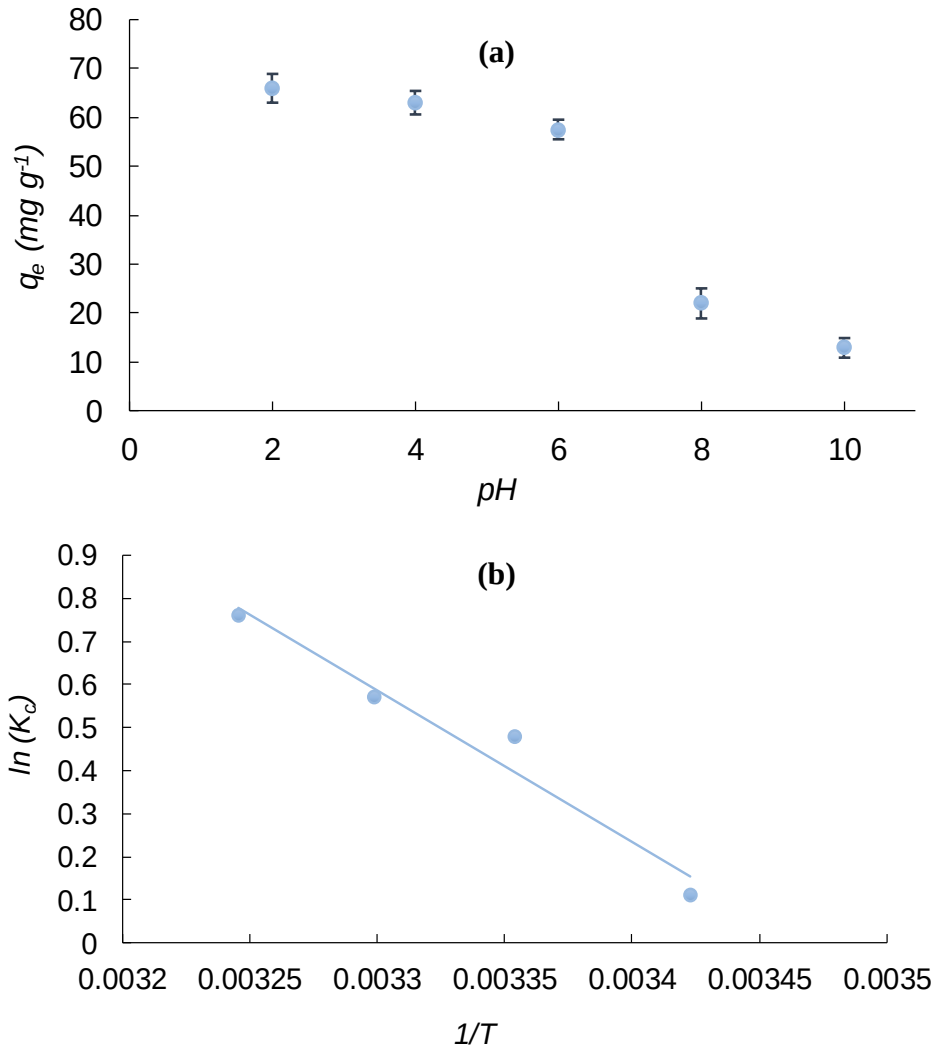

Fig. 29. Variation of the adsorption capacity of beads with pH (at 19 °C; adsorbent = 5 g; C_0 = 4,000 mg L^{-1}) (a) *Kc* as function of *1/T* (R^2 = 0.959) (b).

2.3.5. Fixed-bed column modeling

During the first 40 min, all the PCs were adsorbed, resulting in a PCs concentration of zero in the outlet water (treated water). As adsorption proceeded, the PCs concentration in the treated water gradually increased. In the up-flow mode, as PCs solution is inserted at the bottom of a clean bed of the SA-AC bead medium, most PCs are first eliminated in a closed layer at the bottom. As the adsorption proceeded, the lower compartment of the SA-AC beads became saturated with PCs, and the adsorption area advanced vertically through the column (Kundu et al., 2016). Finally, the adsorption area reached the top of the column, and the PCs concentration in the treated water began to increase. A breakthrough curve was generated by plotting the PCs concentration (in mg L^{-1}) in the treated water against time (in min). Fig. 30 shows the breakthrough curve of the adsorption of the phenolic compound onto SA-AC beads. The instant breakthrough time observed was 40 min, and the exhaustion time was 25 min. Different column parameters were determined.

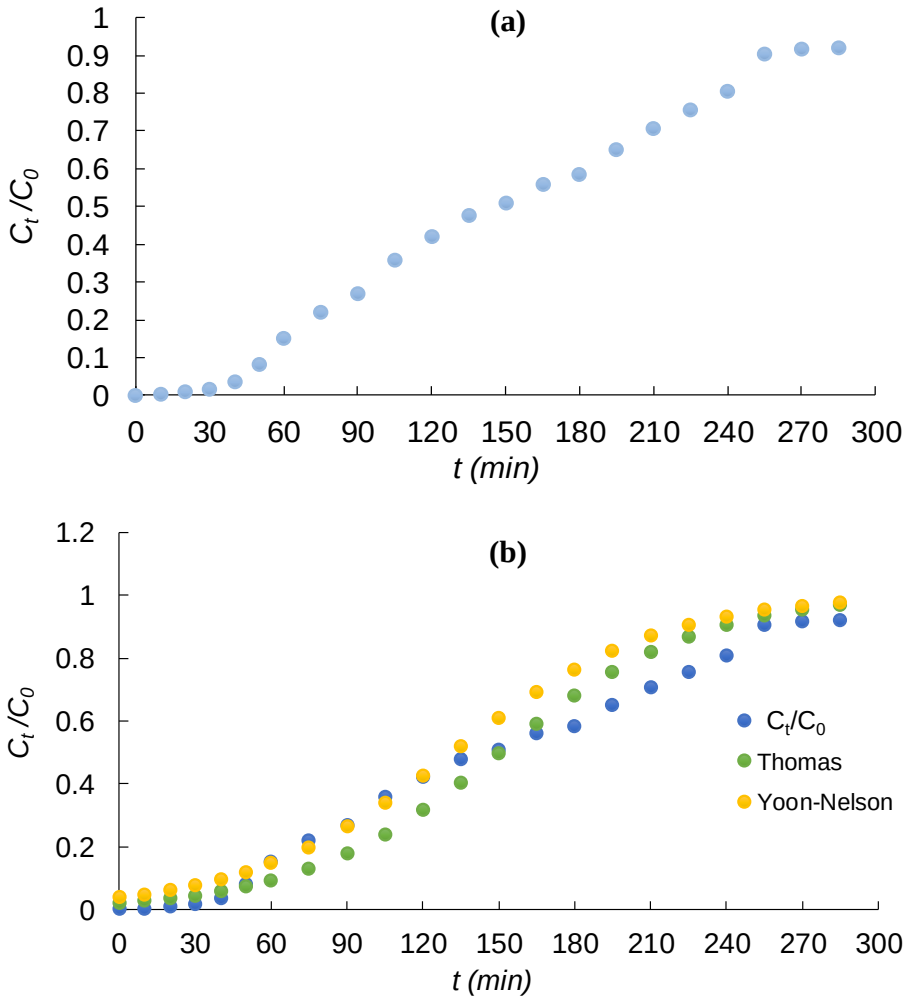

Fig. 30. Experimental and predicted breakthrough curves for PCs adsorption onto the SA-AC beads.

The values of the important design parameters of the breakthrough curves of the bed column for PCs adsorption onto the SA-AC beads were calculated and are shown in Table 13. As shown in this table, for C_i = 4,700 mg L^{-1} and Q = 2 mL min^{-1}, the value of q_e reached 159 mg g^{-1}, while the R was 41.6%. Thus, the SA-AC beads tested in this study for PCs removal using a fixed-bed column yielded promising results than other reported adsorbents (Kumar and Jena, 2016; Víctor-Ortega et al., 2016; Annab et al., 2019). The adsorbent SA-AC beads were able to remove 159 mg g^{-1} PCs. In comparison to Amberlyst A26 exchange resin (148 mg g^{-1}), AC (76 mg g^{-1}) and bead-AC with calcium alginate (16 mg g^{-1}), SA-AC beads showed higher removal capacity. Furthermore, the adsorbent (SA-AC beads) used in the present study was easily prepared at a rather low cost than traditional adsorbents.

Table 13. Parameters of breakthrough curves of the packed-bed column for PCs adsorption onto the SA-AC beads.

C_i (mg L^{-1})	Q (mL min^{-1})	V_{ef} (mL)	q_{total} (mg)	m_{total} (mg)	R (%)	q_e (mg g^{-1})
4700	2	570	704	1,692	41.6	159

Data from HPLC analysis of PCs adsorption onto the SA-AC beads before and after treatment in a fixed-bed column are depicted in Fig. 31. HPLC analysis of the PCs of OMWW after adsorption on the SA-AC beads at 10 min of treatment (Fig. 31a) showed the removal of 100% tyrosol (361 mg L^{-1}), caffeic acid (99 mg L^{-1}), ferulic acid (8.4 mg L^{-1}), coumaric acid (9.1 mg L^{-1}), and cinnamic acid (264 mg L^{-1}). It can be noted that the adsorption capacity of tyrosol, caffeic acid, coumaric acid, ferulic acid and cinnamic acid is greater than that of gallic acid (40 mg L^{-1}). This could be due to the effect of the structure and pKa of PCs present in the OMWW.

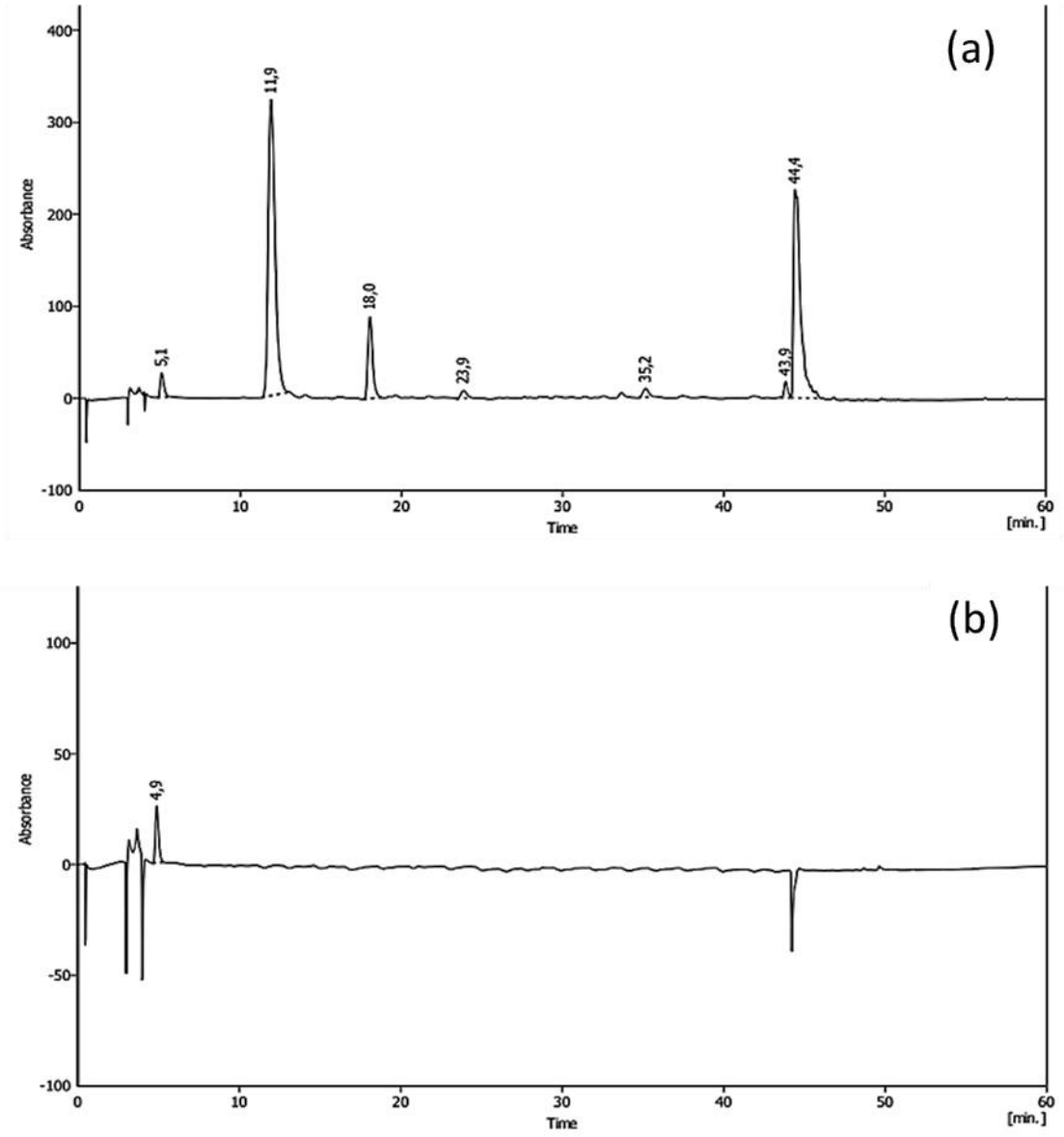

Fig. 31. Chromatograms (HPLC) of OMWW before (a) and after (b) treatment.

OMWW contains a considerable quantity of mineral ions and organic matter. The physicochemical parameters of the OMWW before and after treatment in a fixed-bed column are described in Table 14. In addition to removing PCs, the SA-AC beads were able to adsorb several ions and colloidal and soluble organic particles with an average of approximately 50%. These contaminants can compete for the adsorption sites and interfere with the removal efficiency. This finding indicates that the surface of the SA-AC bead is highly attractive to multiple elements of OMWW contaminants, which was confirmed by the greater decrease in

electrical conductivity after treatment. SA-AC was also efficient in raising the pH from 4.79 to 6.12, so we could use it directly without pH adjustment after treatment.

Table 14. Physicochemical parameters of the OMWW before and after adsorption.

Parameters	Before adsorption	After adsorption
pH	4.79	6.12
Electrical conductivity (mS cm^{-1})	23	12
COD (g-O_2 L^{-1})	66	36
Sodium (mg L^{-1})	130	40
Potassium (mg L^{-1})	5,900	2,950
Calcium (mg L^{-1})	240	130

The parameters given by modeling the experimental breakthrough curves with the Thomas and Yoon-Nelson models for PCs adsorption into SA-AC are presented in Table 15. The R^2 values (0.977) demonstrated that the Yoon-Nelson model was compatible and coulddescribe the PCs in SA-AC continuous mode. Furthermore, it is shown in Table 15 that the 50% breakthrough time (τ) for 50% adsorbate breakthrough from the Yoon-Nelson model complies with the experimental values ($\tau(exp)$ = 141 min). Moreover, error analysis was based on obtaining the best model among the models used for this study. The MAE values equaled 0.0619 and 0.0710 for the Thomas model and Yoon-Nelson model, respectively, as shown in Table 15. In contrast, both models' root-mean-square error (RMSE) values were calculated as 0.073 and 0.090, respectively. The MAE and RMSE for the Thomas model were lower than those for the Yoon-Nelson model. The Thomas model fit the experimental data well, meaning that the results followed the kinetics of Langmuir with the hypothesis applicable in a system with a constant flow and a negligible axial dispersion in the adsorption of the column because the motive force of speed follows the reversible reaction of the second-order (Chue, 2010). These results are consistent with those obtained previously in batch experiments.

In addition to their utility in terms of kinetics and isotherms obtained with real effluents, these data will allow us to design an OMWW treatment system by simulating a full-

scale process. To accurately design a full-scale SA-AC bead adsorption system, in several cases, pilot-scale tests are still required in several cases. However, these modeling results facilitate implementation and offer promising results on PCs breakthroughs in a short time. Consequently, the time and cost of a full-scale design are significantly reduced (Merle et al., 2020).

Table 15. Parameters of Yoon-Nelson and Thomas models for the adsorption of PCs by SA-AC in a fixed-bed column.

Model	**Parameters**	**Value**
Thomas	K_{th} (mL mg^{-1} min^{-1})	0.0053
	$q_{0\ cal}$ (mg g^{-1})	276
	R^2	0.967
	MAE	0.062
	RMSE	0.073
Yoon-Nelson	K_{YN} (min^{-1})	0.024
	τ_{Cal} (min)	134
	R^2	0.977
	MAE	0.071
	RMSE	0.090

Desorption studies will serve to recover precious PCs from OMWW to regenerate SA-AC beads and to understand the adsorption process. As we showed, PCs adsorption on SA-AC beads is ensured by chemisorption, so desorption experiments were carried out with ethanol according to the procedure described in Part II. This was due to the high solubility of PCs in ethanol. The results showed that ethanol recovered almost 43% of the PCs adsorbed. This indicates that ethanol could access SA-AC bead micropores. A similar desorption investigation was also performed and examined for the desorption of phenol using 30% (*v/v*) ethanol solution by neem leaves (*Azadirachta indica*). Maximum desorption of phenol was achieved (58%) with the batch system (Mandal et al., 2020). Shim et al. (2014) worked with actual Ca-alginate beads containing corn cob silica, immobilized *Pseudomonas putida YNSI*, and reported successful phenol desorption using 0.05 M HCl. These studies showed that phenol recovery from beads were substantial (69%) and that optimization of the desorption step in the continuous process is still needed (Mandal et al., 2014).

Solvent regeneration has numerous advantages for SA-AC bead regeneration since. It requires less energy, enables the recovery of PCs and SA-AC beads, and avoids the loss of SA-AC beads. Adsorbent regeneration allows the feasibility of recycling beads for several cycles of OMWW treatment and phenol recovery. However, the regeneration of adsorbent is affected by several physico-chemical parameters, including the pressure drop. Shen et al. (2010) highlighted that an increase of feed pressure from 131.32 to 202.65 kPa, increases the adsorbate recovery rate from 49% to 78%. The pressure drop is impacted by the beads bed thickness (i.e. column height), the bed porosity, as well as the friction at the surface of the beads (Franchin et al., 2020). The pressure drop across the column increases approximately linearly with the breakthrough time (Kratochvil et al., 1998). For this reason and in order to reduce the pressure drop across the bed, it is recommended to periodically backwash the column (Cooney et al., 1998). To selectively desorb PCs, electrosorption/desorption experiments will be carried out in the future using a fixed bed column reactor. Specific attention will be given to study the influence of the acidity constants of PCs on the efficiency of electrosorption to desorb the PCs selectively.

3. Conclusions

New composite beads based on olive pomace with alginate hydrogel were formulated successfully for PCs elimination from OMWW. The structure and porous morphology of SA-AC beads was confirmed by FTIR, SEM and EDS, which revealed the feasibility of SA-AC beads as potential and low-cost biosorbents. The adsorption of PCs by the SA-AC bead composite fits second-order kinetics and Langmuir isotherms. The results indicated that PC adsorption on SA-AC beads is strongly dependent on pH and phenol solubility. Thermodynamic analysis indicated that PCs adsorption was spontaneous and endothermic. Thomas and Yoon-Nelson models were selected to fit the experimental data, and the modified Thomas model was better at predicting PCs column adsorption. Finally, the regeneration investigation of SA-AC beads showed that the recovery of phenols from OMWW can be carried out with ethanol.

References

Abdelhay, A., Al Bsoul, A., Al-Othman, A., Al-Ananzeh, N. M., Jum'h, I., Al-Taani, A. A., 2017. Kinetic and thermodynamic study of phosphate removal from water by adsorption onto (Arundodonax) reeds. Adsorpt. Sci. Technol. 36, 46-61. https://doi.org/10.1177/0263617416684347

Achak, M., Hafidi, A., Ouazzani, N., Sayadi, S., Mandi, L., 2009. Low cost biosorbent "banana peel" for the removal of PCs from olive mill wastewater: Kinetic and equilibrium studies. J. Hazard. Mater. 166, 117-125. https://doi.org/10.1016/j.jhazmat.2008.11.036

Al-Bsoul, A., Hailat, M., Abdelhay, A., Tawalbeh, M., Al-Othman, A., Al-kharabshehIsra' Nawaf, Al-Taani, A. A., 2020. Efficient removal of phenol compounds from water environment using ziziphus leaves adsorbent. Sci. Total Environ., 143229. https://doi.org/10.1016/j.scitotenv.2020.143229

Al-Bsoul, A., Al-Shannag, M., Tawalbeh, M., Al-Taani, A. A., Lafi, W. K., Al-Othman, A., Alsheyab, M., 2020. Optimal conditions for olive mill wastewater treatment using ultrasound and advanced oxidation processes. Sci. Total Environ. 700, 134576. https://doi.org/10.1016/j.scitotenv.2019.134576

Allwar, A., 2020. Preparation and characterizations of activated carbon from banana fruit bunch with chemical treatments using hydrothermal processes. In: AIP Conf. Proc. AIP Publishing LLC, 030028. https://doi.org/10.1063/5.0002794

Alwan, Ghanim. (2008). pH control problems of a wastewater treatment plant. Al-Khawarizmi Eng. J. 4, 37-45.

Annab, H., Fiol, N., Villaescusa, I., Essamri, A., 2019. A proposal for the sustainable treatment and valorisation of olive mill wastes.J. Environ. Chem. Eng., 7, 102803. https://doi.org/10.1016/j.jece.2018.11.047

Arenales-Sierra, I. M., Lobato-Calleros, C., Vernon-Carter, E. J., Hernández-Rodríguez, L., Alvarez-Ramirez, J., 2019. Calcium alginate beads loaded with $Mg(OH)_2$ improve L. casei viability under simulated gastric condition. LWT - Food Sci Technol, 112, 108220. https://doi.org/10.1016/j.lwt.2019.05.118

Aziz, F., El Achaby, M., Lissaneddine, A., Aziz, K., Ouazzani, N., Mamouni, R., Mandi, L., 2020. Composites with alginate beads: A novel design of nano-adsorbents impregnation for large-scale continuous flow wastewater treatment pilots. Saudi J. Biol. Sci. 27, 2499-2508. https://doi.org/10.1016/j.sjbs.2019.11.019

Azzam, M. O., Hazaimeh, S. A., 2021. Olive mill wastewater treatment and valorization by extraction/concentration of hydroxytyrosol and other natural phenols. Process SAF Environ. 148, 495-523. https://doi.org/10.1016/j.psep.2020.10.030

Badawi, M. A., Negm, N. A., Abou Kana, M. T. H., Hefni, H. H., Abdel Moneem, M. M., 2017. Adsorption of aluminum and lead from wastewater by chitosan-tannic acid modified biopolymers: Isotherms, kinetics, thermodynamics and process mechanism. Int. J. Biol. Macromol. 99, 465-476. https://doi.org/10.1016/j.ijbiomac.2017.03.003

Baierle, F., John, D. K., Souza, M. P., Bjerk, T. R., Moraes, M. S., Hoeltz, M., Schneider, R. C., 2015. Biomass from microalgae separation by electroflotation with iron and aluminum spiral electrodes. Chem. Eng. J, 267, 274-281. https://doi.org/10.1016/j.cej.2015.01.031

Bampalioutas, K., Vlysidis, A., Lyberatos, G., Vlyssides, A., 2019. Detoxification and methane production kinetics from threephase olive mill wastewater using Fenton's reagent followed by anaerobic digestion. J. Chem. Technol. 94, 265-275.

https://doi.org/10.1002/jctb.5772

Basu, M., Guha, A. K., Ray, L., 2019. Adsorption of lead on lentil husk in fixed bed column bioreactor. Bioresour. Technol. 283, 86-95. https://doi.org/10.1016/j.biortech.2019.02.133

Braghiroli, F. L., Bouafif, H., Hamza, N., Neculita, C. M., Koubaa, A., 2018. Production, characterization, and potential of activated biochar as adsorbent for PCs from leachates in a lumber industry site. Environ. Sci. Pollut. Res. 25, 26562-26575. https://doi:10.1007/s11356-018-2712-9

Cheng, W. P., Gao, W., Cui, X., Ma, J. H., Li, R. F., 2016. Phenol adsorption equilibrium and kinetics on zeolite X/activated carbon composite. J. Taiwan Inst. Chem. Eng. 62, 192-198. https://doi.org/10.1016/j.jtice.2016.02.004

Chu, K. H., 2010. Fixed bed sorption: setting the record straight on the Bohart-Adams and Thomas models. J. Hazard. Mater. 177, 1006-1012. https://doi.org/10.1016/j.jhazmat.2010.01.019

Cooney, E., Stevens, G., Booker, N., Shallcross, D., 1999. Ammonia removal from wastewaters using natural Australian zeolite. II. Pilot-scale study using continuous packed column process. Sep. Sci. Technol. 34, 2741-2760. https://doi:10.1081/ss-100100802

Duarte, K. R., Justino, C., Panteleitchouk, T., Zrineh, A., Freitas, A. C., Duarte, A. C., Rocha-Santos, T. A. P., 2014. Removal of PCs in olive mill wastewater by silica-alginate-fungi biocomposites. Int. J. Environ. Sci. Technol. 11, 589-596. https://doi:10.1007/s13762-013-0268-2

El Ghadraoui, A., Ouazzani, N., Ahmali, A., El Mansour, T. E. H., Aziz, F., Hejjaj, A., Mandi, L., 2020. Treatment of olive mill and municipal wastewater mixture by pilot scale vertical flow constructed wetland. Desalin. Water Treat. 198, 126-139. https://doi: 10.5004/dwt.2020.26009

El Hanandeh, A., Albalasmeh, A., Gharaibeh, M., Alajlouni, M. 2020. Modification of biochar prepared from olive oil processing waste to enhance phenol removal from synthetic and olive mill wastewater. Sep. Sci. Technol. 1-13, 1659-1671.https://doi.org/10.1080/01496395.2020.1794897

El Moudden, H., El Idrissi, Y., El Yadini, A., Harhar, H., Tabyaoui, B., Tabyaoui, M., 2019. Effect of filtration of olive mill wastewater on the phenolic composition and its influence on antioxidant activity. Pharmacology OnLine.2, 161-176.

Elayadi, F., Achak, M., Beniich, N., Belaqziz, M., El Adlouni, C., 2020. Factorial design for optimizing and modeling the removal of organic pollutants from olive mill wastewater using a novel low-cost bioadsorbent. Water Air Soil Pollut. 231, 1-16. https://doi:10.1007/s11270-020-04695-8

Elmansour, T. E., Mandi, L., Ahmali, A., Elghadraoui, A., Aziz, F., Hejjaj, A., Ouazzani, N., 2020. Effect of polyphenols on activated sludge biomass during the treatment of highly diluted olive mill wastewaters: Biomass dynamics and purifying performances. Water Sci. Technol. 82, 1416-1429. https://doi.org/10.2166/wst.2020.423

Es-Sahbany, H., Berradi, M., Nkhili, S., Hsissou, R., Allaoui, M., Loutfi, M., El Youbi, M. S., 2019. Removal of heavy metals (nickel) contained in wastewater-models by the adsorption technique on natural clay. Mater. Today: Proc. 13, 866-875. https://doi.org/10.1016/j.matpr.2019.04.050

Franchin, G., Pesonen, J., Luukkonen, T., Bai, C., Scanferla, P., Botti, R., Colombo, P., 2020. Removal of ammonium from wastewater with geopolymer sorbents fabricated via additive manufacturing. Mater. Des. 195, 109006.

https://doi.org/10.1016/j.matdes.2020.109006

Hassan, A. F., Abdel-Mohsen, A. M., Elhadidy, H., 2014. Adsorption of arsenic by activated carbon, calcium alginate and their composite beads. Int. J. Biol. Macromol. 68, 125-130. https://doi.org/10.1016/j.ijbiomac.2014.04.006

Ho, Y. S., McKay, G., 1999. Pseudo-second-order model for sorption processes. Process Biochem. 34, 451-465. https://doi.org/10.1016/S0032-9592(98)00112-5

Iqbal, J., Shah, N. S., Sayed, M., Imran, M., Muhammad, N., Howari, F. M., Polychronopoulou, K., 2019. Synergistic effects of activated carbon and nano-zerovalent copper on the performance of hydroxyapatite-alginate beads for the removal of As^{3+} from aqueous solution. J. Clean. Prod. 235, 875-886. https://doi.org/10.1016/j.jclepro.2019.06.316

Iwanow, M., Gärtner, T., Sieber, V., König, B., 2020. Activated carbon as catalyst support: precursors, preparation, modification and characterization. Beilstein J. Org. Chem. 16, 1188-1202. https://doi.org/10.3762/bjoc.16.104

Ji, M., Jiang, X., Wang, F., 2015. A mechanistic approach and response surface optimization of the removal of oil and grease from restaurant wastewater by electrocoagulation and electroflotation. Desalin. Water Treat. 55, 2044-2052. https://doi.org/10.1080/19443994.2014.929034

Jodra, Y., Mijangos, F., 2003. Phenol adsorption in immobilized activated carbon with alginate gels. Sep. Sci. Technol. 38, 1851-1867. https://doi.org/10.1081/SS-120019412

Kaleh, Z., Geißen, S. U., 2016. Selective isolation of valuable biophenols from olive mill wastewater. J. Environ. Chem. Eng. 4, 373-384. https://doi.org/10.1016/j.jece.2015.11.010

Kilic, M. Y., Abdelraheem, W. H., He, X., Kestioglu, K., Dionysiou, D. D., 2019. Photochemical treatment of tyrosol, a model phenolic compound present in olive mill wastewater, by hydroxyl and sulfate radical-based advanced oxidation processes (AOPs. J. Hazard. Mater. 367, 734-742. https://doi.org/10.1016/j.jhazmat.2018.06.062

Kim, T. Y., Jin, H. J., Park, S. S., Kim, S. J., Cho, S. Y., 2008. Adsorption equilibrium of copper ion and phenol by powdered activated carbon, alginate bead and alginate-activated carbon bead. J. Ind. Eng. Chem. 14, 714-719. https://doi.org/10.1016/j.jiec.2008.07.004

Kratochvil, D., Volesky, B., 1998. Biosorption of Cu from ferruginous wastewater by algal biomass. Water Res. 32, 2760-2768. https://doi.org/10.1016/S0043-1354(98)00015-3

Kumar, A., Jena, H. M., 2016. Removal of methylene blue and phenol onto prepared activated carbon from Fox nutshell by chemical activation in batch and fixed-bed column. J. Clean. Prod. 137, 1246-1259. https://doi.org/10.1016/j.jclepro.2016.07.177

Kundu, S. Gupta, A. K. 2005. Analysis and modeling of fixed bed column operations on As(V) removal by adsorption onto iron oxide-coated cement (IOCC). J. Colloid Interface Sci. 290(1), 52-60. https://doi.org/10.1016/j.jcis.2005.04.006

Kwak, H. W., Hong, Y., Lee, M. E., Jin, H. J., 2018. Sericin-derived activated carbon-loaded alginate bead: An effective and recyclable natural polymer-based adsorbent for methylene blue removal. Int. J. Biol. Macromol. 120, 906-914. https://doi.org/10.1016/j.ijbiomac.2018.08.116

Lagergren, S., 1898. Zur Theorie der Sogenannten Adsorption Gelöster Stoffe, Kongl. Vetensk. Acad. Handl. 24, 1-39.

Lawal, A. A., Hassan, M. A., Farid, M. A. A., Yasim-Anuar, T. A. T., Yusoff, M. Z. M., Zakaria, M. R., Shirai, Y., 2020. One-step steam pyrolysis for the production of mesoporous biochar from oil palm frond to effectively remove phenol in facultatively

treated palm oil mill effluent. Environ. Technol. Innov. 18, 100730. https://doi.org/10.1016/j.eti.2020.100730

Leouifoudi, I., Zyad, A., Amechrouq, A., Oukerrou, M. A., Mouse, H. A., Mbarki, M., 2014. Identification and characterization of PCs extracted from Moroccan olive mill wastewater. Food Sci. Technol. 34, 249-257. http://dx.doi.org/10.1590/fst.2014.0051

Li, W., Yan, J., Yan, Z., Song, Y., Jiao, W., Qi, G., Liu, Y., 2018. Adsorption of phenol by activated carbon in rotating packed bed: Experiment and modeling. Appl. Therm. Eng. 142, 760-766. https://doi.org/10.1016/j.applthermaleng.2018.07.051

Li, Y., Fu, F., Cai, W., Tang, B., 2019. Synergistic effect of mesoporous feroxyhyte nanoparticles and Fe(II) on phosphate immobilization: Adsorption and chemical precipitation. Powder Technol. 345, 786-795. https://doi.org/10.1016/j.powtec.2019.01.075

Liu, S., Cheng, G., Xiong, Y., Ding, Y., Luo, X., 2020. Adsorption of low concentrations of bromide ions from water by cellulose-based beads modified with TEMPO-mediated oxidation and Fe(III) complexation. J. Hazard. Mater. 384, 121195. https://doi.org/10.1016/j.jhazmat.2019.121195

Magdich, S., Jarboui, R., Rouina, B. B., Boukhris, M., Ammar, E., 2012. A yearly spraying of olive mill wastewater on agricultural soil over six successive years: impact of different application rates on olive production, phenolic compounds, phytotoxicity and microbial counts. Sci. Total Environ. 430, 209-216. https://doi.org/10.1016/j.scitotenv.2012.05.004

Mandal, A., Bar, N., Das, S. K., 2020. Phenol removal from wastewater using low-cost natural bioadsorbent neem (Azadirachtaindica) leaves: Adsorption study and MLR modeling. Sustain. Chem. Pharm. 17, 100308. https://doi.org/10.1016/j.scp.2020.100308

Merle, T., Knappe, D. R., Pronk, W., Vogler, B., Hollender, J., von Gunten, U., 2020. Assessment of the breakthrough of micropollutants in full-scale granular activated carbon adsorbers by rapid small-scale column tests and a novel pilot-scale sampling approach. Environ. Sci. Water Res. Technol. 6, 2742-2751. https://doi.org/10.1039/D0EW00405G

Mojoudi, N., Soleimani, M., Mirghaffari, N., Belver, C., Bedia, J., 2019. Removal of phenol and phosphate from aqueous solutions using activated carbons prepared from oily sludge through physical and chemical activation. Water Sci. Technol. 80, 575-586. https://doi.org/10.2166/wst.2019.305

Nadavala, S. K., Swayampakula, K., Boddu, V. M., Abburi, K., 2009. Biosorption of phenol and o-chlorophenol from aqueous solutions on to chitosan-calcium alginate blended beads. J. Hazard. Mater. 162, 482-489. https://doi.org/10.1016/j.jhazmat.2008.05.070

Nasrullah, A., Bhat, A. H., Naeem, A., Isa, M. H., Danish, M., 2018. High surface area mesoporous activated carbon-alginate beads for efficient removal of methylene blue. Int. J. Biol. Macromol. 107, 1792-1799. https://doi.org/10.1016/j.ijbiomac.2017.10.045

Olusegun, S. J., de Sousa Lima, L. F., Mohallem, N. D. S., 2018. Enhancement of adsorption capacity of clay through spray drying and surface modification process for wastewater treatment. Chem. Eng. J. 334, 1719-1728. https://doi.org/10.1016/j.cej.2017.11.084

Pinto, R. T. P., Lintomen, L., Luz Jr, L. F. L., Wolf-Maciel, M. R., 2005. Strategies for recovering phenol from wastewater: thermodynamic evaluation and environmental concerns. Fluid Phase Equilib. 228, 447-457. https://doi.org/10.1016/j.fluid.2004.09.005

Quesada, H. B., de Araújo, T. P., Vareschini, D. T., de Barros, M. A. S. D., Gomes, R. G., Bergamasco, R., 2020. Chitosan, alginate and other macromolecules as activated carbon

immobilizing agents: A review on composite adsorbents for the removal of water contaminants. Int. J. Biol. Macromol. 164, 2535-2549. https://doi.org/10.1016/j.ijbiomac.2020.08.118

Rahmanian, N., Jafari, S. M., Galanakis, C. M., 2014. Recovery and removal of PCs from olive mill wastewater. J. Am. Oil Chem. Soc. 91, 1-18.

Ren, H., Gao, Z., Wu, D., Jiang, J., Sun, Y., Luo, C., 2016. Efficient Pb(II) removal using sodium alginate-carboxymethyl cellulose gel beads: Preparation, characterization, and adsorption mechanism. Carbohydr. Polym. 137, 402-409. https://doi.org/10.1016/j.carbpol.2015.11.002

Shen, C., Yu, J., Li, P., Grande, C. A., Rodrigues, A. E., 2010. Capture of CO_2 from flue gas by vacuum pressure swing adsorption using activated carbon beads. Adsorption 17, 179-188. https://doi.org/10.1007/s10450-010-9298-y

Shim, J., Kumar, M., Goswami, R., Mazumder, P., Oh, B. T., Shea, P. J., 2019. Removal of p-cresol and tylosin from water using a novel composite of alginate, recycled MnO_2 and activated carbon. J. Hazard. Mater. 364, 419-428. https://doi.org/10.1016/j.jhazmat.2018.09.065

Shim, J., Lim, J.-M., Shea, P. J., Oh, B.-T., 2014. Simultaneous removal of phenol, Cu and Cd from water with corn cob silica-alginate beads. J. Hazard. Mater. 272, 129-136. https://doi.org/10.1016/j.jhazmat.2014.03.010

Soto, M. L., Moure, A., Domínguez, H., Parajó, J. C., 2011. Recovery, concentration and purification of PCs by adsorption: A review. J. Food Eng. 105, 1-27. https://doi.org/10.1016/j.jfoodeng.2011.02.010

Srivastava, V. C., Swamy, M. M., Mall, I. D., Prasad, B., Mishra, I. M., 2006. Adsorptive removal of phenol by bagasse fly ash and activated carbon: equilibrium, kinetics and thermodynamics. Colloids Surf. A Physicochem. Eng. 272, 89-104. https://doi.org/10.1016/j.colsurfa.2005.07.016

Sun, J., Liu, X., Zhang, F., Zhou, J., Wu, J., Alsaedi, A., Li, J., 2019. Insight into the mechanism of adsorption of phenol and resorcinol on activated carbons with different oxidation degrees. Colloids Surf. A Physicochem. Eng. 563, 22-30. https://doi.org/10.1016/j.colsurfa.2018.11.042

Tafesh, A., Najami, N., Jadoun, J., Halahlih, F., Riepl, H., Azaizeh, H., 2011. Synergistic antibacterial effects of poly PCs from olive mill wastewater. Evid.-Based Complementary Altern. Med. 2011, 1-9. https://doi.org/10.1155/2011/431021

Tahermansouri, H., Dehghan, Z., Kiani, F., 2015. Phenol adsorption from aqueous solutions by functionalized multiwalled carbon nanotubes with a pyrazoline derivative in the presence of ultrasound. RSC Adv., 5, 44263-44273. https://doi.org/10.1039/C5RA02800K

Tao, J., Huo, P., Fu, Z., Zhang, J., Yang, Z., Zhang, D., 2019. Characterization and phenol adsorption performance of activated carbon prepared from tea residue by NaOH activation. Environ. Technol. 40, 171-181. https://doi.org/10.1080/09593330.2017.1384069

Víctor-Ortega, M. D., Ochando-Pulido, J. M., Martínez-Ferez, A., 2016. Performance and modeling of continuous ion exchange processes for phenols recovery from olive mill wastewater. Process Saf. Environ. Prot. 100, 242-251. https://doi.org/10.1016/j.psep.2016.01.017

Wang, W., Xu, S., Wang, K., Liang, J., Zhang, W., 2019. De-intercalation of the intercalated potassium in the preparation of activated carbons by KOH activation. Fuel Process. Technol. 189, 74-79. https://doi.org/10.1016/j.fuproc.2019.03.001

Yuney, K., Oladipo, A. A., Gazi, M., Younis, D. Z., 2020. CuO coated olive cake nanocomposites for rapid phenol removal and effective discoloration of high strength olive mill wastewater. Chemosphere 253, 126703. https://doi.org/10.1016/j.chemosphere.2020.126703

Zagklis, D. P., Vavouraki, A. I., Kornaros, M. E., Paraskeva, C. A., 2015. Purification of olive mill wastewater phenols through membrane filtration and resin adsorption/desorption. J. Hazard. Mater. 285, 69-76. https://doi.org/10.1016/j.jhazmat.2014.11.038

II. Electrosorption of phenolic compounds from olive mill wastewater: mass transport consideration under transient regime through alginate-activated carbon fixed-bed electrode

1. Introduction

The electrode material is of primary importance in such an electrochemical systembecause it impacts the electrosorption rates and yields. It depends on the specific surface area, pore size distribution, electric conductivity, surface function, and wettability (Sun et al., 2016b; Yue et al., 2019c; Lissaneddine et al., 2021b). Three-dimensional (3D) particle electrodes provide high electroactive surface area and can be easily implemented in fixed-bed reactors to favor mass transfer (Andrés García et al., 2018; Macías-García et al., 2019; Yue et al., 2019c; Lissaneddine et al., 2021b). Different studies have already demonstrated the performance of 3D electrodes for the electrosorption of organic compounds (e.g., acid red 88, orange II, methylene blue and metribuzin) from wastewater (Lissaneddine et al., 2021b). However, it has been recently reviewed that no studies have reported the electrosorption efficiency of organic pollutants from real aqueous effluents, while a supporting electrolyte has always beenadded (Lissaneddine et al., 2021b). Matrix effects are known to interfere with the electrochemical process efficiency and the addition of salts constitutes a supplementary source of pollution (Mousset et al., 2018, 2020a, 2020b; Lissaneddine et al., 2021b). Moreover, the few existing models about organics electrosorption do not include physico-chemical properties of the compounds as well as mass transport phenomena. However, though they are of primary importance in process efficiency (Lissaneddine et al., 2021b).

Within this context, a detailed investigation has been carried out for the first time to understand and predict the electrosorption of PCs from simulated and actual OMWW. The bio-sourced SA-AC beads have been implemented as a packed-bed electrode. In addition, novel theoretical models have been proposed to predict the evolution of electrosorption of organic compounds in simulated and real effluents considering the mass transport and difference of pKa of the PCs.

2. Modeling

A new model is proposed to predict the rate of phenol electrosorption onto the beads by incorporating the transport phenomena defined by the Nernst-Planck equation (Jasielec, 2021) that include diffusion electro-migration and convection. Electro-migration was neglected with the simulated effluent since the phenol molecule (pKa = 9.95) is uncharged at the applied pH of 4. Though the setup is under forced convection within the column, the low flow rate would imply that the diffusion of phenol towards the 3D porous material is not occurring in a stationary regime. Supposing that the beads are all spherical with the same diameter (~ 3.5 mm), the phenol rate towards the 3D porous material (r_c) can obey the Fick's law under transient regime according to Eq. 30 (Miomandre et al., 2005):

$$r_c = -\frac{1}{S}\frac{dC}{dt} = \frac{1}{V}(C_t - C_t^{el})\sqrt{\frac{D}{\pi t}} \quad (30)$$

where D is the diffusion coefficient of phenol, S is the specific surface area of the beads, t is the time, C_t and C_t^{el} are the concentrations of phenol in the solution and at electrode surface at time t, respectively.

C_t^{el} can be expressed as a function of C_0, as follow:

$$C_t^{el} = C_0 - C_{t-1} \quad (31)$$

where $C_{t-1}$and $C_0$are the phenol concentrations at time t-1 and t = 0 (in min), respectively, in the discrete model.

Then $C_t - C_t^{el}$ can be expressed according to Eq. 32:

$$C_t - C^{el} = C_t + C_{t-1} - C_0 \quad (32)$$

After incorporating Eq. 32 into Eq. 30 and integrating Eq. 30 from $C_t = C_0$ to C_t, Eq. 33 can be obtained:

$$ln\ (C_t + C_{t-1} - C_0) = \frac{2S\sqrt{D}}{\pi V} t^{\frac{1}{2}} + ln(C_0) \quad (33)$$

When dealing with real effluents (OMWW), a mixture of PCs with different pKa (3.0–4.0 to 10.0–11.0) should be considered (Lissaneddine et al., 2021a). Therefore, the influence of electromigration of ionic PCs must be added into Eq. 34:

$$r_c = -\frac{1}{S}\frac{dC}{dt} = \frac{1}{V}(C_t - C_t^{el})\sqrt{\frac{D}{\pi t}} + j_k \quad (34)$$

With

$$j_k = \frac{F}{RT} Z_k D_k C_k E = \frac{F}{RT} Z_k D_k C_k \rho_s j_{app} \quad (35)$$

where $j_k, D_{k,} Z_k \; and \; C_k$ are the flux, the diffusion coefficient, the valence and the concentration of the charged PCs (*k*), respectively, R is the gas constant, T is the absolute temperature, F is the Faraday constant, E is the electric field, ρ_s is the solution resistivity, j_{app} is the applied current density.

After integrating Eq. 34 from C_t = C_0 to C_t, the following Eq. 36 can be obtained:

$$t^{\frac{1}{2}} = \frac{X+\sqrt{X^2-4YZ}}{2Y} \quad (36)$$

With

$$X = \frac{2S\sqrt{D}}{\pi V} \quad (37)$$

$$Y = \frac{FZ_k D_k \rho_s j_{app}}{RT} \quad (38)$$

$$Z = ln\left(\frac{C_t + C_{t-1} - C_0}{C_0(C_t - C_0)}\right) \quad (39)$$

The fittings of the models with experimental results were evaluated with the RMSE as written in Eq. 26.

3. Results and discussion

3.1.Electrochemical characterization of the 3D porous electrodes

The electrochemical properties of the initial SA-AC beads electrodes have been determined to evaluate their electrochemical performance as an active electrode material. It has been shown that the electroactive surface area, I_0, the charge transfer resistance (R_{CT}) and the C_{DL} values were not impacted by the content of AC in the beads. Therefore, only their average values have been reported.

The electroactive surface area of porous electrodes determines the amount of polarized active sites, which in turn determines the rate and yield of electrosorption. Besides,

the electroactive surface area is a key parameter for the electrosorption efficiency (Zhu & Zhao, 2019a). The CV showed that the beads possess a high electroactive surface area that equaled $23 \times 10^3 \pm 5.5 \times 10^3$ cm^2 (Fig. 32). Comparatively, surfaces of 0.14 cm^2 with an oxidized AC electrode (Deryło-Marczewska et al., 2019), 0.93 cm^2 with an AC nanotubes-supported palladium electrode (Wang et al., 2010) and 531 cm^2 with an ACF electrode (Ergan & Gengec, 2020) were previously estimated. The value obtained with SA-AC emphasized that the encapsulation of AC in the beads allowed maintaining a high electroactive surface compared to porous electrodes proposed in the literature. This is of prime interest to reach high electrosorption capacity.

I_0 was determined to evaluate the electrode's catalyst performance and the electron transfer across the electrode (Sharma et al., 2013; Situmorang et al., 2020). The calculated I_0 obtained from Tafel slopes was 3.24 mA (Fig. 32b). This value was high compared to electrodes based on other materials and described in the literature, such as AC derived from rice husk (0.06 to 0.17 mA) (Jiao et al., 2020) and ammonium bicarbonate and AC (0.084 to 1.5 mA) (Li et al., 2014). Knowing that a higher I_0 leads to a quicker response towards a change in potential (Sharma et al., 2013; Sun & Chen, 2016), better electrode performance would be expected.

To further characterize the porous electrode/electrolyte interface, EIS data have been obtained after validation of impedance spectra with the linear Kramers-Kronig transform (KKT) technique (Fasmin & Srinivasan, 2015) (Fig. 32c). The chi-squared residues (χ^2) calculated for KKT fitting with experimental spectra as well as for Randle's type EEC model fitting with KKT were determined to be 1.5×10^{-5} and 9.3×10^{-7}, respectively. The good agreement with EIS spectra could validate the Randle's type circuit model that is drawn in Fig. 33. This model further demonstrated that the electrolyte exchangesoccur directly within the SA-AC beads and not at the beads and current collector surfaces. This could also explain why the parameters related to electrode/electrolyte interface (electroactive surface area, I_0, R_{CT} and C_{DL}) were relatively constant, whatever the load of AC within the beads. The associated R_{CT} and C_{DL} values of the EEC model were 1.7± 0.7 Ω and 0.15± 0.084 μF cm^{-2}, respectively. The R_{CT} was low compared with other reported porous electrodes such as almond shell-based activated nanoporous carbon (5.8 Ω) (Jain & Tripathi, 2014), AC (4.2 Ω) (Tian et al., 2020) and Cu_2O doped AC (9.39 Ω) (Zhang et al., 2015). This trend of R_{CT} compared with other porous materials corroborated with the higher I_0 value in the present

case. This would therefore promote the electrosorption on the SA-AC beads electrodes. In addition, a higher C_{DL} value was found compared to AC (0.0058 µF cm^{-2}) (Tian et al., 2020), which should increase the electric double layer and, therefore, the electrosorption efficiency (Lissaneddine, et al., 2021b). This is discussed in the next sub-section.

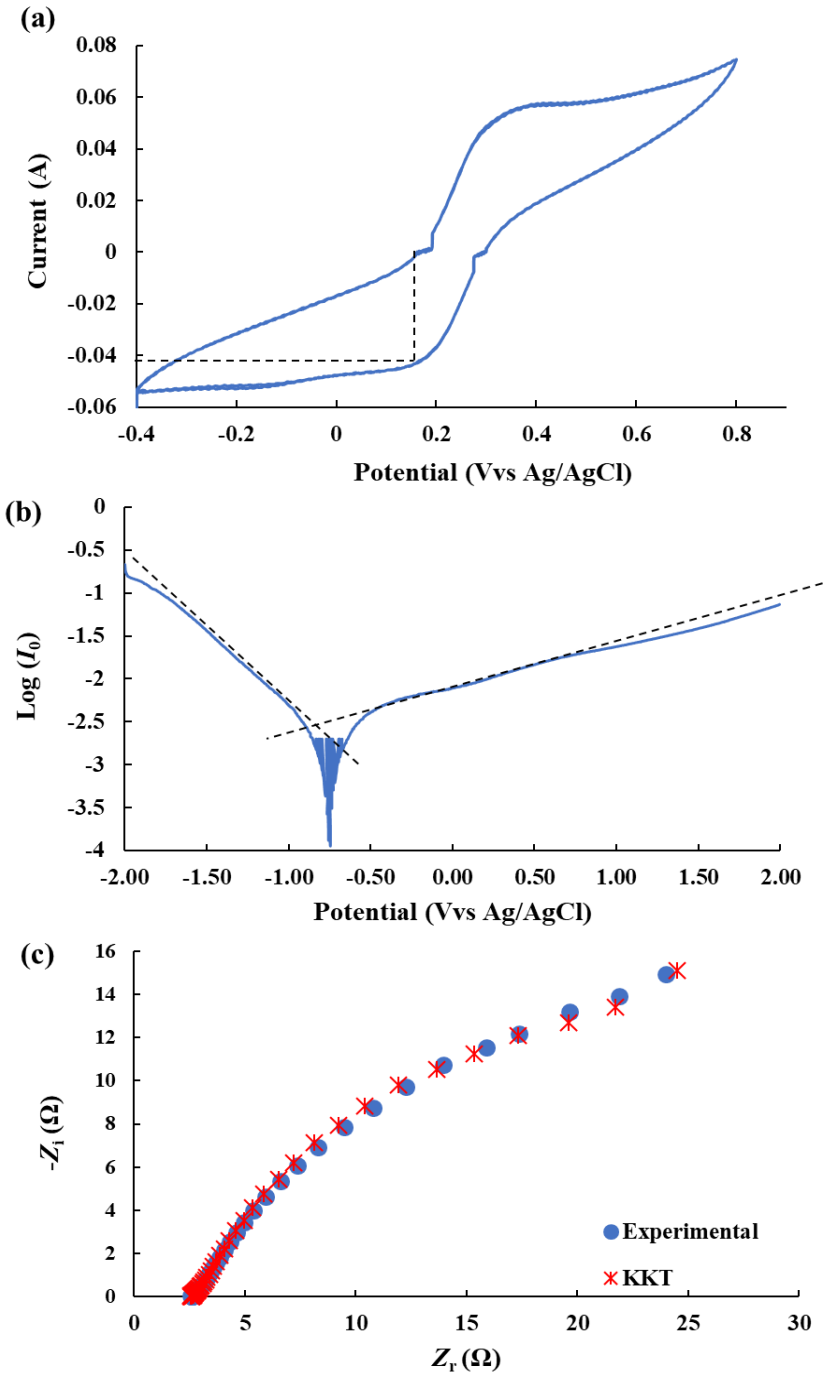

Fig. 32. Electrochemical properties of the prepared SA-AC beads electrode using CV (a), LSV (b) and EIS (c).

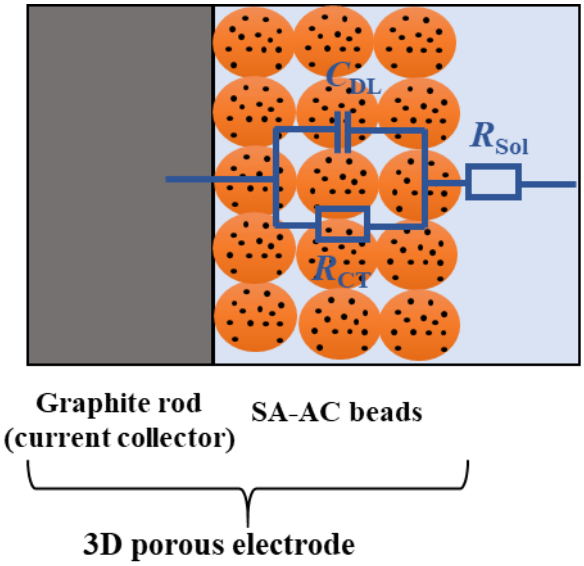

Fig. 33. Scheme of the EEC model integrated into the 3D porous electrodes.

3.2.Electrosorption efficiency

3.2.1. Effect of iron and calcium contents in the beads

To optimize the stability of the bio-sourced adsorbent during the electrosorption, iron or calcium has been added in beads preparation (Fig. 34). The results showed that the electrosorption capacities were almost similar, in the order of 204 ± 3 mg g^{-1} and 197 ± 10 mg g^{-1} after 240 min for 100% w/v Fe and 100% w/v Ca, respectively.

In order to be able to select the optimal element, the electrical conductivities of the two porous electrodes (100% w/v Fe and 100% w/v Ca) were compared by EIS measurements. Fig. 34b illustrates the Nyquist representations. The R_{CT} values ranked as follows: 100% w/v Fe (1.7 Ω) < 100% w/v Ca (2.6 Ω). The R_{CT} values decreased by 1.5-fold between 100% w/v Ca and 100% w/v Fe, highlighting an increase of electrode conductivity with the 100% w/v Fe. This trend was assumed to be due to differences in electron hopping, polaron and ionic radii. The transition energy between Fe^{2+} and Fe^{3+} is 0.2 eV (Iqbal & Farooq, 2007), indicating pronounced electron hopping and, hence, a rapid increase in conductivity with iron. Similar results have been observed in a previous study involving divalent and trivalent metal ions' doping on magnesium aluminate. The magnesium aluminate doped by Fe^{3+} had lower resistivity, i.e. higher conductivity, than the one doped by Ca^{2+} (Iqbal & Farooq, 2007). This was explained by the fact that the ionic radii of Ca^{2+} (0.99 Å)

was larger than that of Fe^{3+} (0.64 Å) along with the small polaron and electron hopping with iron (Iqbal & Farooq, 2007).

This could further explain why in this study, beads preparation with 100% w/v Fe displayed slightly higher electrosorption capacitiesin this study. Since the increase of material conductivity has previously been demonstrated to increase the electrosorption efficiency (Lissaneddine et al., 2021b), the selected optimal content of crosslinking agent used for the beads preparation was 100% w/v Fe.

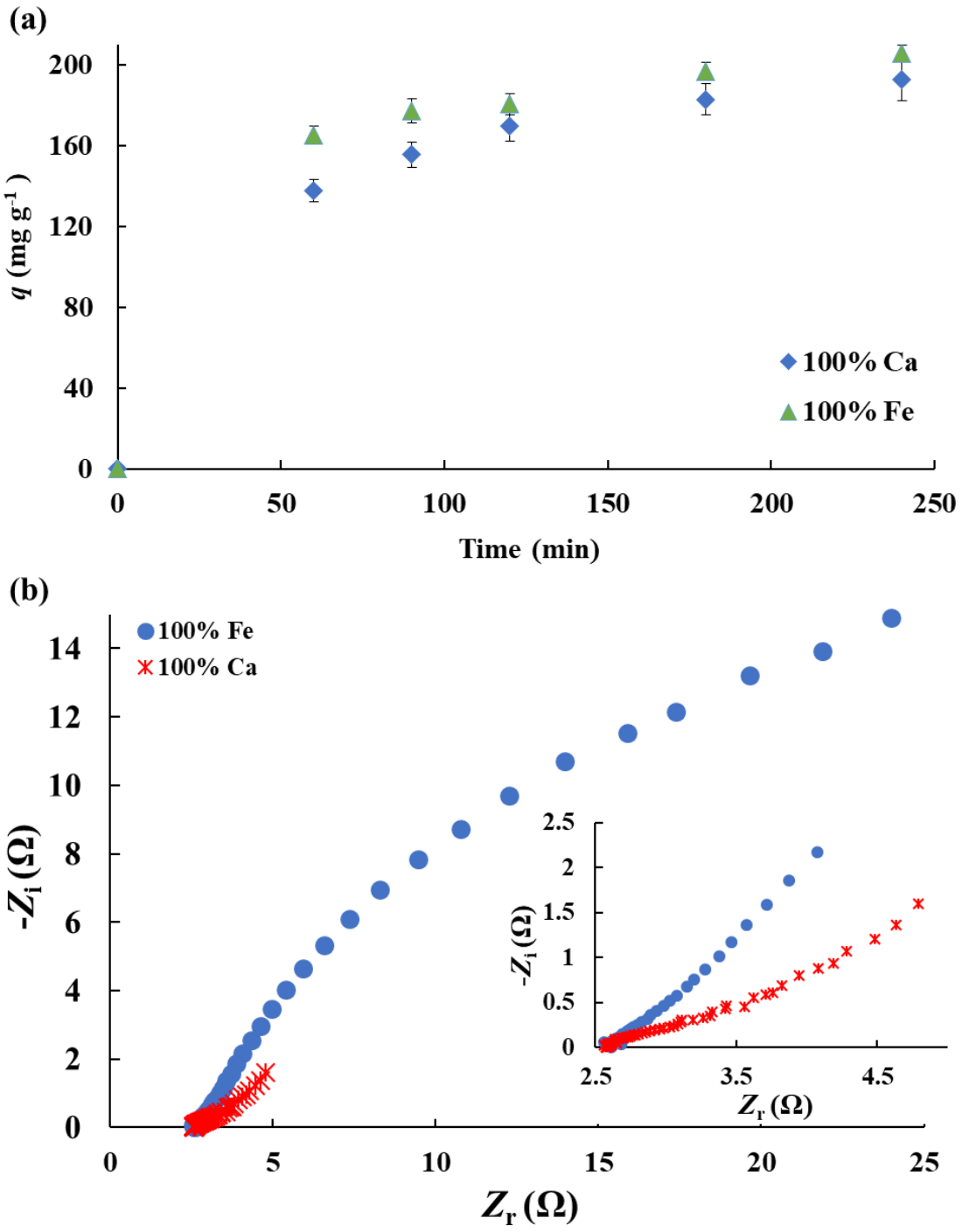

Fig. 34. Effect of the presence of iron (100% w/v) or calcium (100% w/v) in the beads preparation: on the electrosorption efficiency of phenol (a) and on electrode conductivity estimated from the Nyquist plot (b). Operating conditions: anode: graphite rod, cathode: graphite rod and 35 g SA-1% w/v AC beads, cathode potential: -1.2 V/(Ag/AgCl), electrolyte: 6 g L^{-1} KCl, pH 4 and 4 g L^{-1} phenol, flow rate: 10 mL min^{-1}, m/V = 0.35 g mL^{-1}.

3.2.2. Influence of AC percentage

The influence of AC percentage, i.e., the adsorbent dose, on phenol electrosorption kinetics in simulated OMWW is illustrated in Fig. 35a. Firstly, it can be observed that the electrosorption capacity increased rapidly over time as the active sites were accessible. This is because with increasing time, the active sites tend to be saturated so that the electrosorption capacity slowly increases until finally reaching adsorption equilibrium. Secondly, the electrosorption capacity increased for all percentages of AC tested with increasing time. In addition, there was an increase in electrosorption capacity with increasing percentages of AC up to 1% w/v (183 mg g^{-1}). This trend was in agreement with literature in which the phenol adsorption capacity increased with the increase of powder-AC in alginate gels (Jodra & Mijangos, 2003). Moreover, a further increase in the percentage of AC (3% w/v) led to a declined electrosorption capacity of phenol to 178 mg g^{-1}.

Interestingly, the trend of k_m evolution with AC percentages (Fig. 35b) was similar to the behavior of phenol electrosorption (Fig. 35a). k_m values increased from 0% w/v AC (8.9 10^{-5} m s^{-1}) to 1% w/v AC (9.7 10^{-5} m s^{-1}) and decreased at 3% w/v AC (8.1 10^{-5} m s^{-1}). This further confirmed that the electrosorption occurred mainly within the beads as suggested by the EEC model (section 3.1 of Part III, sub-chapter I.II) and not at the graphite rod and beads interfaces. Moreover, this suggests that the electrosorption capacity strongly depended on the diffusivity of the phenol within the beads. It has been previously shown that when the AC particles were trapped in a SA gel, the PCs diffused into the micropores of the SA gels and were adsorbed by the AC enveloped in the SA matrix (Chung et al., 2003). The increase of AC could then increase the diffusivity and, therefore the mass transport. At too high content of AC (3% w/v), agglomeration of AC may occur, which could lead to a reduction in the elasticity of the hydrogel network and the formation of a denser network (Tiwari et al., 2012; Thakur, 2018). In a previous adsorption work, AC was agglomerated in the beads, which increased the diffusional path length and the decreased adsorption capacity (Iqbal et al., 2016; Araga et al., 2017). In addition, the mass transfer coefficient has been shown to decrease with the increase in adsorbent particle size (Krishna et al., 1966). These statements agree with the declined electrosorption capacity of phenol at 3% w/v AC. To better visualize the mechanism of electrosorption with an increase of AC content within the beads, a scheme has been proposed in Fig. 36. This drawing highlights the constant external diffusion layer, whatever

the AC content, while the internal diffusion within the beads is affected. The mass transport is then influenced along with the electrosorption efficiency.

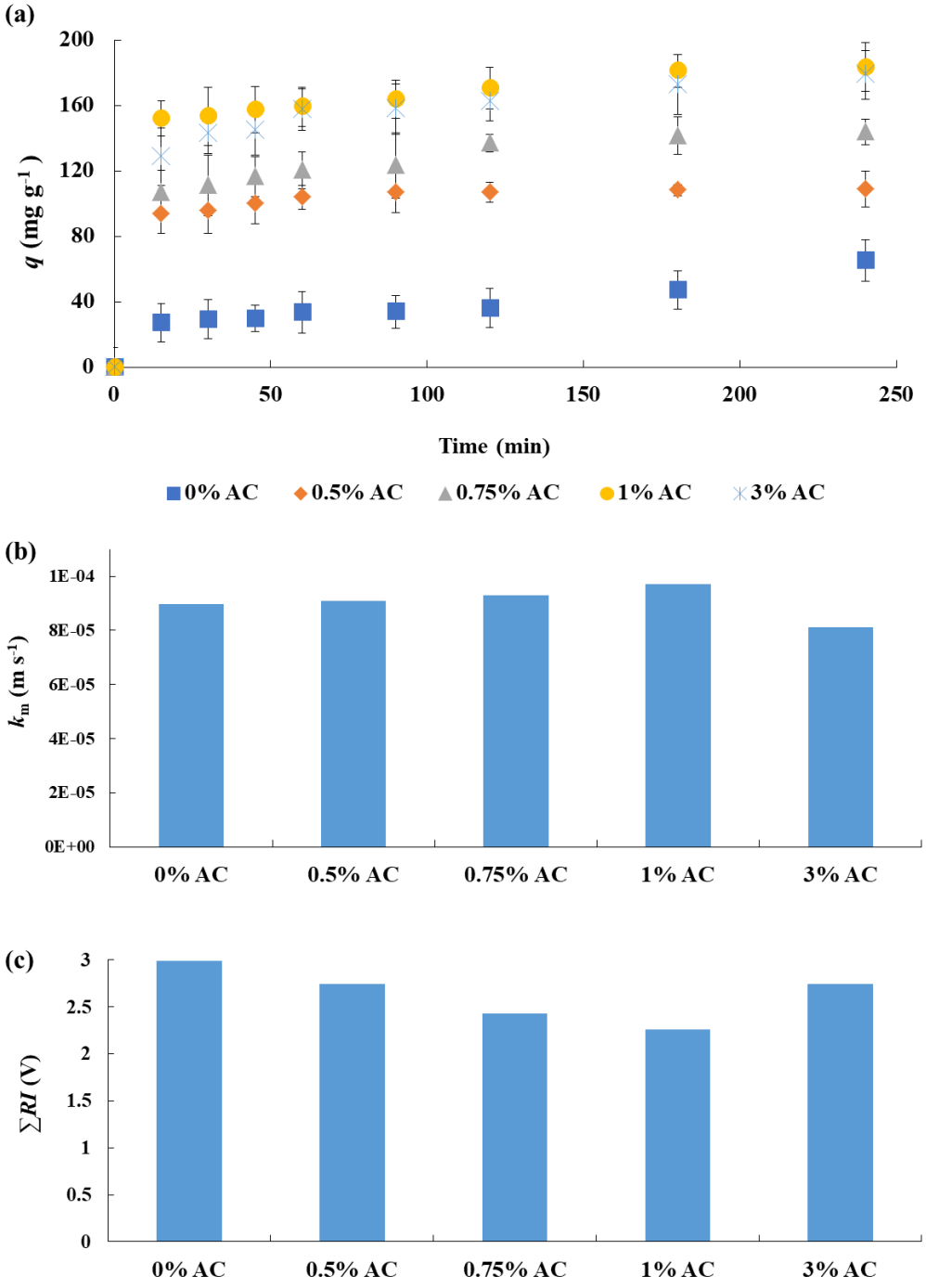

Fig. 35. Effect of AC percentage (% w/v) on: the evolution of electrosorption capacity of phenol (a), the mass transport (b) and internal ohmic resistance (c). Operating conditions: anode: graphite rod, cathode: graphite rod and 35 g SA (100% w/v Fe)-AC beads, cathode potential: -1.2 V/(Ag/AgCl), electrolyte: 6 g L^{-1} KCl, pH 4 and 4 g L^{-1} phenol, flow rate: 10 mL min^{-1}, m/V = 0.35 g mL^{-1}.

Furthermore, increasing the percentage of AC might have decreased the internal ohmic resistance of the SA-AC beads electrode from 2.9 V (0% w/v AC) to 2.2 V (1% w/v AC) (Fig. 35c), which subsequently resulted in a higher electrosorption capacity. A further increase of AC content (3% w/v AC) led to an increase of $\sum RI$ to 2.7 V. The reasons for this latter trend could be explained as follows. First, the mass transport decreased at 3% w/v AC (Fig. 35b). According to the results of Fang et al. (2005, 2006) the delayed transport of the ions into electrode (modified AC aerogel) pores increased internal ohmic resistance (Fang et al., 2005; Fang & Binder, 2006). Consequently, the AC percentage influenced the ion's transport and, next the internal ohmic resistance. Bian et al. (2016) demonstrated that the electrosorption performance significantly improved with a decrease in the electrode's internal ohmic resistance (14 to 3.6 Ω) for inorganic compounds on a membrane capacitive deionization reactor (Bian et al., 2016). This was further evidenced in this study for organic compounds electrosorption on a fixed-bed column reactor with beads electrode. To conclude, $\sum RI$ seemed, therefore, to be correlated with the mass transport as well as the AC content in the beads and the related electrosorption efficiency.

Upon these results, the optimum percentage of AC was taken as 1% w/v for the next electrosorption experiments.

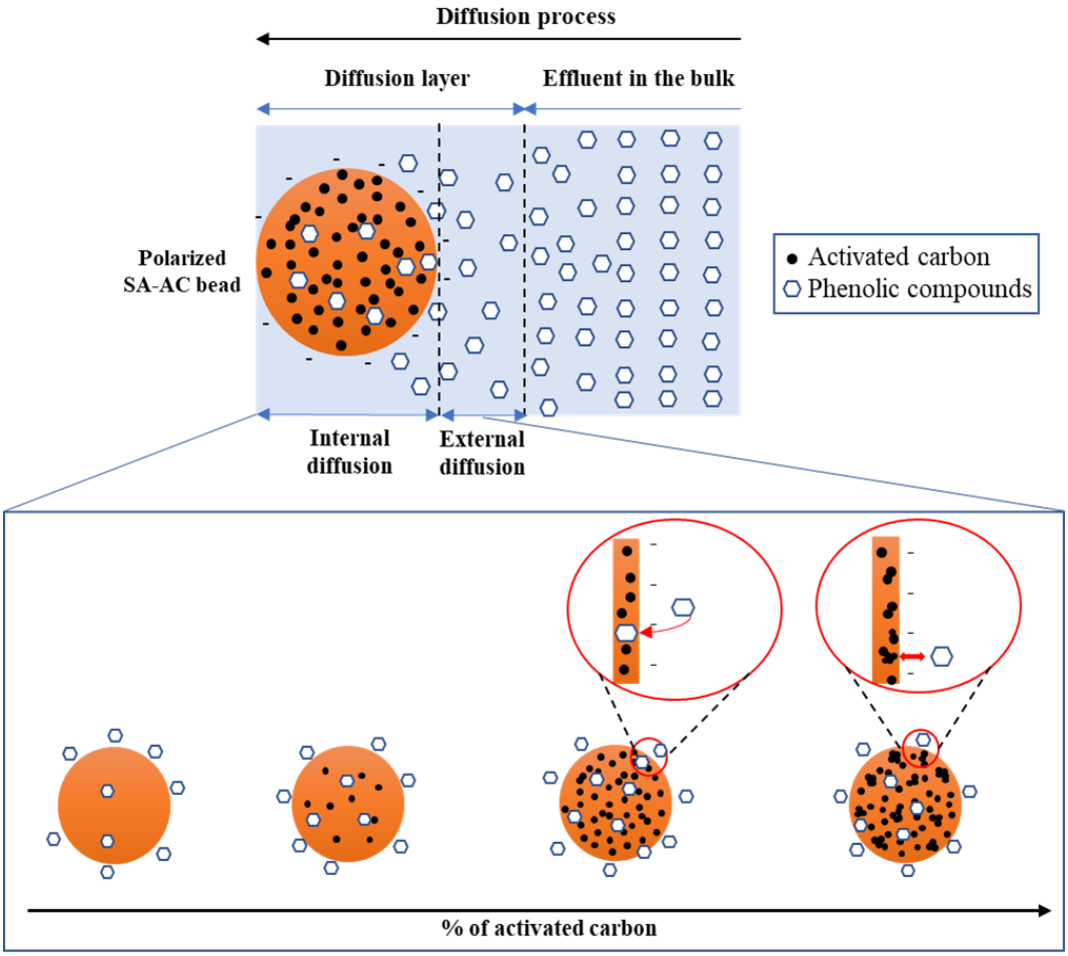

Fig. 36. Mechanism of phenol electrosorption in SA-AC beads with increasing AC content.

4.2.1. Effect of cathode potential

The influence on phenol electrosorption efficiency of E_{cat} varying from -0.8 to -1.3 V/(Ag/AgCl) compared to OC condition is shown in Fig. 37. The electrosorption capacity increased with decreasing applied potential from -0.8 to -1.2 V/(Ag/AgCl), reaching a maximum electrosorption capacity of 170 mg g^{-1} at equilibrium (Fig. 37a). It has been previously demonstrated that the potential could impact the electrosorption capacity of uncharged molecules (Gileadi, 1966b), which was the case of phenol (pKa = 9.95) considering the solution pH of 4. The electrode pola rization induces the replacement of solvent molecules with the organic compound at the interface, enhancing its electrosorption. However, the electrosorption capacity decreased to 73 mg g^{-1}, when the applied potential equaled -1.3 V/(Ag/AgCl). At this range of cathode potential, the reduction of water (H_2O) starts occurring according to Eq. (40), in which hydrogen gas (H_2) is produced on the surface of the 3D electrode (Ziati & Hazourli, 2019).

$$2H_2O + 2e^- \rightarrow H_2 + 2OH^- \quad (40)$$

This H_2 electrogeneration limit the availability of the active sites on the cathode surface (Hazourli et al., 1996b; Adnan et al., 2021b). Therefore, the involvement of this faradaic reaction strongly reduced the electrosorption capacity to 73 mg g^{-1}, which was even lower than in OC condition (123 mg g^{-1}). In this latter case, the absence of electric current emphasized the gain (38%) obtained with electrosorption at optimal voltage compared with the sole adsorption.

The energy requirement is an important economic parameter to take into account in the electrosorption process optimization. Considering the electrosorption efficiency as function of specific charge values (Fig. 37b), decreasing the applied potential increased the specific charge. The maximum electrosorption capacity (around 170 mg g^{-1}) was reached after only 0.28 Ah L^{-1} at -1.1 V/(Ag/AgCl), compared to 2 Ah L^{-1} at -1.2 V/(Ag/AgCl). Thus, the applied E_{cat} was taken as -1.1 V/(Ag/AgCl) for the next electrosorption experiment with real OMWW.

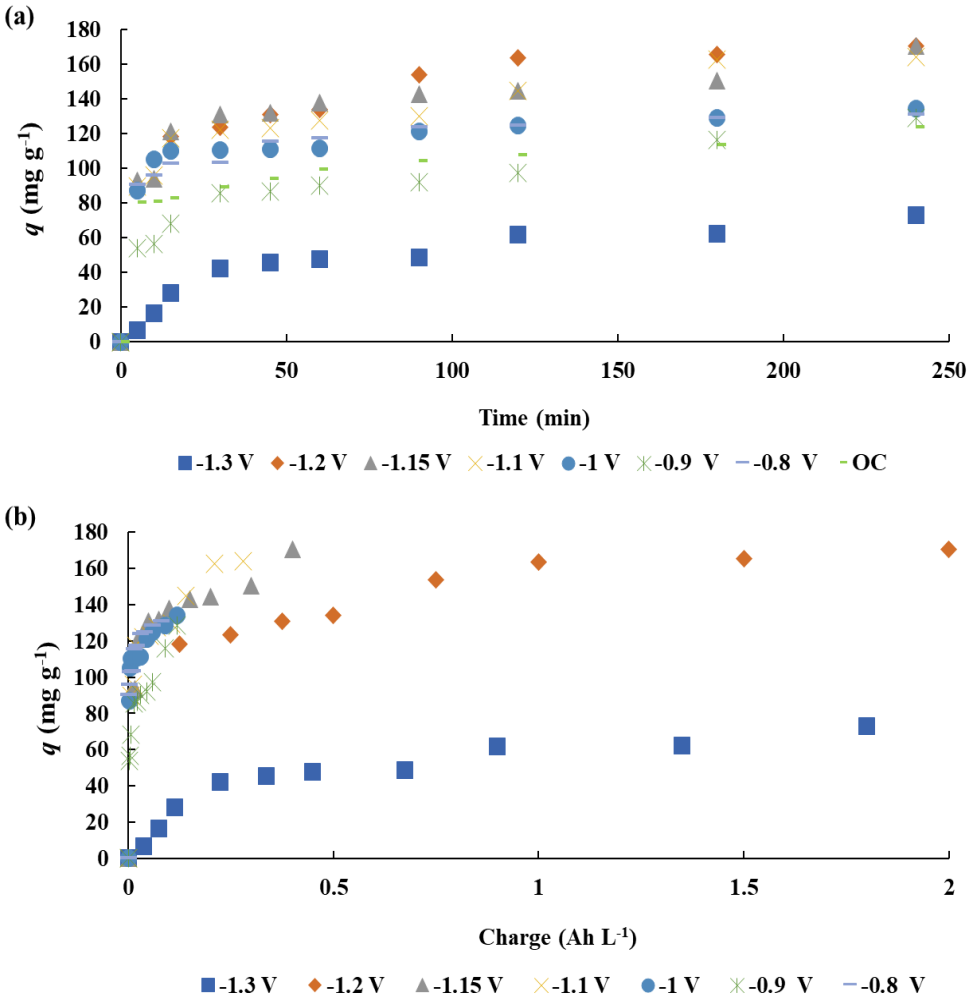

Fig. 37. Effect of E_{cat} (V/(Ag/AgCl)) considering the contact time (a) and the specific charge (b) on the electrosorption of phenol. Operating conditions: anode: graphite rod, cathode: graphite rod and 35 g SA (100% w/v Fe)-1% w/v AC beads, electrolyte: 6 g L^{-1} KCl, pH 4 and 4 g L^{-1} phenol, flow rate: 10 mL min^{-1}, m/V = 0.35 g mL^{-1}.

4.2.2. Multi-components effect with actual effluent

Electrosorption experiment with real OMWW has been carried out under optimal conditions: 1% w/v of AC, 100% w/v of Fe and -1.1 V/(Ag/AgCl) of E_{cat} (Fig. 38). The results showed that the maximum electrosorption capacity of PCs was higher (307 mg g^{-1}) than with phenol solutions (164 mg g^{-1}) in simulated OMWW. This difference could be explained by the presence of multiple PCs having different physico-chemical properties, such as diverse pKa values. The main PCs identified in actual OMWW have been listed in a previous paper (Lissaneddine et al., 2021a) and their pKa ranged from 3.0-4.0 to 10.0-11.0. It is usually assumed that the acidic forms of the PCs remain uncharged, while their basic forms are ionized due to the presence of many hydroxyl (OH/O^-) and carboxyl ($COOH/COO^-$) functions in these molecules (Baransi et al., 2012; Liu et al., 2020). The charged PCs were therefore subjected to electro-migration in supplement to diffusion. Though the surface of the SA-AC beads was negatively charged (cathode), electrostatic repulsion between the PCs negatively charged and negative charge of the surface of the SA-AC beads could still promote contact with the beads (Parida & Pradhan, 2010). In addition, since the hydraulic flow is ascending, from the negative fixed-bed electrode to the positive counter electrode, the electro-migration could also favor the contact of PCs already within the fixed-bed electrode. Therefore, their electrosorption rates and yields were maximized. The influence of electro-migration was previously noticed with other organic compounds (e.g., acid red 88, orange II, and methylene blue) in simulated effluents (Sun et al., 2016b; Yue et al., 2019c; Lissaneddine et al., 2021b). The present results newly demonstrated the influence of electro-migration with a multi-component system containing organics in an actual effluent.

Based on this trend, the SA-AC beads electrode could be used to separate not only phenol but also other PCs (47%) from actual OMWW by electrosorption for subsequent valorization upon further research studies.

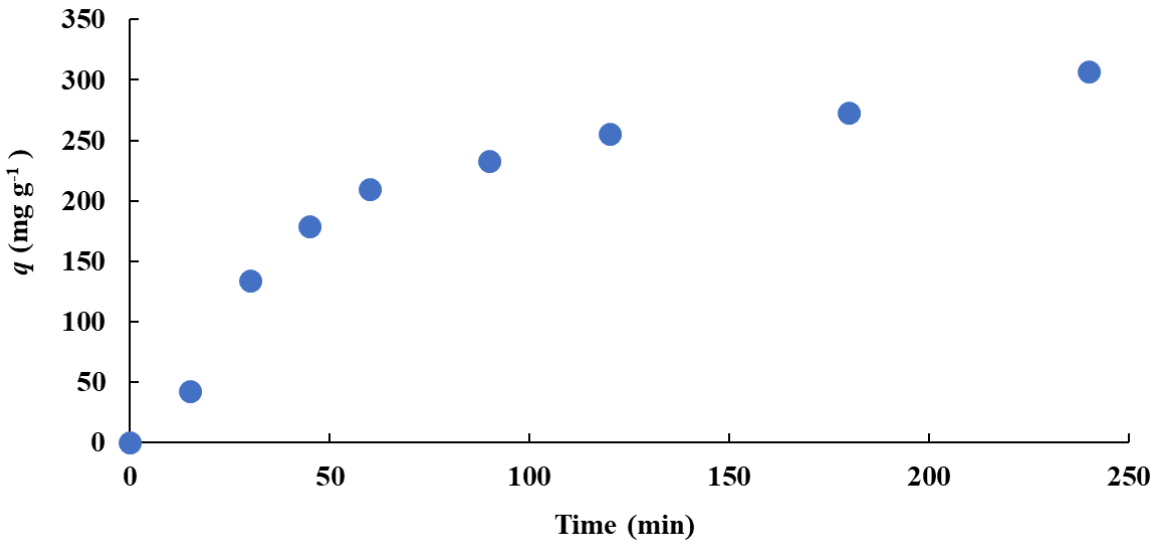

Fig. 38. Effect of contact time on the electrosorption of PCs from real OMWW at optimal operating conditions. Operating conditions: anode: graphite rod, cathode: graphite rod and 35 g SA (100% w/v Fe)-1% w/v AC beads, cathode potential: -1.1 V/(Ag/AgCl), flow rate: 10 mL min^{-1}, *m*/*V* ratio = 0.35 g mL^{-1}.

4.2.3. Theoretical evolution of organic compounds electrosorption in simulated and actual effluents

The models developed in section 2 of Part III, sub-chapter I.II have been used to predict the electrosorption evolution of phenol in simulated OMWW as a function of AC content (Fig. 39a) and of PCs in real OMWW (Fig. 39b). All the RMSE values were lower than 2.95×10^{-2}, which confirmed the good agreement of the model with the experimental data. Thus, the diffusion in simulated effluent and diffusion along with electro-migration in real effluent would be the main phenomena involved in the kinetics of organic compounds electrosorption.

The good fitting with real effluent further supported the estimated average value of valence of ionic PCs that was estimated to be 3.8. This value was obtained by weighting the valence of each PC supposed to be charged under the solution pH of 4.8 by the proportion of their basic form and their average concentrations in real effluent. The main ionic PCs identified in actual OMWW were gallic acid (valence of 5), ferulic acid (valence of 5), caffeic acid (valence of 4), cinnamic acid (valence of 2), and coumaric acid (valence of 3), according to a previous study (Lissaneddine et al., 2021a).

Furthermore, based on slopes values ($\frac{2S\sqrt{D}}{\pi V}$) of $ln\ (C_t + C_{t-1} - C_0)$ = f($t^{1/2}$) (Eq. 33), the diffusivity constant for phenol could be estimated as function of AC content ($D_{X\%}$) as follows (Eq. 41):

$$D_{X\%} = \frac{\pi V^2}{4S^2} \quad (41)$$

The evolution of $D_{X\%}$ as a function of AC content has been plotted in Fig. 39c. The trend was following the electrosorption capacity of phenol at different AC percentages (Fig. 35a), i.e. optimal diffusion (7.3×10^{-9} m^2 s^{-1}) at 1% w/v AC. This was also in agreement with k_m values evolution (Fig. 35b). This further corroborated that the electrosorption capacity strongly depended on the diffusivities of the PCs within the beads.

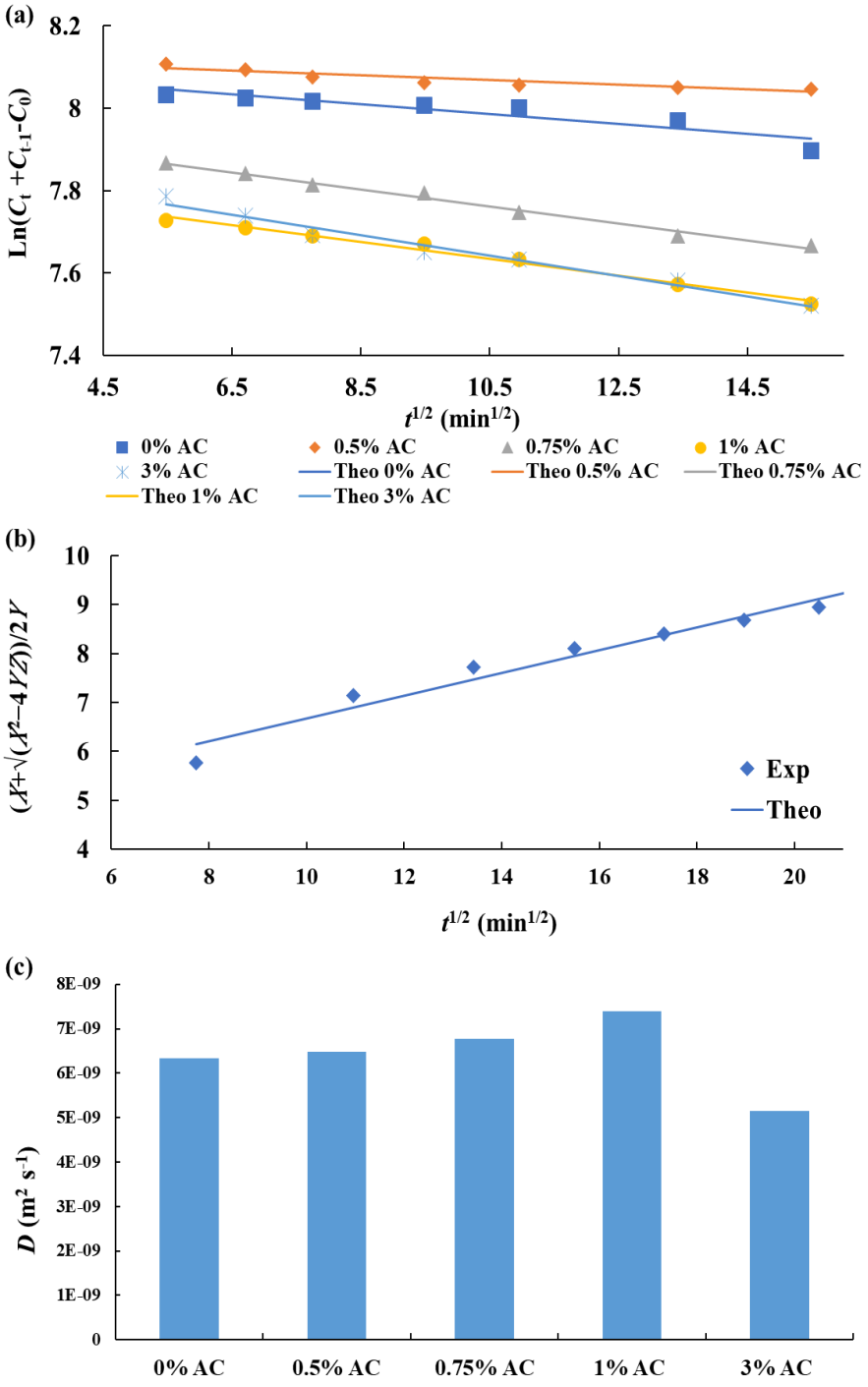

Fig. 39. Experimental (symbol) versus theoretical correlations (continuous line) as a function of $t^{1/2}$ in simulated OMWW as function of AC content (a) and of PCs in real OMWW (b), effect of the percentage of AC on the diffusion coefficient (c).

4. Conclusions

This study proposed a novel approach to remove the PCs from simulated and actual OMWW by implementing electrosorption onto SA-AC beads as a porous electrode. The impacts of key parameters (crosslinking agent (iron and calcium), AC content and cathode potential) on the removal efficiency of PCs were explored. The main new insights can be listed as follows:

- The higher conductivity obtained with Fe crosslinking agent led to slightly higher electrosorption efficiency compared to Ca.
- The AC content within the beads impacted the mass transfer and the diffusion coefficients as well as the internal ohmic resistance. An optimal AC amount was noticed (1% w/v), because too high a concentration implied agglomeration.
- An E_{cat} of -1.1 V/(Ag/AgCl) was found optimal considering the electrosorption capacity and energy requirements. However, too high voltage leads to faradaic reactions that hamper the electrosorption mechanism.
- The electrosorption efficiency was higher with real wastewater compared to simulated effluent. This could be due to the presence of multiple organic components that have different pKa.
- New discrete models have been proposed to understand and predict electrosorption efficiency. The kinetics were mainly limited by diffusion in transient regime in synthetic effluent, while electro-migration of ionic PCs also impacted the electrosorption with real OMWW.
- The results, the EEC model and the kinetic models could confirm that electrosorption mainly occurred within the beads and not at the 3D electrode/electrolyte interface, unlike often assessed.

The good electrosorption efficiency obtained for PCs removal from OMWW is promising for PCs recovery for subsequent valorization. A further possibility would be to combine electrosorption for recovery with a degradation process to eliminate unwanted compounds, which is the subject of ongoing research.

References

Adebayo, M.A., Areo, F.I., 2021. Removal of phenol and 4-nitrophenol from wastewater using a composite prepared from clay and Cocos nucifera shell: Kinetic, equilibrium and thermodynamic studies. Resour. Environ. Sustain. 3, 100020. https://doi.org/10.1016/j.resenv.2021.100020

Adnan, F.H., Mousset, E., Pontvianne, S., Pons, M., 2021a. Mineral cathodic electro-precipitation and its kinetic modelling in thin-film microfluidic reactor during advanced electro-oxidation process. Electrochim. Acta 387, 138487. https://doi.org/10.1016/j.electacta.2021.138487

Adnan, F.H., Pons, M.-N., Mousset, E., 2021b. Mass transport evolution in microfluidic thin film electrochemical reactors: New correlations from millimetric to submillimetric interelectrode distances. Electrochem. commun. 130, 107097. https://doi.org/10.1016/j.elecom.2021.107097

Aharonov-Nadborny, R., Raviv, M., Graber, E.R., 2016. Soil spreading of liquid olive mill processing wastes impacts leaching of adsorbed terbuthylazine. Chemosphere 156, 220–227. https://doi.org/10.1016/j.chemosphere.2016.04.104

Andrés García, E., Agulló-Barceló, M., Bond, P., Keller, J., Gernjak, W., Radjenovic, J., 2018. Hybrid electrochemical-granular activated carbon system for the treatment of greywater. Chem. Eng. J. 352, 405–411. https://doi.org/10.1016/j.cej.2018.07.042

Araga, R., Soni, S., Sharma, C.S., 2017. Fluoride adsorption from aqueous solution using activated carbon obtained from KOH-treated jamun (Syzygium cumini) seed. J. Environ. Chem. Eng. 5, 5608–5616. https://doi.org/10.1016/j.jece.2017.10.023

Azzam, M.O.J., Hazaimeh, S.A., 2021. Olive mill wastewater treatment and valorization by extraction/concentration of hydroxytyrosol and other natural phenols. Process Saf. Environ. Prot. 148, 495–523. https://doi.org/10.1016/j.psep.2020.10.030

Baransi, K., Dubowski, Y., Sabbah, I., 2012. Synergetic effect between photocatalytic degradation and adsorption processes on the removal of phenolic compounds from olive mill wastewater. Water Res. 46, 789–798. https://doi.org/10.1016/j.watres.2011.11.049

Bian, Y., Liang, P., Yang, X., Jiang, Y., Zhang, C., Huang, X., 2016. Using activated carbon fiber separators to enhance the desalination rate of membrane capacitive deionization. Desalination 381, 95–99. https://doi.org/10.1016/j.desal.2015.11.016

Brillas, E., Garcia-Segura, S., 2020. Benchmarking recent advances and innovative technology approaches of Fenton, photo-Fenton, electro-Fenton, and related processes: A review on the relevance of phenol as model molecule. Sep. Purif. Technol. 237, 116337. https://doi.org/10.1016/j.seppur.2019.116337

Cañizares, P., Marcos, I.F. De, Rodrigo, M.A., Lobato, J., 2006. Measurement of mass-transfer coefficients by an electrochemical technique. J. Chem. Educ. 83, 1204–1207. https://doi.org/10.1021/ed083p1204

Chai, Y., Qin, P., Wu, Z., Bai, M., Li, W., Pan, J., Cao, R., Chen, A., Jin, D., Peng, C., 2021. A coupled system of flow-through electro-Fenton and electrosorption processes for the efficient treatment of high-salinity organic wastewater. Sep. Purif. Technol. 267, 118683. https://doi.org/10.1016/j.seppur.2021.118683

Chung, T., Tseng, H., Juang, R., 2003. Mass transfer effect and intermediate detection for phenol degradation in immobilized Pseudomonas putida systems 38, 1497–1507. https://doi.org/10.1016/S0032-9592(03)00038-4

Deryło-Marczewska, A., Skrzypczyńska, K., Kuśmierek, K., Świątkowski, A., Zienkiewicz-Strzałka, M., 2019. The adsorptive properties of oxidized activated carbons and their

applications as carbon paste electrode modifiers. Adsorption 25, 357–366. https://doi.org/10.1007/s10450-019-00016-6

Ergan, B.T., Gengec, E., 2020. Dye degradation and kinetics of online electro-Fenton system with thermally activated carbon fiber cathodes. J. Environ. Chem. Eng. 8, 104217. https://doi.org/10.1016/j.jece.2020.104217

Esteves, B.M., Morales-Torres, S., Maldonado-Hódar, F.J., Madeira, L.M., 2021. Integration of olive stones in the production of Fe/AC-catalysts for the CWPO treatment of synthetic and real olive mill wastewater. Chem. Eng. J. 411. https://doi.org/10.1016/j.cej.2021.128451

Fang, B., Binder, L., 2006. A modified activated carbon aerogel for high-energy storage in electric double layer capacitors. J. Power Sources 163, 616–622. https://doi.org/10.1016/j.jpowsour.2006.09.014

Fang, B., Wei, Y.Z., Maruyama, K., Kumagai, M., 2005. High capacity supercapacitors based on modified activated carbon aerogel. J. Appl. Electrochem. 35, 229–233. https://doi.org/10.1007/s10800-004-3462-6

Fang, Z., Cao, X., Li, Xuexiao, Wang, H., Li, Xianning, 2017. Electrode and azo dye decolorization performance in microbial-fuel-cell- coupled constructed wetlands with different electrode size during long-term wastewater treatment. Bioresour. Technol. 238, 450–460. https://doi.org/10.1016/j.biortech.2017.04.075

Fasmin, F., Srinivasan, R., 2015. Detection of nonlinearities in electrochemical impedance spectra by Kramers–Kronig transforms. J. Solid State Electrochem. 19, 1833–1847. https://doi.org/10.1007/s10008-015-2824-9

Genethliou, C., Kornaros, M., Dailianis, S., 2020. Biodegradation of olive mill wastewater phenolic compounds in a thermophilic anaerobic upflow packed bed reactor and assessment of their toxicity in digester effluents. J. Environ. Manage. 255, 109882. https://doi.org/10.1016/j.jenvman.2019.109882

Gileadi, E., 1966. Electrosorption of uncharged molecules on solid electrodes. J. Electroanal. Chem. 11, 137–151. https://doi.org/10.1016/0022-0728(66)80073-6

Haddad, K., Jeguirim, M., Jellali, S., Thevenin, N., Ruidavets, L., Limousy, L., 2021. Biochar production from Cypress sawdust and olive mill wastewater: Agronomic approach. Sci. Total Environ. 752, 141713. https://doi.org/10.1016/j.scitotenv.2020.141713

Hazourli, S., Bonnecaze, G., Astruc, M., 1996. Adsorption et electrosorption de composes organiques sur charbon actif en grains partie i - influence du potentiel imposé et du nombre de cycles adsorption and electrosorption of organic compounds on granular activated carbon part i - influence of applied. Environ. Technol. (United Kingdom) 17, 1275–1283. https://doi.org/10.1080/09593330.1996.9618457

He, F., Hemmatifar, A., Bazant, M.Z., Hatton, T.A., 2020. Selective adsorption of organic anions in a flow cell with asymmetric redox active electrodes. Water Res. 182, 115963. https://doi.org/10.1016/j.watres.2020.115963

Iqbal, M., Iqbal, N., Bhatti, I.A., Ahmad, N., Zahid, M., 2016. Response surface methodology application in optimization of cadmium adsorption by shoe waste: A good option of waste mitigation by waste. Ecol. Eng. 88, 265–275. https://doi.org/10.1016/j.ecoleng.2015.12.041

Iqbal, M.J., Farooq, S., 2007. Effect of doping of divalent and trivalent metal ions on the structural and electrical properties of magnesium aluminate. Mater. Sci. Eng. B Solid-State Mater. Adv. Technol. 136, 140–147. https://doi.org/10.1016/j.mseb.2006.09.009

Jain, A., Tripathi, S.K., 2014. Almond shell-based activated nanoporous carbon electrode for

EDLCs. https://doi.org/10.1007/s11581-014-1282-1

Jasielec, J.J., 2021. Electrodiffusion Phenomena in neuroscience and the Nernst–Planck–Poisson equations. Electrochem 2, 197–215. https://doi.org/10.3390/electrochem2020014

Jiao, Y., Hu, Y., Han, L., Zhou, M., 2020. Activated carbon derived from rice husk as efficient oxygen reduction catalyst in microbial fuel cell. Electroanalysis 32, 2969–2975. https://doi.org/10.1002/elan.202060409

Jodra, Y., Mijangos, F., 2003. Phenol adsorption in immobilized activated carbon with alginate gels phenol adsorption in immobilized activated. Sep. Sci. Technol. 37–41. https://doi.org/10.1081/SS-120019412

Krishna, M. S., Raju, G. J., & Rao, C. V., 1966. Mass transfer in packed beds in annuli electrolytic redox reactions. Period. Polytech. Chem. Eng. 11, 95–102.

Li, D., Qu, Y., Liu, J., He, W., Wang, H., Feng, Y., 2014. Using ammonium bicarbonate as pore former in activated carbon catalyst layer to enhance performance of air cathode microbial fuel cell. J. Power Sources 272, 909–914. https://doi.org/10.1016/j.jpowsour.2014.09.053

Li, Y., Zhang, C., Jiang, Y., Wang, T., Wang, H., 2016. Effects of the hydration ratio on the electrosorption selectivity of ions during capacitive deionization. DES 399, 171–177. https://doi.org/10.1016/j.desal.2016.09.011

Lissaneddine, A., Mandi, L., Achaby, M. El, Mousset, E., Rene, E.R., Ouazzani, N., Pons, M.-N., Aziz, F., 2021a. Performance and dynamic modeling of a continuously operated pomace olive packed bed for olive mill wastewater treatment and phenol recovery. Chemosphere 280, 130797. https://doi.org/10.1016/j.chemosphere.2021.130797

Lissaneddine, A., Pons, M.-N., Aziz, F., Ouazzani, N., Mandi, L., Mousset, E., 2021b. A critical review on the electrosorption of organic compounds in aqueous effluent – Influencing factors and engineering considerations. Environ. Res. J. 204, 112128. https://doi.org/10.1016/j.envres.2021.112128

Liu, B., Zhong, F., Yokoyama, W., Huang, D., Zhu, S., Li, Y., 2020. Interactions in starch co-gelatinized with phenolic compound systems: Effect of complexity of phenolic compounds and amylose content of starch. Carbohydr. Polym. 116667. https://doi.org/10.1016/j.carbpol.2020.116667

Macías-García, A., Carrasco-Amador, J.P., Encinas-Sánchez, V., Díaz-Díez, M.A., Torrejón-Martín, D., 2019. Preparation of activated carbon from kenaf by activation with H_3PO_4. Kinetic study of the adsorption/electroadsorption using a system of supports designed in 3D, for environmental applications. J. Environ. Chem. Eng. 7, 103196. https://doi.org/10.1016/j.jece.2019.103196

Miller, A., Singh, L., Wang, L., Liu, H., 2019. Linking internal resistance with design and operation decisions in microbial electrolysis cells. Environ. Int. 126, 611–618. https://doi.org/10.1016/j.envint.2019.02.056

Miomandre, F., Sadki, S., Audebert, P., Méallet-Renault, R., 2005. Electrochimie - Des concepts aux applications. Dunod, Paris. (in French), Paris.

Mousset, E., 2020a. Unprecedented reactive electro-mixing reactor: Towards synergy between micro- and macro-reactors? Electrochem. Commun. 118, 106787. https://doi.org/10.1016/j.elecom.2020.106787

Mousset, E., Frunzo, L., Esposito, G., Hullebusch, E.D. van, Oturan, N., Oturan, M.A., 2016a. A complete phenol oxidation pathway obtained during electro-Fenton treatment and validated by a kinetic model study. Appl. Catal. B Environ. 180, 189–198. https://doi.org/10.1016/j.apcatb.2015.06.014

Mousset, E., Huang Weiqi, V., Foong Yang Kai, B., Koh, J.S., Tng, J.W., Wang, Z., Lefebvre, O., 2017. A new 3D-printed photoelectrocatalytic reactor combining the benefits of a transparent electrode and the Fenton reaction for advanced wastewater treatment. J. Mater. Chem. A 5, 24951–24964. https://doi.org/10.1039/c7ta08182k

Mousset, E., Loh, W.H., Lim, W.S., Jarry, L., Wang, Z., Lefebvre, O., 2021. Cost comparison of advanced oxidation processes for wastewater treatment using accumulated oxygen-equivalent criteria. Water Res. 200, 117234. https://doi.org/https://doi.org/10.1016/j.electacta.2021.138466

Mousset, E., Pontvianne, S., Pons, M.-N., 2018. Fate of inorganic nitrogen species under homogeneous Fenton combined with electro-oxidation/reduction treatments in synthetic solutions and reclaimed municipal wastewater. Chemosphere 201, 6–12. https://doi.org/10.1016/j.chemosphere.2018.02.142

Mousset, E., Quackenbush, L., Schondek, C., Gerardin-Vergne, A., Pontvianne, S., Kmiotek, S., Pons, M.N., 2020b. Effect of homogeneous Fenton combined with electron transfer on the fate of inorganic chlorinated species in synthetic and reclaimed municipal wastewater. Electrochim. Acta 334, 135608. https://doi.org/10.1016/j.electacta.2019.135608.

Mousset, E., Wang, Z., Hammaker, J., Lefebvre, O., 2016b. Physico-chemical properties of pristine graphene and its performance as electrode material for electro-Fenton treatment of wastewater. Electrochim. Acta 214, 217–230. https://doi.org/10.1016/j.electacta.2016.08.002

Parida, K.M., Pradhan, A.C., 2010. Removal of phenolic compounds from aqueous solutions by adsorption onto manganese nodule leached residue. J. Hazard. Mater. 173, 758–764. https://doi.org/10.1016/j.jhazmat.2009.09.003

Sahin, E.M., Tongur, T., Ayranci, E., 2020. Removal of azo dyes from aqueous solutions by adsorption and electrosorption as monitored with in-situ UV-visible spectroscopy. Sep. Sci. Technol. 55, 3287–3298. https://doi.org/10.1080/01496395.2019.1676786

Selman, J.R., Tobias, C.W., 1978. Mass-Transfer Measurements by the limiting-current technique. Adv. Chem. Eng. 10, 211–318.

Sharma, M., Jain, P., Varanasi, J.L., Lal, B., Rodríguez, J., Lema, J.M., Sarma, P.M., 2013. Enhanced performance of sulfate reducing bacteria based biocathode using stainless steel mesh on activated carbon fabric electrode. Bioresour. Technol. 150, 172–180. https://doi.org/10.1016/j.biortech.2013.09.069

Singleton, V. L., & Rossi, J.A., 1965. Colorimetry of total phenolic substances. US Am. Chem. Soc. Symp. Ser. 26, 47–70.

Situmorang, R.S., Seri, O., Kawai, H., 2020. Estimation of exchange current density for hydrogen evolution reaction of copper electrode by using the differentiating polarization method. Appl. Surf. Sci. 505, 144300. https://doi.org/10.1016/j.apsusc.2019.144300

Sun, D., Chen, Y., 2016. Electrode Kinetics of CO_2 Electroreduction. https://doi.org/10.1201/b20177-4

Sun, X.-F., Guo, B.-B., He, L., Xia, P.-F., Shu-Guang Wang, 2016. Electrically accelerated removal of organic pollutants by a three-dimensional graphene aerogel. AIChE J. 59, 215–228. https://doi.org/10.1002/aic

Taylor, P., Ji, M., Jiang, X., Wang, F., 2015. Desalination and water treatment a mechanistic approach and response surface optimization of the removal of oil and grease from restaurant wastewater by electrocoagulation and electroflotation. Desalin. water Treat. 37–41. https://doi.org/10.1080/19443994.2014.929034

Thakur, S., Arotiba, O., 2018. Synthesis, characterization and adsorption studies of an acrylic

acid-grafted sodium alginate-based TiO_2 hydrogel nanocomposite. Adsorption Science and Technology 36. https://doi.org/10.1177/0263617417700636

Tian, X., Bao, S., Zhang, Y., 2020. Adsorption properties of V(IV) on the resin-activated carbon composite electrodes in capacitive deionization. International Journal of Minerals, Metallurgy and Materials. 28(11),, 1777-1787. https://dx.doi.org/10.1007/s12613-020-2100-6

Tiwari, A., Soni, A., Bajpai, A.K., 2012. Nanoparticles loaded alginate beads as potential adsorbent for removal of phenol from aqueous solution. Synth. React. Inorganic, Met. Nano-Metal Chem. 42, 1158–1166. https://doi.org/10.1080/15533174.2012.682835

Tundis, R., Conidi, C., Loizzo, M.R., Sicari, V., Cassano, A., 2020. Olive mill wastewater polyphenol-enriched fractions by integrated membrane process: A promising source of antioxidant, hypolipidemic and hypoglycaemic compounds. Antioxidants, 9(7), 602.

Ververi, M., Goula, A.M., 2019. Pomegranate peel and orange juice by-product as new biosorbents of phenolic compounds from olive mill wastewaters. Chem. Eng. Process. Process Intensif. 138, 86–96. https://doi.org/10.1016/j.cep.2019.03.010

Wang, Y., Sheng, Z.M., Yang, H., Jiang, S.P., Li, C.M., 2010. Electrocatalysis of carbon black- or activated carbon nanotubes-supported Pd-Ag towards methanol oxidation in alkaline media. Int. J. Hydrogen Energy 35, 10087–10093. https://doi.org/10.1016/j.ijhydene.2010.07.172

Yang, W., Zhou, M., Ma, L., 2021. A continuous flow-through system with integration of electrosorption and peroxi-coagulation for efficient removal of organics. Chemosphere 274, 129983. https://doi.org/10.1016/j.chemosphere.2021.129983

Yao, C., Zhang, W., Xu, L., Cheng, M., Su, Y., Xue, J., Liu, J., Hou, S., 2021. A facile synthesis of porous MXene-based freestanding film and its spectacular electrosorption performance for organic dyes. Sep. Purif. Technol. 263, 118365. https://doi.org/10.1016/j.seppur.2021.118365

Yue, F., Zhang, Q., Xu, L., Zheng, Y., Yao, C., Jia, J., Leng, W., Hou, S., 2019. Porous reduced graphene oxide/single-walled carbon nanotube film as freestanding and flexible electrode materials for electrosorption of organic dye. ACS Appl. Nano Mater. 2, 6258–6267. https://doi.org/10.1021/acsanm.9b01236

Zhang, X., Li, K., Yan, P., Liu, Z., Pu, L., 2015. N-type Cu_2O doped activated carbon as catalyst for improving power generation of air cathode microbial fuel cells. Bioresour. Technol. 187, 299–304. https://doi.org/10.1016/j.biortech.2015.03.131

Zhu, P., Zhao, Y., 2019. Cyclic voltammetry measurements of electroactive surface area of porous nickel: Peak current and peak charge methods and diffusion layer effect. Mater. Chem. Phys. 233, 60–67. https://doi.org/10.1016/j.matchemphys.2019.05.034

Ziati, M., Hazourli, S., 2019. Experimental investigation of activated carbon prepared from date stones adsorbent electrode for electrosorption of lead from aqueous solution. Microchem. J. 146, 164–169. https://doi.org/10.1016/j.microc.2018.12.041

Chapter II: Granular activated carbon

I. Granular activated carbon based on pomace olive for olive mill wastewater treatment and phenol recovery

1. Introduction

Generally, the OMWW treatment by adsorption on GAC is mostly used after coagulation, flocculation, sedimentation and advanced oxidation processes (Bertin et al., 2004; Yonar & Azbar, 2005; Ena et al., 2009; Enaime et al., 2019). Unfortunately, few researchers have studied the treatment of OMWW by adsorption alone without combining it with any other method except the work of Ena et al. (2012). The latter investigated the GAC of PCs adsorption at concentrations in the 12.5–200 g L^{-1} range, which showed the GAC had a great adsorbing capacity, starting from the lowest concentration tested (12.5 g L^{-1}) (Ena et al., 2012). Also, Garcia-Araya et al. (2003) studied the adsorption of three PCs on a GAC with a relatively small surface area (Alvarez & Ingenier, 2003). To the authors' knowledge, GAC used in these works is commercial GAC.

This chapter investigates the production of high surface GAC from olive pomace and studies in more detail the removal of PCs from real OMWW in fixed-bed column adsorption using the developed GAC. These works provide a fundamental understanding of the real OMWW effects on adsorption and its impact on the adsorptive properties of PCs on GAC. In addition, the effects of bed depth influent and flow rate on PCs removal are studied. Finally, the Thomas and the Yoon-Nelson kinetic models are employed to simulate experimental data to evaluate their column performance on PCs.

2. Results and discussion

2.1.Physicochemical properties of effluent

The OMWW exhibited a brown to reddish-brown coloring, cloudy appearance and a strong olive oil smell. Table 16 shows the physicochemical properties of the investigated raw OMWW. The OMWW has shown an acidic pH (4.54) caused by the presence of organic acids (Elabdouni et al., 2020). The pH value recorded in our study was in the same range (between 4.2 and 5.9) as the one cited in the literature (Bagheri et al., 2020). The effluent was also characterized by a high electrical conductivity value (16.2 mS cm^{-1}); this high value was

ascribed to the high content of salts in OMWW. The predominance of toxic substances also characterized the OMWW; mostly, the content of PCs in OMWW was 10.6 g L^{-1}.

Table 16. Physicochemical parameters of OMWW.

Parameters	Value
pH	4.54 ± 0.004
Electrical conductivity (mS cm^{-1})	16.2 ± 0.04
Total dry matter (g L^{-1})	80.6 ± 3.8
Mineral matter (g L^{-1})	17.3 ± 2.3
Suspended matter (g L^{-1})	14.4 ± 2.1
COD (g-O_2 L^{-1})	192 ± 12
Total phosphorus (g L^{-1})	2.1 ± 0.03
Orthophosphate (g L^{-1})	0.31 ± 0.004
Nitrite (g L^{-1})	0.21 ± 0.004
Ammonia nitrogen (g L^{-1})	0.20 ± 0.09
Total PCs (g L^{-1})	10.6 ± 0.04
Total sugars (g L^{-1})	20.2 ± 1.2
Chloride (g L^{-1})	8.5 ± 0.94

2.2.Preparation and characterization of GAC

The results about the GAC preparation with different mass ratios of activator/precursor (1: 1, 2: 1, 3: 1, 5: 1) have been shown in Fig. 40. It was observed after three repetitions that the 3: 1 mass ratio was the best. This is because the pore volume of the GAC increased continuously with the rate of impregnation. As a result, it created a micropore structure and increased the enlargement of the micropores to the mesopores (Sudaryanto et al., 2006). In addition, the adsorption of PCs (small sizes: average molecular diameter = 0.557 nm) was favored on microporous AC. Therefore, the optimum mass ratio was taken as (3: 1) for GAC production by considering these results.

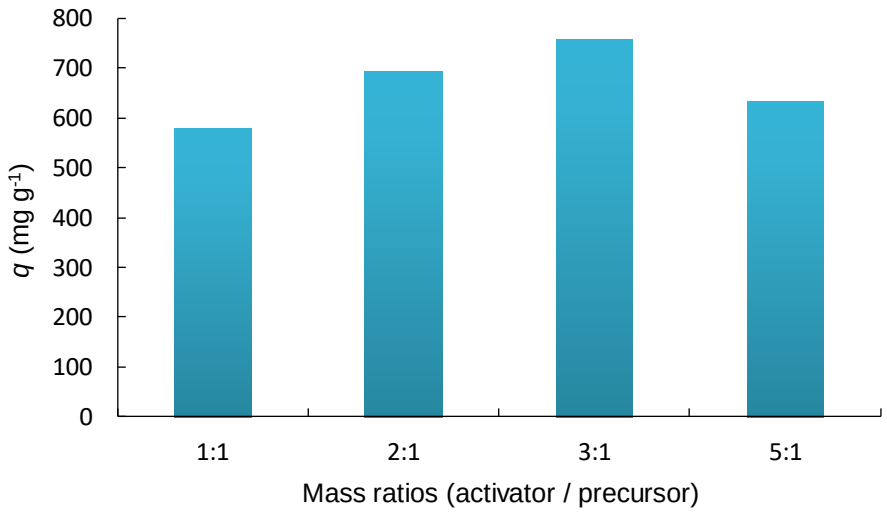

Fig. 40. Effect of the mass ratio of activator / precursor on the adsorption of phenol in batch. Phenol concentration = 4,000 mg L^{-1}, pH = 4, stirring = 200 rpm^{-1}.

FTIR was used to determine the functional groups on the GAC's surface before and after adsorption by the infrared spectra transmission (Fig. 41). It can be observed that many absorption bands belong to the –OH groups. The broadbands at 3400 and 3600 cm^{-1} were assigned to –OH stretching, corresponding to the water as moisture (Orha et al., 2017). Both bands around 2957 and 2878 cm^{-1} represented the (C–H) asymmetric, symmetric vibrations in methyl and methylene groups, respectively (Alhamed & Bamufleh, 2009). A major band was observed at 1444 cm^{-1} (asymmetric vibrations), representing the aqueous carboxylates (COO^{-}) (Shafeeyan et al., 2011; Orha et al., 2017). A small shoulder at 1118 cm^{-1} could be assigned to alcohol (R–OH) groups (Alhamed & Bamufleh, 2009).

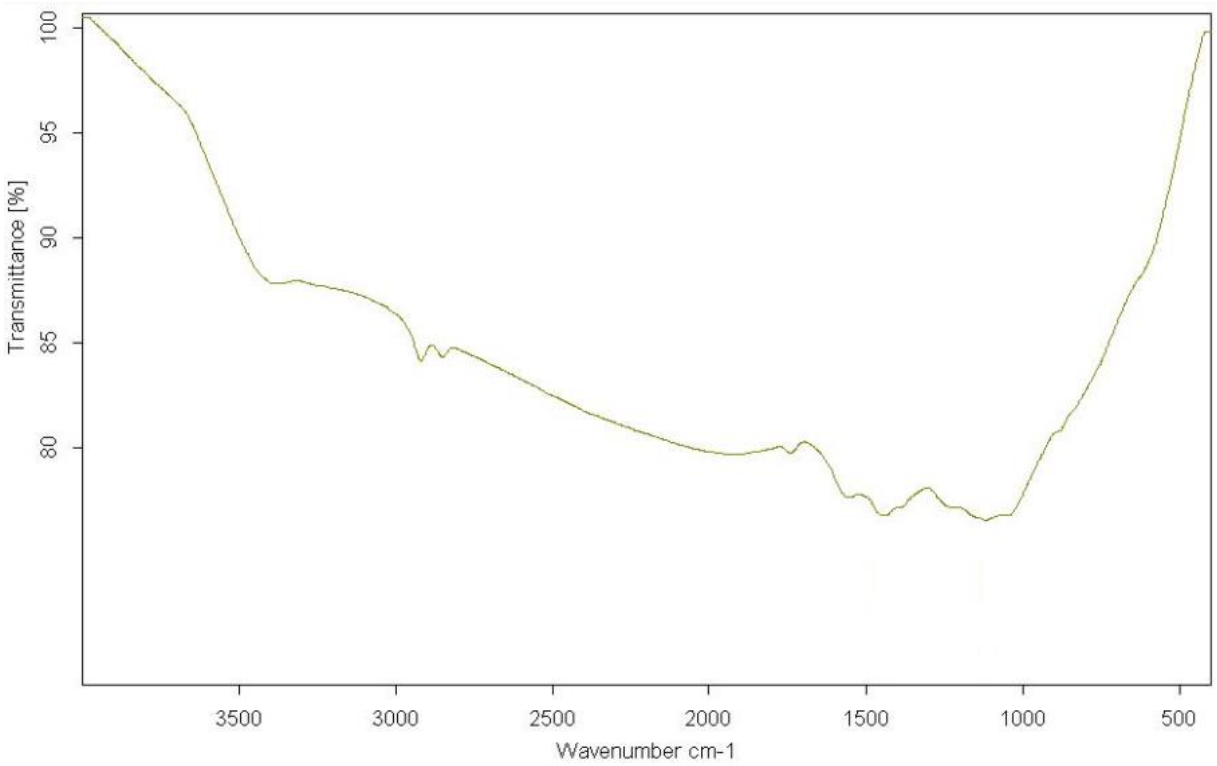

Fig. 41. FTIR spectra of GAC.

The surface morphology of GAC was characterized by SEM (Fig. 42). It is observed that GAC had a porous surface and rough areas with pores of different sizes. EDS results of GAC are shown in Table 17, the semiquantitative elemental analysis of the GAC surface indicating the major elements on the GAC were C (81.48 W%) and O (14.62 W%). In addition, traces of Na (1.96 W%), P (0.15 W%), Cl (0.25 W%), K (0.91 W%) and Ca (0.63 W%) species were identified as impurities of the olive pomace material and activation.

Under optimal conditions, the generated AC had a specific surface area of 1,012 m^2 g^{-1} with an average pore size of 1.5 nm.

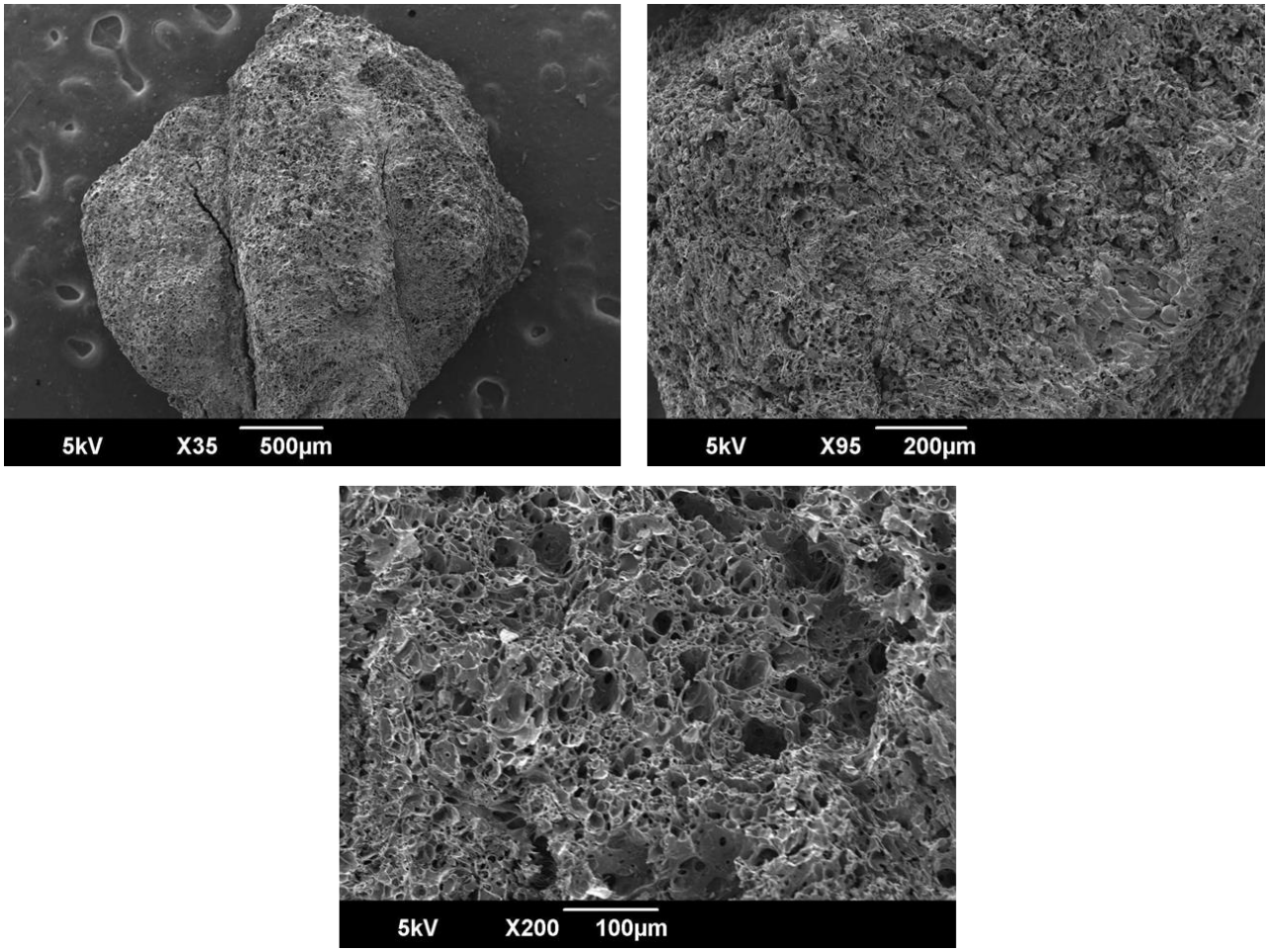

Fig. 42. SEM spectra of GAC at different magnification.

Table 17. EDS of GAC.

Element	W%	at.%
C	81.48	86.58
O	14.62	11.68
Na	1.96	1.09
P	0.15	0.06
Cl	0.25	0.09
K	0.91	0.30
Ca	0.63	0.20
	100.00	100.00

2.3.Adsorption efficiency

2.3.1. Adsorption equilibrium study

The initial concentration of PCs effect on the GAC adsorbent was examined at 20–5,000 mg L^{-1}. The results obtained are given in Fig. 43a. The adsorption capacity of PCs increased with the concentration of PCs in solution from 20 to 1,733 mg g^{-1} at 20 and 5,000 mg L^{-1}, respectively. The curves were favorable, presenting an inclined shape at a low equilibrium concentration of PCs. A plateau was observed at higher concentrations of PCs, indicating the saturation of the GAC surface. This behavior indicates the high active adsorption sites and the high efficiency of the GAC to remove PCs.

In order to clarify and understand the sorption process of PCs onto GAC, Langmuir and Freundlich's adsorption isotherm models were investigated in this study. The adsorption isotherms for adsorption of PCs on GAC from different adsorption models are shown in Figs. 43b and 43c. It was found that the R^2 values of the Langmuir isotherm were higher than those of the Freundlich isotherm, with R^2 of 0.997. These results demonstrate that the adsorption of PCs by GAC was better, followed by the Langmuir isotherm model. Accordingly, the monolayer maximum adsorption capacity of PCs was 1,666 mg g^{-1}. This result indicated that the adsorption of PCs behaviors over GAC was mainly a monolayer adsorption reaction, which involved chemical-physical adsorption equilibrium mechanism (Dong et al., 2021; Lissaneddine et al., 2021a). Furthermore, the $K_L$value, which usually describes adsorption energy, equaled 6.10^{-4} L mg^{-1}. This suggests that the spontaneity of the adsorption of PCs

could easily occur on the GAC surface (Dong et al., 2021; Franco et al., 2021). Moreover, it was notable that the value of 1/*n* from the Freundlich isotherm model was in range of 0–1, suggesting that chemical adsorption was favored on the surface of GAC (Dong et al., 2021).

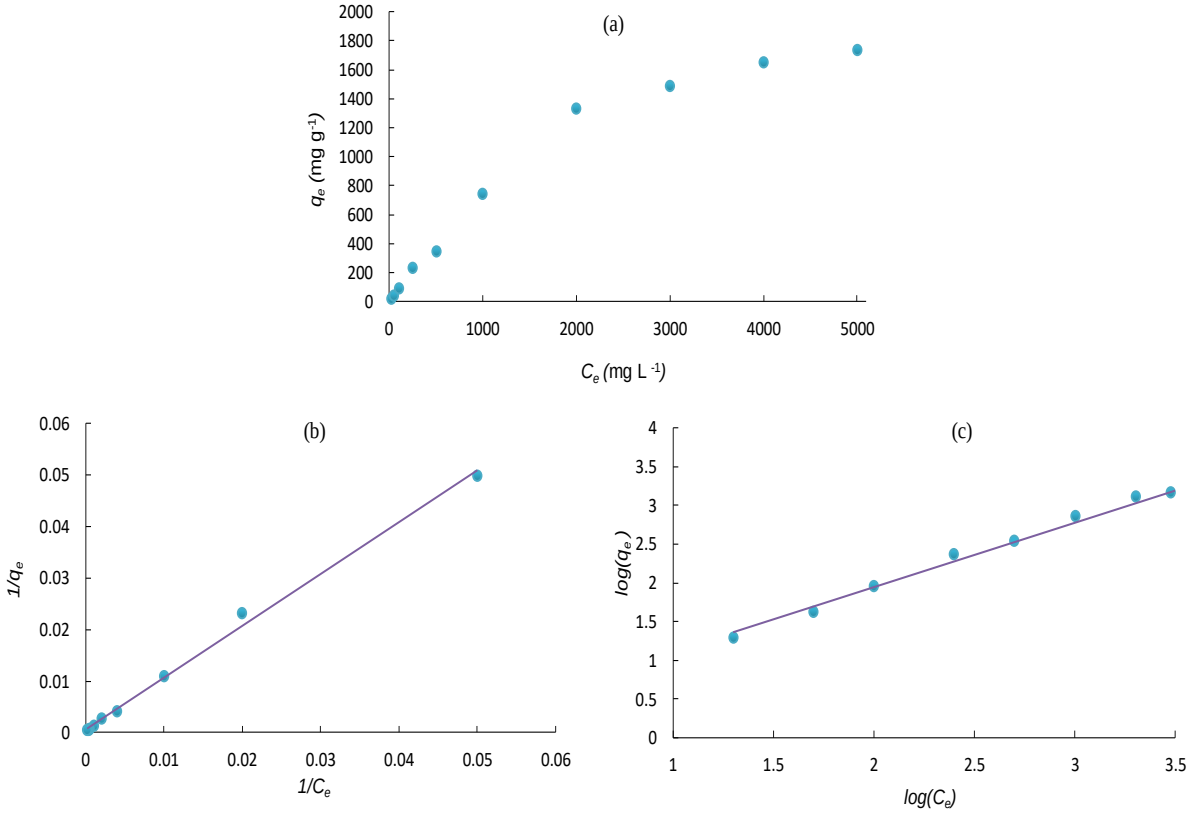

Fig. 43. Effect of the initial concentration on the adsorption of PCs (a), adsorption isotherm: (b) Langmuir and (c) Freundlich. Initial concentration, 20-4,000 mg L^{-1}; volume of OMWW, 5 mL; temperature, 19°C; pH=4; and contact time, 24h.

Table 18. Isotherm parameters of PCs adsorption onto the GAC (Conditions: 5 g of the adsorbent, 20-5,000 mg $L^{-1}$of PCs, pH=4, contact time 24h).

Isotherm	Parameters	Value of parameters
Langmuir	Q_m (mg g^{-1})	1667
	K_L (L mg^{-1})	6×10^{-4}
	R^2	0.997
	RMSE	1.15×10^{-6}
Freundlich	1/*n*	0.83
	K_F (L mg^{-1})	1.87
	R^2	0.988
	RMSE	2.35×10^{-3}

2.3.2. Modeling of adsorption kinetics

The effect of contact time on the adsorption of PCs on the GAC was examined between 0 and 480 min. The results obtained are given in Fig. 44a. The adsorption capacity of PCs increased rapidly over time as the active sites were accessible. With increasing time, the active sites tend to be saturated so that the adsorption capacity slowly increases until finally reaching adsorption equilibrium of 1,753 mg g^{-1} at 480 min.

To further study the removal process of PCs onto GAC, two kinetic models were presented. The sorption kinetics data have been compared with the pseudo-first-order and pseudo-second-order rate equations. The kinetic plots for adsorption of PCs onto GAC are shown in Figs. 44b and 44c, while kinetic parameters and correlation coefficients are listed in Table 19. The pseudo-second-order model expressed a lowest RMSE and a higher R^2 of 0.996 than 0.919 of the pseudo-first-order model, indicating the good fitting of the pseudo-second-order model. Specifically, the theoretical adsorption capacity value equaled 1,785 mg g^{-1}, which was not that far from the one obtained in the experimental study (1,753 mg g^{-1}). It was concluded that the adsorption of PCs onto the GAC process obeyed the pseudo-second-order model. This further indicated that the interactions between PCs molecules and the GAC active sites were governed by chemisorption phenomena, i.e. the valence changed by sharing or exchanging electrons between the GAC and the PCs (Kong et al., 2020; Lissaneddine et al., 2021a; Dehmani et al., 2021).

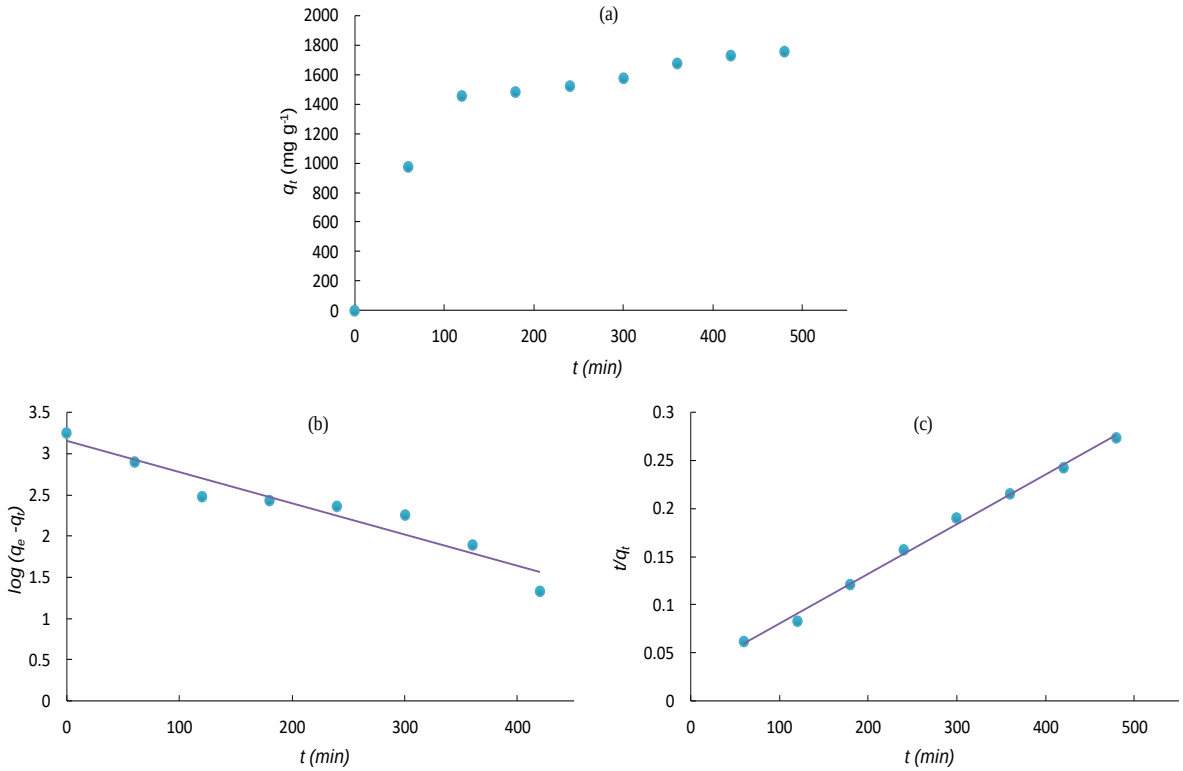

Fig. 44. Effect of the contact time on the adsorption of PCs (a), kinetic adsorption models: pseudo-first-order (b) and pseudo-second-order (c). Initial concentration, 4,000 mg L^{-1}; volume of OMWW, 5 mL; temperature, 19°C; pH=4; and contact time, 480 min).

Table 19. Kinetic parameters of PCs adsorption onto GAC (Conditions: 5 g of the adsorbent, 4,000 mg L^{-1} of PCs, 480 min contact time under optimum conditions of other variables).

Model	**Parameters**	**Value of parameters**
Pseudo-first-order	k_1 (min^{-1})	87.10^{-4}
	$q_{e\ (Calc.)}$ (mg g^{-1})	1438
	R^2	0.919
	RMSE	3,48.10^{-1}
Pseudo-second-order	k_2 (min^{-1})	10^{-5}
	$q_{e\ (Calc.)}$ (mg g^{-1})	1785
	R^2	0.996
	RMSE	3,24.10^{-3}

2.3.3. Effect of pH

The initial pH of the solution is an important factor, since it can influence the ionization state of the outer GAC surface and the charge characteristics of PCs, and the

adsorption mechanism. Therefore, it also influences the adsorption capacity of the PCs. Therefore, the effect of pH was studied over a pH range of 2 to 6 under optimum operating conditions. Fig. 45 shows the pH effect on adsorption of PCs onto the GAC. By increasing the pH from 2 to 6, adsorption of PCs onto GAC decreased from 1,010 to 639 mg g^{-1}, respectively. This could be due to the protonated forms of PCs thatwere predominant from acidic to neutral pH (effect of pKa) (Lissaneddine et al., 2021a). This form is more prone to be adsorbed on GAC than the unprotonated form. A similar trend was also observed in the study conducted by Annab et al. (2019) to remove PCs from OMWW onto beads based on AC (Annab et al., 2019). This was also in agreement with Ziati et al. (2017), who studied the adsorption of PCs from OMWW onto AC prepared with peach stones (Ziati et al., 2017).

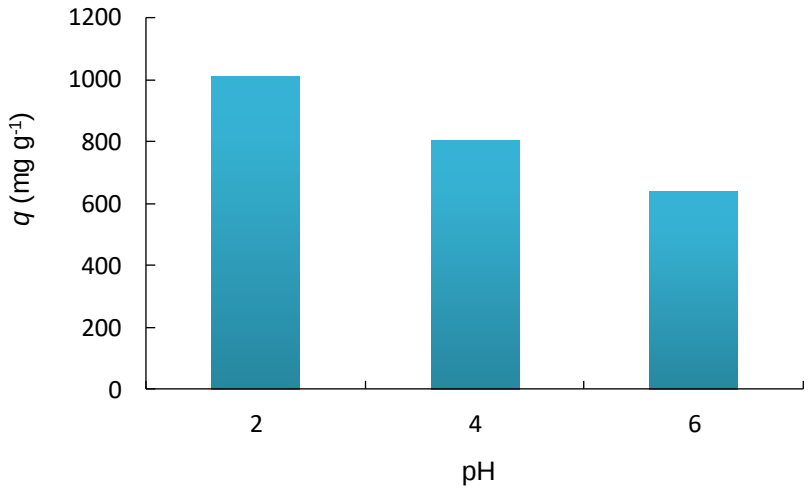

Fig. 45. Variation of the adsorption capacity of GAC with pH (at 19 °C; adsorbent = 5 g; C_0 = 4,000 mg L^{-1}).

2.3.4. Effect of temperature

The temperature effect (19-35°C) on the adsorption of PCs on GAC was performed. The thermodynamic properties *ΔG, ΔH* and *ΔS* values were calculated from the slope and the intercept of the linear correlation between $Ln(K_c)$ and 1/*T* known as the Van't Hoff plot (Fig. 46) and listed in Table 20. The results revealed the endothermic nature of the overall process ($\Delta H > 0$). In addition, the values of *ΔG* were negatives, which indicated that the process was spontaneous. However, the absolute values of *ΔG* increased with the temperature enhancement, suggesting that the adsorption was favorable at higher temperature. The obtained positive *ΔS* for GAC suggested a modification of their surface during the adsorption

process. Similar results have been obtained in other studies regarding the adsorption of PCs into the olive pit–derived AC (Eder et al., 2021), AC beads (Lissaneddine et al., 2021a), AC coated with milk proteins (Yangui & Abderrabba, 2018) and amine-modified mesoporous silica (Yangui et al., 2017).

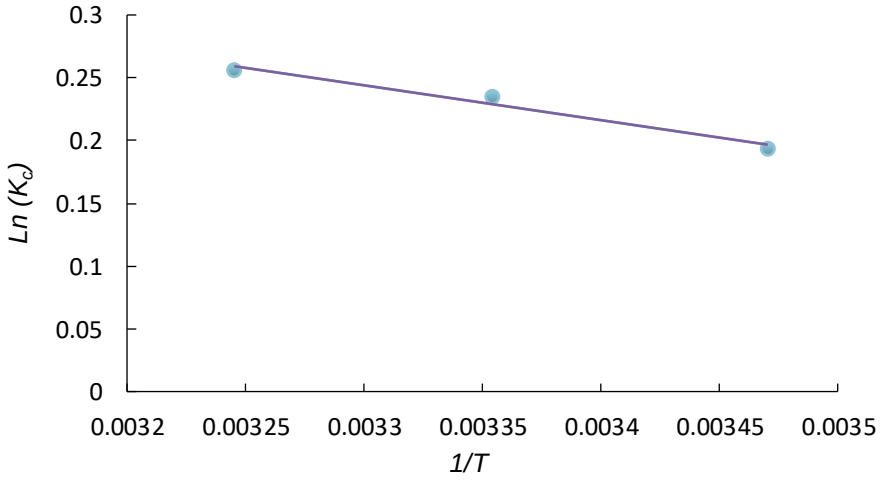

Fig. 46. Plot of $Ln(K_c)$ as a function of $1/T$ ($R^2 = 0.97$).

Table 20. Thermodynamic parameters of the adsorption process of PCs on GAC at various temperatures.

ΔH (KJ mol^{-1})	**ΔS (J mol^{-1} K^{-1})**	**ΔG (J mol^{-1})**		
		19°C	25°C	35°C
2,303	9.62	-464	-582	-656

2.3.5. Fixed-bed column

Different flow rates (0.5, 0.8 and 1.5 mL min^{-1}) were investigated in order to study its effect on the breakthrough curve of PCs. In these experiments, all the parameters (initial concentration, bed height, pH and temperature) were kept constant. The effect of flow rates on the breakthrough curves is presented in Fig. 47a. It could be observed that an increase in flow rate from 0.5 to 1 mL min^{-1} gave rise to steeper breakthrough curves and reduced breakthrough and saturation times. These trends were due to the residence time of the OMWW in the column, which was not long enough to reach adsorption equilibrium at a high flow rate (Abdelkreem, 2013). Iheanacho et al. (2021) and Abdelkreem et al. (2013) reported a similar observation in the recovery of phenol (Abdelkreem, 2013; Iheanacho et al., 2021).

The influence of bed heights (10, 15 and 20 cm) on the breakthrough curves of PCs has also been carried out. In these experiments, all the parameters (initial concentration, flow rates, pH and temperature) were also kept constant. The effect of bed height on the breakthrough curves is presented in Fig. 47b. It could be observed that the higher the bed heights, the more contact time of PCs with the GAC. This made increase PCs removal efficiency in the column. This was also due to the fact that the longer bed had more amount of GAC and, therefore more active sites for PCs adsorption. Moreover, more time was required for the bed saturation for higher bed heights, as previously reported (Abdelkreem, 2013; Iheanacho et al., 2021).

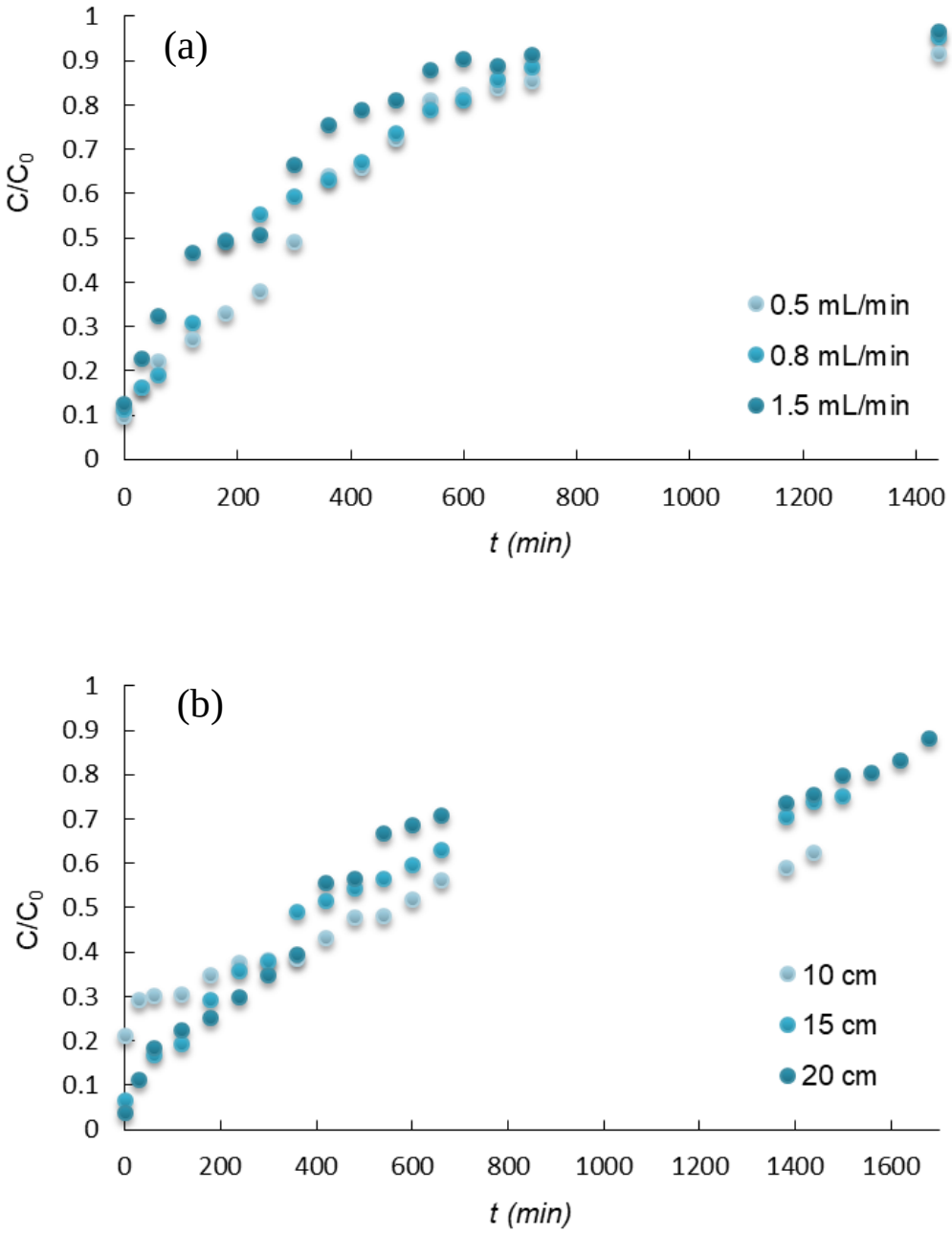

Fig. 47. Effects of operating parameters on breakthrough curves: (a) effect of flowrate and (b) effect of bed height.

The experimental data resulting from different flow rates and different bed heights variation were fitted with two empirical models Thomas and Yoon-Nelson column kinetic models and analyzed via linear regression tools. The results of the linear regression analysis are presented in Tables 21 and 22. The models were in good agreement with the experimental data, based on R^2 values ($R^2 > 0.9$). This meant that both Thomas and Yoon–Nelson models could be used to describe the dynamic behavior of the column.

Thomas model follows the kinetics of Langmuir with a hypothesis applicable in a system with a constant flow and a negligible axial dispersion in the column. This is because the motive force of speed follows a reversible reaction of second-order (Lissaneddine et al., 2021b). Thomas kinetic constants increased with improved in flow rate and bed height, but adsorption capacity decreased, maybe due to mass transfer resistance being greater as bed height increased (Satya et al., 2021). The application of Yoon–Nelson model to the experimental data resulted in K_{YN} and τ values that adequately described the fixed-bed adsorption of PCs onto the GAC layer. Yoon–Nelson constants increased with the flow rate and bed height. However, the time required for the breakthrough of 50% of adsorbate decreased, which was probably due to the broadened mass transfer zone (Lai et al., 2021).

Table 21. Thomas model parameters for PCs adsorption into GAC in a fixed-bed column at different conditions using linear regression analysis.

GAC bed height (cm)	Flow rate (mL min^{-1})	K_{Th} (mL min^{-1} mg^{-1})	q_0 (mg g^{-1})	R^2
10	0.5	12×10^{-4}	265	0.97
10	0.8	12×10^{-4}	189	0.94
10	1.5	13×10^{-4}	143	0.96
10	1	45×10^{-5}	655	0.98
15	1	84×10^{-5}	425	0.93
20	1	12×10^{-4}	247	0.97

Table 22. Yoon–Nelson model parameters for PCs adsorption into GAC in a fixed-bed column at different conditions using linear regression analysis.

GAC bed height (cm)	Flow rate (mL min^{-1})	K_{YN} (min^{-1})	T (min)	R^2
10	0.5	51×10^{-5}	385	0.97
10	0.8	53×10^{-5}	171	0.94
10	1.5	57×10^{-5}	103	0.96
10	1	18×10^{-5}	500	0.98
15	1	36×10^{-5}	447	0.93
20	1	43×10^{-5}	423	0.97

2.4.Desorption

Desorption studies allow clarifying the mechanism of adsorption and of value-added PCs recovering. The results of the desorption experiments in a stirred batch reactor with different kinds of solvents, i.e., distilled water, ethanol, a mixture of methanol and ethanol (50%/50% M) and HCl (0.05 M), are presented in Fig. 48. The solvent efficiency for PCs desorption was

following this rank (from the best to the worse): HCl (0.05 M) > mixture of methanol and ethanol (50%/50% M) > ethanol > distilled water. Thus, HCl (0.05 M) led to the highest enhancement of PCs desorption from GAC and was used for the desorption experiments in column (Fig. 49), according to the procedure described in part II, section 1.5.1. Figure 49 show the concentration of PCs accumulated over 360 min in HCl (0.05 M) solution. The results showed that HCl could recover almost 90% of the compounds adsorbed in the GAC packed-bed column.

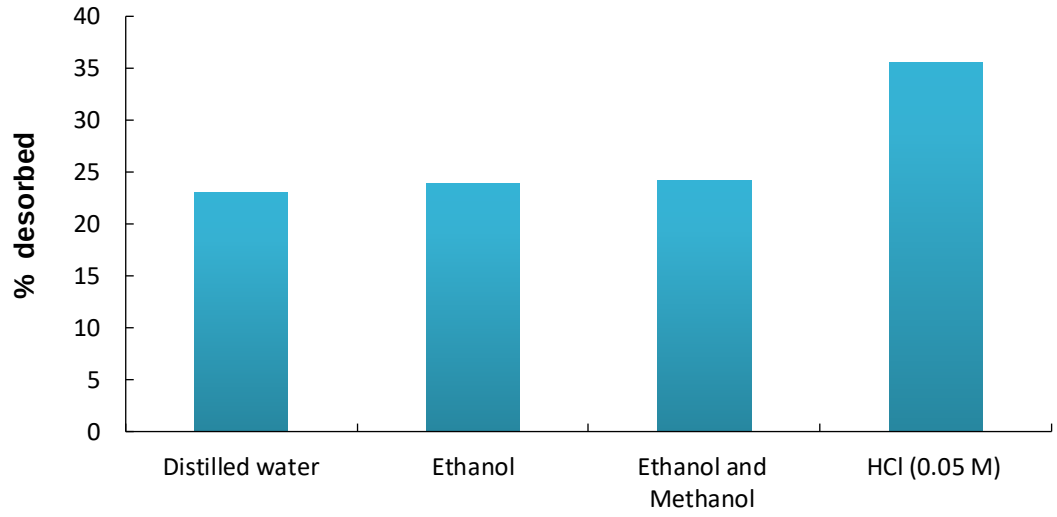

Fig. 48. Effects of different solvents on PCs desorption efficiency.

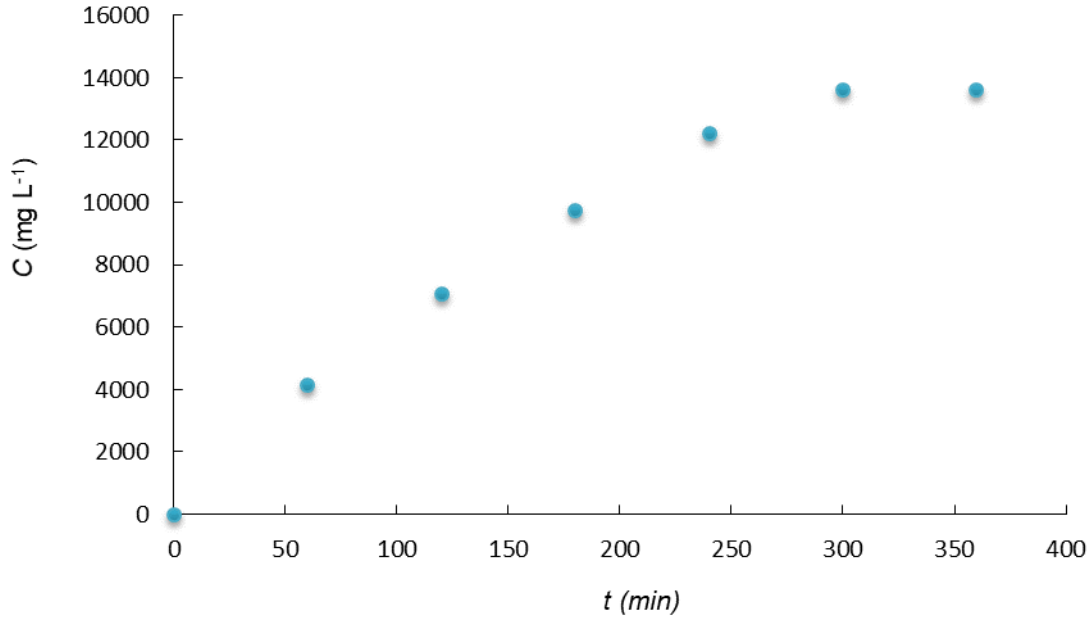

Fig. 49. Fraction of desorbed PCs from GAC by HCl (0.05 M).

3. Conclusions

Olive pomace was effectively converted into GAC. The reliability of the adsorbent properties for adsorption was confirmed using FTIR, SEM, EDS and BET studies. The Langmuir monolayer adsorption capacity was 1,666 mg g^{-1}. The experimental kinetic data fitted well with the pseudo-second-order kinetic model. The thermodynamic parameters for the PCs adsorption onto the GAC highlighted that the negative value of ΔG confirmed the feasibility of the process and the spontaneous nature of adsorption. The values of ΔH and ΔS suggested an endothermic reaction and a modification of GAC surface during the adsorption process. In the dynamic mode, the breakthrough time for PCs adsorption decreased with the flow rate but increased with the bed height. Therefore, the adsorption capacity of PCs depended on the bed height and the flow rate. The modeling about the adsorption in the column indicated that both Thomas and Yoon-Nelson models fitted well with the experimental data. Finally, considering the several advantages of GAC (i.e., low cost and high efficiency in this application), it could be used as a promising adsorbent for PCs adsorption and desorption from OMWW.

References

Adnan, F.H., Mousset, E., Pontvianne, S., Pons, M., 2021. Mineral cathodic electro-precipitation and its kinetic modelling in thin-film microfluidic reactor during advanced electro-oxidation process. Electrochim. Acta 387, 138487. https://doi.org/10.1016/j.electacta.2021.138487

Ania, C.O., Béguin, F., 2007. Mechanism of adsorption and electrosorption of bentazone on activated carbon cloth in aqueous solutions. Water Res. 41, 3372–3380. https://doi.org/10.1016/j.watres.2007.03.031

Ayoubi-Feiz, B., Aber, S., Khataee, A., Alipour, E., 2014a. Preparation and application of α-Fe_2O_3/TiO_2/activated charcoal plate nanocomposite as an electrode for electrosorption-assisted visible light photoelectrocatalytic process. J. Mol. Catal. A Chem. 395, 440–448. https://doi.org/10.1016/j.molcata.2014.09.006

Ayoubi-Feiz, B., Aber, S., Khataee, A., Alipour, E., 2014b. Electrosorption and photocatalytic one-stage combined process using a new type of nanosized TiO_2/activated charcoal plate electrode. Environ. Sci. Pollut. Res. 21, 8555–8564. https://doi.org/10.1007/s11356-014-2777-z

Ayoubi-Feiz, B., Mashhadizadeh, M.H., Sheydaei, M., 2018. Preparation of reusable nano N-TiO_2/graphene/titanium grid sheet for electrosorption-assisted visible light photoelectrocatalytic degradation of a pesticide: Effect of parameters and neural network modeling. J. Electroanal. Chem. 823, 713–722. https://doi.org/10.1016/j.jelechem.2018.07.020

Ayranci, E., Conway, B.E., 2001. Removal of phenol, phenoxide and chlorophenols from waste-waters by adsorption and electrosorption at high-area carbon felt electrodes. J. Electroanal. Chem. 513, 100–110. https://doi.org/10.1016/S0022-0728(01)00529-0

Bán, A., Schäfer, A., Wendt, H., 1998. Fundamentals of electrosorption on activated carbon for wastewater treatment of industrial effluents. J. Appl. Electrochem. 28, 227–236. https://doi.org/10.1023/A:1003247229049

Barhoum, A., El-Maghrabi, H.H., Iatsunskyi, I., Coy, E., Renard, A., Salameh, C., Weber, M., Sayegh, S., Nada, A.A., Roualdes, S., Bechelany, M., 2020. Atomic layer deposition of Pd nanoparticles on self-supported carbon-Ni/NiO-Pd nanofiber electrodes for electrochemical hydrogen and oxygen evolution reactions. J. Colloid Interface Sci. 569, 286–297. https://doi.org/10.1016/j.jcis.2020.02.063

Bayram, E., 2016. Electrosoption of aromatic organic acids from aqueous solutions onto granular activated carbon electrodes for water purification. Hacettepe J. Biol. Chem. 3, 273–273. https://doi.org/10.15671/hjbc.20164420570

Bayram, E., Ayranci, E., 2012a. Structural effects on electrosorptive behavior of aromatic organic acids from aqueous solutions onto activated carbon cloth electrode of a flow-through electrolytic cell. J. Electroanal. Chem. 683, 14–20. https://doi.org/10.1016/j.jelechem.2012.07.028

Bayram, E., Ayranci, E., 2012b. Electrosorption based waste water treatment system using activated carbon cloth electrode: Electrosorption of benzoic acid from a flow-through electrolytic cell. Sep. Purif. Technol. 86, 113–118. https://doi.org/10.1016/j.seppur.2011.10.032

Bayram, E., Kizil, Ç., Ayranci, E., 2018. Flow-through electrosorption process for removal of 2,4-D pesticide from aqueous solutions onto activated carbon cloth fixed-bed electrodes. Water Sci. Technol. 77, 848–854. https://doi.org/10.2166/wst.2017.598

Bousba, S., Meniai, A.H., 2014. Removal of phenol from water by adsorption onto sewage

sludge based adsorbent. Chem. Eng. Trans. 40, 235–240. https://doi.org/10.3303/CET1440040

Chen, Q., Wang, L., Xu, Y., Li, P., Wang, X., Wang, M., Kong, Y., 2018. Electrochemical investigation of phenol oxidation by a TiO_2/GAC based packed-bed electrode reactor. Int. J. Electrochem. Sci. 13, 7301–7309. https://doi.org/10.20964/2018.08.59

Chen, Y., Tu, Y., Bai, Y., Li, J., Lu, J., 2018. Electrosorption enhanced electrooxidation of a model organic pollutant at 3D SnO_2-Sb electrode in superimposed pulse current mode. Chemosphere 195, 63–69. https://doi.org/10.1016/j.chemosphere.2017.12.074

Damaskin, B. B., Baturina, O.A., 1999. Co-adsorption of anions and low-adsorbing cations within the Alekseev-Popov-Kolotyrkin model. Russ. J. Electrochem. 35(11), 1182–1185.

Damaskin, B.B., 2011. Modeling of co adsorption of cations and anions localized in different layers of the dense part of electrical double layer under the conditions of linear charge dependence of the adsorption energy. Russ. J. Electrochem. 47, 988–994. https://doi.org/10.1134/S1023193511090047

Damaskin, B.B., 2008. Modeling of synergism effect at different orientation of co-adsorbing molecules. Russ. J. Electrochem. 44, 1411–1417. https://doi.org/10.1134/S102319350812001X

Damaskin, B.B., Baturina, O.A., 2001a. Some anomalies in coadsorption of two organic substances due to differences in molecular interaction of species undergoing coadsorption. Russ. J. Electrochem. 37, 1482–1489.

Damaskin, B.B., Baturina, O.A., 2001b. Simulating coadsorption of surface active anions and organic molecules capable of forming two-dimensional condensed layers on the electrode. Russ. J. Electrochem. 37, 121–126.

Damaskin, B.B., Baturina, O.A., 2001c. Simulation of coadsorption of inorganic ions and organic molecules on electrodes. Russ. J. Electrochem. 37, 73–79.

Damaskin, B.B., Safonov, V.A., Safonov, N. V, 2003. Adsorption of an organic compound in two different positions: Simulation taking into account all three parameters of intermolecular interaction. Russ. J. Electrochem. 39, 814–819.

Eisinger, R.S., Alkire, R.C., 1980. Electrosorption of b-naphthol on graphite. J Electroanal.Chem. 112, 327–337.

Eisinger, R.S., Keller, G.E., 1990. Electrosorption: A case study on removal of dilute organics from water. Environ. Prog. 9, 235–244. https://doi.org/10.1002/ep.670090418

Gennero, M.R., Chialvo, A.C., 2012. Exchange current density, electrocatalytic activity and volcano curve for the hydrogen electrode reaction: theoretical analysis 17.

Gileadi, E., 1966. Electrosorption of uncharged molecules on solid electrodes. J. Electroanal. Chem. 11, 137–151. https://doi.org/10.1016/0022-0728(66)80073-6

Haider, S.S., Iqbal, M.Z., Zakar, S., Afzal, A.M., Yaqoob, K., Aftab, S., 2021. Superior performance of electrodeposited CoMnS as novel electrode material for supercapattery devices. J. Energy Storage 39, 102608. https://doi.org/10.1016/j.est.2021.102608

Han, Y., Quan, X., Chen, S., Zhao, H., Cui, C., Zhao, Y., 2006a. Electrochemically enhanced adsorption of phenol on activated carbon fibers in basic aqueous solution. J. Colloid Interface Sci. 299, 766–771. https://doi.org/10.1016/j.jcis.2006.03.007

Han, Y., Quan, X., Chen, S., Zhao, H., Cui, C., Zhao, Y., 2006b. Electrochemically enhanced adsorption of aniline on activated carbon fibers. Sep. Purif. Technol. 50, 365–372. https://doi.org/10.1016/j.seppur.2005.12.011

Han, Y., Quan, X., Ruan, X., Zhang, W., 2008. Integrated electrochemically enhanced adsorption with electrochemical regeneration for removal of acid orange 7 using

activated carbon fibers. Sep. Purif. Technol. 59, 43–49. https://doi.org/10.1016/j.seppur.2007.05.026

Hazourli, S., Bonnecaze, G., Astruc, M., 1996. Adsorption et electrosorption de composes organiques sur charbon actif en grains partie I - Influence du potentiel imposé et du nombre de cycles adsorption and electrosorption of organic compounds on granular activated carbon part I- Influence of applied. Environ. Technol. 17, 1275–1283. https://doi.org/10.1080/09593330.1996.9618457

Hou, C.H., Huang, J.F., Lin, H.R., Wang, B.Y., 2012. Preparation of activated carbon sheet electrode assisted electrosorption process. J. Taiwan Inst. Chem. Eng. 43, 473–479. https://doi.org/10.1016/j.jtice.2011.12.003

Jayson, G.G., Sangster, J.A., Thompson, G., Wilkinson, M.C., 1987. Adsorption and electrosorption of mercury (II) acetate onto activated charcoal cloth from aqueous solution. Carbon N. Y. 25, 523–531. https://doi.org/10.1016/0008-6223(87)90193-X

Jiang, D., Li, B., 2009. Granular activated carbon single-chamber microbial fuel cells (GAC-SCMFCs): A design suitable for large-scale wastewater treatment processes. Biochem. Eng. J. 47, 31–37. https://doi.org/10.1016/j.bej.2009.06.013

Jin, Y., Wu, M., Zhao, G., Li, M., 2011. Photocatalysis-enhanced electrosorption process for degradation of high-concentration dye wastewater on TiO2/carbon aerogel. Chem. Eng. J. 168, 1248–1255. https://doi.org/10.1016/j.cej.2011.02.026

Kitous, O., Cheikh, A., Lounici, H., Grib, H., Pauss, A., Mameri, N., 2009. Application of the electrosorption technique to remove Metribuzin pesticide. J. Hazard. Mater. 161, 1035–1039. https://doi.org/10.1016/j.jhazmat.2008.04.091

Lissaneddine, A., Pons, M.-N., Aziz, F., Ouazzani, N., Mandi, L., Mousset, E., 2021b. A critical review on the electrosorption of organic compounds in aqueous effluent – Influencing factors and engineering considerations. Environ. Res. J. 204, 112128. https://doi.org/10.1016/j.envres.2021.112128

Liu, L., Liu, Y., Che, N., Gao, B., Li, C., 2021. Electrochemical adsorption of perfluorooctanoic acid on a novel reduced graphene oxide aerogel loaded with Cu nanoparticles and fluorine. J. Hazard. Mater. 416, 125866. https://doi.org/10.1016/j.jhazmat.2021.125866

López-Bernabeu, S., Ruiz-Rosas, R., Quijada, C., Montilla, F., Morallón, E., 2016. Enhanced removal of 8-quinolinecarboxylic acid in an activated carbon cloth by electroadsorption in aqueous solution. Chemosphere 144, 982–988. https://doi.org/10.1016/j.chemosphere.2015.09.071

Mcquillan, A.R. V, Stevens, G.W., Mumford, A., 2018. The Electrochemical regeneration of granular activated carbons: A review. J. Hazard. Mater. https://doi.org/10.1016/j.jhazmat.2018.04.079

Meng, H.-S., Liu, Y., Liu, P.-X., Zhou, L.-L., Chen, C., Wang, W.-K., Xu, J., 2021. Development of a three-dimensional photoelectrocatalytic reactor packed with granular sludge carbon photoelectrocatalyst for efficient wastewater treatment, Sep. Purif. Technol. 277, 119642. https://doi.org/10.1016/j.seppur.2021.119642

Moeini, B., Avval, T.G., Linford, M.R., Ghalkhani, M., Kaykhaii, M., Abdullah Mirzaie, R., 2021. Surface-orientated platinum nanoparticles electrodeposited on a carbon substrate as a high performance electrocatalyst for glucose oxidation reaction in alkaline media. Mater. Sci. Eng. B Solid-State Mater. Adv. Technol. 268, 115147. https://doi.org/10.1016/j.mseb.2021.115147

Mohamed, E.F., Andriantsiferana, C., Wilhelm, A.M., Delmas, H., 2011. Competitive adsorption of phenolic compounds from aqueous solution using sludge-based activated

carbon. Environ. Technol. 32, 1325–1336. https://doi.org/10.1080/09593330.2010.536783

Mohanraj, R., Brindha, R., Kandeeban, R., Mahendhar, M., Saminathan, K., Ayyappadasaa, G., 2021. Electrochemical detection of 5-hydroxytryptamine using sustainable SnO_2-Graphite nanocomposite modified electrode. Mater. Lett. 305, 130796. https://doi.org/10.1016/j.matlet.2021.130796

Niamlaem, M., Boonyuen, C., Sangthong, W., Limtrakul, J., Zigah, D., Kuhn, A., Warakulwit, C., 2020. Highly defective carbon nanotubes for sensitive, low-cost and environmentally friendly electrochemical H_2O_2 sensors: Insight into carbon supports. Carbon 170, 154–164. https://doi.org/10.1016/j.carbon.2020.07.081

Nie, C., Dai, Z., Meng, H., Duan, X., Qin, Y., Zhou, Y., Ao, Z., Wang, S., An, T., 2019. Peroxydisulfate activation by positively polarized carbocatalyst for enhanced removal of aqueous organic pollutants. Water Res. 166, 115043. https://doi.org/10.1016/j.watres.2019.115043

Niu, J., Conway, B.E., 2003. Adsorption of organics onto an high-area C-cloth electrode from organic solvents and organic solvent/water mixtures. J. Electroanal. Chem. 546, 59–72. https://doi.org/10.1016/S0022-0728(03)00146-3

Pierpaoli, M., Jakobczyk, P., Sawczak, M., Łuczkiewicz, A., Fudala-Książek, S., Bogdanowicz, R., 2021. Carbon nanoarchitectures as high-performance electrodes for the electrochemical oxidation of landfill leachate. J. Hazard. Mater. 401, 123407. https://doi.org/10.1016/j.jhazmat.2020.123407

Plaisance, H., Mocho, P., Bonnecaze, G., 1996. Adsorption et electrosorption de benzene sur charbon actif en grains - Adsorption and electrosorption of benzene on granular activated carbon. Environ. Technol. 17, 1313–1325. https://doi.org/10.1080/09593331708616501

Rong, C., Xien, H., 2009. Reversible electrosorption of thiocyanate anions by active carbon felt. Sep. Sci. Technol. 44, 3984–3999. https://doi.org/10.1080/01496390903182453

Rong, C., Xien, H., 2005. Electrosorption of thiocyanate anions on active carbon felt electrode in dilute solution. J. Colloid Interface Sci. 290, 190–195. https://doi.org/10.1016/j.jcis.2005.04.022

Sahin, E.M., Tongur, T., Ayranci, E., 2020. Removal of azo dyes from aqueous solutions by adsorption and electrosorption as monitored with in-situ UV-visible spectroscopy. Sep. Sci. Technol. 55, 3287–3298. https://doi.org/10.1080/01496395.2019.1676786

Sekar, S., Aqueel Ahmed, A.T., Pawar, S.M., Lee, Y., Im, H., Kim, D.Y., Lee, S., 2020. Enhanced water splitting performance of biomass activated carbon-anchored WO_3 nanoflakes. Appl. Surf. Sci. 508, 145127. https://doi.org/10.1016/j.apsusc.2019.145127

Stenina, E. V, Baturina, O.A., Sviridova, L.N., Damaskin, B.B., 2001. Coadsorption of halide anions and 1-adamantanol molecules on a mercury electrode. Russ. J. Electrochem. 37, 931–938.

Strohl, J.H., Dunlap, K.L., 1972. Electrosorption and separation of quinones on a column of graphite particles. Anal. Chem. 44, 2166–2170. https://doi.org/10.1021/ac60321a012

Sun, X.-F., Guo, B.-B., He, L., Xia, P.-F., Shu-Guang Wang, 2016. Electrically accelerated removal of organic pollutants by a three-dimensional graphene aerogel. AIChE J. 59, 215–228. https://doi.org/10.1002/aic

Wang, X., Hu, Y., Min, J., Li, S., Deng, X., Yuan, S., Zuo, X., 2018. Adsorption characteristics of phenolic compounds on graphene oxide and reduced graphene oxide: A batch experiment combined theory calculation. Appl. Sci. 8, 1–13. https://doi.org/10.3390/app8101950

Yue, F., Zhang, Q., Xu, L., Zheng, Y., Yao, C., Jia, J., Leng, W., Hou, S., 2019. Porous reduced graphene oxide/single-walled carbon nanotube film as freestanding and flexible electrode materials for electrosorption of organic dye. ACS Appl. nano Mater. 2, 6258–6267. https://doi.org/10.1021/acsanm.9b01236

Zhu, P., Zhao, Y., 2019. Cyclic voltammetry measurements of electroactive surface area of porous nickel: Peak current and peak charge methods and diffusion layer effect. Mater. Chem. Phys. 233, 60–67. https://doi.org/10.1016/j.matchemphys.2019.05.034

Ziati, M., Khemmari, F., Cherifi, O., & Didouche, F. Y., 2017. Removal of polyphenols from olive mill wastewater by adsorption on activated carbon prepared from peach stones. Rev. Roum. Chim., 62(11), 865-874.

II. Electrosorption with bio-sourced granular activated carbon electrode for phenols recovery and combination with electrooxidation for residual olive mill wastewater treatment

1. Introduction

Electrode materials have a great impact on the performance of electrosorption. Electrosorption efficiency partly depends on the nature of the electrode materials and their characteristics (Lissaneddine et al., 2021b). Various carbonaceous materials such as GAC (Eisinger & Keller, 1990; Hazourli et al., 1996a; Plaisance et al., 1996; Bán et al., 1998; Kitous et al., 2009; Bayram, 2016;), carbon cloth (Jayson et al., 1987; López- Niu & Conway, 2003; Ania & Béguin, 2007; Bayram & Ayranci, 2012b; Bernabeu et al., 2016; Bayram et al., 2018; Sahin et al., 2020), carbon fiber (Strohl & Dunlap, 1972; Han et al., 2006b, 2006a, 2008), carbon felt (Ayranci & Conway, 2001; Rong & Xien, 2005, 2009), graphite (Strohl & Dunlap, 1972; Eisinger & Alkire, 1980) and graphene (Sun et al., 2016a; Yue et al., 2019b; Liu et al., 2021) have been commonly utilized as electrode materials for the removal of organics. GAC is frequently used as an adsorbent in water and wastewater treatment processes due to its high surface area with values usually ranging between 600 and 1,200 m^2 g^{-1} (Jiang & Li, 2009).

The results reported by many authors in the literature showed that the GAC electrode has high efficiency for eliminating different organic pollutants. This was the case for instance with the removal of BA (90.6%) and nicotinic acid (91%) (Bayram, 2016), metribuzin (22 mg g^{-1}) (Kitous et al., 2009), naphthalenesulfonic acid (100 mg g^{-1}), benzyl alcohol (100 mg g^{-1}), naphthoic acid (100 mg g^{-1}), methylquinolinium chloride (100 mg g^{-1}) (Bán et al., 1998), benzene (238 mg g^{-1}) (Plaisance et al., 1996) and chloroform (340 mg g^{-1}) (Hazourli et al., 1996a). However, GAC has never been used for the PCs elimination from OMWW. In addition, the production of GAC can be obtained directly from natural raw materials (biomass waste), while preserving great stability. Contrastingly, it is necessary to add an additive (alginate) for composite beads. These latters are also less stable, since they can be degraded easier at high current intensity. Therefore, GAC has some advantages compared to the composite beads.

In this context, the GAC was implemented as an electrode material for the electrosorption of PCs from OMWW. The electrochemical characterization of the GAC electrode was studied in order to determine its performance. The objective of this study is to investigate the effect of electrode polarization on the electrosorption of phenol and explore the relationship between the PCs properties and their electrosorption efficiency. The electrochemical regeneration of GAC electrodes and the electrochemical organic degradation of residual OMWW were also studied.

2. Results and discussion

2.1.Characterization of GAC

2.1.1. Influence of electrochemical conditioning on GAC characteristics

Additional electrochemical conditioning of the GAC has been tested to further enhance its properties compared to the GAC manufactured in Part III, sub-chapter II.I. The morphologies of GAC before and after electrochemical conditioning were analyzed by SEM, as shown in Fig. 50. Before conditioning, it wasobserved large voids and rifts made the surface quite heterogeneous and porous. However, the GAC after conditioning had rough surfaces with smaller irregular and interspatial pores within the matrix of the GAC, which could facilitate the diffusion of more PCs molecules into the pores structure. The difference of morphologies of GAC before and after conditioning could be explained by the pitting corrosion that may occur during the application of high anode potential (E_{an} = 1.8 V/(Ag/AgCl)). This potential was higher than the standard potential (0.011 V/(Ag/AgCl)) at which corrosion of carbon started to occur (Lissaneddine et al., 2021b).

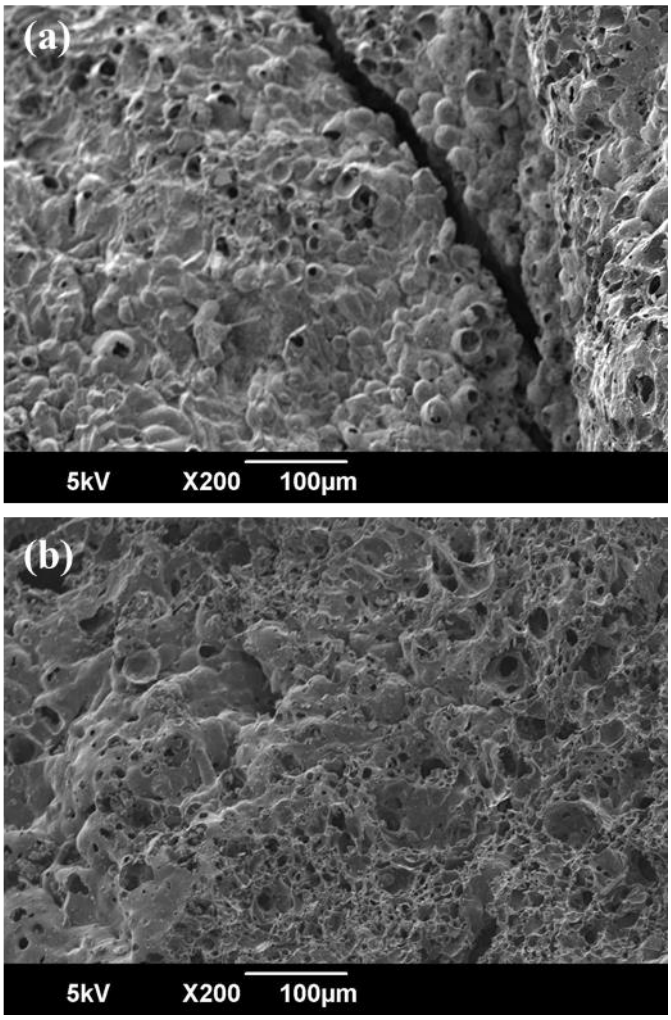

Fig. 50. SEM images: (a) GAC before conditioning, (b) GAC after conditioning.

EDS results of both GAC are shown in Table 23. The semi-quantitative elemental analysis of the GAC surfaces indicated that the major elements on both GAC were C and O. The carbon content was slightly decreased (from 86.6 to 85.6 at.%) after electrochemical treatment, which could be ascribed to the localized corrosion of the GAC. In the meantime, the oxygen content slightly increased (from 11.7 to 12.2 at.%). This could be explained by the electrooxidation of GAC that occurred at a potential higher than the oxygen evolution potential (1.03 V/(Ag/AgCl)) and might contribute to the slight oxygenation. In addition, traces of Na, P, Cl, K and Ca species were identified in both GAC and should be attributed to the impurities of the raw olive pomace material. They could also come from the chemical activation stage.

Table 23. EDS of GAC before and after conditioning.

	GAC-Before conditioning		GAC-After conditioning	
Element	**W%**	**at.%**	**W%**	**at.%**
C	81.48	86.58	80.33	85.61
O	14.62	11.68	15.28	12.25
Na	1.96	1.09	3.01	1.68
P	0.15	0.06	0.13	0.05
Cl	0.25	0.09	0.15	0.05
K	0.91	0.3	0.3	0.1
Ca	0.63	0.2	0.81	0.26
	100	100	100	100

The results of phenol electrosorption of into GAC before conditioning and GAC after conditioningare represented in the Fig. 51. The phenol removal increased from 72% for GAC before conditioning to 75% for GAC after conditioning. These properties indicated that the conditioned GAC electrode should have significant electrosorption efficiency and was therefore employed in the subsequent electrosorption experiments.

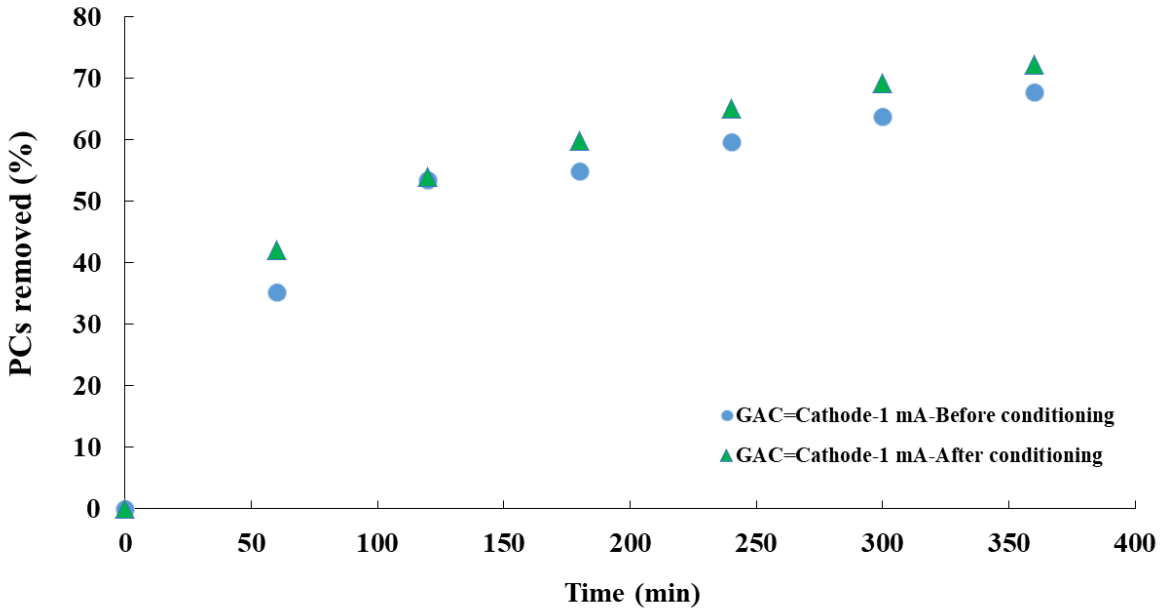

Fig. 51. Electrosorption of phenol into GAC before conditioning and GAC after conditioning. Operating conditions: anode: platinum wire, cathode: graphite rod and 10 g of GAC, electrolyte: 6 g L^{-1} KCl, pH 4 and 4 g L^{-1} phenol, flow rate: 10 mL min^{-1}, m/V = 0.1 g mL^{-1}.

2.1.2. Electrochemical characterization of the conditioned GAC

The electrochemical performance of the GAC electrode was studied with CV, LSV and EIS. The CV curve of GAC is shown in Fig. 52a. The electroactive surface area for the GAC electrode was found to be 7.8 × 10^3 cm^2. This value was high compared to other porous carbon-based electrodes used in literature such as AC-anchored WO_3 nanoflakes electrode (299 cm^2) (Sekar et al., 2020), SnO_2-Graphite nanocomposite modified electrode (0.291 cm^2) (Mohanraj et al., 2021), composite carbon nanofiber electrodes (1,750 to 2,125 cm^2) (Barhoum et al., 2020) and hybrid Au-(polyvinylpyrrolidone and 4-dimethylaminopyridine)/carbon electrode (0.007 to 0.206 cm^2) (Niamlaem et al., 2020). High electroactive surface area leads to high number of active sites, and consequently high electrosorption capacity would be expected (Zhu & Zhao, 2019b).

In addition, a value of I_0 was found to be around 5.5 × 10^{-3} A from Tafel slopes (Fig. 52b). The performance of GAC electrode is much better than those of the most reported carbon-based electrodes in literature. For example, I_0 of graphene before and after electrochemical oxidation were 7 × 10^{-5} and 4 × 10^{-3} A, respectively (Pierpaoli et al., 2021). Other values of I_0 with platinum nanoparticles electrodeposited on a carbon substrate were varying from 0.41 to 2.1 × 10^{-3} A (Moeini et al., 2021). The lower I_0 values obtained in

literature would imply a lower electrosorption efficiency compared to the GAC employed in this work.

Figure 52c illustrates the Nyquist plot of the GAC electrode, which showed two regions with different characteristic of impedance. The inclined straight lines approximating 45° angle demonstrated that diffusion process mechanism should occur on GAC electrode (Chen et al., 2018). EIS data have been obtained after validation of impedance spectra with linear KKT method (Fig. 51c). The χ^2 calculated for KKT fitting with experimental spectra as well as for EEC model fitting with KKT were determined to be 5.6 10^{-5} and 1.1 10^{-6}, respectively. The best EEC model of GAC electrode was demonstrated to be R (Q (R (QR))) as shown in Fig. 52. The first one was the resistance of the bulk electrolyte (R_{Sol}) whose value approximated 33 Ω. The parallel combination of C_{DL} and R_{CT} reached values of 2.5 µF cm^{-2} and 4 Ω, respectively. Compared to other porous electrodes used in the literature R_{CT} had a lower value than TiO_2/GAC based packed-bed electrode (206 Ω) (Chen et al., 2018), granular sewage sludge carbons (94 Ω) (Meng et al., 2021) and platinum nanoparticles electrodeposited on a carbon substrate (89 Ω) (Moeini et al., 2021). This lower value of R_{CT} is beneficial to efficient electrosorption. Another interesting feature is that a capacitance/resistance couple was connected in series to R_{CT} (Fig. 53). The respective values of the internal capacitance of GAC (C_{GAC}), in parallel to the internal resistance of GAC (R_{GAC}) were 0.38 µF cm^{-2} and 1.2 Ω, respectively. Based on the values of electroactive surface area, I_0, resistances and capacitances, the GAC electrode would depict good performance of electrosorption.

When the GAC was compared with the composite beads (Part III, sub-chapter I.II), it could be noticed that the electroactive surface area of composite beads (23 × 10^3 cm^2) was greater than the one of GAC. Moreover, the values of I_0 (3.24 × 10^{-3} A), C_{DL} (0.15 µF cm^{-2}) and R_{CT} (1.7 Ω) were lower with the composite beads compared to the GAC. These trends mean that SA-AC beads had better electrochemical performance than GAC. Therefore, lower electrosorption efficiency with the GAC could be expected. Still, GAC has interesting advantages over composite beads: (i) easy to manufacture, (ii) higher stability at high current intensity, (iii) possibility of regeneration. These statements further justify the interest to pursue with GAC as electrode in the following sections.

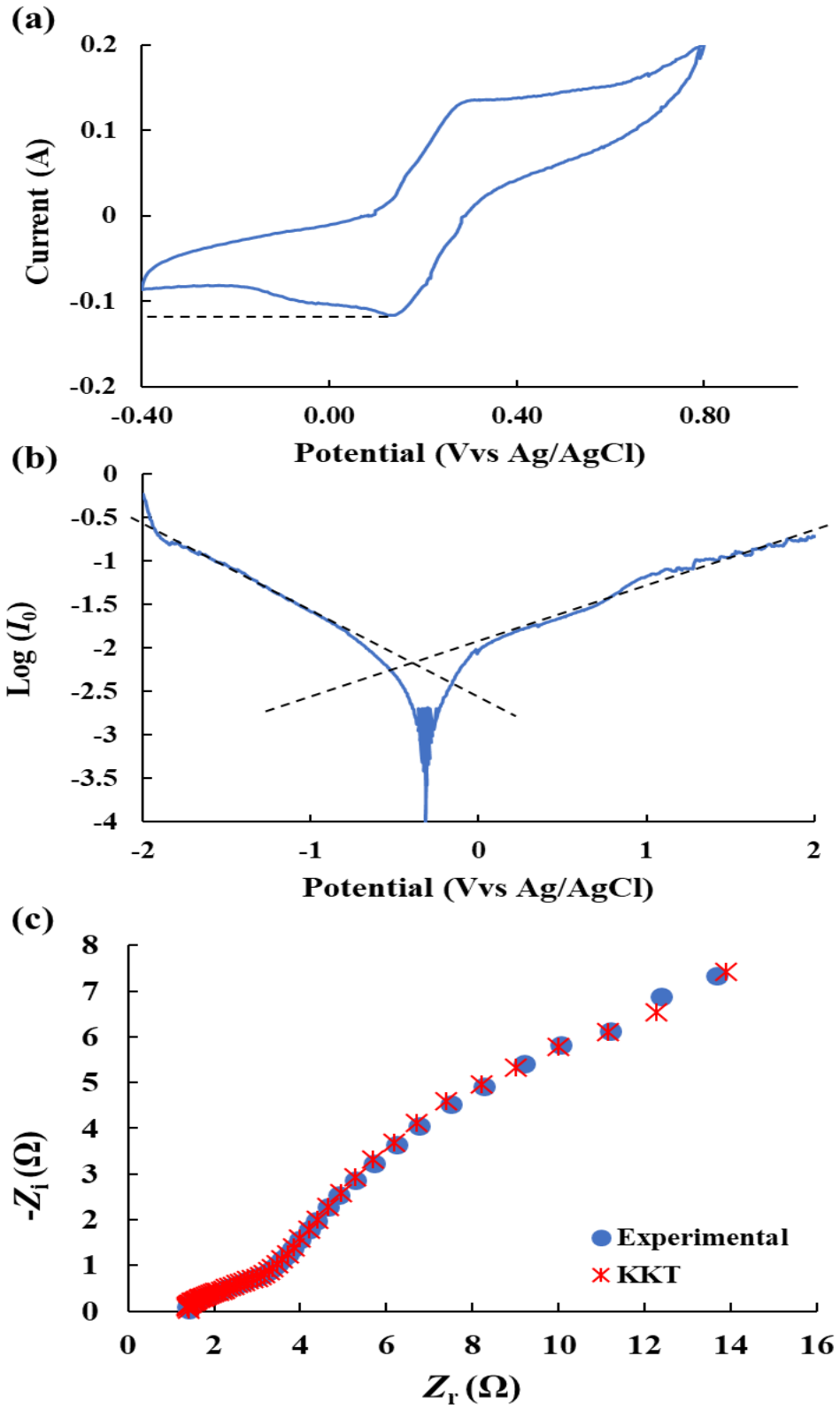

Fig. 52. Electrochemical properties of GAC electrode using CV (a), LSV (b) and EIS (c).

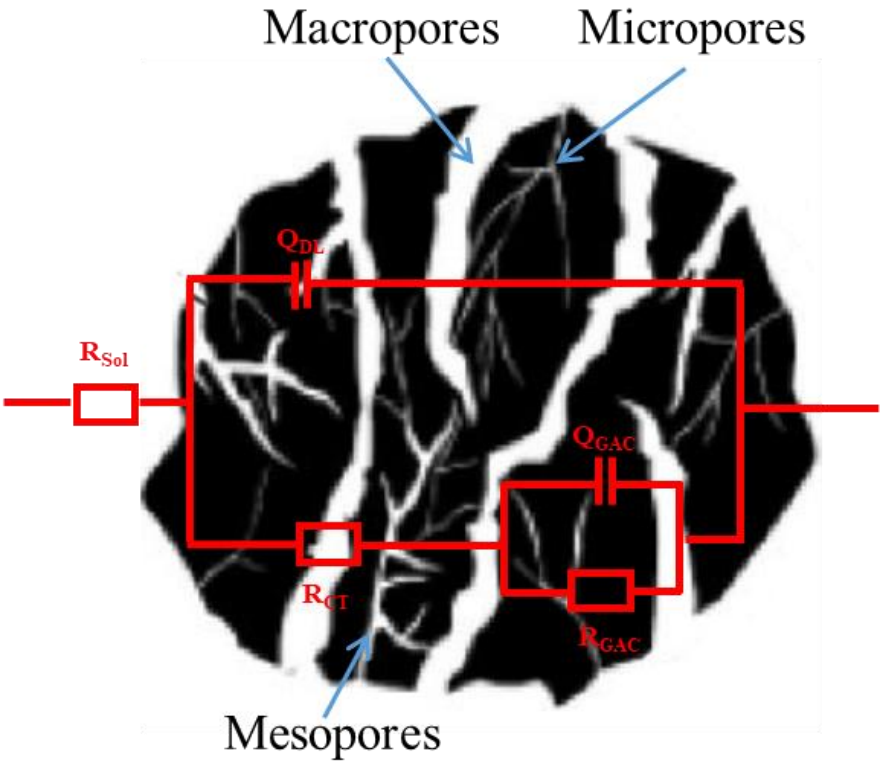

Fig. 53. Scheme of the EEC model integrated into the GAC porous electrodes.

2.2.Electrosorption

2.2.1. Phenol electrosorption

Electrode polarity and applied current are the main factors prevailing the electrosorption efficiency (Lissaneddine et al., 2021b). The effects of current intensity on the electrosorption of phenol have been therefore investigated for the 3D electrode when used as either cathode or anode. Figure 54a illustrates the effect of current intensity as a function of contact time on the percentage of phenol electrosorbed in anode configuration. The phenol removal increased with the applied current from 69% at 5 mA (E_{an} = 0.65 V/(Ag/AgCl)) to 74% at 100 mA (E_{an} = 1.70 V/(Ag/AgCl)). This trend could be explained by the increase of phenol diffusion from the bulk solution into the mesopores and micropores of the GAC according to the results of EIS and EEC. Similar results have been observed by Rong and Xien (2009) for electrosorption of thiocyanate into active carbon felt (Rong & Xien, 2009). Then the efficiency of electrosorption decreased to 68%, when the applied current equaled 150 mA (E_{an} = 1.90 V/(Ag/AgCl)). This could be ascribed to the O_2 production from H_2O electrooxidation that could occur in this range of current (150 mA), considering the higher E_{an}

value (1.70 V/(Ag/AgCl)) compared to the potential of oxygen evolution reaction (1.03 V/(Ag/AgCl)). The O_2 generation limited the GAC surface availability for phenol electrosorption. Therefore, the gas electrogeneration strongly reduced the electrosorption efficiency, which was even lower than in adsorption (66%). Still, the optimal electrosorption led to higher efficiency (74%) than adsorption itself.

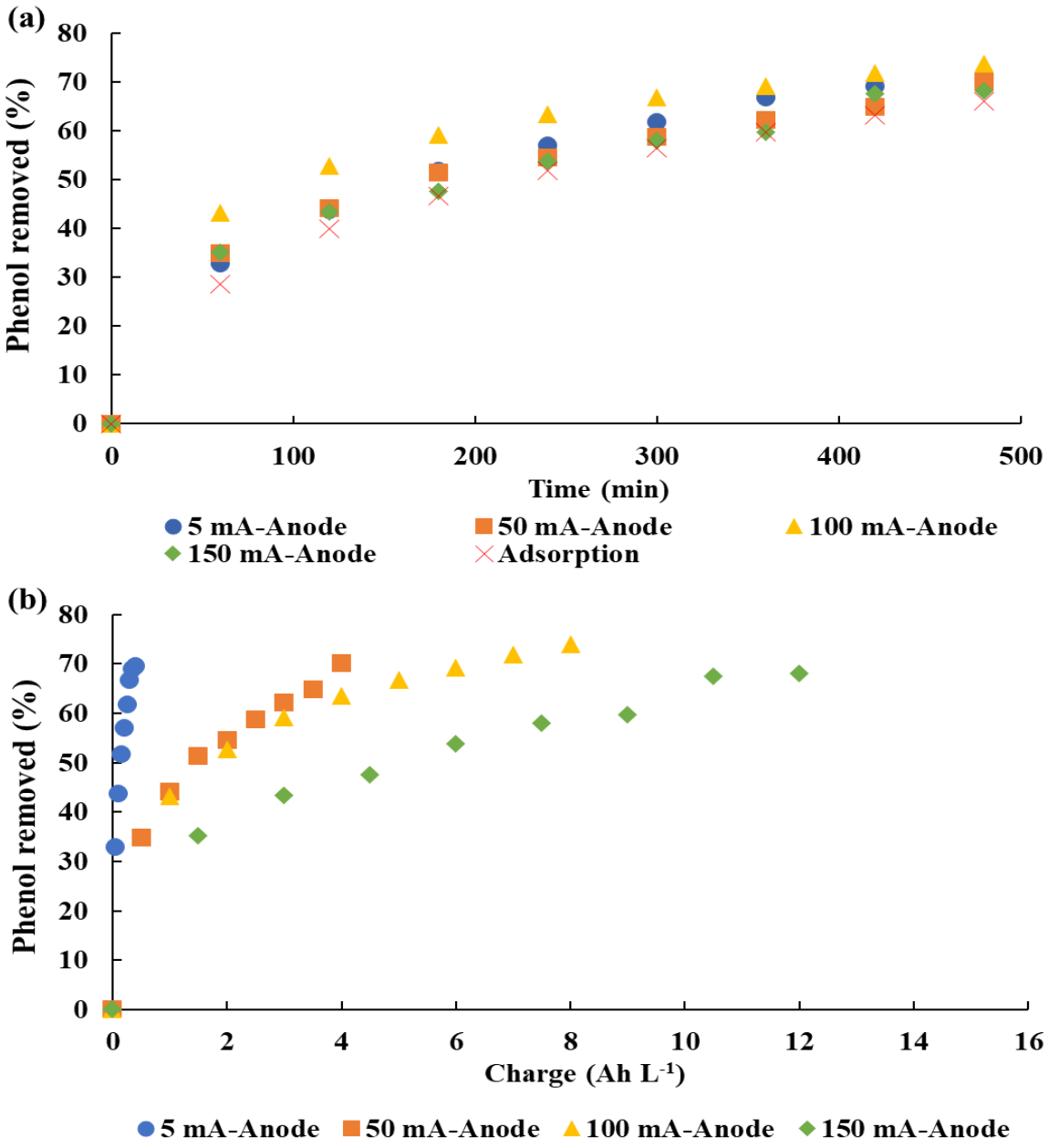

Fig. 54. Effect of the current intensity considering the contact time (a) and the specific charge (b) on the electrosorption of phenol. Operating conditions: cathode: platinum wire, anode: graphite rod and 10 g of GAC, electrolyte: 6 g L^{-1} KCl, pH 4 and 4 g L^{-1} phenol, flow rate: 10 mL min^{-1}, m/V = 0.1 g mL^{-1}.

Figure 55a showed the effect of the current intensity on the percentage of phenol removed when the GAC was employed as a cathode. The maximum removal percentage of phenol was 72%, when the applied current equaled 1 mA (E_{cat} = 0.26 V/(Ag/AgCl)). Then the efficiency decreased with the increasing current until 100 mA (E_{cat} = -1.1 V/(Ag/AgCl)), where the efficiency of electrosorption was 65%. Similar to the anode configuration, the gaseous H_2 electrogeneration from H_2O reduction started at a higher current intensity and it subsequently reduced the electrosorption efficiency.

In addition to the improved electrosorption capacity, another necessary feature of the process is the low energy requirements. The influence of current intensity considering the specific charge on phenol removal percentage in both anode and cathode setups are shown in Fig. 54b and Fig. 55b, respectively. The specific charge increased by increasing the applied current from 1 to 150 mA at both cathode and anode configurations. The maximum removal percentage of phenol was reached after only 0.08 Ah L^{-1} at 1 mA with GAC cathode, compared to 8 Ah L^{-1} at 100 mA with GAC anode. The specific charge with GAC anode was found to be a hundred times greater than that of GAC cathode system. Upon these results, the applied current of 1 mA with GAC as cathode was applied for the subsequent electrosorption experiments. This was to prevent the formation of faradaic reactions (gaseous H_2 and O_2 evolutions) at the GAC surface and to keep the energy demand as low as possible.

The morphology of conditioned GAC cathode after 8 h of electrosorption at 1 mA was analyzed by SEM, as shown in Fig. 56. Morphological changes on the surface of GAC after electrosorption were observed. The surfaces were smoother after electrosorption. This could be primarily due to the pores saturation with a high amount of phenolelectrosorbed. Differences were also noticed with EDS results (Table 24). The semi-quantitative elemental analysis of the GAC surface indicated that the major elements on the GAC were still carbon and oxygen. However, after electrosorption, the weight percentages of C decreased from 80.3% to 72.7 %, respectively, while the weight percentage of O increased from 12.2% to 19.8%. The oxygenation could be maybe due to the oxygen adsorption on the cathode before its subsequent reduction since it is known that oxygen can be easily reduced on carbon cathode materials (Du et al., 2021).

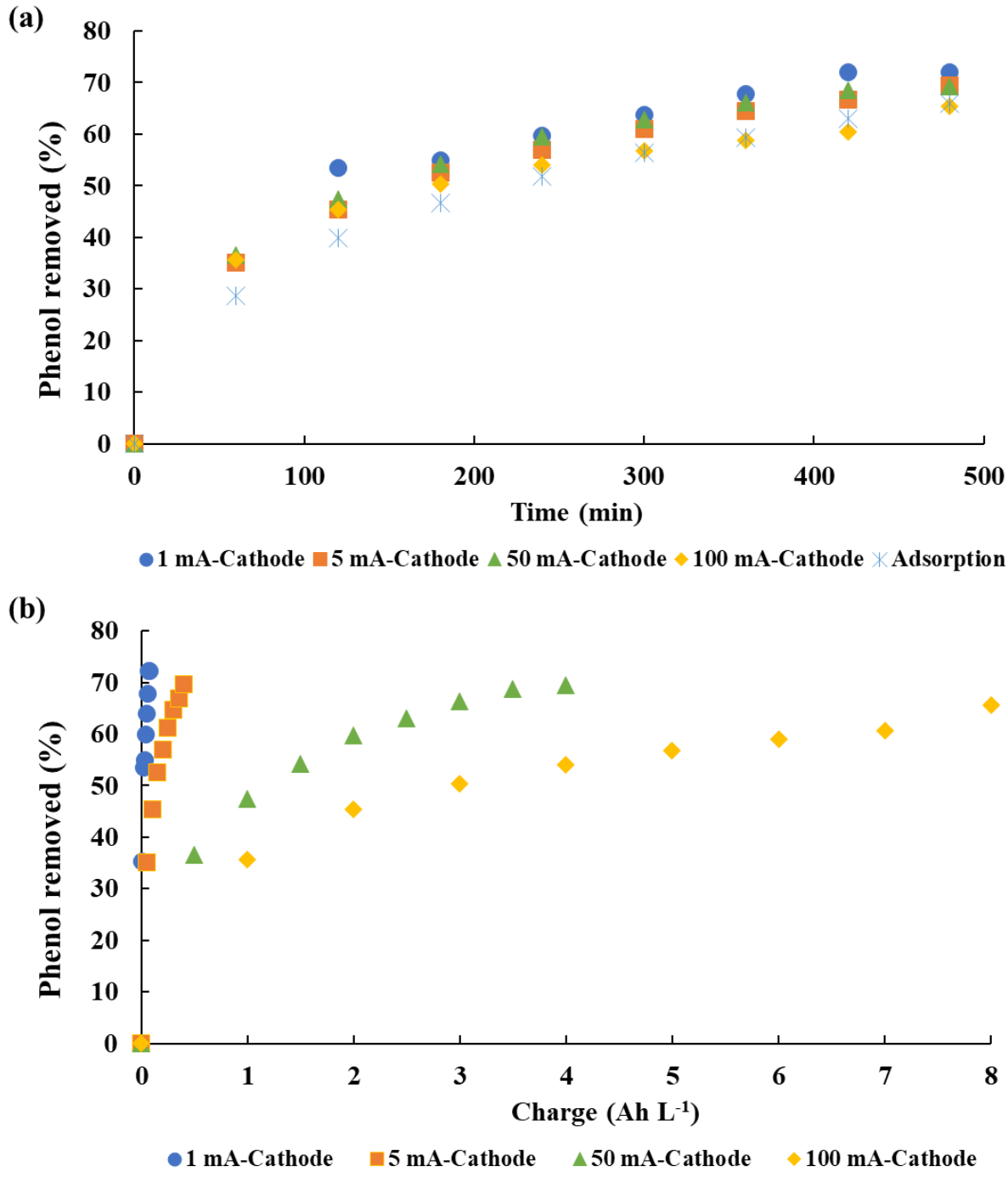

Fig. 55. Effect of the current intensity considering the contact time (a) and the specific charge (b) on the electrosorption of phenol. Operating conditions: anode: platinum wire, cathode: graphite rod and 10 g of GAC, electrolyte: 6 g L^{-1} KCl, pH 4 and 4 g L^{-1} phenol, flow rate: 10 mL min^{-1}, m/V = 0.1 g mL^{-1}.

Table 24. EDS of conditioned GAC cathode after electrosorption at 1 mA for 8 h.

	Conditioned GAC-After electrosorption (1 mA, 8 h)-Cathode	
Element	**W%**	**at.%**
C	72.71	79.04
O	24.27	19.80
Na	0.55	0.31
P	0.20	0.08
Cl	0.29	0.11
K	1.39	0.46
Ca	0.60	0.20
	100	100

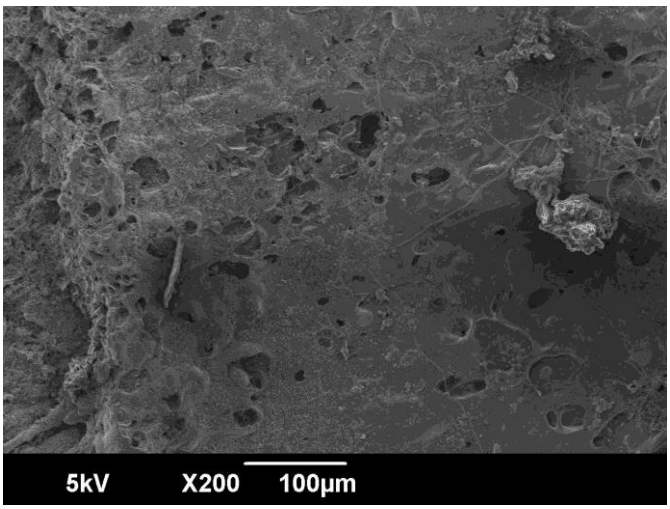

Fig. 56. SEM images conditioned GAC cathode after 8 h of electrosorption at 1 mA.

2.2.2. Effect of phenolic compounds properties

The effect of the kinds of PCs on their electrosorption efficiency was studied considering the following PCs having different pKa and molar weight (MW): phenol (pKa = 9.9, MW = 94 g mol^{-1}), gallic acid (pKa = 3.1, MW = 170 g mol^{-1}), caffeic acid (pKa = 4.6, MW = 180 g mol^{-1}), coumaric acid (pKa = 4.0, MW = 164 g mol^{-1}) and quercetin (pKa = 6.4, MW = 302 g mol^{-1}).

The kinetics of PCs electrosorptions at 1 mA (E_{cat} = 0.26 V/(Ag/AgCl)) with GAC as cathode and initial solution pH of 4 are illustrated in Fig. 56. The PCs removal increased rapidly over time as the active sites were accessible until saturation of active sites leading to equilibrium. The removal percentages of phenol, gallic acid, caffeic acid, coumaric acid and

quercetin were 72.3%, 36.8%, 72.5%, 60.6% and 26.5%, respectively, after 360 min. In addition, the trend clearly highlighted the fact that PCs removal was not dependent only on the pKa values of PCs. The high performance of caffeic acid could be attributed to its pKa value (4.6) that is close to the initial solution pH (4). In this condition, the basic form of caffeic acid also presents in solution, meaning that part of the molecules (23%) were preferentially negatively charged. Therefore, these charged molecules were subjected to electro-migration in addition to diffusion phenomena. Then electrostatic repulsion between the negatively charged GAC surface (cathode) and caffeic acid ionic form could increase the contact of caffeic acid with the adsorbent. This was also stated in the experiments with SA-AC beads electrode with real OMWW (Part III, sub-chapter I.II). The high electrosorption efficiency with coumaric acid could be also explained by this mechanism since its pKa (4) was also close to the initial pH. However, the high removal efficiency of phenol compared to quercetin could not be explained by the single influence of pKa. Both compounds had a pKa value much higher than the initial pH and therefore their uncharged acidic forms predominated. The efficiency difference could be ascribed to the different MW and size of the PCs compared to the GAC pore size distribution (Mohamed et al., 2011; Lissaneddine et al., 2021a). The average pore size of GAC was 1.5 nm (Part III, sub-chapter II.I), while the quercetin size was around 0.9 nm. Contrastingly, the phenol size was lower (0.557 nm), considering its MW value. Therefore, less numbers of potential active sites were available for the quercetin electrosorption. It subsequently decreased its electrosorption efficiency compared to phenol.

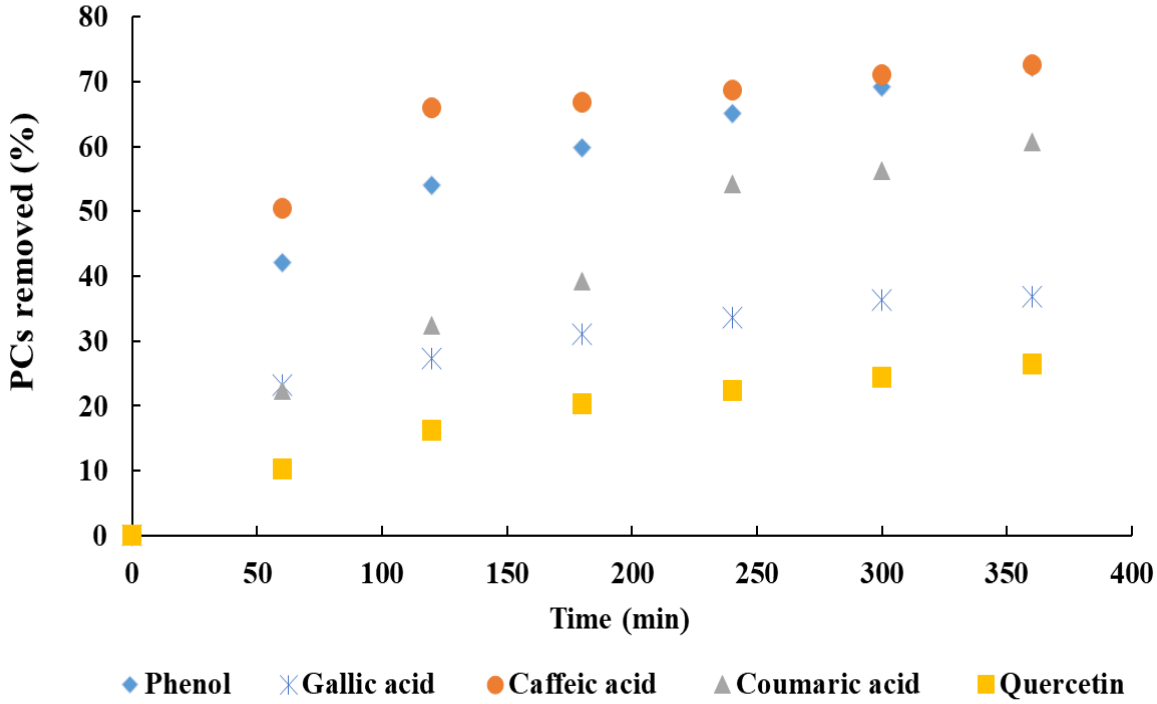

Fig. 57. Effect of the kinds of PCs on the electrosorption at cathode. Operating conditions: anode: platinum wire, cathode: graphite rod and 10 g of GAC, electrolyte: 6 g L^{-1} KCl, pH 4 and PC, current intensity: 1 mA, flow rate: 10 mL min^{-1}, m/V = 0.1 g mL^{-1}.

2.2.3. OMWW electrosorption

The PCs electrosorption from actual OMWW has been investigated to understand the mechanism of co-electrosorption into GAC electrodes. From the previous section it could be expected that the optimal current intensity should vary with the type of PC. The current has been therefore varied from 1 mA to 100 mA with GAC as a cathode in order to optimize the electrosorption efficiency with the real effluent (Fig. 57). After 6 h, the PCs removal increased by raising the applied current from 1 mA (E_{cat} = 0.26 V/(Ag/AgCl)) (42.6%) to 10 mA (E_{cat} = -0.05 V/(Ag/AgCl)) (68.1%). The electric current should promote the ionic PCs electro-migration from the bulk solution to the pores of the GAC. The uncharged molecules could be also impacted by the electric potential (Gileadi, 1966a), which enhanced the electrosorption efficiency of PCs as already stated in Part III, sub-chapter I.II. Then the PCs removal dropped down to 44% at 100 mA (E_{cat} = -1.1 V/(Ag/AgCl)). This should be due to the H_2 electrogeneration that hamper the electrosorption, as previously explained in section 2.2.1 of Part III, sub-chapter II.II.

Moreover, the PCs removal at 1 mA (0.26 V/(Ag/AgCl)) was lower (42%) in actual OMWW compared with simulated OMWW (72%). This could be explained by the intermolecular interaction between the mixture of PCs in the actual OMWW (Damaskin, Baturina, 1999; Stenina et al., 2001; Damaskin, 2001c, 2001a, 2001b, 2003, 2008, 2011; Lissaneddine et al., 2021b).

Additionally, the specific charge increased with the applied current, from 1 mA (0.06 Ah L^{-1}) to 100 mA (6 Ah L^{-1}) after 6 h (Fig. 57b). The maximum removal percentage of PCs was reached after 0.6 Ah L^{-1} at 10 mA, which made this applied current as of the optimal one for subsequent experiments. Furthermore, the internal ohmic resistance of the GAC electrode increased by increasing the applied current from 0.7 Ω (1 mA) to 4.6 Ω (100 mA) (Fig. 57c). The increases in internal ohmic resistance limited the electrochemical performance of GAC electrode (Haider et al., 2021). This could explain the decrease of electrosorption efficiency at 50 mA (4.3 Ω) on the contrary to 10 mA (1.6 Ω). Since an increase of resistance usually leads to higher energy requirement, this trend is also in agreement with the specific charge evolution in Fig. 57b that showed an optimal value of 10 mA.

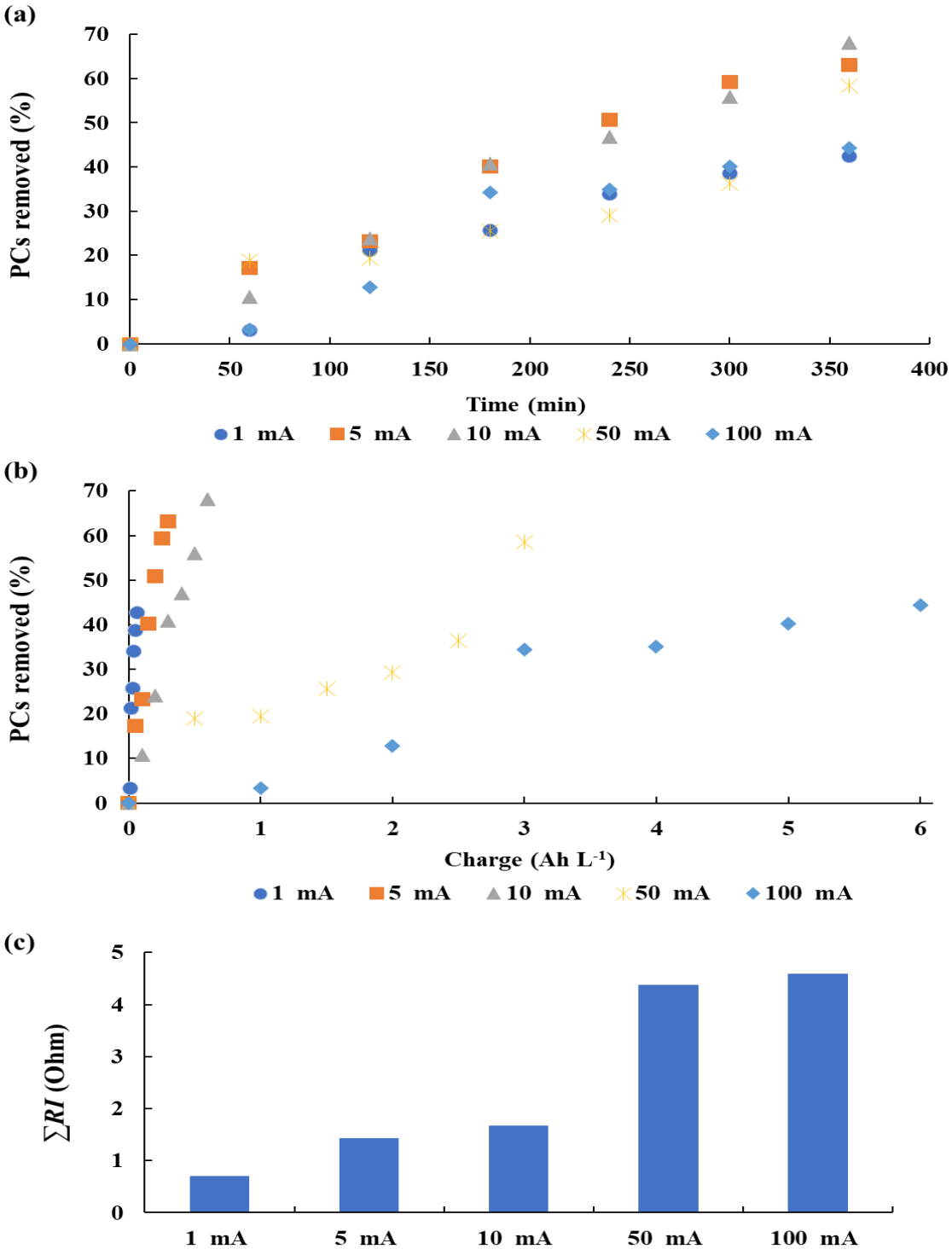

Fig. 58. Effect of the current intensity considering the contact time (a) the specific charge (b) on the electrosorption of PCs from real OMWW and internal resistance (c) at optimal operating conditions. Operating conditions: anode: platinum wire, cathode: graphite rod and 10 g of GAC, flow rate: 10 mL min^{-1}, m/V = 0.1 g mL^{-1}.

2.3.Electrochemical regeneration of the GAC electrode

Electrochemical regeneration of the porous electrodes refers to the regeneration in electrolyte solution by a given potential or current through an electrodesorption step (Mcquillan et al., 2018; Lissaneddine et al., 2021b). One advantage of electrochemical regeneration is the reduction of energy consumption compared with the thermal processes (Bayram & Ayranci, 2012a).

The regeneration of GAC electrode aims to restore the original active sites of the GAC electrode by removing and recovering PCs that have accumulated into the different pore sizes of the GAC electrodes. The 3D material was employed as an anode by reversing the polarity. The influence of applied current was evaluated and the results of PCs electro-desorption are shown in Fig. 58. The percentage of PCs recovered increased by rising the applied current from 1 mA (E_{an} = 0.35 V/(Ag/AgCl)) (21.4%) to 10 mA (E_{an} = 1.25V/(Ag/AgCl)) (34.5%), after 360 min. This was explained by the fact that current density is the driving force for contaminant degradation (Mcquillan et al., 2018). Similar results have been obtained in other studies involving the desorption of methylquinolinium chloride from AC by increasing the potential from 0 mV/(Ag/saturated KCl) to 600 mV/(Ag/saturated KCl) (Bán et al., 1998). However, a further increase of current should damage too much the GAC material, since carbon can be already oxidized at a potential of 0.407 V/(Ag/AgCl) (Lissaneddine et al., 2021b). This is why higher current intensity was not tested.

Moreover, the experimental results showed that the electrodesorption efficiency achieved an equilibrium after only 2 h (Fig. 58), while it was barely reached after 6 h in electrosorption experiments (Fig. 57a). Therefore, 120 min was sufficient for electrodesorption tests. In the aim of further increasing the desorption efficiency, successive electrodesorption cycles have been performed with the same GAC electrode and with fresh electrolyte at each cycle. The results showed that the second and third cycles were less colorful in comparison with cycle 1 (Fig. 59). This suggested that less molecules absorbing visible light were extracted from the GAC. However, there were no PCs recovery from the electrode at the second and third cycles (Figs. 59a and 59b), which means that this color was not an indicator for PCs recovery. It further exhibited the fact that all the recoverable PCs from the GAC were completed after only one cycle. This further means that the reversible electrosorbed PCs fraction was already recovered at the first cycle. Subsequent cycles could

not remove the fractions within the micro- and meso- pores that are more irreversible, which represented around 65%. It is also important to note that applying a higher current than 10 mA would have improved the recovery efficiency, but this would be to the detriment of the electrode integrity. As shown in section 2.1.1 of Part III, sub-chapter II.II, applying higher current intensity led to pitting corrosion of the GAC anode, which could therefore increase the release of PCs initially electrosorbed.

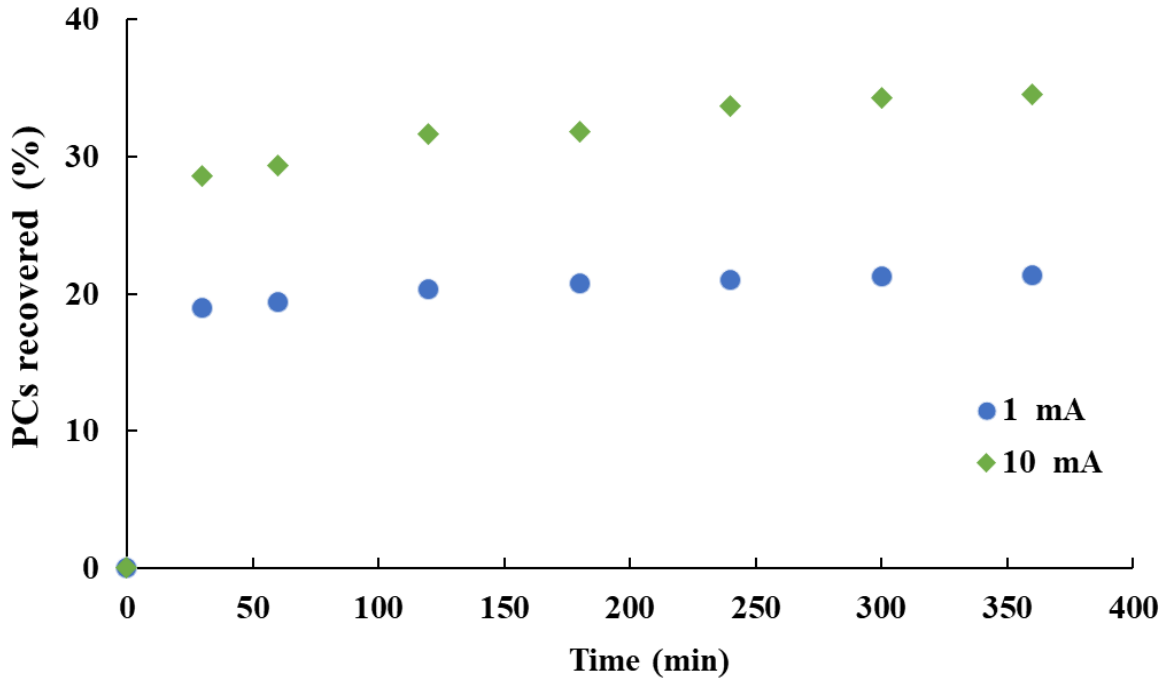

Fig. 59. Effect of the current intensity on the electro-desorption of PCs from GAC. Operating conditions: cathode: platinum wire, anode: graphite rod and 10 g of GAC, electrolyte: 0.1 g L^{-1} KCl, flow rate: 10 mL min^{-1}, m/V = 0.1 g mL^{-1}.

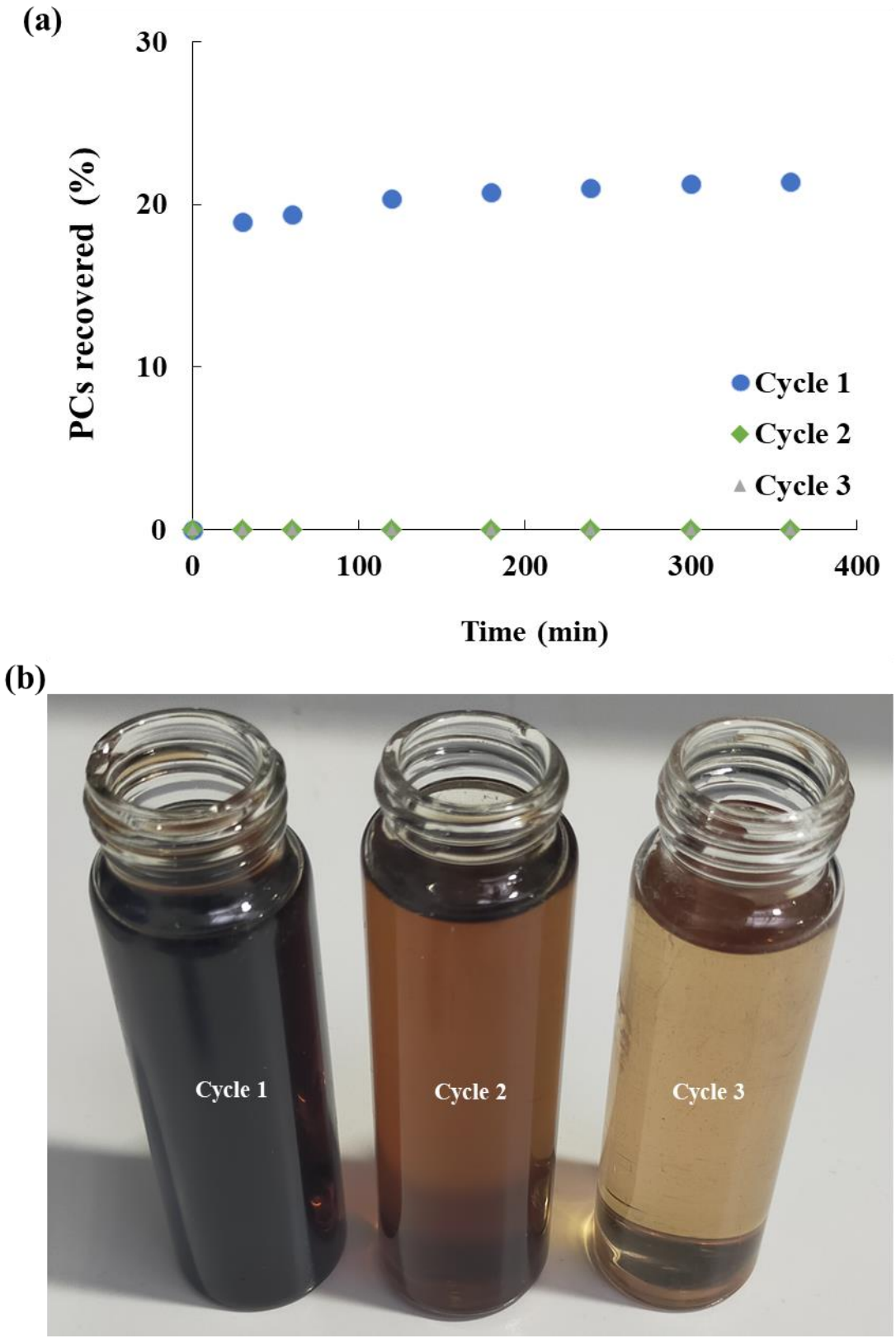

Fig. 60. Pictures about three successive electro-desorption cycles of PCs from GAC electrode.

2.4.Electrochemical degradation of OMWW

For a more integrated treatment of OMMW, the combination of electrosorption as a separation technology with a degradation process should be an effective strategy. This would permit to recover the value-added compounds, while the residual effluent would be treated before disposal. Some studies investigated the electrooxidation combined with electrosorption to remove BA (Chen et al., 2018), acyclovir and phenol (Nie et al., 2019) in simulated effluents. The results were promising and it has been therefore decided to apply this combination in this study, but with actual effluent (OMWW).

The COD and PCs removal efficiencies for the electrosorption combined with advanced electrooxidation process compared with the electrosorption are shown in Table 25. The COD removal efficiency obtained were 84% and 91% for the combined processes before and after filtration of the actual OMWW, respectively. Contrastingly, it was 40% for the sole electrosorption process. The coupling, therefore, led to two times higher removal efficiency. This could be partly explained by the BDD scaling with maybe soluble and insoluble organic compounds as shown in the picture in Fig. 60. In addition, the PCs that could not be electrosorbed during the first step were subsequently removed during the electrooxidation experiments. The PCs removal efficiencies were around 97% with the combined process with or without filtration of the initial effluent, while 77% was removed during the preliminary electrosorption. This trend was in agreement with literature in which the removal efficiency increased with the combined process for various organic pollutants in synthetic solution, such as reactive yellow 39 (Ayoubi-Feiz et al., 2014b), diazinon (Ayoubi-Feiz et al., 2018b), alizarin red (Jin et al., 2011b) and lanasol red 5B (Ayoubi-Feiz et al., 2014a).

Fig. 61. Scaling on BDD anode after electrooxidation experiments of OMWW.

To conclude, the electrosorption combined with electrooxidation could offer promising results for the actual OMWW, only after better understanding the scaling issue on the BDD anode and after optimizing then the electrooxidation process.

Table 25. OMWW characterization before and after electrochemical degradation.

Kind of effluent	pH	COD (g-O_2 L^{-1}) (removal %)	Total PCs (mg L^{-1}) (removal %)
OMWW	5.0	163	4,801
OMWW after electrosorption (480 min)	5.0	98 (40%)	1,083 (77%)
OMWW after electrosorption (480 min) followed by electrooxidation (420 min)	4.6	26 (84%)	134 (97%)
OMWW after filtration (≈ 10 µm) and electrosorption (480 min) followed by electrooxidation (420 min)	4.4	13 (91%)	102 (97.7%)

3. Conclusions

Performance of biosourced GAC electrode in an electrosorption technology has been investigated for PCs removal from OMWW for the first time. The results of electrochemical characterization of GAC electrode showed that the high electroactive surface area (7.8×10^3 cm^2), high value of I_0 (5.5×10^{-3} A), and low value of R_{CT} (4 Ω), could be promising properties for electrosorption studies. Still, the properties of GAC seemed less performant

than the AS-AC beads, but the other advantages of GAC (i.e., stability, regeneration, manufacturing) could overcome the expected higher electrosorption efficiency of the beads. The electrosorption study of PCs was performed at different current intensities for Artificial OMWW (1 to 200 mA) for actual OMWW (1 to 100 mA). The most suitable current intensities were 1 mA (0.26 V/(Ag/AgCl)) for artificial OMWW and 10 mA (-0.05 V/(Ag/AgCl)) for actual OMWW, recording the highest electrosorption efficiencies of 72% and 68%, respectively. The influence of kinds of PCs having different pKa and molecular size has shown that both parameters impacted, according to the solution pH and the GAC pore size distribution.

Moreover, the PCs recovery from the GAC electrode by using the electrochemical regeneration method was carried out. The percentage of PCs recovered was 34.5% at optimal conditions, i.e., 0.1 g L^{-1} of KCl and a current intensity of 10 mA during 120 min after one cycle. Further cycles could not permit the recovery of electrosorbed fractions, while higher current should lead to corrosion of the GAC material.

The combination of electrosorption as a separation technique for PCs recovery and advanced electro-oxidation as degradation process for the treatment of residual OMWW was finally studied. The removal efficiency of COD was 84% and 91% for the combined processes before and after filtration, respectively. This combination could be suitable for the future, but the scaling issues need to be overcome and the optimization should be then performed.

References

Adnan, F.H., Mousset, E., Pontvianne, S., Pons, M., 2021. Mineral cathodic electro-precipitation and its kinetic modelling in thin-film microfluidic reactor during advanced electro-oxidation process. Electrochim. Acta 387, 138487. https://doi.org/10.1016/j.electacta.2021.138487

Ania, C.O., Béguin, F., 2007. Mechanism of adsorption and electrosorption of bentazone on activated carbon cloth in aqueous solutions. Water Res. 41, 3372–3380. https://doi.org/10.1016/j.watres.2007.03.031

Ayoubi-Feiz, B., Aber, S., Khataee, A., Alipour, E., 2014a. Preparation and application of α-Fe_2O_3/TiO_2/activated charcoal plate nanocomposite as an electrode for electrosorption-assisted visible light photoelectrocatalytic process. J. Mol. Catal. A Chem. 395, 440–448. https://doi.org/10.1016/j.molcata.2014.09.006

Ayoubi-Feiz, B., Aber, S., Khataee, A., Alipour, E., 2014b. Electrosorption and photocatalytic one-stage combined process using a new type of nanosized TiO_2/activated charcoal plate electrode. Environ. Sci. Pollut. Res. 21, 8555–8564. https://doi.org/10.1007/s11356-014-2777-z

Ayoubi-Feiz, B., Mashhadizadeh, M.H., Sheydaei, M., 2018. Preparation of reusable nano N-TiO_2/graphene/titanium grid sheet for electrosorption-assisted visible light photoelectrocatalytic degradation of a pesticide: Effect of parameters and neural network modeling. J. Electroanal. Chem. 823, 713–722. https://doi.org/10.1016/j.jelechem.2018.07.020

Ayranci, E., Conway, B.E., 2001. Removal of phenol, phenoxide and chlorophenols from waste-waters by adsorption and electrosorption at high-area carbon felt electrodes. J. Electroanal. Chem. 513, 100–110.

Bán, A., Schäfer, A., Wendt, H., 1998. Fundamentals of electrosorption on activated carbon for wastewater treatment of industrial effluents. J. Appl. Electrochem. 28, 227–236. https://doi.org/10.1023/A:1003247229049

Barhoum, A., El-Maghrabi, H.H., Iatsunskyi, I., Coy, E., Renard, A., Salameh, C., Weber, M., Sayegh, S., Nada, A.A., Roualdes, S., Bechelany, M., 2020. Atomic layer deposition of Pd nanoparticles on self-supported carbon-Ni/NiO-Pd nanofiber electrodes for electrochemical hydrogen and oxygen evolution reactions. J. Colloid Interface Sci. 569, 286–297. https://doi.org/10.1016/j.jcis.2020.02.063

Bayram, E., 2016. Electrosoption of aromatic organic acids from aqueous solutions onto granular activated carbon electrodes for water purification. Hacettepe J. Biol. Chem. 3, 273–273. https://doi.org/10.15671/hjbc.20164420570

Bayram, E., Ayranci, E., 2012a. Structural effects on electrosorptive behavior of aromatic organic acids from aqueous solutions onto activated carbon cloth electrode of a flow-through electrolytic cell. J. Electroanal. Chem. 683, 14–20. https://doi.org/10.1016/j.jelechem.2012.07.028

Bayram, E., Ayranci, E., 2012b. Electrosorption based waste water treatment system using activated carbon cloth electrode: Electrosorption of benzoic acid from a flow-through electrolytic cell. Sep. Purif. Technol. 86, 113–118. https://doi.org/10.1016/j.seppur.2011.10.032

Bayram, E., Kizil, Ç., Ayranci, E., 2018. Flow-through electrosorption process for removal of 2,4-D pesticide from aqueous solutions onto activated carbon cloth fixed-bed electrodes. Water Sci. Technol. 77, 848–854. https://doi.org/10.2166/wst.2017.598

Bousba, S., Meniai, A.H., 2014. Removal of phenol from water by adsorption onto sewage

sludge based adsorbent. Chem. Eng. Trans. 40, 235–240. https://doi.org/10.3303/CET1440040

Chen, Q., Wang, L., Xu, Y., Li, P., Wang, X., Wang, M., Kong, Y., 2018. Electrochemical investigation of phenol oxidation by a TiO_2/GAC based packed-bed electrode reactor. Int. J. Electrochem. Sci. 13, 7301–7309. https://doi.org/10.20964/2018.08.59

Chen, Y., Tu, Y., Bai, Y., Li, J., Lu, J., 2018. Electrosorption enhanced electrooxidation of a model organic pollutant at 3D SnO_2-Sb electrode in superimposed pulse current mode. Chemosphere 195, 63–69. https://doi.org/10.1016/j.chemosphere.2017.12.074

Damaskin, B. B., Baturina, O.A., 1999. Co-adsorption of anions and low-adsorbing cations within the Alekseev-Popov-Kolotyrkin model. Russ. J. Electrochem. 35(11), 1182–1185.

Damaskin, B.B., 2011. Modeling of co adsorption of cations and anions localized in different layers of the dense part of electrical double layer under the conditions of linear charge dependence of the adsorption energy. Russ. J. Electrochem. 47, 988–994. https://doi.org/10.1134/S1023193511090047

Damaskin, B.B., 2008. Modeling of synergism effect at different orientation of co-adsorbing molecules. Russ. J. Electrochem. 44, 1411–1417. https://doi.org/10.1134/S102319350812001X

Damaskin, B.B., Baturina, O.A., 2001a. Some anomalies in coadsorption of two organic substances due to differences in molecular interaction of species undergoing coadsorption. Russ. J. Electrochem. 37, 1482–1489.

Damaskin, B.B., Baturina, O.A., 2001b. Simulating coadsorption of surface active anions and organic molecules capable of forming two-dimensional condensed layers on the electrode. Russ. J. Electrochem. 37, 121–126.

Damaskin, B.B., Baturina, O.A., 2001c. Simulation of coadsorption of inorganic ions and organic molecules on electrodes. Russ. J. Electrochem. 37, 73–79.

Damaskin, B.B., Safonov, V.A., Safonov, N. V, 2003. Adsorption of an organic compound in two different positions: Simulation taking into account all three parameters of intermolecular interaction. Russ. J. Electrochem. 39, 814–819.

Du, X., Oturan, M.A., Zhou, M., Belkessa, N., Su, P., Cai, J., Trellu, C., Mousset, E., 2021. Nanostructured electrodes for electrocatalytic advanced oxidation processes: From materials preparation to mechanisms understanding and wastewater treatment applications. Appl. Catal. B Environ. 296, 120332. https://doi.org/10.1016/j.apcatb.2021.120332

Eisinger, R.S., Alkire, R.C., 1980. Electrosorption of b-naphthol on graphite. J Electroanal.Chem. 112, 327–337.

Eisinger, R.S., Keller, G.E., 1990. Electrosorption: A case study on removal of dilute organics from water. Environ. Prog. 9, 235–244. https://doi.org/10.1002/ep.670090418

Gileadi, E., 1966. Electrosorption of uncharged molecules on solid electrodes. J. Electroanal. Chem. 11, 137–151. https://doi.org/10.1016/0022-0728(66)80073-6

Haider, S.S., Iqbal, M.Z., Zakar, S., Afzal, A.M., Yaqoob, K., Aftab, S., 2021. Superior performance of electrodeposited CoMnS as novel electrode material for supercapattery devices. J. Energy Storage 39, 102608. https://doi.org/10.1016/j.est.2021.102608

Han, Y., Quan, X., Chen, S., Zhao, H., Cui, C., Zhao, Y., 2006a. Electrochemically enhanced adsorption of phenol on activated carbon fibers in basic aqueous solution. J. Colloid Interface Sci. 299, 766–771. https://doi.org/10.1016/j.jcis.2006.03.007

Han, Y., Quan, X., Chen, S., Zhao, H., Cui, C., Zhao, Y., 2006b. Electrochemically enhanced adsorption of aniline on activated carbon fibers. Sep. Purif. Technol. 50, 365–372.

https://doi.org/10.1016/j.seppur.2005.12.011

Han, Y., Quan, X., Ruan, X., Zhang, W., 2008. Integrated electrochemically enhanced adsorption with electrochemical regeneration for removal of acid orange 7 using activated carbon fibers. Sep. Purif. Technol. 59, 43–49. https://doi.org/10.1016/j.seppur.2007.05.026

Hazourli, S., Bonnecaze, G., Astruc, M., 1996. Adsorption et electrosorption de composes organiques sur charbon actif en grains partie I - Influence du potentiel imposé et du nombre de cycles adsorption and electrosorption of organic compounds on granular activated carbon part I- Influence of applied. Environ. Technol. 17, 1275–1283. https://doi.org/10.1080/09593330.1996.9618457

Hou, C.H., Huang, J.F., Lin, H.R., Wang, B.Y., 2012. Preparation of activated carbon sheet electrode assisted electrosorption process. J. Taiwan Inst. Chem. Eng. 43, 473–479. https://doi.org/10.1016/j.jtice.2011.12.003

Jayson, G.G., Sangster, J.A., Thompson, G., Wilkinson, M.C., 1987. Adsorption and electrosorption of mercury (II) acetate onto activated charcoal cloth from aqueous solution. Carbon N. Y. 25, 523–531. https://doi.org/10.1016/0008-6223(87)90193-X

Jiang, D., Li, B., 2009. Granular activated carbon single-chamber microbial fuel cells (GAC-SCMFCs): A design suitable for large-scale wastewater treatment processes. Biochem. Eng. J. 47, 31–37. https://doi.org/10.1016/j.bej.2009.06.013

Jin, Y., Wu, M., Zhao, G., Li, M., 2011. Photocatalysis-enhanced electrosorption process for degradation of high-concentration dye wastewater on TiO_2/carbon aerogel. Chem. Eng. J. 168, 1248–1255. https://doi.org/10.1016/j.cej.2011.02.026

Kitous, O., Cheikh, A., Lounici, H., Grib, H., Pauss, A., Mameri, N., 2009. Application of the electrosorption technique to remove Metribuzin pesticide. J. Hazard. Mater. 161, 1035–1039. https://doi.org/10.1016/j.jhazmat.2008.04.091

Lissaneddine, A., Pons, M.-N., Aziz, F., Ouazzani, N., Mandi, L., Mousset, E., 2021b. A critical review on the electrosorption of organic compounds in aqueous effluent – Influencing factors and engineering considerations. Environ. Res. J. 204, 112128. https://doi.org/10.1016/j.envres.2021.112128

Liu, L., Liu, Y., Che, N., Gao, B., Li, C., 2021. Electrochemical adsorption of perfluorooctanoic acid on a novel reduced graphene oxide aerogel loaded with Cu nanoparticles and fluorine. J. Hazard. Mater. 416, 125866. https://doi.org/10.1016/j.jhazmat.2021.125866

López-Bernabeu, S., Ruiz-Rosas, R., Quijada, C., Montilla, F., Morallón, E., 2016. Enhanced removal of 8-quinolinecarboxylic acid in an activated carbon cloth by electroadsorption in aqueous solution. Chemosphere 144, 982–988. https://doi.org/10.1016/j.chemosphere.2015.09.071

Mcquillan, A.R. V, Stevens, G.W., Mumford, A., 2018. The electrochemical regeneration of granular activated carbons: A review. J. Hazard. Mater. https://doi.org/10.1016/j.jhazmat.2018.04.079

Meng, H.-S., Liu, Y., Liu, P.-X., Zhou, L.-L., Chen, C., Wang, W.-K., Xu, J., 2021. Development of a three-dimensional photoelectrocatalytic reactor packed with granular sludge carbon photoelectrocatalyst for efficient wastewater treatment, Sep. Purif. Technol. 277, 11964. https://doi.org/10.1016/j.seppur.2021.119642

Moeini, B., Avval, T.G., Linford, M.R., Ghalkhani, M., Kaykhaii, M., Abdullah Mirzaie, R., 2021. Surface-orientated platinum nanoparticles electrodeposited on a carbon substrate as a high performance electrocatalyst for glucose oxidation reaction in alkaline media. Mater. Sci. Eng. B Solid-State Mater. Adv. Technol. 268, 115147.

https://doi.org/10.1016/j.mseb.2021.115147

Mohamed, E.F., Andriantsiferana, C., Wilhelm, A.M., Delmas, H., 2011. Competitive adsorption of phenolic compounds from aqueous solution using sludge-based activated carbon. Environ. Technol. 32, 1325–1336. https://doi.org/10.1080/09593330.2010.536783

Mohanraj, R., Brindha, R., Kandeeban, R., Mahendhar, M., Saminathan, K., Ayyappadasaa, G., 2021. Electrochemical detection of 5-hydroxytryptamine using sustainable SnO_2-graphite nanocomposite modified electrode. Mater. Lett. 305, 130796. https://doi.org/10.1016/j.matlet.2021.130796

Niamlaem, M., Boonyuen, C., Sangthong, W., Limtrakul, J., Zigah, D., Kuhn, A., Warakulwit, C., 2020. Highly defective carbon nanotubes for sensitive, low-cost and environmentally friendly electrochemical H_2O_2 sensors: Insight into carbon supports. Carbon 170, 154–164. https://doi.org/10.1016/j.carbon.2020.07.081

Nie, C., Dai, Z., Meng, H., Duan, X., Qin, Y., Zhou, Y., Ao, Z., Wang, S., An, T., 2019. Peroxydisulfate activation by positively polarized carbocatalyst for enhanced removal of aqueous organic pollutants. Water Res. 166, 115043. https://doi.org/10.1016/j.watres.2019.115043

Niu, J., Conway, B.E., 2003. Adsorption of organics onto an high-area C-cloth electrode from organic solvents and organic solvent/water mixtures. J. Electroanal. Chem. 546, 59–72. https://doi.org/10.1016/S0022-0728(03)00146-3

Pierpaoli, M., Jakobczyk, P., Sawczak, M., Łuczkiewicz, A., Fudala-Książek, S., Bogdanowicz, R., 2021. Carbon nanoarchitectures as high-performance electrodes for the electrochemical oxidation of landfill leachate. J. Hazard. Mater. 401, 123407. https://doi.org/10.1016/j.jhazmat.2020.123407

Plaisance, H., Mocho, P., Bonnecaze, G., 1996. Adsorption et electrosorption de benzene sur charbon actif en grains adsorption and electrosorption of benzene on granular activated carbon. Environ. Technol. 17, 1313–1325. https://doi.org/10.1080/09593331708616501

Rong, C., Xien, H., 2009. Reversible electrosorption of thiocyanate anions by active carbon felt. Sep. Sci. Technol. 44, 3984–3999. https://doi.org/10.1080/01496390903182453

Rong, C., Xien, H., 2005. Electrosorption of thiocyanate anions on active carbon felt electrode in dilute solution. J. Colloid Interface Sci. 290, 190–195. https://doi.org/10.1016/j.jcis.2005.04.022

Sahin, E.M., Tongur, T., Ayranci, E., 2020. Removal of azo dyes from aqueous solutions by adsorption and electrosorption as monitored with in-situ UV-visible spectroscopy. Sep. Sci. Technol. 55, 3287–3298. https://doi.org/10.1080/01496395.2019.1676786

Sekar, S., Aqueel Ahmed, A.T., Pawar, S.M., Lee, Y., Im, H., Kim, D.Y., Lee, S., 2020. Enhanced water splitting performance of biomass activated carbon-anchored WO_3 nanoflakes. Appl. Surf. Sci. 508, 145127. https://doi.org/10.1016/j.apsusc.2019.145127

Stenina, E. V, Baturina, O.A., Sviridova, L.N., Damaskin, B.B., 2001. Coadsorption of halide anions and 1-adamantanol molecules on a mercury electrode. Russ. J. Electrochem. 37, 931–938.

Strohl, J.H., Dunlap, K.L., 1972. Electrosorption and separation of quinones on a column of graphite particles. Anal. Chem. 44, 2166–2170. https://doi.org/10.1021/ac60321a012

Sun, X.-F., Guo, B.-B., He, L., Xia, P.-F., Shu-Guang Wang, 2016. Electrically accelerated removal of organic pollutants by a three-dimensional graphene aerogel. AIChE J. 59, 215–228. https://doi.org/10.1002/aic

Wang, X., Hu, Y., Min, J., Li, S., Deng, X., Yuan, S., Zuo, X., 2018. Adsorption characteristics of phenolic compounds on graphene oxide and reduced graphene oxide:

A batch experiment combined theory calculation. Appl. Sci. 8, 1–13. https://doi.org/10.3390/app8101950

Yue, F., Zhang, Q., Xu, L., Zheng, Y., Yao, C., Jia, J., Leng, W., Hou, S., 2019. Porous reduced graphene oxide/single-walled carbon nanotube film as freestanding and flexible electrode materials for electrosorption of organic dye. ACS Appl. Nano Mater. 2, 6258–6267. https://doi.org/10.1021/acsanm.9b01236

Zhu, P., Zhao, Y., 2019. Cyclic voltammetry measurements of electroactive surface area of porous nickel: Peak current and peak charge methods and diffusion layer effect. Mater. Chem. Phys. 233, 60–67. https://doi.org/10.1016/j.matchemphys.2019.05.034

General conclusion and Perspectives

The objective of this work was to perform a cycle of olive mill waste treatment in which the olive pomace was first converted into a highly porous adsorbent and then into a porous electrode that could be subsequently used for the treatment of OMWW by adsorption or electrosorption. This is in the framework of a zero liquid and waste discharge approach and promotes the circular economy concept.

The composite beads are a promising adsorbent for the selective removal of organic pollutants in wastewater treatment; due to its high adsorption capacity, exceptional regeneration capacity as well as the simple preparation method. First of all, the solid waste of olive oil extraction processes (i.e., olive pomace) was converted into AC by treating it with NaOH and then encapsulating it within SA in beads by crosslinking. Then, the prepared SA-AC beads were applied as an adsorbent for the recovery of PCs from OMWW. The structure and porous morphology of SA-AC beads was confirmed by FTIR, SEM and EDS, which revealed the feasibility of SA-AC beads as potential and low-cost biosorbents. The adsorption performance of these beads was evaluated in batch and fixed-bed reactors operated in a concurrent flow system. The results revealed that an adsorption capacity of 68 mg g^{-1} was reached with initial total PCs concentration of 4,000 mg L^{-1}. The kinetics of the adsorption process of the PCs fitted a pseudo-second-order model, and the most likely mechanism took place in two stages. The adsorption isotherm was in agreement with the Langmuir model, representing a monolayer adsorption of the PCs. The dynamic models could also accurately represent the breakthrough curves. Considering PC recovery, a regeneration experiment of SA-AC beads was carried out in fixed-bed reactors. SA-AC beads depicted a higher percentage of desorption (> 40%) using ethanol as solvent and they could be reused for subsequent cycles for OMWW treatment and phenol recovery.

Then the electrosorption of PCs from simulated and real OMWW has been studied with SA-AC beads packed-bed electrode. 100% w/v Fe crosslinking agents led to slightly higher electrosorption efficiency (204 mg g^{-1}) and higher conductivity of the fixed-bed electrode compared with 100% w/v Ca. The AC content was then varied from 0% w/v to 3% w/v, while an optimal value was found to be around 1% w/v. At this percentage, the internal ohmic drop voltage was lower (2.26 V), the mass transport was higher (9.7×10^{-5} m s^{-1}) and

the diffusivity was higher (7.3×10^{-9} m^2 s^{-1}) as well, which led to enhanced electrosorption rates. The applied electrode potential variation from -0.8 to -1.2 V/(Ag/AgCl) led to an increase in electrosorption efficiency. At too high voltage (-1.3 V/(Ag/AgCl)), faradaic reaction started to occur. Therefore, the E_{cat} of -1.1 V/(Ag/AgCl) was found optimal. At an open circuit, the adsorption capacity was lower (123 mg g^{-1} against 170 mg g^{-1}), demonstrating the interest of electrosorption over adsorption. Comparing the electrosorption between simulated and real OMWW, the electrosorption capacity was found higher (307 mg g^{-1}) with actual effluents. Upon these results, new models were developed to better understand and predict the PCs electrosorption kinetics, including mass transport in transient regime. Electro-migration was added to diffusion in the model with real effluent as an explanation about the superiority of efficiency. The evolution of estimated diffusivity constant values allowed confirming that the electrosorption efficiency depended mainly on the diffusion within the beads and not at interfaces.

On the way to manufacture low-cost adsorbent directly from olive pomace waste, by limiting the preparation steps and adding chemicals, GAC was proposed to recover PCs from simulated and actual OMWW during either adsorption or electrosorption process. The suitability of GAC properties to ensure good separation efficiency was confirmed using FTIR, SEM, EDS and BET studies. Batch and fixed-bed column studies were used to understand the OMWW adsorption into GAC. For batch equilibrium studies, the adsorption of PCs onto the optimized GAC showed a strong dependence on the pH, temperature, contact time, and initial PCs concentration. The adsorption isotherm models followed the Langmuir and pseudo-second-order kinetic models. The Langmuir monolayer adsorption capacity of PCs adsorption onto GAC was 1,666 mg g^{-1}. Adsorption capacity of PCs depended on the bed height and the flow rate in column experiments. Both the Thomas and the Yoon-Nelson kinetic models fitted well the experimental data in the column. The desorption experiments of PCs from GAC have been realized. Therefore, the GAC could be used as a promising adsorbent for PCs adsorption and desorption from OMMW.

Afterward, the electrosorption of PCs from simulated and real OMWW has been studied with GAC packed-bed electrodes. The electrochemical characterization of GAC electrode showed that a high electroactive surface area (7.8×10^3 cm^2), a high value of I_0 (5.5×10^{-3} A), and low value of R_{CT} (4 Ω) could be advantages for electrosorption studies. The electrosorption study of PCs was performed at different current intensities for artificial

OMWW (1 to 200 mA) and for actual OMWW (1 to 100 mA). The highest electrosorption efficiencies were found at 1 mA (0.26 V/(Ag/AgCl)) for artificial OMWW and 10 mA (-0.05 V/(Ag/AgCl)) for actual OMWW, 72% and 68%, respectively. The influence of PCs types with different pKa and molecular sizes showed that both parameters had an impact on the electrosorption efficiency, depending on the solution pH and GAC pore size distribution. In addition, the recovery of PCs from the GAC electrode using the electrochemical regeneration method was performed and the percentage of PCs recovered was 34.5%. Finally, the combination of electrosorption as a separation technique for PCs recovery and advanced electrooxidation as a degradation process for OMWW was investigated. The COD removal efficiency was 84% and 91% for the combined processes before and after filtration, respectively.

The combination of electrosorption with a degradation process appears to be a promising strategy for treating OMWW, but still requires adjustments. In addition, some aspects need to be integrated to validate these processes and their uses for the treatment of OMWW:

- Other more powerful chemical activators should be tested to avoid carbonization to produce an even more efficient activated carbon, i.e. cheaper, stiffer, and containing more mesopores and micropores; thermal activation could also be tried in the absence of oxygen to avoid carbon loss,
- The selectivity of organic compounds with respect to separation technologies could be studied in more details by developing sufficiently elaborate analytical protocols. This would allow distinguishing the different types of PCs (and organic compounds in general) present in complex matrices such as real effluents, before, during and after adsorption/electrosorption and desorption/electrodesorption,
- The treatment of residual margines by electro-oxidation could be optimized after having well identified the problems related to the fouling of the anode,
- The efficiency of the various treatments (adsorption/desorption, electrodesorption/electrodesorption, electro-oxidation) must be tested on pilot scale processes and then on an industrial scale; the optimization must also be done on a larger scale in order to estimate the costs which will be more representative with real conditions. This will also allow a better comparison of the efficiency of these technologies compared to other existing processes.